NEUROMODULATION IN NEUROLOGICAL DISEASES: NEW TECHNOLOGY, UNCONVENTIONAL IDEAS AND ADVANCES

EDITED BY: Wayne Feng, Gottfried Schlaug and Yuping Wang
PUBLISHED IN: Frontiers in Neuroscience

frontiers Research Topics

ISSN 1664-8714
ISBN 978-2-88963-684-6
DOI 10.3389/978-2-88963-684-6

About Frontiers

Frontiers is more than just an open-access publisher of scholarly articles: it is a pioneering approach to the world of academia, radically improving the way scholarly research is managed. The grand vision of Frontiers is a world where all people have an equal opportunity to seek, share and generate knowledge. Frontiers provides immediate and permanent online open access to all its publications, but this alone is not enough to realize our grand goals.

Frontiers Journal Series

The Frontiers Journal Series is a multi-tier and interdisciplinary set of open-access, online journals, promising a paradigm shift from the current review, selection and dissemination processes in academic publishing. All Frontiers journals are driven by researchers for researchers; therefore, they constitute a service to the scholarly community. At the same time, the Frontiers Journal Series operates on a revolutionary invention, the tiered publishing system, initially addressing specific communities of scholars, and gradually climbing up to broader public understanding, thus serving the interests of the lay society, too.

Dedication to Quality

Each Frontiers article is a landmark of the highest quality, thanks to genuinely collaborative interactions between authors and review editors, who include some of the world's best academicians. Research must be certified by peers before entering a stream of knowledge that may eventually reach the public - and shape society; therefore, Frontiers only applies the most rigorous and unbiased reviews.
Frontiers revolutionizes research publishing by freely delivering the most outstanding research, evaluated with no bias from both the academic and social point of view. By applying the most advanced information technologies, Frontiers is catapulting scholarly publishing into a new generation.

What are Frontiers Research Topics?

Frontiers Research Topics are very popular trademarks of the Frontiers Journals Series: they are collections of at least ten articles, all centered on a particular subject. With their unique mix of varied contributions from Original Research to Review Articles, Frontiers Research Topics unify the most influential researchers, the latest key findings and historical advances in a hot research area! Find out more on how to host your own Frontiers Research Topic or contribute to one as an author by contacting the Frontiers Editorial Office: researchtopics@frontiersin.org

NEUROMODULATION IN NEUROLOGICAL DISEASES: NEW TECHNOLOGY, UNCONVENTIONAL IDEAS AND ADVANCES

Topic Editors:
Wayne Feng, Medical University of South Carolina, United States
Gottfried Schlaug, Harvard Medical School, United States
Yuping Wang, Capital Medical University, China

Echnology development and the investigation of new disease indications in neuromodulation is accelerating in the past decade. Non-invasive and invasive technologies are moving in an unusually rapid pace from the bench-side to the bedside. There are many renewed focuses on mechanisms of actions and new targets that are closely connecting the basic and clinical research. Artificial intelligence and machine learning are somewhat disrupting but also infusing new excitements to the traditional models of experiments and clinical trials.

This Research Topic on “Neuromodulation in Neurological Diseases: New Technology, Unconventional Ideas and Advances” collects articles that span pre-clinical, translational, clinical and population sciences in various formats of neuromodulation.

Citation: Feng, W., Schlaug, G., Wang, Y., eds. (2020). Neuromodulation in Neurological Diseases: New Technology, Unconventional Ideas and Advances. Lausanne: Frontiers Media SA. doi: 10.3389/978-2-88963-684-6

Table of Contents

frontiers in Neuroscience

ORIGINAL RESEARCH
published: 24 October 2018
doi: 10.3389/fnins.2018.00783

Check for updates

Axonal Stimulations With a Higher Frequency Generate More Randomness in Neuronal Firing Rather Than Increase Firing Rates in Rat Hippocampus

Zhaoxiang Wang[1], Zhouyan Feng[1]* and Xuefeng Wei[2]

[1] Key Lab of Biomedical Engineering for Education Ministry, College of Biomedical Engineering & Instrument Science, Zhejiang University, Hangzhou, China, [2] Department of Biomedical Engineering, The College of New Jersey, Ewing, NJ, United States

Deep brain stimulation (DBS) has been used for treating many brain disorders. Clinical applications of DBS commonly require high-frequency stimulations (HFS, ∼100 Hz) of electrical pulses to obtain therapeutic efficacy. It is not clear whether the electrical energy of HFS functions other than generating firing of action potentials in neuronal elements. To address the question, we investigated the reactions of downstream neurons to pulse sequences with a frequency in the range 50–200 Hz at afferent axon fibers in the hippocampal CA1 region of anesthetized rats. The results show that the mean rates of neuronal firing induced by axonal HFS were similar even for an up to fourfold difference (200:50) in the number and thereby in the energy of electrical pulses delivered. However, HFS with a higher pulse frequency (100 or 200 Hz) generated more randomness in the firing pattern of neurons than a lower pulse frequency (50 Hz), which were quantitatively evaluated by the significant changes of two indexes, namely, the peak coefficients and the duty ratios of excitatory phase of neuronal firing, induced by different frequencies (50–200 Hz). The findings indicate that a large portion of the HFS energy might function to generate a desynchronization effect through a possible mechanism of intermittent depolarization block of neuronal membranes. The present study addresses the demand of high frequency for generating HFS-induced desynchronization in neuronal activity, which may play important roles in DBS therapy.

Keywords: high frequency stimulation, unit spikes, firing rate, randomness, desynchronization, electrical energy

OPEN ACCESS

Edited by:
Ioan Opris,
University of Miami, United States

Reviewed by:
Marcus Thomas Wilson,
University of Waikato, New Zealand
Yael Hanein,
Tel Aviv University, Israel

****Correspondence:***
Zhouyan Feng
fengzhouyan@139.com

Specialty section:
This article was submitted to Neural Technology, a section of the journal Frontiers in Neuroscience

Received: *15 May 2018*
Accepted: *10 October 2018*
Published: *24 October 2018*

Citation:
Wang Z, Feng Z and Wei X (2018) Axonal Stimulations With a Higher Frequency Generate More Randomness in Neuronal Firing Rather Than Increase Firing Rates in Rat Hippocampus. Front. Neurosci. 12:783. doi: 10.3389/fnins.2018.00783

INTRODUCTION

Deep brain stimulation (DBS) is an established therapy for treating motor disorders such as Parkinson's disease and essential tremor (Cury et al., 2017). Due to its fast and reversible actions, as well as fewer side effects than pharmacological treatments, DBS therapy has also shown promise for treating other neurological diseases such as epilepsy, depression, and Alzheimer's disease (Laxton et al., 2010; Kennedy et al., 2011; Vonck et al., 2013). However, the precise mechanisms of DBS have not yet been determined, limiting the development and informed application of DBS treatment to various neurological disorders (Udupa and Chen, 2015; Florence et al., 2016). One of the key questions desired to be addressed is why DBS requires a high-frequency persistent pulse stimulation to obtain therapeutic efficacy in most treatments (Herrington et al., 2016). Because stimulation frequency is an important determinant of the consumption of electrical energy and the battery life-span of implantable pulse generators, answers to the question are important for the advancement of DBS therapy.

Clinical investigations have shown that a pulse frequency higher than 90 Hz is effective, whereas a pulse frequency lower than 60 Hz is ineffective or even worsens the symptoms in treating tremors by DBS (Birdno and Grill, 2008; McConnell et al., 2012). Additionally, high-frequency stimulation (HFS) (around 130 Hz) has been shown to be more effective than low-frequency stimulation in treating epilepsy (Jobst, 2010; Vonck et al., 2013). Thus, regular DBS therapy utilizes HFSs (commonly above 100 Hz) of electrical pulses in treating most brain disorders.

According to biophysical theory of excitable cells, a sequence of stimulation pulses could induce neuronal firing by transferring electrical energy into "neuronal energy" by depolarizing membranes to generate action potentials and to transmit excitation signals. Therefore, it seems reasonable to speculate that more electrical energy delivered by stimulations of a higher frequency would generate more neuronal firing. However, over-delivery of electrical energy by intensive HFS can generate a depolarization block of voltage-gated channels in neuronal membranes thereby preventing continuous firing of action potentials (Benazzouz et al., 1995; Beurrier et al., 2001). Therefore, the stimulated neurons (or neuronal elements) could only generate action potentials with a frequency far lower than the frequency of HFS (Hashimoto et al., 2003; Hamani and Temel, 2012; Florence et al., 2016; Feng et al., 2017). Such a low firing rate could be achieved by a lower stimulation frequency that consumes less electrical energy without inducing depolarization block. Then, what is the role of HFS that consumes more electrical energy?

Hypotheses on the mechanisms of DBS originally focused on whether the targeted nuclei are being excited or suppressed by HFS (Vitek, 2002; Florence et al., 2016), but the focus has shifted from excitability to desynchronization in recent years (Medeiros and Moraes, 2014; Popovych and Tass, 2014). Increase of synchronous bursting and rhythmic oscillation of large neuronal populations are associated with many brain diseases such as motor disorders and epilepsy (Gatev et al., 2006; Rampp and Stefan, 2006; Hammond et al., 2007; Jiruska et al., 2013). Studies have shown that HFS utilized by DBS can reduce pathological oscillations and synchronous activity of target neurons (Wingeier et al., 2006; Deniau et al., 2010; Eusebio et al., 2011; Medeiros and Moraes, 2014). Therapeutic effects of DBS may be attributed to a desynchronization effect rather than a rate change of neuronal firing (Hashimoto et al., 2003; McCairn and Turner, 2009). Therefore, we hypothesize that HFS with a higher frequency could generate more randomness in neuronal firing thereby resulting in a desynchronization effect of DBS.

To test the hypothesis, we investigated the reactions of downstream neurons to pulse stimulation with different frequencies (50–200 Hz) at afferent axon fibers in the hippocampal CA1 region of anaesthetized rats. Axons are more prone to be excited by extracellular pulses of HFS than other structure elements of neurons (Ranck, 1975; Nowak and Bullier, 1998; Johnson and McIntyre, 2008). The outputs of axonal HFS can spread widely through projections of axonal fibers (Nowak and Bullier, 1998), which may play important roles in DBS therapy (Girgis and Miller, 2016; Herrington et al., 2016). Therefore, the present study of axonal stimulation could reveal important mechanisms of DBS and especially provide a new explanation for the demand of high frequency pulses in effective DBS.

We conducted the investigation in hippocampal region because the clear lamellar organizations of neuronal structures in hippocampus facilitate the manipulation of stimulation and recording *in vivo* (Andersen et al., 2000, 2007). In addition, hippocampus *per se* is a potential target for the treatments of brain disorders such as epilepsy and Alzheimer's disease (Jobst, 2010; Laxton et al., 2010). Therefore, the results of axonal HFS in hippocampal regions could be valuable in advancing the applications of DBS.

MATERIALS AND METHODS

Animal Surgery

All surgical procedures were carried out in accordance with the Guide for the Care and Use of Laboratory Animals (China Ministry of Health). The protocol was approved by the Institutional Animal Care and Use Committee, Zhejiang University, Hangzhou. Twenty adult male Sprague-Dawley rats (321 ± 49 g) were used in this study under anesthesia with urethane. Details of surgery and electrode placements were similar to previous reports (Feng et al., 2013, 2017). Briefly, a 16-channel silicon electrode probe (Model Poly2, NeuroNexus Technologies, United States) was inserted into hippocampal CA1 region to record electrical potentials (**Figure 1A**). A stimulation electrode, concentric bipolar stainless steel electrode (FHC, Bowdoin, ME, United States) was inserted into Schaffer collaterals of the CA1 region to apply orthodromic stimulation in the upstream of the recording probe. Four neighboring contacts in the recording probe located in pyramidal cell layer were used to collect unit spikes. Another contact located in stratum radiatum, approximate 0.2 mm from the pyramidal layer, was used to collect post-synaptic potentials induced by the stimulation of Schaffer collaterals.

Recording and Stimulating

Details of recording and stimulating apparatuses have been reported previously (Feng et al., 2017). Briefly, sixteen-channel signals collected by the recording probe were amplified with a frequency band of 0.3–5000 Hz and then sampled at a rate of 20 kHz/channel with 16-bit analog-to-digital conversions. HFS sequences were biphasic current square-pulses with each phase width of 0.1 ms, current intensity of 0.3–0.5 mA, and pulse frequency of 50, 100, or 200 Hz. The duration of pulse sequences was 1 min.

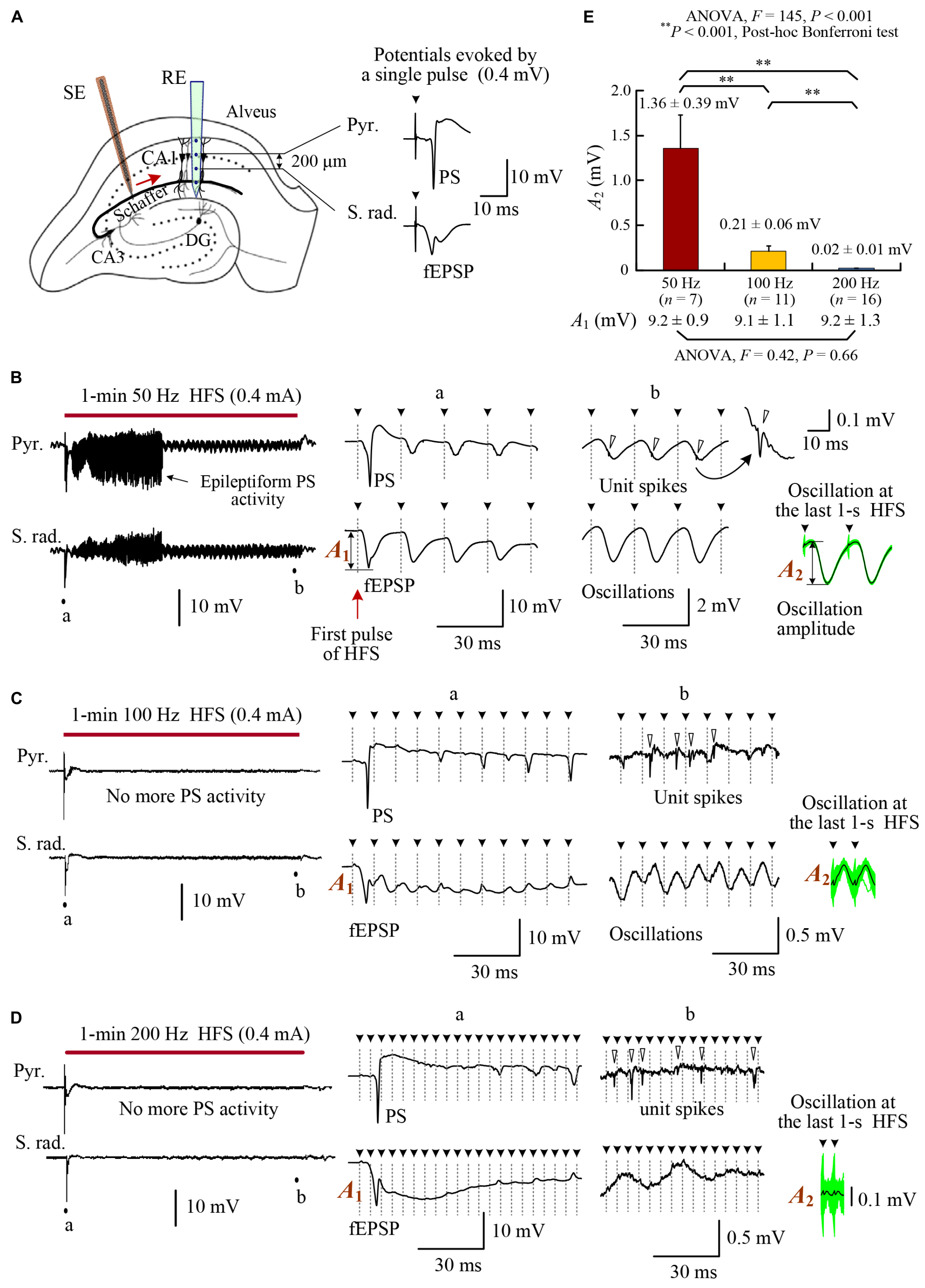

FIGURE 1 | Changes of evoked potentials in the downstream region during HFS of afferent fibers in the rat hippocampal CA1 region. **(A)** Schematic diagram of the locations of recording electrode array (RE) and orthdromic stimulation electrode (SE) in the CA1 region. Two contacts on the recording array separated 0.2 mm were used to collect the potentials in the pyramidal layer (Pyr.) and stratum radiatum (S. rad.), respectively. Typical evoked potentials (PS and fEPSP) by a single pulse are showed on the right. **(B–D)** Neuronal responses to 1-min HFS trains with 50, 100, and 200 Hz pulse frequencies (denoted by the bars). Large PS and fEPSP were evoked by the first stimulation pulse at the onset of HFS. However, in the late HFS period, no more PS potentials appeared in the pyramidal layer and only small oscillations paced pulses in the stratum radiatum. Nevertheless, unit spikes (indicated by hollow arrow heads in the expanded plots) persisted. **(E)** Comparison of the oscillation amplitudes among HFS with different pulse frequencies of 50, 100, and 200 Hz. With similar amplitudes at the onset of HFS (denoted by A_1 and listed on the bottom), the mean oscillation amplitudes at the end of HFS (denoted by A_2) were suppressed more by higher frequencies. The A_2 values were calculated by superposing and averaging the inter-pulse signals in the last 1 s of HFS. See the insets at the lower right of plots **(B–D)**. The green waveforms are superposed signals, and the black curves are average waveforms. Two repeated inter-pulse intervals are drawn for clarity. The solid arrow heads (with dot lines) over the waveforms indicate the removed stimulation artifacts.

Data Analysis of Unit Spikes

After removing stimulation artifacts, signals of multiple unit activity (MUA) were obtained by high-pass filtering the raw recording signals with a cut-off frequency of 500 Hz. MUA signals of four neighboring channels located in the pyramidal layer were used to extract single unit activity (SUA) of pyramidal cells and interneurons. See the reference for the processing details of artifact removal, spike detection, and spike sorting (Feng et al., 2017).

To investigate the effects of axonal HFS on the downstream neurons, mean firing rates of MUA and SUA were calculated during the late 30-s period of 1-min HFS and during the baseline (30 s) before HFS as a control. The initial 30-s period of the 1-min HFS was not used to analyze unit spikes, because population spikes (PS) possibly appeared in the period and might contaminate unit spikes, especially during HFS with a lower stimulation frequency of 50 Hz (Feng et al., 2013).

To evaluate the changes of phase-locked relationship between unit spikes and stimulation pulses during HFS with different frequencies, peri-stimulus time histograms (PSTH) were calculated with a bin width of 0.5 ms and a unit of "spike counts per bin." Two indexes, the peak coefficient and the duty ratio of excitatory phase, were used to quantify the distribution of unit spikes in the inter-pulse intervals of HFS. The definition of the peak coefficient is as follows:

$$\text{Peak coefficient} = \Delta C / C_{\text{ave}} \tag{1}$$

where ΔC = (maximum value of PSTH − C_{ave}), and C_{ave} = average value of PSTH over the time span of inter-pulse interval. A large value of peak coefficient indicates a non-uniform PSTH with a sharp peak; otherwise, a peak coefficient ≈0 indicates an even distribution of PSTH.

The definition of duty ratio of excitatory phase is as follows:

$$\text{Duty ratio of excitatory phase} = \frac{\text{number of "excitatory" PSTH bins}}{\text{total number of PSTH bins}} \times 100\% \tag{2}$$

where the "excitatory" PSTH bin is defined as a bin with the unit spike counts above 1.2 times of the mean value of baseline recording in the mimic PSTH (see below for the measurement of mimic PSTH). A redundancy of 20% is used in the threshold setting for anti-interference, because the mean coefficient of variation (CV = standard deviation/mean value) of bins in baseline equivalent PSTHs was ∼0.1 and 2-fold CV (∼0.2) would cover ∼95% interferences of a normal distribution. Thus, the duty ratio is the percentage of "excitatory" bins in a PSTH, and describes the concentration of excitatory effects that increase neuronal firing. A small value of duty ratio indicates a narrow phase of excitation or no excitatory phase (duty ratio = 0); otherwise, a duty ratio ≈100% indicates that neuronal firing increases in the entire time span of inter-pulse intervals.

The two indexes together offer a quantification of the phase-lock relationship between neuronal firing and stimulation pulses. A PSTH with a larger peak coefficient and a smaller duty ratio indicates a stronger phase-locked excitatory effect of stimulation on neuronal firing; otherwise, a PSTH with a smaller peak coefficient and a larger duty ratio indicates a more random effect of stimulation on neuronal firing.

For control, mimic PSTHs were calculated from baseline recordings of unit spikes by setting mimic inter-pulse intervals as 20, 10, and 5 ms corresponding to "stimulation" frequencies of 50, 100, and 200 Hz. Average value (spike counts per bin) of baseline mimic-PSTH was used to calculate the duty ratio of excitatory phase in the formula (2).

Additionally, during HFS, coupling ratio between stimulation pulses and single unit spikes was used to evaluate the efficiency of stimulus pulses in inducing action potentials in the downstream neurons:

$$\text{Coupling ratio} = \frac{\text{number of unit spikes}}{\text{number of stimuation pulses}} \tag{3}$$

All statistical data were shown as mean ± standard deviation. Paired *t*-test for two data groups (e.g., HFS group vs. corresponding baseline group) or one-way ANOVA with *post hoc* Bonferroni tests for three data groups were used to determine statistical significances of the differences among data groups.

RESULTS

Field Potentials and Unit Activity Evoked by HFS With Different Frequencies

To investigate the effects of afferent stimulation on the downstream CA1 neurons, we examined the evoked potentials both in the pyramidal cell layer (Pyr.) and in the stratum radiatum (S. rad.) during stimulations of Schaffer collaterals (**Figure 1A**). Similar to previous reports (Feng et al., 2013, 2017), large PS and field excitatory postsynaptic potentials (fEPSP) (i.e., highly synchronous responses of downstream neurons) appeared in the initial periods of HFS sequences with any stimulation frequencies of 50, 100, and 200 Hz (see expanded insets "a" in **Figures 1B–D**). The duration of epileptiform PS activity was longer for lower stimulation frequency 50 Hz, similar to the previous report (Feng et al., 2013).

Following disappearance of PS activity, in the pyramidal layer, unit spikes persisted without integrating into PS potentials. In the stratum radiatum, small potential oscillations paced with each stimulation pulse, indicating impulses of HFS coming from the afferent fibers (see expanded insets "b" in **Figures 1B–D**). The amplitudes of oscillations decreased significantly with the increase of HFS frequency (**Figure 1E**). With similar amplitudes of fEPSP (A_1) at the onset of 1-min HFS sequences, the mean oscillation amplitudes (A_2) of post-synaptic potentials at the last 1 s of HFS were only ∼15, ∼2, and ∼0.2% of A_1 for 50, 100, and 200 Hz stimulations, respectively. The data indicate a frequency-dependent attenuation of the effect of individual pulses on post-synaptic potentials.

The stimulations in the late steady-state period of HFS failed to induce large PS events; however, they did increase the firing rates of post-synaptic neurons in the pyramidal layer (**Figure 2A**). The

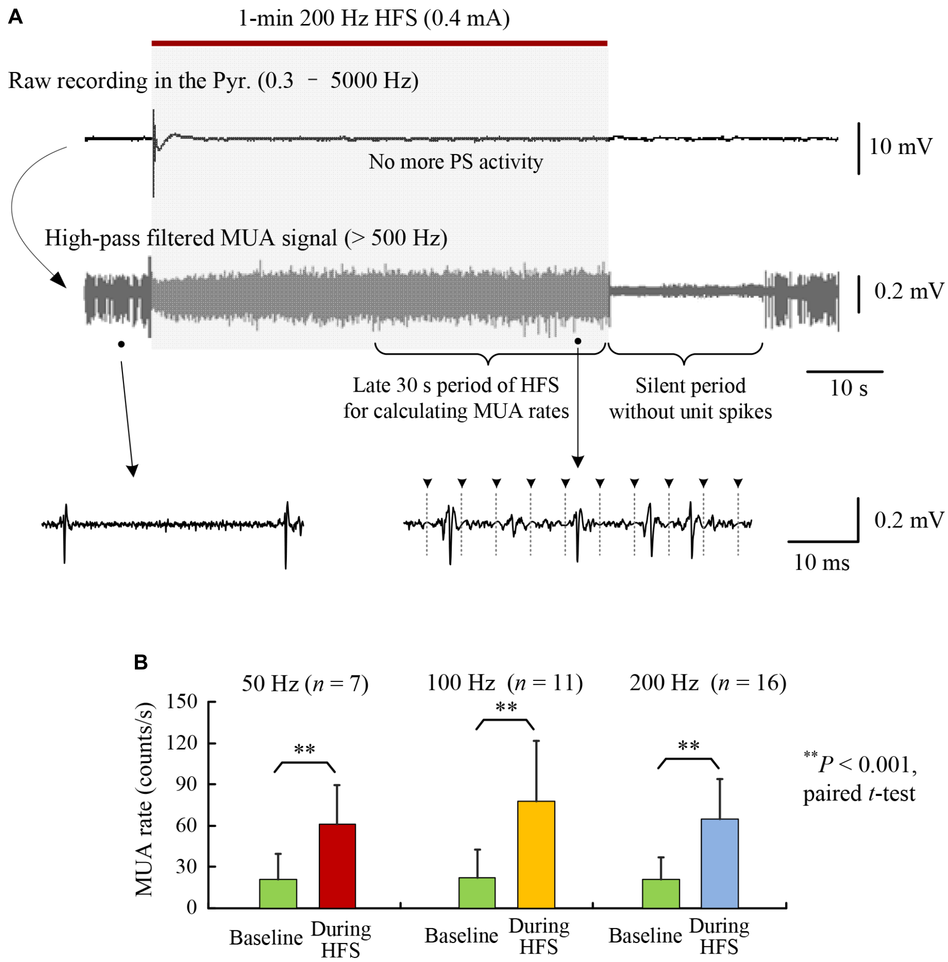

FIGURE 2 | Increase of multiple unit activity (MUA) in the CA1 region during HFS of afferent axons. **(A)** A typical example of neuronal responses to a 1-min train of 200 Hz HFS. The high-pass filtered signal (>500 Hz) shows that the MUA increased during the late period of HFS that was absent of obvious PS activity. **(B)** Comparisons of MUA firing rates between baseline recordings and during late 30-s periods of 1-min HFS with 50, 100, and 200 Hz pulse frequencies. No significant differences existed among the firing rates of the baseline recordings and during HFS, respectively, for the three groups with different frequencies (ANOVA $F < 1.1$, $P > 0.34$).

rates of multiple unit spikes (MUA) during the late 30-s periods of HFS with 50, 100, and 200 Hz were all significantly greater than baseline rates of MUA before HFS. Nevertheless, there was no significant differences among the mean MUA rates during HFS of different frequencies (**Figure 2B**; ANOVA $F = 1.1$, $P = 0.34$). A silent period (10–30 s) without neuronal firing always appeared immediately after the termination of HFS, indicating that the unit spikes during late HFS must have been induced by the stimulation (**Figure 2A**).

These results suggest that the difference of pulse frequencies did not cause significant differences in the firing rates of downstream neurons at MUA level, whereas up to a fourfold difference (200:50 frequency) of electrical energy existed among the delivered HFS sequences. The similarity in firing rates posed a difficulty in explaining the frequency-dependent effects of DBS. Nevertheless, the post-synaptic potentials evoked by individual pulses were frequency dependent (**Figure 1E**), which might change the patterns of neuronal firing. We hypothesize that the extra electrical energy delivered by pulses of a higher frequency would change the firing timing of downstream neurons, rather than their firing rates. Therefore, we next tested the hypothesis by analyzing the distributions of unit spikes in PSTHs during HFS with different frequencies.

Flattening PSTH Distributions of MUA by Stimulation With a Higher Frequency

As a control, mimic PSTH of baseline recording showed that the MUA distribution in mimic inter-pulse intervals was flat, indicating a random distribution of neuronal firing under the situation without stimulation. **Figure 3A** shows an example of mimic PSTH of 100 Hz HFS for a 30-s segment of baseline recording.

During 50 Hz HFS, the PSTH of MUA was highly non-uniform with a sharp peak at ~10 ms within the 20 ms inter-pulse intervals. Most unit spikes appeared in the time range of 8–13 ms (**Figure 3B**, *left*). The non-uniformity of the PSTH decreased with

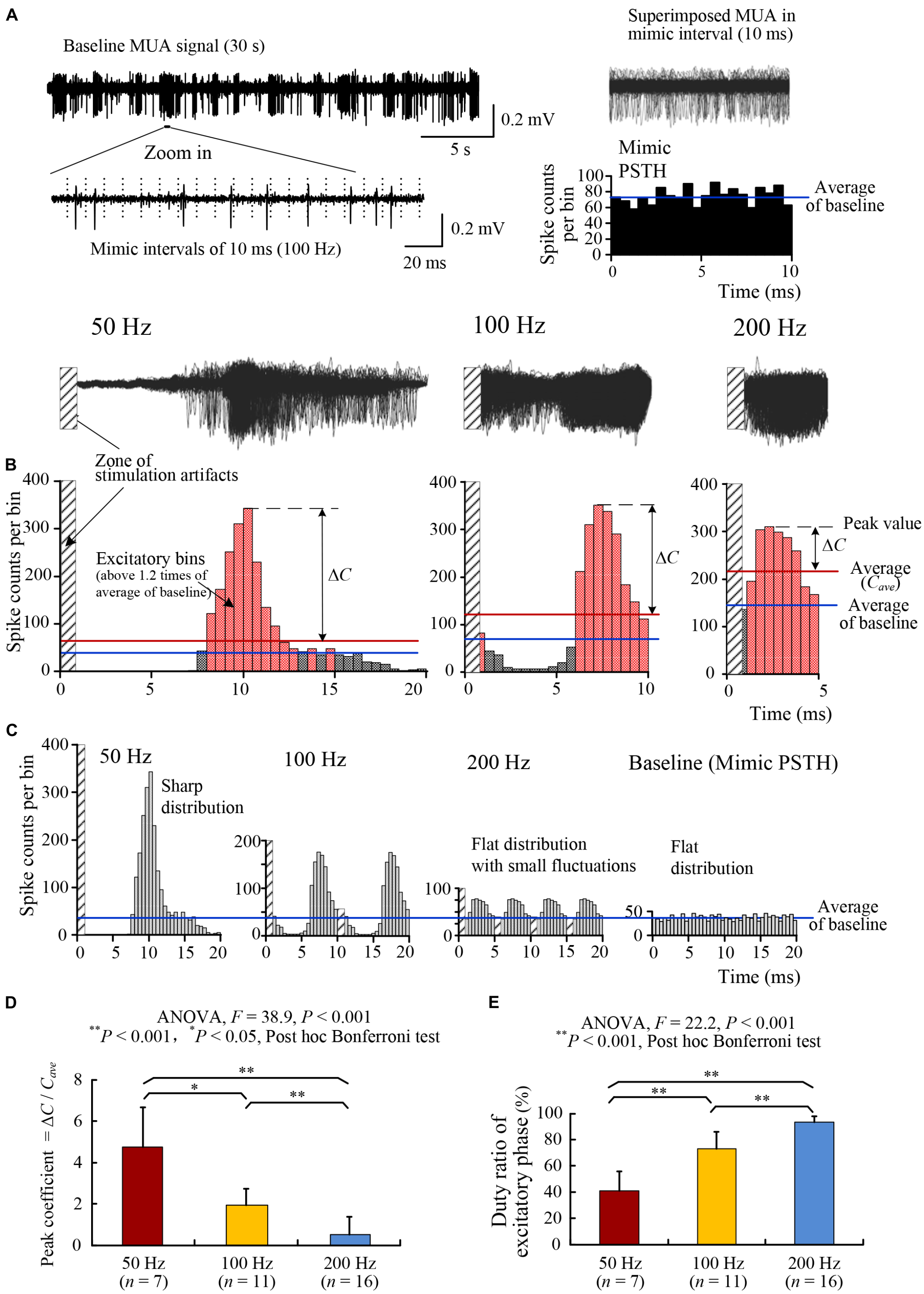

FIGURE 3 | Changes of the PSTH distributions of MUA firing by HFS with various pulse frequencies. **(A)** Making mimic PSTH of MUA firing from 30-s baseline recording for control. *Left*: a typical baseline MUA signal (30 s) was divided by virtual intervals of 10 ms (100 Hz). *Right*: superimposed signals of all 10 ms segments in the 30-s MUA (*up*) and the corresponding mimic PSTH (*down*). The blue line denotes the mean value of PSTH. **(B)** Typical plots of MUA PSTH during late 30-s HFS with 50, 100, and 200 Hz pulse frequencies. *Up*: superimposed signals of all inter-pulse intervals. *Down*: PSTH plots. In the PSTH plots, the red lines and blue lines denote the self-mean values (C_{ave}) and the baseline mean values, respectively. ΔtextitC is the difference between the peak value and the self-mean. The pink bins of PSTH are with values greater than the baseline mean values (termed as excitatory bins). **(C)** Comparisons of the PSTH distributions under the identical time duration of 20 ms by dividing the PSTH of 100 and 200 Hz into two and four same portions, respectively. **(D,E)** Comparisons of the peak coefficient ($\Delta C/C_{ave}$) and the percentage of excitatory bins (i.e., duty ratio of excitatory phase) among HFS with stimulation frequencies of 50, 100, and 200 Hz.

the increase of stimulation frequency (**Figure 3B**, *middle and right*).

Because the amount of unit spikes are cumulated in different time spans of 20, 10, and 5 ms (4:2:1) for 50-, 100-, and 200-Hz PSTHs, respectively; in order to intuitively compare the PSTH distributions of various frequencies, we divided the PSTHs of 100- and 200-Hz HFS evenly into two and four portions, respectively, and connected the portions together to form a PSTH with 20 ms time span, the same as 50-Hz HFS. Similarly, a mimic PSTH of baseline MUA with 20-ms intervals was also made as a control (**Figure 3C**). These PSTHs with an identical time span clearly show that the increase of stimulation frequency flattened the distribution of MUA in the inter-pulse intervals, indicating a decrease of phase-locked relationship between the neuronal firing and the HFS pulses.

Statistical data of PSTH suggest that with the increase of stimulation frequency, the mean values of peak coefficient decreased significantly (ANOVA with *post hoc* Bonferroni tests, $P < 0.001$ for comparisons 50 vs. 200 Hz or 100 vs. 200 Hz, $P < 0.05$ for comparison 50 vs. 100 Hz, **Figure 3D**); meanwhile, the mean values of duty ratio increased significantly (ANOVA with *post hoc* Bonferroni tests, $P < 0.001$ for all three multiple comparisons, **Figure 3E**).

These data indicate that with similar rates of HFS-evoked firing, stimulations with a lower frequency 50 Hz induced a phase-locked firing, while HFS with higher frequencies 100 and 200 Hz generated a more random pattern of neuronal firing. The extra energy delivered by more pulses of a higher frequency might function to randomize the neuronal firing.

Because MUA signals include unit spikes from a group of neurons, the change of phase-locked relationship revealed from MUA did not necessarily represent the behavior of individual neurons. The dispersion in firing time could be a result of randomized firing time of different neurons, or a result of regular firing time of individual neurons but out of phase from each other. Therefore, we next examined the firing distributions of SUA.

Flattening PSTH Distributions of SUA by Stimulation With a Higher Frequency

High-frequency stimulation of Schaffer collaterals can excite two types of neurons in the downstream CA1 region: pyramidal cells and interneurons. Analysis of SUA from the two types of neurons showed that, during the late 30-s periods of 1-min HFS with 50, 100, and 200 Hz, the mean firing rates of the neurons all increased significantly comparing to baseline firing (**Table 1**), although the mean firing rates during HFS of the three different frequencies were not statistically different for both interneurons (ANOVA, $F = 1.8$, $P = 0.17$) and pyramidal cells (ANOVA, $F = 1.6$, $P = 0.20$). Additionally, the coupling ratios between single unit spikes and stimulation pulses decreased significantly with the increase of stimulation frequencies (**Table 1**). The coupling ratios and firing rates of interneurons were greater than pyramidal cells because of the lower excitation threshold of interneurons (Csicsvari et al., 1998).

Scatter plots of SUA timing in sequential inter-pulse intervals illustrated the distribution of neuronal firing (**Figure 4A**). For control, during baseline recording before HFS, the unit spikes distributed randomly in mimic intervals of 20 ms (**Figure 4A**, *Top row*). However, during 50 Hz HFS, the unit spikes distributed centrally in a narrow band except a minor portion of postponed unit spikes (**Figure 4A**, *Middle row*). Because the coupling ratios were far smaller than 100% (**Table 1**), even at the stimulation frequency of 50 Hz, the neurons already failed to respond to every stimulation pulse. Even if an action potential was induced, its latency could be lengthened thereby resulting some of the unit firing out of the phase-locked firing timing.

With the increase of stimulation frequencies to 100 and 200 Hz, the coupling ratios decreased further and the distributions of spikes became more and more randomized to finally lose an obvious phase-locked firing timing (**Figure 4A**, *Middle row*). The PSTHs of SUA with a same interval of 20 ms showed a decrease of peak and an increase of flattening with the increase of stimulation frequency (**Figure 4A**, *Bottom row*).

Statistical data suggest that for both pyramidal cells and interneurons, the peak coefficients of PSTHs decreased significantly (ANOVA, $P < 0.001$ for all multiple comparisons, **Figure 4B**) and the duty ratios of PSTHs increased significantly (ANOVA, $P < 0.001$ for all multiple comparisons, **Figure 4C**) with the increase of HFS frequency.

The obvious peak at around 8–9 ms in the PSTH plots of 50 and 100 Hz indicated the latency of neuronal responses to stimulation pulses. If the interval between stimulation pulses coincided with the peak time of PSTH, the distribution pattern of PSTH would be similar to the PSTH of 100 Hz (corresponding to an inter-pulse interval of 10 ms), except that the peak would overlap more exactly with the zone of stimulation artifacts. However, the firing was not induced by the overlapped stimulation pulse but by the preceding pulse. Additionally, according to the small coupling ratios (**Table 1**), many of the stimulation pulses failed to induce an action potential.

These results indicate that the changes of PSTH distributions of SUA were similar to those of MUA. The flattening trend of MUA distributions by HFS with higher frequencies should be attributed to a more random firing of individual neurons, but not a collective effect of a population of neurons firing at regular intervals yet mutually out of phase. Moreover, the results suggest that with an adequately high frequency, the axonal HFS was able to generate a temporally random excitatory effect on the downstream neurons instead of a sharp effect phase-locked with stimulation pulses, thereby resulting in a desynchronization effect of DBS.

DISCUSSION

The major findings in this study include the following: (1) the neuronal firing rates induced by axonal HFS with different frequencies (50, 100, and 200 Hz) were similar despite an up to fourfold difference in the number of stimulation pulses and in the electrical energy delivered by stimulations. (2) Stimulation with a higher pulse frequency generated more randomness

TABLE 1 | Changes of mean firing rates and coupling ratios of pyramidal cells and interneurons downstream during the late 30-s periods of 1-min 50, 100, and 200 Hz HFS in the Schaffer collaterals of hippocampal CA1 region.

Neuron type	HFS frequency (Hz)	Neuron number	Firing rate in baseline (counts/s)	Firing rate during HFS (counts/s)[a]	Coupling ratio (%)[b]
Interneurons	50	12	5.6 ± 5.0	24.1 ± 15.5	48.3 ± 30.9
	100	17	5.5 ± 5.7	32.5 ± 28.1	32.5 ± 28.5
	200	31	5.9 ± 6.2	20.2 ± 17.8	10.1 ± 8.9
Pyramidal cells	50	26	1.3 ± 1.5	5.1 ± 3.0	10.3 ± 5.9
	100	45	1.2 ± 1.1	6.6 ± 4.3	6.6 ± 4.3
	200	79	1.4 ± 1.3	5.2 ± 4.8	2.6 ± 2.4

[a] *Mean firing rates during HFS of 50, 100, and 200 Hz were all significantly greater than their corresponding firing rates in baseline recordings before HFS (paired t-test, $P < 0.001$), but were not statistically different from each other for both interneurons (ANOVA, $F = 1.8$, $P = 0.17$) and pyramidal cells (ANOVA, $F = 1.6$, $P = 0.20$).*
[b] *Mean coupling ratios of the three HFS frequencies were significantly different from each other for both interneurons and pyramidal cells (one-way ANOVA, $F > 20$, $P < 0.001$; post hoc Bonferroni tests $P < 0.001$ for all multiple comparisons: 100 vs. 50 Hz, 200 vs. 50 Hz, and 100 vs. 200 Hz).*

in neuronal firing timing instead of increasing firing amount. Possible mechanisms underlying the findings and their clinic implications are discussed below.

HFS-Induced Axonal Block Might Limit the Increase of Neuronal Firing Rate With Increasing Stimulation Frequency

Previous studies have shown that HFS with a frequency over 50 Hz can partially block the activation of axons in hippocampus and subthalamus *in vitro* and *in vivo* (Jensen and Durand, 2009; Zheng et al., 2011; Feng et al., 2013; Rosenbaum et al., 2014). Simulation studies suggest that the outflow of potassium ions induced by intense excitation of axons may accumulate in the small peri-axonal space, thereby generating a depolarization block on axonal membranes because of inactivation of sodium channels (Bellinger et al., 2008; Liu et al., 2009). Under the situation of partial block of axons, HFS pulses can still generate intermittent impulses to the projecting neurons (Garcia et al., 2003; Jensen and Durand, 2009; Feng et al., 2014, 2017). Based on those previous results, here we might as well focus on the mechanism of HFS-induced axonal failures to explain our first finding: a saturation in the increase of neuronal firing rates with the increase of stimulation frequency, although involvements of other mechanisms, such as failures in synaptic transmissions, cannot be excluded currently.

Axonal block induced by HFS is frequency dependent (Jensen and Durand, 2009; Feng et al., 2013, 2014). Each pulse of HFS with a higher frequency could only generate action potentials in a smaller amount of axons thereby generating smaller field post-synaptic potentials (**Figure 1**). Nevertheless, stimulations with a higher frequency had more pulses and generated more synaptic inputs to the post-synaptic neurons. The summed excitation of smaller but more inputs could counter balance the excitation from larger but less inputs generating by stimulations with a lower frequency (Feng et al., 2014). Therefore, the mean firing rates of both MUA and SUA did not change significantly within 50–200 Hz frequency range of stimulations (**Figure 2** and **Table 1**). The extra electrical energy delivered by stimulations with a higher frequency could have other functions (e.g., randomizing firing) than increasing firing rates of neurons.

Additionally, despite of no statistical significances, the mean rates of neuronal firing seemed reaching a peak at the middle frequency 100 Hz for both types of neurons. That is, the mean firing rates during 200 Hz stimulation were even smaller than the values during 100 Hz stimulation (**Table 1**). The decline of firing rates by 200 Hz stimulation is reasonable given that a further higher frequency up to kilohertz can completely block axonal firing in peripheral nerves (McGee et al., 2015).

HFS With Higher Frequency Generates More Randomness in Neuronal Firing

The second interesting finding of our study is that increasing stimulation frequency from 50 to 200 Hz can weaken the phase-locked relationship between unit spikes and stimulation pulses. The smaller coupling ratio induced by axonal HFS with a higher frequency could cause randomness in neuronal firing. For example, during 200 Hz HFS, the mean coupling ratio was ∼10% for interneurons, indicating an interneuron might fire once following one of every 10 pulses, that is, about 10 firing opportunities could be "randomly" chosen in every 50 ms. By contrast, during 50 Hz HFS, only about two opportunities could be chosen because of the mean coupling ratio was ∼50%, meaning more concentrated (i.e., less random) in firing timing. In addition, the loss of phase-locked firing time in the inter-pulse intervals of a higher frequency stimulation generated additional randomness (**Figures 3**, **4**). Both the decreased coupling ratio and the loss of phase-locked relationship could be caused by the mechanism of HFS-induced axonal block and nonlinear dynamics in the recovery course of the block. Presumably, with a higher frequency (e.g., 200 Hz), stimulated axons could constantly be on the way to repolarize, or to recover from a state of prolonged depolarization caused by continuous inputs of stimuli. More randomness in the timing of neuronal firing could result because of the nonlinear dynamics of membrane repolarization (Hodgkin and Huxley, 1952; Grill, 2015). Therefore, the "extra electric energy" delivered by a higher frequency might bring randomness to the firing timing of neurons through elevating the membrane potentials of stimulated axons.

Additionally, although the random neuronal firing during stimulations with a higher frequency seemed close to baseline

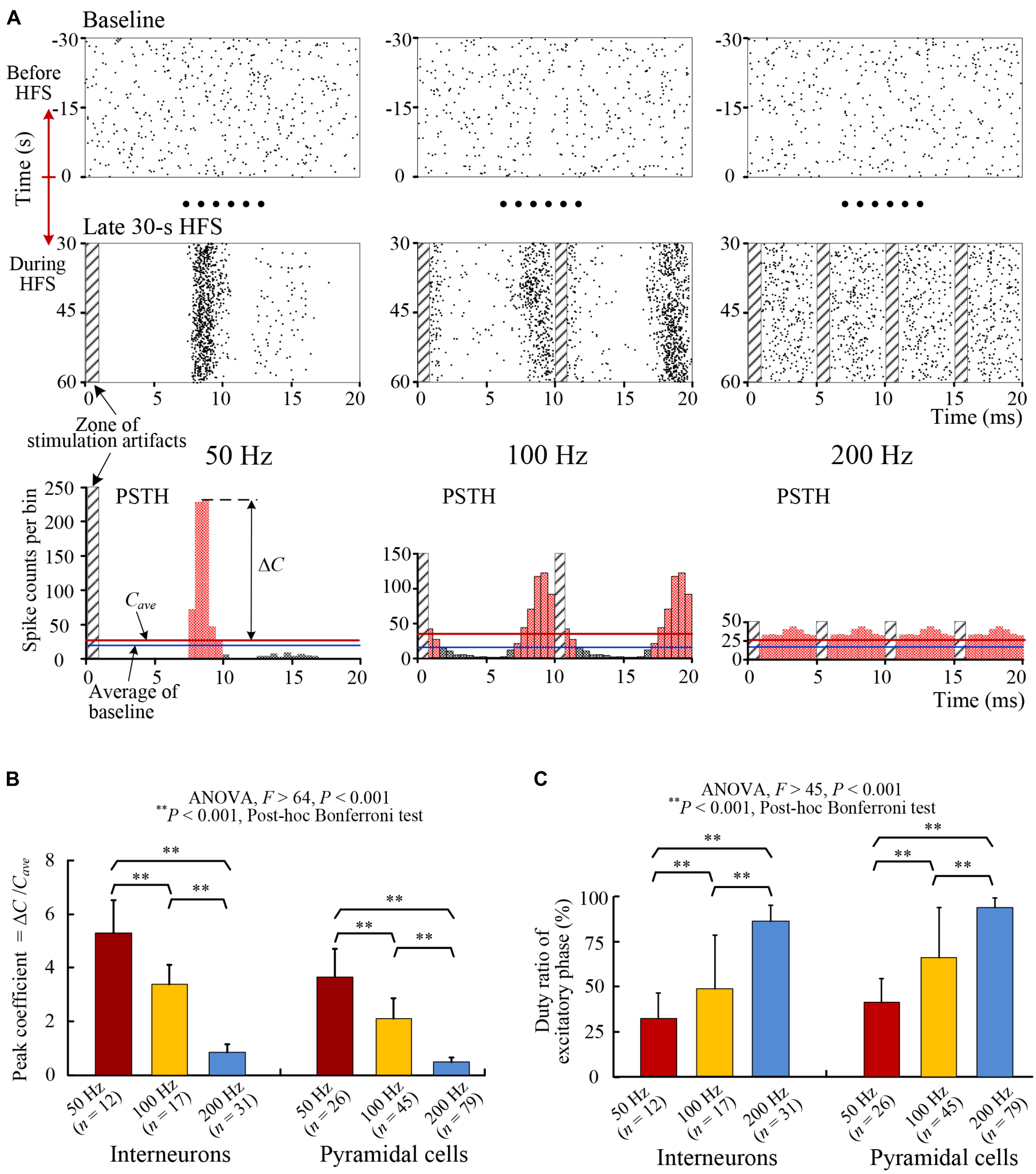

FIGURE 4 | Changes of the PSTH distributions of SUA firing. **(A)** Examples of raster plots and PSTH plots of an interneuron's firing with HFS of 50, 100, and 200 Hz frequencies. *Top*: raster plots of spikes in baseline before HFS (–30 to 0 s) in mimic interval 20 ms. *Middle*: raster plots of spikes during the late 30-s period of HFS. *Bottom*: PSTH plots during the late period of HFS. The time spans of the three groups of plots were unified to 20 ms to facilitate the comparison of firing rates directly. The PSTH plots of 100 and 200 Hz are duplications of two and four same portions, respectively. **(B,C)** Comparisons of the peak coefficients ($\Delta C/C_{ave}$) and the duty ratio of excitatory phase of PSTH for individual interneurons and pyramidal cells during HFS with different stimulation frequency of 50, 100, and 200 Hz.

firing, it could not be a return to baseline firing because of the "silent period" of tens of seconds without unit spikes immediately following the withdrawal of HFS (**Figure 2**). The silent period clearly showed that the neuronal firing during HFS was driven by the stimuli, not "spontaneous" baseline firing. Otherwise, the baseline firing should have continued following the withdrawal of HFS.

In summary, axonal HFS of a higher frequency generated more randomness in the firing timing of downstream neurons. With similar total amount of firing, the increase of firing randomness suggests not only a decrease of synchronized firing among different neurons but also a decrease of rhythmic firing of individual neurons. The present study provides a novel viewpoint for revealing the mechanism of frequency-dependent efficacy of DBS.

Implication to the New Findings of HFS

Synchronized and rhythmic firing events are related to pathological reactions of many brain disorders. For example, increase of synchronous bursts and low frequency oscillations in neurons of the basal ganglia and thalamus accompany motor symptoms of Parkinson's disease (Birdno and Grill, 2008; Gale et al., 2008). Populations of neurons fire in an excessive and synchronized manner in epileptic seizures (Le Van et al., 2003; Lopes et al., 2003).

Recent studies have suggested that desynchronization of neuronal firing is an important mechanism to the therapeutic effects of DBS (Wilson et al., 2011; McConnell et al., 2012; Medeiros and Moraes, 2014). Effective DBS for treating movement disorders overrides pathological oscillations and synchronous activity by replacing them with HFS-induced patterns of activity (Llinas et al., 1999; Birdno and Grill, 2008). Electrical stimulation therapy for epilepsy control has also utilized a strategy to de-synchronize epileptogenic neural networks (Cota et al., 2009; Medeiros and Moraes, 2014). However, the desynchronization effect of DBS requires a stimulation with a high enough frequency (Brown et al., 2004).

The present study addresses the necessarity of a higher frequency for generating HFS-induced desynchronization. With a pulse frequency over 100 Hz, a large portion of the HFS energy utilized by regular DBS might not aim to generate transmissible signals – action potentials, but to add more randomness in the sequences of action potentials thereby causing desynchronization of firing among neurons. As suggested above, a possible mechanism underlying this function of HFS might be intermittent depolarization block of neuronal membranes. The generation of depolarization block may consume a substantial portion of electrical energy.

CONCLUSION

The present study shows that neuronal firing rates induced by HFS at afferent axons are similar for stimulation frequencies of 50–200 Hz with an up to fourfold difference in electrical energy. The extra energy delivered by a higher frequency may function to randomize the neuronal firing to avoid phase-locked firing. Possible mechanism of the findings might be the intermittent block of axonal excitation induced by HFS. The findings provide a novel explanation for the demand of high frequency pulses in effective DBS through the mechanisms of desynchronization and dysrhythmia of neuronal firing.

AUTHOR CONTRIBUTIONS

ZF, ZW, and XW designed the experiments and/or interpreted the data. ZW and ZF performed the experiments and analyzed the data. ZW and ZF drafted the manuscript. XW revised the manuscript critically for important intellectual content. All authors approved the final version of the manuscript to be published and agreed to be accountable for all aspects of the manuscript.

FUNDING

This work was supported by the National Natural Science Foundation of China (No. 30970753) and by the National Basic Research Program of China (No. 2011CB504400).

REFERENCES

Andersen, P., Morris, R., and Amaral, D. (2007). *The Hippocampus Book*. Oxford: Oxford University Press.

Andersen, P., Soleng, A. F., and Raastad, M. (2000). The hippocampal lamella hypothesis revisited. *Brain Res.* 886, 165–171. doi: 10.1016/S0006-8993(00)02991-7

Bellinger, S. C., Miyazawa, G., and Steinmetz, P. N. (2008). Submyelin potassium accumulation may functionally block subsets of local axons during deep brain stimulation: a modeling study. *J. Neural Eng.* 5, 263–274. doi: 10.1088/1741-2560/5/3/001

Benazzouz, A., Piallat, B., Pollak, P., and Benabid, A. L. (1995). Responses of substantia nigra pars reticulata and globus pallidus complex to high frequency stimulation of the subthalamic nucleus in rats: electrophysiological data. *Neurosci. Lett.* 189, 77–80. doi: 10.1016/0304-3940(95)11455-6

Beurrier, C., Bioulac, B., Audin, J., and Hammond, C. (2001). High-frequency stimulation produces a transient blockade of voltage-gated currents in subthalamic neurons. *J. Neurophysiol.* 85, 1351–1356. doi: 10.1152/jn.2001.85.4.1351

Birdno, M. J., and Grill, W. M. (2008). Mechanisms of deep brain stimulation in movement disorders as revealed by changes in stimulus frequency. *Neurotherapeutics* 5, 14–25. doi: 10.1016/j.nurt.2007.10.067

Brown, P., Mazzone, P., Oliviero, A., Altibrandi, M. G., Pilato, F., Tonali, P. A., et al. (2004). Effects of stimulation of the subthalamic area on oscillatory pallidal activity in Parkinson's disease. *Exp. Neurol.* 188, 480–490. doi: 10.1016/j.expneurol.2004.05.009

Cota, V. R., Medeiros, D. C., Vilela, M. R., Doretto, M. C., and Moraes, M. F. (2009). Distinct patterns of electrical stimulation of the basolateral amygdala influence pentylenetetrazole seizure outcome. *Epilepsy Behav.* 14, 26–31. doi: 10.1016/j.yebeh.2008.09.006

Csicsvari, J., Hirase, H., Czurko, A., and Buzsaki, G. (1998). Reliability and state dependence of pyramidal cell-interneuron synapses in the hippocampus: an ensemble approach in the behaving rat. *Neuron* 21, 179–189. doi: 10.1016/S0896-6273(00)80525-5

Cury, R. G., Fraix, V., Castrioto, A., Perez, F. M., Krack, P., Chabardes, S., et al. (2017). Thalamic deep brain stimulation for tremor in Parkinson disease, essential tremor, and dystonia. *Neurology* 89, 1416–1423. doi: 10.1212/WNL.0000000000004295

Deniau, J. M., Degos, B., Bosch, C., and Maurice, N. (2010). Deep brain stimulation mechanisms: beyond the concept of local functional inhibition. *Eur. J. Neurosci.* 32, 1080–1091. doi: 10.1111/j.1460-9568.2010.07413.x

Eusebio, A., Thevathasan, W., Doyle, G. L., Pogosyan, A., Bye, E., Foltynie, T., et al. (2011). Deep brain stimulation can suppress pathological synchronisation in parkinsonian patients. *J. Neurol. Neurosurg. Psychiatry* 82, 569–573. doi: 10.1136/jnnp.2010.217489

Feng, Z., Wang, Z., Guo, Z., Zhou, W., Cai, Z., and Durand, D. M. (2017). High frequency stimulation of afferent fibers generates asynchronous firing in the downstream neurons in hippocampus through partial block of axonal conduction. *Brain Res.* 1661, 67–78. doi: 10.1016/j.brainres.2017.02.008

Feng, Z., Yu, Y., Guo, Z., Cao, J., and Durand, D. M. (2014). High frequency stimulation extends the refractory period and generates axonal block in the rat hippocampus. *Brain Stimul.* 7, 680–689. doi: 10.1016/j.brs.2014.03.011

Feng, Z., Zheng, X., Yu, Y., and Durand, D. M. (2013). Functional disconnection of axonal fibers generated by high frequency stimulation in the hippocampal CA1 region in-vivo. *Brain Res.* 1509, 32–42. doi: 10.1016/j.brainres.2013.02.048

Florence, G., Sameshima, K., Fonoff, E. T., and Hamani, C. (2016). Deep brain stimulation: more complex than the inhibition of cells and excitation of fibers. *Neuroscientist* 22, 332–345. doi: 10.1177/1073858415591964

Gale, J. T., Amirnovin, R., Williams, Z. M., Flaherty, A. W., and Eskandar, E. N. (2008). From symphony to cacophony: pathophysiology of the human basal ganglia in Parkinson disease. *Neurosci. Biobehav. Rev.* 32, 378–387. doi: 10.1016/j.neubiorev.2006.11.005

Garcia, L., Audin, J., D'Alessandro, G., Bioulac, B., and Hammond, C. (2003). Dual effect of high-frequency stimulation on subthalamic neuron activity. *J. Neurosci.* 23, 8743–8751. doi: 10.1523/JNEUROSCI.23-25-08743.2003

Gatev, P., Darbin, O., and Wichmann, T. (2006). Oscillations in the basal ganglia under normal conditions and in movement disorders. *Mov. Disord.* 21, 1566–1577. doi: 10.1002/mds.21033

Girgis, F., and Miller, J. P. (2016). White matter stimulation for the treatment of epilepsy. *Seizure* 37, 28–31. doi: 10.1016/j.seizure.2016.02.004

Grill, W. M. (2015). Model-based analysis and design of waveforms for efficient neural stimulation. *Prog. Brain Res.* 222, 147–162. doi: 10.1016/bs.pbr.2015.07.031

Hamani, C., and Temel, Y. (2012). Deep brain stimulation for psychiatric disease: contributions and validity of animal models. *Sci. Transl. Med.* 4, 142–148. doi: 10.1126/scitranslmed.3003722

Hammond, C., Bergman, H., and Brown, P. (2007). Pathological synchronization in Parkinson's disease: networks, models and treatments. *Trends Neurosci.* 30, 357–364. doi: 10.1016/j.tins.2007.05.004

Hashimoto, T., Elder, C. M., Okun, M. S., Patrick, S. K., and Vitek, J. L. (2003). Stimulation of the subthalamic nucleus changes the firing pattern of pallidal neurons. *J. Neurosci.* 23, 1916–1923. doi: 10.1523/JNEUROSCI.23-05-01916.2003

Herrington, T. M., Cheng, J. J., and Eskandar, E. N. (2016). Mechanisms of deep brain stimulation. *J. Neurophysiol.* 115, 19–38. doi: 10.1152/jn.00281.2015

Hodgkin, A. L., and Huxley, A. F. (1952). A quantitative description of membrane current and its application to conduction and excitation in nerve. *J. Physiol.* 117, 500–544. doi: 10.1113/jphysiol.1952.sp004764

Jensen, A. L., and Durand, D. M. (2009). High frequency stimulation can block axonal conduction. *Exp. Neurol.* 220, 57–70. doi: 10.1016/j.expneurol.2009.07.023

Jiruska, P., de Curtis, M., Jefferys, J. G., Schevon, C. A., Schiff, S. J., and Schindler, K. (2013). Synchronization and desynchronization in epilepsy: controversies and hypotheses. *J. Physiol.* 591, 787–797. doi: 10.1113/jphysiol.2012.239590

Jobst, B. C. (2010). Electrical stimulation in epilepsy: vagus nerve and brain stimulation. *Curr. Treat. Options Neurol.* 12, 443–453. doi: 10.1007/s11940-010-0087-4

Johnson, M. D., and McIntyre, C. C. (2008). Quantifying the neural elements activated and inhibited by globus pallidus deep brain stimulation. *J. Neurophysiol.* 100, 2549–2563. doi: 10.1152/jn.90372.2008

Kennedy, S. H., Giacobbe, P., Rizvi, S. J., Placenza, F. M., Nishikawa, Y., Mayberg, H. S., et al. (2011). Deep brain stimulation for treatment-resistant depression: follow-up after 3 to 6 years. *Am. J. Psychiatry* 168, 502–510. doi: 10.1176/appi.ajp.2010.10081187

Laxton, A. W., Tang-Wai, D. F., McAndrews, M. P., Zumsteg, D., Wennberg, R., Keren, R., et al. (2010). A phase I trial of deep brain stimulation of memory circuits in Alzheimer's disease. *Ann. Neurol.* 68, 521–534. doi: 10.1002/ana.22089

Le Van, Q. M., Navarro, V., Martinerie, J., Baulac, M., and Varela, F. J. (2003). Toward a neurodynamical understanding of ictogenesis. *Epilepsia* 44, 30–43. doi: 10.1111/j.0013-9580.2003.12007.x

Liu, H., Roppolo, J. R., de Groat, W. C., and Tai, C. (2009). The role of slow potassium current in nerve conduction block induced by high-frequency biphasic electrical current. *IEEE Trans. Biomed. Eng.* 56, 137–146. doi: 10.1109/TBME.2008.2006013

Llinas, R. R., Ribary, U., Jeanmonod, D., Kronberg, E., and Mitra, P. P. (1999). Thalamocortical dysrhythmia: a neurological and neuropsychiatric syndrome characterized by magnetoencephalography. *Proc. Natl. Acad. Sci. U.S.A.* 96, 15222–15227. doi: 10.1073/pnas.96.26.15222

Lopes, D. S. F., Blanes, W., Kalitzin, S. N., Parra, J., Suffczynski, P., and Velis, D. N. (2003). Epilepsies as dynamical diseases of brain systems: basic models of the transition between normal and epileptic activity. *Epilepsia* 44, 72–83. doi: 10.1111/j.0013-9580.2003.12005.x

McCairn, K. W., and Turner, R. S. (2009). Deep brain stimulation of the globus pallidus internus in the parkinsonian primate: local entrainment and suppression of low-frequency oscillations. *J. Neurophysiol.* 101, 1941–1960. doi: 10.1152/jn.91092.2008

McConnell, G. C., So, R. Q., Hilliard, J. D., Lopomo, P., and Grill, W. M. (2012). Effective deep brain stimulation suppresses low-frequency network oscillations in the basal ganglia by regularizing neural firing patterns. *J. Neurosci.* 32, 15657–15668. doi: 10.1523/JNEUROSCI.2824-12.2012

McGee, M. J., Amundsen, C. L., and Grill, W. M. (2015). Electrical stimulation for the treatment of lower urinary tract dysfunction after spinal cord injury. *J. Spinal Cord Med.* 38, 135–146. doi: 10.1179/2045772314Y.0000000299

Medeiros, D. C., and Moraes, M. F. (2014). Focus on desynchronization rather than excitability: a new strategy for intraencephalic electrical stimulation. *Epilepsy Behav.* 38, 32–36. doi: 10.1016/j.yebeh.2013.12.034

Nowak, L. G., and Bullier, J. (1998). Axons, but not cell bodies, are activated by electrical stimulation in cortical gray matter. I. Evidence from chronaxie measurements. *Exp. Brain Res.* 118, 477–488. doi: 10.1007/s002210050304

Popovych, O. V., and Tass, P. A. (2014). Control of abnormal synchronization in neurological disorders. *Front. Neurol.* 5:268. doi: 10.3389/fneur.2014.00268

Rampp, S., and Stefan, H. (2006). Fast activity as a surrogate marker of epileptic network function? *Clin. Neurophysiol.* 117, 2111–2117. doi: 10.1016/j.clinph.2006.02.023

Ranck, J. J. (1975). Which elements are excited in electrical stimulation of mammalian central nervous system: a review. *Brain Res.* 98, 417–440. doi: 10.1016/0006-8993(75)90364-9

Rosenbaum, R., Zimnik, A., Zheng, F., Turner, R. S., Alzheimer, C., Doiron, B., et al. (2014). Axonal and synaptic failure suppress the transfer of firing rate oscillations, synchrony and information during high frequency deep brain stimulation. *Neurobiol. Dis.* 62, 86–99. doi: 10.1016/j.nbd.2013.09.006

Udupa, K., and Chen, R. (2015). The mechanisms of action of deep brain stimulation and ideas for the future development. *Prog. Neurobiol.* 133, 27–49. doi: 10.1016/j.pneurobio.2015.08.001

Vitek, J. L. (2002). Mechanisms of deep brain stimulation: excitation or inhibition. *Mov. Disord.* 17, 69–72. doi: 10.1002/mds.10144

Vonck, K., Sprengers, M., Carrette, E., Dauwe, I., Miatton, M., Meurs, A., et al. (2013). A decade of experience with deep brain stimulation for patients with refractory medial temporal lobe epilepsy. *Int. J. Neural Syst.* 23:1250034. doi: 10.1142/S0129065712500347

Wilson, C. J., Beverlin, B. N., and Netoff, T. (2011). Chaotic desynchronization as the therapeutic mechanism of deep brain stimulation. *Front. Syst. Neurosci.* 5:50. doi: 10.3389/fnsys.2011.00050

Wingeier, B., Tcheng, T., Koop, M. M., Hill, B. C., Heit, G., and Bronte-Stewart, H. M. (2006). Intra-operative STN DBS attenuates the prominent beta rhythm in the STN in Parkinson's disease. *Exp. Neurol.* 197, 244–251. doi: 10.1016/j.expneurol.2005.09.016

Zheng, F., Lammert, K., Nixdorf-Bergweiler, B. E., Steigerwald, F., Volkmann, J., and Alzheimer, C. (2011). Axonal failure during high frequency stimulation of rat subthalamic nucleus. *J. Physiol.* 589, 2781–2793. doi: 10.1113/jphysiol.2011.205807

Conflict of Interest Statement: The authors declare that the research was conducted in the absence of any commercial or financial relationships that could be construed as a potential conflict of interest.

frontiers in Neuroscience

REVIEW
published: 11 December 2018
doi: 10.3389/fnins.2018.00929

Mechanisms Involved in the Neuroprotection of Electroacupuncture Therapy for Ischemic Stroke

Ying Xing[1], *Min Zhang*[2], *Wen-Bin Li*[2], *Fang Dong*[3] *and Feng Zhang*[1,4]*

[1] *Department of Rehabilitation Medicine, The Third Hospital of Hebei Medical University, Shijiazhuang, China,* [2] *Department of Pathophysiology, Hebei Medical University, Shijiazhuang, China,* [3] *Department of Clinical Laboratory Medicine, The Third Hospital of Hebei Medical University, Shijiazhuang, China,* [4] *Hebei Provincial Orthopedic Biomechanics Key Laboratory, The Third Hospital of Hebei Medical University, Shijiazhuang, China*

Stroke is one of the main causes of death all over the world. As the combination of acupuncture and electric stimulation, electroacupuncutre is a safe and effective therapy, which is commonly applied in ischemic stroke therapy in both experimental studies and clinical settings. The review was performed via searching for related articles in the databases of OVID, PUBMED, and ISI Web of Science from their respective inceptions to May 2018. In this review, we summarized the mechanism of EA for ischemic stroke via a series of factors, consisting of apoptosis related-factors, inflammatory factors, autophagy-related factors, growth factors, transcriptional factors, cannabinoid CB1 receptors, and other factors. In summary, EA stimulation may effectively alleviate ischemic brain injury via a series of signal pathways and various other factors.

Keywords: electroacupuncture, ischemic stroke, apoptosis, neuroprotection, neurotrophic factors (NTFs)

OPEN ACCESS

Edited by:
Gottfried Schlaug,
Harvard Medical School,
United States

Reviewed by:
Yaohui Tang,
Shanghai Jiao Tong University, China
Jing Tao,
Fujian University of Traditional Chinese Medicine, China

Correspondence:
Feng Zhang
zjk20019@126.com

Specialty section:
This article was submitted to Neural Technology, a section of the journal Frontiers in Neuroscience

Received: *06 June 2018*
Accepted: *27 November 2018*
Published: *11 December 2018*

Citation:
Xing Y, Zhang M, Li W-B, Dong F and Zhang F (2018) Mechanisms Involved in the Neuroprotection of Electroacupuncture Therapy for Ischemic Stroke. Front. Neurosci. 12:929. doi: 10.3389/fnins.2018.00929

INTRODUCTION

Ischemic stroke is a primary cause for dependency, disability, and death worldwide (Liao et al., 2017). Occlusion of the middle cerebral artery is the most common cause of ischemic stroke, resulting in high death rates ranging from 40 to 80% (Wicha et al., 2017). Ischemic stroke activates several detrimental cascades that regulate many pathological changes, consisting of apoptosis, excitotoxicity, inflammatory response, and oxidative stress (Li et al., 2017b). Electroacupuncture (EA) stems from the combination of modern electrical stimulation and traditional acupuncture and is a special type of acupuncture (Zhan et al., 2018). Compared to other conventional therapies, EA is widely accepted because it is a relatively safe, cheap, and straightforward therapy (Zhan et al., 2018). EA treatment following ischemic brain injury may produce neuroregenerative or neuroprotective effects via suppressing apoptosis, alleviating glutamate excitotoxicity, enhancing cerebral blood flow and growth factor production, regulating oxidative injury, maintaining blood-brain barrier integrity, and generating cerebral ischemic tolerance (Chang et al., 2018).

LITERATURE RESEARCH CRITERIA

In this Narrative Review, the MEDLINE (PubMed), EMBASE, Cochrane Central Register of Controlled Trials (CENTRAL) databases (from inception to May 2018) were queried to identify related abstracts and articles. The search terms were "electroacupuncture" and "stroke" or "cerebral ischemia," and the concerned disease is ischemic stroke.

The Effect of EA Therapy on the Pathogenesis and Pathological Process of Ischemic Stroke

Neurogenesis

Regulation of various growth factors may prompt both neurogenesis and angiogenesis, and improve motor function in the early phases post-stroke (Talwar and Srivastava, 2014). Shin et al. suggest that acupuncture may improve adult neurogenesis via upregulating the expression levels of neurotrophic factors (NTFs) in the brain (Shin et al., 2017). Cheng et al. indicate that the combination of EA and intranasal administration of NGF may effectively promote functional recovery and mitigate ischemic brain injury following focal ischemic stroke via elevating cell proliferation and survival (Cheng et al., 2009). Kim et al. suggest that 2 Hz EA stimulation at Baihui and Dazhui following ischemic brain injury may upregulate endogenous neurogenesis via enhancing differentiation and proliferation of NSCs via the VEGF and brain-derived neurotrophic factor (BDNF) pathway, which contributes to prompting post-ischemic functional recovery (Kim et al., 2014). Tao et al. show that EA intervention with 1–20 Hz following ischemic stroke could increase the proliferation of reactive astrocytes by promoting the expression of crucial trophic factors, such as BDNF, to provide a protective effect against ischemic damage in peri-ischemic regions (Tao et al., 2016).

Kim et al. show that EA at a frequency of 2 Hz and an intensity of 1 mA may induce prominent improvement of motor and neurological functions and exert neuroprotection against ischemic brain injury via elevating the expression of SDF-1α and BDNF (Kim et al., 2013b). EA combined with mesenchymal stem cell transplantation may improve the recovery of neurological function and upregulate the expression of neurotrophic factors, for instance neurotrophin-4/5 (NT4) and BDNF, involved in neurogenesis in mice with ischemic stroke (Kim et al., 2012, 2018). The promotion of NT4 and BDNF secretion in the ischemic brain was accomplished via their common receptor, tropomyosin receptor kinase B (TrkB) (Ahn et al., 2018). In addition, EA may improve synaptic plasticity in rats with ischemic stroke via protecting synaptic ultrastructure and promoting the levels of NGF, BDNF, GAP-43 and p38 in the ischemic brain's cortex (Yi et al., 2006).

Ephrins and Eph receptors are regarded as growth-associated inhibiting factor and are the largest tyrosine kinase family, participating in development processes of the central nervous system. Ren et al. show that EA intervention may improve neural plasticity in peri-ishcemic brain cortexes of rats with acute ischemic stroke, which might involve the enhancement of the ephrin-A5 expression (Liu et al., 2008). Retinoic acid is a crucial regulator of neurogenesis in the hippocampus and subventricular zone. EA may promote neurological deficit recovery via regulation of retinoic acid expression to effectively alleviate ischemic brain damage (Hong et al., 2013). Nestin is a cytoplasmic intermediate filament protein and normally expressed during CNS development (Michalczyk and Ziman, 2005). Ki67, a nuclear protein, is considered as a mitotic marker and expressed at the outset stage of mitosis in the neurogenesis process. EA at 2 Hz may decrease nestin immunoreactive cells and Ki67 in rats after cerebral ischemia/reperfusion (Liao et al., 2017). Heparan sulfate proteoglycans (HSPGs) exist in the extracellular matrix and the cell surface, which is closely associated with synapse function and development (Long et al., 2016). EA treatment can reduce modified neurological severity scores (mNSS) and prompt neural functional recovery following cerebral ischemic stroke via elevating the expression of HSPGs and Slit2 (Long et al., 2016).

GAP-43, as a key factor of axonal growth cones, participates in the process of axonal regeneration (Huang et al., 2017b). EA at acupoints of Neiguan and Zusanli may prompt neural remodeling and improve neural function in cerebral ischemic rats, which is related to promoted expression of GAP-43 surrounding the brain infarction region (Zhou et al., 2011). Nogo protein-A (Nogo-A) is a key myelin-related axonal growth inhibitory protein, mainly inhibiting axonal regeneration after ischemic stroke (Huang et al., 2017b). EA treatment at acupoints along both the Lung Meridian and the Pericardium Meridian may decrease the level of serum Nogo-A in post-stroke rats. Moreover, stimulation in the Pericardium Meridian exerts a better effect than in the Lung Meridian (Chen et al., 2015b). Huang et al. suggest that a treatment of EA at Quchi and Zusanli with 20 Hz for 30 min may promote axonal regeneration via increasing the expression of Gap-43 and decreasing the expression of the Nogo-A signal pathway (Huang et al., 2017b). In addition, the upregulation of phospho-LIMK1 and total LIMK1 levels was related to the synaptic-dendritic plasticity in the hippocampal CA1 region, and EA may down-regulate the expression of miR-134, negatively modulating LIMK1 to elevate synaptic-dendritic plasticity (Liu et al., 2017). Guo et al. show that EA stimulation may significantly increase the expression of IGF-1 mRNA in the striatum and hippocampus, involving the neuroprotective mechanism of EA (Guo et al., 2004). Wang et al. suggest that glia maturation factor (GMF) activation is involved in glial activation. EA intervention is reported to suppress ischemia-elicited astrocyte activation and reduce the expression of GMF. Thus, it is speculated that EA might inhibit astroglial activation via decreasing GMF (Wang et al., 2014) (as shown in **Table 1**).

Astrocytes are important for the regeneration and recovery of neuronal function and glial fibrillary acidic protein (GFAP) is regarded as a biomarker of astrocytes in the central neuronal system (Seri et al., 2001). High-frequency EA treatment with 15 HZ for 30 min daily for 5 days may decrease the GFAP expression in the hippocampus and the neocortex in rats with post-stroke pain (Tian et al., 2016). EA stimulation with 2 Hz at the acupoints of ST36 and ST37 may improve neurological dysfunction, increase rotarod test times, and decrease cerebral infarct areas. In addition, 2 Hz EA may elevate the number of GFAP immunoreactive cells and decrease nestin immunoreactive cells and Ki67 in rats after cerebral ischemia/reperfusion(Liao

TABLE 1 | Summary for mechanisms of EA for regulating neurotropic and transcriptional factors against ischemic brain injury.

References	Species/model	Acupuncture type/frequency/intensity/time	Acupoints	Results
Wang et al., 2003	Wistar rat/MCAO	EA/20–3 HZ/3 mA/30 min	Baihui (DU20) Renzhong (DU26)	Enhancement of the VEGF expression
Pan et al., 2012	SD rat/MCAO	EA/20 HZ/2–4 V/30 min	Hegu (LI4) Quchi (LI 11)	Up-regulation of serum VEGF
Tao et al., 2016	SD rat/MCAO	EA/1–20 HZ/30 min	Quchi (LI11) Zusanli(ST36)	Enhancement of BDNF
Kim et al., 2013b	C57BL/6J/photothrombotic cortical ischemia model	EA/20 HZ/1 mA/20 min	Baihui (GV20) Dazhui(GV14)	Increase of BDNF and SDF-1α
Kim et al., 2012	SD rat/MCAO	EA/3 HZ/until the limb and the ear twitched/5 min	Baihui (GV20)	Motor recovery improvement and BDNF/trkB promotion
Ma and Luo, 2008	Wistar rat/MCAO	EA/40–60HZ/5 V/15 min	Hegu (LI 4)	Angiogenesis factors promotion and anti-angiogenesis factors down-regulation
Zhou et al., 2011	rat/MCAO	EA/20 min	Zusanli (ST36) Neiguan (PC 6)	Promotion of GAP-43
Huang et al., 2017b	SD rat/MCAO	EA/ 20 Hz/30 min	Zusanli (ST36) Quchi (LI11)	Up-regulation of Gap-43; down-regulation of Nogo-A.

et al., 2017). Wang et al. suggest that glia maturation factor (GMF) activation is involved in glial activation, while EA intervention of 5–20Hz for 30 min at Baihui and Shuigou is reported to suppress ischemia-elicited astrocyte activation and reduce the expression of GMF. Thus, it is speculated that EA might inhibit astroglial activation via decreasing GMF (Wang et al., 2014).

Angiogenesis

Vascular endothelial growth factor (VEGF) is usually related to angiogenesis formation after cerebral ischemic damage, consequently exerting neuroprotective effects to alleviate the infarct volume (Kim et al., 2018). EA at the acupoints of Baihui and Renzhong induced an elevation of VEGF, which might be associated with a reduction of the infarct area via activating angiogenesis and promoting tissue repair by the proliferation of activating astrocytes following ischemic stroke (Wang et al., 2003). High levels of VEGF induced by EA intervention at Quchi and Zusanli may promote chemotaxis, mobilization and homing of EPCs so as to promote neovascularization (Zhao et al., 2010). EA stimulation with 20 Hz for 30min at both the Pericardium Meridian and the Large Intestine Meridian may elevate VEGF expression and the VEGF-positive microvessel number in ischemic stroke rats, indicating an elevation of cerebral angiogenesis, and stimulation at Quze-Neiguan exerts a better effect than Hegu-Quchi (Pan et al., 2012). Xie et al. show that EA may upregulate and accelerate the formation of stromal cell-derived factor-1α (SDF-1α) concentration gradient and result in the enhancement of angiogenesis and endothelial progenitor cells in an ischemic brain as well as promote the recovery of neurological function (Xie et al., 2016). EA stimulation may promote the expression level of angiogenic growth factors Ang-1 and VEGF and decrease the expression level of endostatin, involved in the process of angiogenesis in ischemic brain tissues from rats (Ma and Luo, 2008) and the mechanism of decreasing ischemic damage (Ma and Luo, 2007).

Autophagy

Cytoplasmic light chain 3(LC3) plays a key role in evaluating levels of autophagy (Glick et al., 2010). LC 3-II may be transformed from LC3-I and localizes in autophagosomal membranes, and the number of autophagosomes is closely related to the ratio of LC3-II/ LC3-I (Li et al., 2017b). Liu et al. demonstrate that EA treatment with 1–20 Hz for 3 days may downregulate the ratio of LC3BII/LC3BI as well as decrease the number of autolysosomes, lysosomes, and autophagosomes in the peri-ischemic cortex (Liu et al., 2016a). Furthermore, Li et al. illustrated the activation of autophagy in neurons after ischemia by way of high expression levels of Beclin 1 and LC3 in the peri-infarct cortex(Li et al., 2017b). The expression of autophagosome membrane makers, such as Unc-51-like kinase 1 (ULK1), autophagy-related gene 13 (Atg13) also may be reduced by EA treatment with 1–20 Hz for 3 days after ischemic stroke (Liu et al., 2016a).

The mammalian target of rapamycin (mTOR) kinase produces two functionally different complexes via interacting with other partners, individually named as mTOR complex 1 (mTORC1) and mTORC2; mTORC1 is a main regulator of autophagy and autophagosome formation (Liu et al., 2016a). Formation of autophagosome is regulated by the mTORC1 pathway and LC3-II (Liu et al., 2016a). Liu et al. indicate that EA treatment at the acupoints of ST36 and LI11 significantly upregulated the expression of mTORC1 and the expression of the ULK complex, indicating that the neuroprotection of EA treatment against ischemic injury might be involved in the suppression of autophagy and autophagosome formation (Liu et al., 2016a).

Apoptosis

EA of 2 Hz combined with melatonin may exert a neuroprotective effect against apoptosis by improving neurological deficits and infarcted volume, elevating B-cell lymphoma 2 (Bcl-2) and decreasing Bcl2-associated X protein(Bax) (Liu and Cheung, 2013). EA with 5–20 Hz for 30 min once daily at Baihui (DU20) and Shenting (DU24) may enhance Bcl-2 at both protein and mRNA level, phosphorylated-CREB at the protein level, and the activity of glutathione peroxidase and superoxide dismutase in the hippocampus of rats after ischemic stroke (Lin et al., 2015a). On the contrary, EA suppressed the production of Bax and reduced the malondialdehyde level (Lin et al., 2015a). Guo et al. indicate that the neuroprotection induced by EA with taurine might be related to the alleviation of P53 over-expression and up-regulation of the radio of Bcl-2/Bax in ischemic cortexes of rats (Guo et al., 2002). Xue et al. show that EA treatment may contribute to upregulating the expression level of Bcl-xL and anti-apoptotic Bcl-2 in ischemic stroke rats (Xue et al., 2014). Chen et al. demonstrate that EA with 1–20 Hz for 30 min at Quchi and Zusanli may improve cerebral infarction and neural function, and elevate the ratio of anti-apoptotic Bcl-2/Bax in ischemic brain tissue via PI3K/Akt signaling pathway activation (Chen et al., 2012). The neuroprotection of EA preconditioning at the Quchi acupoint against neuronal apoptosis might be partly regulated by the expression of Bcl-2 and Bax via εPKC activation (Wang et al., 2011). EA may increase bcl-2 expression and reduce caspase-3 expression, which might contribute to alleviation of neuronal apoptosis in cerebral ischemia-reperfusion rats (Chen et al., 2009). Xue et al. demonstrated that EA of Zusanli (ST36) and Quchi (LI11) may notably suppress the activities of pro-apoptosis factors, including caspase-3,—8, and—9 (Xue et al., 2014). Wang et al. show that EA may inhibit the activation of caspase-9 and decrease the number of apoptotic cells (Wang et al., 2002).

EA treatment with 4–20 Hz may suppress the death receptor (DR)-mediated apoptotic pathway, which may induce neuronal apoptosis after hypoxia-ischemia, alleviating DR5-induced neuronal apoptosis following ischemic stroke (Xue et al., 2014). Among the members of the apoptosis protein family inhibitor (IAP), anti-apoptotic cIAP-1 and—2 levels were significantly elevated in the cerebral cortex of post-stroke rats after EA treatment (Xue et al., 2014). Shi demonstrates that acupuncture exerts anti-apoptotic effects via inducing the nerve growth factor receptor (trk-A) expression following cerebral ischemic stroke (Shi, 1999) (as shown in **Table 2**).

Inflammatory

1–20 Hz EA treatment were inserted at 2–3 mm depth into Quchi and Zusanli, and may reduce the levels of pro-inflammatory cytokines, including IL-1β, IL-6, and TNF-α, in rats following ischemic stroke (Lan et al., 2013). Acupuncture may alleviate the enhancement of IL-6, IL-1β, and TNF-α, and suppress the microglia activation in ischemic brain tissues, suggesting that the microglia activation may be closely associated with the anti-inflammation effect of acupuncture (Han et al., 2015). EA treatment of 1–20 Hz at Quchi (LI11) and Zusanli (ST36) mediated the miR-9/ NF-κB signaling pathway and decreased the production of the proinflammatory cytokines, IL-1β and TNF-α (Liu et al., 2016c). Huang et al. show that EA treatment with 2–20Hz at Baihui and Shenting may effectively decrease the excessive expression of pro-inflammatory cytokine interleukin-1β (IL-1β) mediated by spinal microglial P2X7R so as to relieve pain hypersensitivity (Huang et al., 2017a). Wang et al. suggest that the mRNA levels of Il6st/Gp130, Cntfr and Lifr were significantly elevated following EA treatment, demonstrating that the IL-6 type cytokines exert a crucial effect in chronic or subacute phases of ischemic stroke following multiple EA interventions (Wang et al., 2014). The combination of EA 2 Hz and melatonin induced an inhibitory effect on COX-2 and TNF-α, playing a key role in neuroprotective effect to alleviate cerebral infarct volume and neurological deficit following ischemic stroke (Liu and Cheung, 2013). Scalp acupuncture may improve ischemic brain injury and inhibit cytokine-mediated inflammation via inhibiting leukocyte infiltration, prompting neurofunctional recovery, downregulating the expression of IL-1β and TNF-α and elevating IL-10 expression in rats (Zhang et al., 2007). Scalp acupuncture with 2–100Hz at the points Baihui and Qubin may elevate TGF-beta1 level and downregulate the expression of NF-κB and COX-2 in cerebrum tissues so as to attenuate ischemic brain injury, inhibiting leukocyte infiltration and improving neurofunctional recovery in rats (Zhang et al., 2009).

MMP-9 and MMP-2, the key members of the MMP family, might result in the degradation of extracellular matrix and aggravate cerebral infarct volume, which are associated with BBB destruction and other pathological processes after ischemic brain damage (Lin et al., 2016). Xu et al. suggest that ischemic brain injury-induced enhancement of MMP2 may be notably alleviated by EA stimulation in ischemic rats (Xu et al., 2014). MMP-2/MMP-9 expression was suppressed by EA treatment in brain ischemic rats and EA may alleviate learning and memory

TABLE 2 | Summary for mechanisms of EA for regulating apoptotic related factors against ischemic brain injury.

References	Species/model	Acupuncture type/frequency/intensity/time	Acupoints	results
Xue et al., 2014	SD rat/MCAO	EA/4–20 HZ/30 min	Quchi (LI11) Zusanli(ST36)	Elevating the ratio of Bcl-2/Bax
Chen et al., 2012	SD rat/MCAO	EA/1–20 HZ/30 min	Quchi (LI11) Zusanli (ST36)	Enhancement of Bcl-2/Bax ratio
Wang et al., 2011	SD rat/MCAO	EA	Quchi (LI11) Zusanli (ST36)	Up-regulation of Bcl-2; down-regulation of Bax
Liu and Cheung, 2013	SD rat/MCAO	EA/2 HZ/0.5 mA	Zusanli (ST36) xiajuxu(ST39)	Promotion of BCL-2 and Bax
Liu et al., 2016a	SD rat/MCAO	EA/6 V/0.2 mA/30 min	Quchi (LI11) Zusanli (ST36)	Inhibition of LC3B)II/I, ULK1, Atg13, Beclin1; promotion of mTORC1
Wang et al., 2002	MCAO	EA		Activation of the Akt and inhibition of the caspase-9
Xue et al., 2014	SD rat/MCAO	EA/4–20 HZ/30 min	Zusanli(ST36) Quchi(LI11)	Promotion of PI3K, p-Akt, p-Bad and Bcl-2
Chen et al., 2009	SD rat	EA		Up-regulation of bcl-2; down-regulation of caspase-3

TABLE 3 | Summary for mechanisms of EA for regulating inflammatory factors against ischemic brain injury.

References	Species/model	Acupuncture type/frequency/intensity/time	Acupoints	Results
Liu et al., 2016b	SD rat/MCAO	EA/1–20HZ/6 V/0.2 mA /30 min	Quchi (LI11) Zusanli (ST36)	Reduction of IL-1β, IL-6, and TNF-α
Huang et al., 2017a	SD rat/MCAO	EA/2–20 Hz/0.2 mA/30 min	Baihui (DU20) Shenting(DU24)	Down-regulation of IL-1βvia P2X7R
Zhang et al., 2007	SD rat/MCAO	scalp acupuncture		Down-regulation of IL-1β, TNF-α, IL-10
Liu and Cheung, 2013	SD rat/MCAO	EA/2 HZ/0.5 mA	Zusanli (ST36) xiajuxu(ST39)	Inhibition of COX-2 and TNF-α
Wang et al., 2014	SD rat/MCAO	EA/5–20 Hz/1.0–1.2 mA/30 min	"Baihui" (GV 20) and "Shuigou" (GV 26)	Promotion of Il6st/Gp130, Cntfr and Lifr
Zhang et al., 2009	SD rat/MCAO	scalp acupuncture /2–100 HZ/2 mA	Baihui(GV20) Qubin (GB7)	Inhibition of COX-2 NF-kappaB; enhancement of TGF-beta1
Liu et al., 2016c	SD rat/MCAO	EA/4 V/1–20 HZ/30 min	Quchi (LI11) Zusanli (ST36)	Inhibition of IL-1β and TNF-α
Ma et al., 2016	SD rat/MCAO	EA/2 Hz/1 mA/30 min	Baihui(GV20) Siguan	Reduction of MMP-9; Promotion of TIMP-1
Jiang et al., 2017	SD rat/MCAO	EA/1 mA/20 Hz for 5 min, 2 Hz for 30 min	Baihui (GV 20), Hegu(LI4),Taichong (LR 3)	Promotion of CYLD and reducing CX3CL1
Xu et al., 2014	SD rat/MCAO	Acupuncture and EA/2 HZ/1 mA/20 min	Zusanli (ST36) Baihui (GV20)	Reduction of MMP2
Lan et al., 2013	SD rat/MCAO	EA/1–20 HZ/muscle twitch threshold	Quchi (LI11) Zusanli (ST36)	Inhibition of TNF-α, IL-1β, and IL-6.
Lin et al., 2015b, 2016	SD rat/MCAO	EA/20 HZ/1–3 mA/30 min	Baihui (DU20) Shenting(DU24)	Reduction of MMP-2 and MMP-9

dysfunction as well as anatomical damage in post-stroke rats (Lin et al., 2016). 2 Hz EA at Baihui and Siguan markedly elevated the expression of tissue inhibitors of metalloproteinases-1 (TIMP-1) and reduced the expression of matrix metalloproteinase−9 (MMP-9) at protein and mRNA levels, leading to a balance disorder of MMP-9/TIMP-1expression, which might be involved in neuroprotection caused by EA at the Siguan and Baihui acupoints against ischemic brain injury (Ma et al., 2016).

Cylindromatosis (CYLD) is mainly expressed in peri-infarct cortical neurons, exerting anti-inflammatory and neuroprotective effects in rats after cerebral ischemia/reperfusion (Jiang et al., 2017). Enhancement of CYLD expression induced by EA at the points of Baihui, Hegu, and Taichong may reduce neuronal CX3CL1 expression and inhibit NF-κB nuclear translocation, subsequently suppressing pro-inflammatory cytokines and microglial activation in peri-infarct regions (Jiang et al., 2017). EA exerted anti-inflammatory effects via inhibition of the neuronal NF-kB pathway, which was related to increases of neuronal A20 expression induced by EA treatment in the ischemic brain of rats (Zhan et al., 2016). EA-induced downregulation of the STAT expression following ischemic stroke may exert benefits for rats with chronic and acute ischemic stroke (Su et al., 2012). Wang et al. show that shot single-time EA stimulation at Baihui and Shuigou may significantly upregulate the levels of Stat5a, Stat5b, and Stat6 and multiple EA treatments may remarkably downregulate the levels of Stat1 and Stat2 (Wang et al., 2014). EA may lower the peak expression level of heat shock protein 70 (Hsp70) and adrenocorticotrophic hormone (ACTH) so as to prompt neuronal repair, decrease inflammatory response and suppress excessive stress (Shi et al., 2017) (as shown in **Table 3**).

Blood-Brain Barrier

The blood-brain barrier (BBB) may maintain and protect homeostasis in the CNS and closely govern signaling transmission with the peripheral nervous system (Zhang et al., 2018). EA stimulation provides a beneficial effect in ischemia-reperfusion injured rats via mediating the expression of tight junction proteins, including claudin-5, occludin and ZO-1 (Zhang et al., 2014). EA (100 Hz, 2 mA) of GV 15 and GV 20 with increased NGF levels in the brain may increase BBB permeability in the ischemic cerebral tissue (Lin et al., 2009). EA stimulation at Renzhong (DU26) and Baihui (DU20) may enhance aquaporin-4 expression after ischemic brain damage, which possibly protects the BBB (Peng et al., 2012). Zhang et al. suggested that 8 min duration of EA pretreatment at GV20 and GV26 may significantly enhance exogenous NGF concentrations and increase BBB permeability in the cerebral cortex of rats with ischemic stroke (Zhang et al., 2018). Zou et al. showed that EA preconditioning with a density-sparse wave at Baihui decreases brain edema and BBB permeability by suppressing the expression of p-caveolin-1 and the degradation of tight junction proteins (Zou et al., 2015). EA preconditioning of GV 26 and GV 20 may effectively improve BBB damage via upregulating the level of MMP-9 mRNA, MMP-9 protein and VEGF mRNA after ischemic brain injury (Lin et al., 2015b).

Different Types of Factors Involved in the Process of EA Therapy Neuroprotection

MiRNAs

MiRNAs are a critical class of non-coding RNAs (ncRNAs) composed of 18–24 nucleotides. MiRNAs are important regulating molecules in the etiology and pathology of ischemic brain injury and the percentage of MiRNA changes can be up to 20% in ischemic stroke (Chen et al., 2017). MiR-9 can bind to NF-κB so as to take part in the process of inflammation caused by ischemic brain damage. EA treatment at Quchi (LI11) and Zusanli (ST36) with 1–20 Hz exerts neuroprotective effects via the miR-9-NF-κB downstream pathway after cerebral ischemic injury (Liu et al., 2016c). Zhou et al. show that the neuroprotective effect of EA may be partly reversed by miR-191a-5p, which may aggravate neuronal damage following ischemic stroke. Moreover, reduction of miR-191a-5p in the cortex and primary neurons of rats may improve neurological deficits, decrease infarct volumes, reduce neuronal apoptosis and elevate cell viability (Zhou et al., 2017). Zheng et al. suggest that EA treatment at Neiguan (PC6) and Renzhong (GV26) with a frequency of 2 Hz may reverse the upregulation of rno-miR-494 at 24 h following ischemic stroke. Therefore, rno-miR-494 might be involved in the neuroprotective effect of EA in the process of ischemic brain damage (Zheng et al., 2016). EA may change the expression level of cell proliferation-associated miRNA, including rno-miR-6216, rno-miR-206-3p, rno-miR-494-3p, and rno-miR-3473, which might be related to the improved functional recovery and cerebral blood supply after stroke (Zheng et al., 2016). Hippocampal synaptic plasticity induced by EA was associated with miR-134-mediated LIMK1, involved in the improvement of memory and learning in the period of ischemic-injury recovery (Liu et al., 2017). MiR-181b may be enhanced by EA with 2/10 Hz for 5 successive days in the penumbras, and EA may prompt neurobehavioral function recovery via regulating the expression of RhoA,GAP43, and PirB (Deng et al., 2016).

Ion and Ionic Channel Proteins

EA for 30 min/day may protect neurons against ischemic damage via modulating the level of Ca^{2+} to suppress Ca^{2+} overload in the infarct region of the brain (Xu et al., 2002). The large-conductance $Ca^{(2+)}$-activated $K^{(+)}$ (BKCa) expression level was down-regulated by EA at the Shuigou acupoint, which may prompt the recovery of pathological damage and improve neurological deficit in cerebral ischemic rats (Wang et al., 2016). Zhang et al. demonstrate that EA treatment at the Shenting and Baihui for 30 min/day exerts an important therapeutic effect in cognitive recovery, and the key mechanism is related to the regulation of CaM-CaMKIV-CREB (Zhang et al., 2016). EA treatment may effectively suppress the activity and expression level of CaM, subsequently increasing the CREB and CaMKIV expression (Zhang et al., 2016). Ren et al. show that EA treatment may regulate the expression of Na(v)1.6 and Na(v)1.1 following ischemic stroke, which may be related to the neuroprotection mechanism of EA treatment (Ren et al., 2010b). EA stimulation (density wave, frequency 10 Hz and intensity 1 mA) at PC6, SJ5, SP6, and ST36 may modulate the expression of Nav1.1 following acute ischemic stroke, which may be involved in the protective mechanism of EA treatment for ischemic brains (Ren et al., 2010a). Sun et al. show that transient receptor potential melastatin7 (TRPM7) plays an important role in the process of ischemic stroke, and EA may reverse the up-regulation of TRPM7 expression in cerebral infarction rats. The pathway of trkA might be involved in the effect of EA on TRPM7 (Zhao et al., 2005). Moreover, the expression level of the water channel proteins, AQP9 and AQP4, may be markedly inhibited after EA treatment with a 2 Hz frequency (intensity, 1 mA) at GV20 and ST36 in the infarct brain, demonstrating that the neuroprotection mechanisms of EA are partially involved in the improvement of inflammation-mediated cerebral edema (Xu et al., 2014).

ACh and Related Receptors

Kim et al. indicate that EA stimulation at a 2 Hz frequency of 1 mA intensity for 20 min may significantly increase the release of acetylcholine (ACh) from the cholinergic nerve in the ischemic brain cortex. ACh upregulation contributes to the release of NO from endothelial cells, and the over-expression of NO leads to vasodilation (Kim et al., 2013a). EA treatment at 2/15 Hz sparse-dense frequency and an intensity of 1 mA for 30 min may significantly reverse downregulation in the mRNA level of α7nAChR, choline acetyltransferase, and five subtypes of muscarinic receptors, subsequently alleviating damage of the central cholinergic system (Chi et al., 2018).

Nitric Oxide Synthase (iNOS)

Shi suggests that enhancement of NO levels in peri-infarction is closely relevant to iNOS immunoactivity and acupuncture may suppress iNOS immunoactivity via reducing the NO content in ischemic stroke rats (Shi, 1999). The effect of EA stimulation at Baihui and Dazhui with 2 Hz for 20 min on moderate ischemic damage is completely inhibited in eNOS KO mice, demonstrating that the neuroprotection of EA is closely related to eNOS (Kim et al., 2013a).

Nogo Protein and Its Receptors

In the spinal cord, the medulla oblongata and the cerebral cortex of ischemic stroke rats, upregulation of Nogo-66 receptor (NgR) expression is a critical cause of remote-organ damage of acute cerebral ischemia (Tan et al., 2014b). The neuroprotective effect induced by EA at Baihui (GV 20), Shuigou (GV 26), and Neiguan (PC 6) might be significantly associated with suppressing the expression level of NgR protein, which is the receptor of myelin growth suppression regulator Nogo-A in the brains of rats with hypertensive ischemic brain damage (Tan et al., 2014b). Tan et al. demonstrate that the up-regulation of NgR1 and Nogo-A induced by ischemia may be reversed by EA treatment at days 14 and 28 following ischemic stroke in renovascular hypertensive rats, and EA may alleviate neural damage following cervical spinal cord injury (Tan et al., 2014a). Deng et al. show that PirB protein and pirb mRNA levels in the penumbra are reduced by EA treatment at a dense-disperse frequency of 2/10 Hz and an intensity of 1–2 mA at the Baihui point within 28 days following ischemia/reperfusion, and the decrease of pirB might promote neurite outgrowth following oxygen-glucose deprivation damage (Deng et al., 2016).

MAPK Signal Pathway

EA treatment may suppress the nuclear translocation of NF-κBp65 and the expression of MyD88 and p38 MAPK so as to inhibit the production of pro-inflammatory cytokines, which is a possible mechanism for explaining how EA ameliorates the excessive activated microglia (Liu et al., 2016b). Liu et al. suggest that EA treatment at Zusanli and Quchi with dense disperse waves of 1–20 Hz may suppress nuclear translocation of NF-κB p65 in the peri-ischemic cortex of rats following ischemic stroke (Liu et al., 2016c). Systemic EA stimulation with 1–20 Hz at the points of Zusanli and Quchi may suppress the activation of the TLR4/NF-κB pathway after ischemia/reperfusion injury by decreasing crucial target points of the TLR4/NF-κB signaling pathway (Lan et al., 2013). As two crucial downstream target points of the NF-κB signaling pathway, pro-apoptotic Fas, and Bax are significantly suppressed by EA treatment. The protection mechanisms of EA at Shenting and Baihui on the improvement of cognitive impairment might be involved in the suppression of NF-κB-mediated cell apoptosis in ischemic/reperfusion rats (Feng et al., 2013).

Huang et al. show that EA stimulation may provide protection against ischemic cerebral damage via activating the ERK1/2 pathway (Huang et al., 2014). EA notably elevates the expression of ERK phosphorylation so as to prompt cerebral cell proliferation, and the expression levels of cyclin-dependent kinase (CDK)4 and cyclin D1 are also enhanced via ERK activation in ischemic brain tissues (Xie et al., 2013).

EA intervention with disperse waves of 4 and 20 Hz for 3 days may activate the PI3K/Akt signal pathway, which might be associated with the anti-apoptotic form of IAP(inhibitor of apoptosis protein) and the Bcl-2 (Xue et al., 2014). Activation of the PI3K/Akt signaling pathway induced by EA intervention may be involved in EA's mechanism against ischemic brain injury (Sun et al., 2005). Furthermore, as the PI3K activators, EA may upregulate the serum levels of GDNF and BDNF (Chen et al., 2012). Li et al. show that EA stimulation at GV26 may partially reduce the enhancement of AngII and its receptor-regulated IP3 signal pathway induced by ischemic stroke, and then improve blood supply and decrease vasoconstriction in the infarct region, providing a neuroprotective effect in ischemic rats (Li et al., 2014).

Zhao et al. demonstrate that EA stimulation with disperse waves of 4 and 20 Hz for 21 days may prompt the neurogenesis of NSCs via enhancing the Notch1 expression level after ischemic brain injury (Zhao et al., 2015). EA therapy with frequencies of 1 or 20 Hz for 30 min/day markedly suppresses the transcription of GSK3 and upregulates the expression of β-catenin and Wnt1 in neural progenitor cells (NPCs), suggesting that EA may prompt the NPCs' proliferation in the peri-ischemic cortex by the Wnt/β-catenin pathway at the Zusanli (ST36) and Quchi (LI11) points (Chen et al., 2015a). Wu et al. show that the phosphorylation level of AMP-activated protein kinase α (AMPKα) in motor cortex, somatosensory cortex and caudate putamen regions may be elevated by EA, promoting motor functional recovery and neural activity following ischemic brain injury (Wu et al., 2017).

Glutamate and Its Receptors

Glutamate accumulation occurs immediately following ischemic stroke, leading to an excessive enhancement of glutamate receptors and resulting in neurotoxicity (Liu et al., 2015). Yue et al. suggest that EA and acupuncture treatment may upregulate the serum gamma-aminobutyric acid (GABA) levels and decrease serum glutamate (Glu) levels as well as the ratio of Glu/GABA compared to those before treatment in patients with stroke, but EA exerts a better effect on those than the acupuncture group (Yue et al., 2012). Zhang et al. demonstrate that acupuncture (twice daily for 1 week, 20 min for each time) at Baihui may prevent damage of synaptic transmission and spike encoding at GABAergic neurons from ischemic stroke, and the preventive effect is related to the resistance ability of GABAergic cells to changes in refractory periods and changes of spike threshold potentials following stroke (Zhang et al., 2011). Shi shows that acupuncture may decrease the N-methyl-D-aspartate receptor subtype 1 (NMDAR1) mRNA mediated excitotoxicity of glutamate after cerebral ischemia-reperfusion injury (Shi, 1999). EA stimulation with dense-sparse frequencies (sparse 4 Hz for 1.5 s and dense 16 Hz for 1.5 s alternately) may increase the expression of TrkA and reduce the over-expression of the NMDAR1 subunit in MCAO rats (Sun et al., 2005). EA with 2 Hz may improve long-term potentiation and behavior impairment after ischemic stroke via reversing the upregulation of transient receptor potential vanilloid subtype 1 (TRPV1) and NMDAR1 in the hippocampal CA1 regions (Lin and Hsieh, 2010). EA stimulation may reverse the promoted level of NMDAR1 mRNA induced by ischemic stroke (Sun et al., 2005). Zhao et al. show that a bidirectional mediation of extracellular inhibitory and excitatory amino acid (glutamate, aspartate, and taurine) levels may be involved in EA, with 15 HZ induced neuroprotection following ischemic stroke (Zhao and Cheng, 1997).

Protein Kinase C

Expression of protein kinase C (PKC) in the vascular smooth muscle of the focal ischemic brain was notably suppressed by EA treatment following cerebral infarction, which might be involved in the protective mechanism of EA for ischemic stroke (Xu et al., 2012). EA treatment (15 Hz, 1 mA) at Shuigou may improve acute cerebral infarction via relieving arterial spasm in acute cerebral infarction rats via up-regulating the activity and immunoactivity of PKC in the vascular smooth muscle of the middle cerebral artery (Lü et al., 2015).

5-Hydroxytryptamin

The possible mechanism of post-stroke insomnia recovery caused by low-frequency EA intervention may be involved in the down-regulation of plasma norepinephrine and the upregulation of plasma 5-hydroxytryptamine (5-HT) (Tang et al., 2015). Head point-through-point EA therapy may effectively treat post-stroke depression via significantly upregulating plasma 5-HT levels in patients (Xue et al., 2007).

Cannabinoid CB1 Receptors

In the central nervous system, endocannabinoids exert a series of different functions through the significantly localized stimulation of cannabinoid CB1 receptors (CB1R) in the cortex, basal ganglia and hippocampus (Liu et al., 2015). Tian et al. suggest that delta-opioid receptors may be up-regulated by EA stimulation at Shuigou and Neiguan for 30 min/day so as to protect the brain against ischemic brain injury (Tian et al., 2008). Enhancement of glutamate receptor subunit 2 (GluR2) induced by EA with 2–15 HZ for 30 min/days exerts a neuroprotective effect against global cerebral ischemia via CB1R, providing a new possible therapy target (Liu et al., 2015).

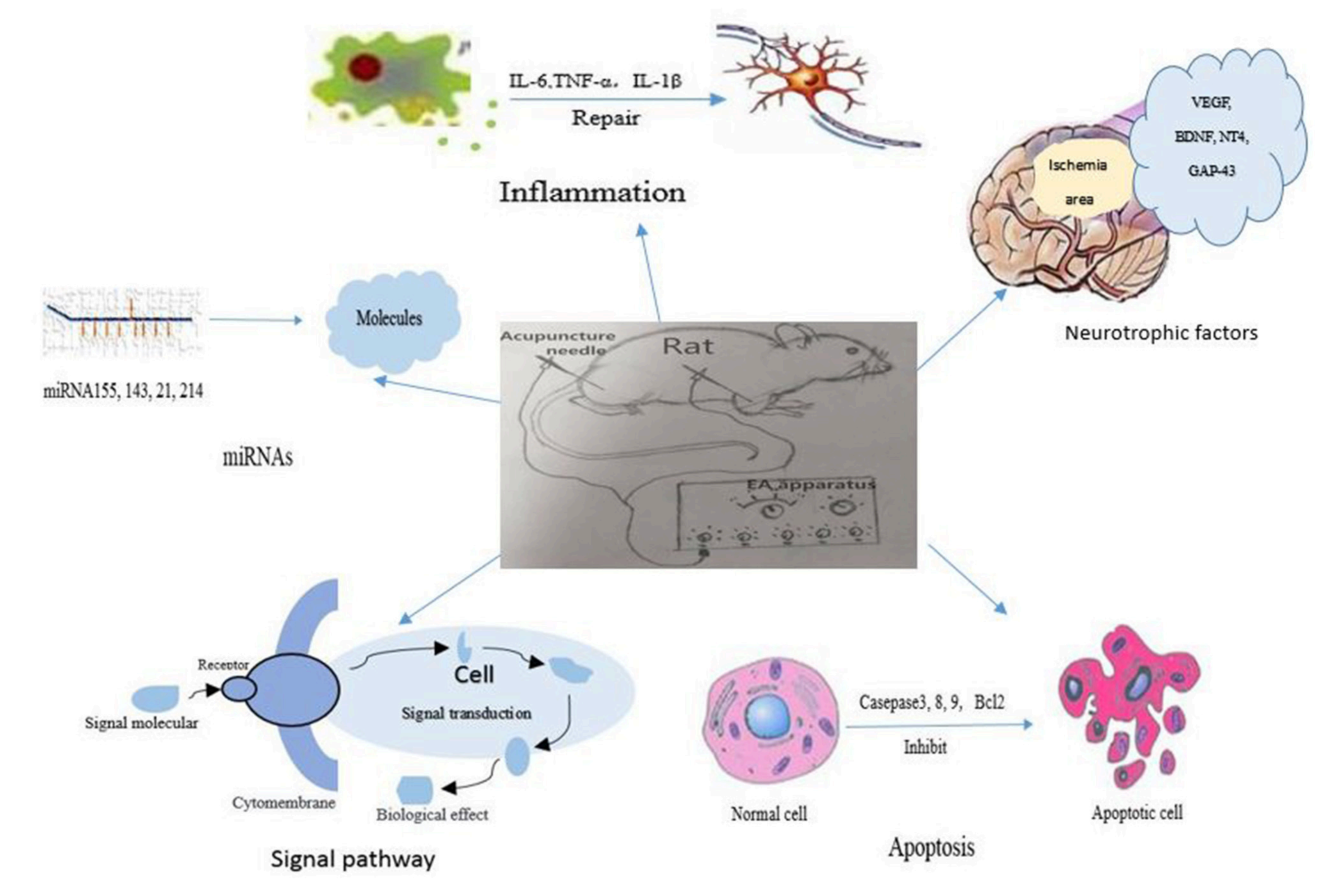

FIGURE 1 | The signal pathways and factors involved in the mechanisms of electroacupuncture therapy for ischemic stroke.

Cell Proliferation Related Molecules

EA at the point of Quchi and Zusanli may enhance the expression of p-Rb, CDK4, and CyclinD1, and BrdU labeling in the peri-ischemic striatum and cortex after stroke (Tao et al., 2016). EA at Zusanli and Quchi with 1–20 Hz may lead to promotion of the gene and protein expression level of cyclin E, CDK2, CDK4, and cyclinD1, shortening the G1-phase, omitting the G0/S and/or G1/S transition point and resulting in continued proliferation (Huang et al., 2014). EA treatment notably decreases the negative regulators p27Kip and p21Cip1 in the protein and gene levels, which may effectively reverse the effect of these factors in suppressing positive regulatory factors, thus enhancing cell proliferation (Huang et al., 2014).

Transcriptional Factors

EA treatment could reduce the neurological score, alleviate neurological dysfunction in rats following ischemic stroke, and promote the expression level of Slit 2 and Robo 1, which might be involved in the mechanism of EA treatment for alleviating brain infarction in the clinic (Lu et al., 2013). EA intervention at acupoints alleviates the downregulation of cell division-cycle 42 (Cdc 42) and upregulation of Slit-Robo GTPase-activating protein-1 (srGAP 1) caused by brain ischemia in rats, demonstrating that EA could exert benefits in neurological function following ischemic stroke (Lin et al., 2016). Lu et al. show that EA promotes the expression of Monocarboxylate transporter 1 (MCT1) in astrocytes and enhances the transportation of lactate from astrocyte to neurons as energy substrates (Chen et al., 2015b). EA (15 Hz, 2 mA) plays a key role in establishing collateral circulation and blood vessel regeneration via enhancing the expression level of Apelin-APJ for vascular endothelial cells in ischemic rat brains (Yang et al., 2017). Li et al. show that EA may raise hypoxia-inducible factor-1α (HIF-1α), reduce cerebral IV and promote recovery of neurological function in cerebral ischemic rats (Li et al., 2017a). After damage of cerebral tissue, abnormal activated astrocytes will prompt the synthesis and release of pain signal transduction-associated mediators, for example cyclooxygenase-2 (COX-2). COX-2 expression was markedly upregulated in the damaged hippocampus of animal models after global cerebral ischemia, and EA may exert an analgesic effect via reducing COX-2 expression in the hippocampus (Tian et al., 2016).

Serum Proteins

Pan et al. show that EA may change the expression level of multiple serum proteins, including upregulation of gelsolin, beta-2-glycoprotein I proteins, C3, C4B, and complement component I, and downregulation of SerpinG1 protein in acute ischemic stroke patients (Pan et al., 2011). EA at Shenting and Baihui with 1–20Hz for 30 min daily for 7 days may downregulate the expression of Ras homologous member A, and upregulate the expression of F-actin proteins, Ras-related C3 botulinum toxin substrate 1 and cell division cycle 42, Which demonstrates that dendritic spine plasticity and Rho GTPases play a key role in the mediation of EA effects related to cognitive function recovery after ischemic brain injury (Lin et al., 2016). Suppression of platelet-associated complement-1 (PAC-1) induced by EA at yangning meridian acupoints may promote the recovery of paralyzed lower extremities in patients with acute ischemic brain injury (Tang et al., 2015).

CONCLUSION

In recent years, EA has not only been applied as a supplementary treatment for post-stroke recovery but also as a preventive intervention for stroke. EA has shown neuroprotective effects in both animal studies and clinical trials. There is growing evidence that EA attenuates ischemic brain injury via regulating considerable molecules, for instance apoptosis-related factors, inflammation-related factors, autophagy-related factors, glutamate and its receptors, miRNAs, neurotropic, and transcriptional factors, becoming involved in different signal pathways, as shown in **Figure 1**. Meanwhile, the clinical effects of EA included life quality improvement, attenuation of pain, enhancement of cerebral blood flow and daily-life activity promotion in stroke patients. These beneficial effects of EA might be closely related to the above-mentioned neuroprotective mechanisms which were confirmed in animal studies. Moreover, the potential adverse effects of EA should be attached with enough importance. If the needle is not disposable, the contaminated needle might help the spread of infectious diseases; if the practitioner is not skillful enough, the needle might damage the internal organs in the abdomen; if the treatment point is not selected appropriately, the needle might hurt the vascular system or nerves in the respective region of body.

In conclusion, EA stimulation is a safe and effective therapy in reducing ischemic brain injury. The mechanisms for neuroprotection of EA might explain the why EA may exert benefits for stroke patients in clinical settings. Further research on molecular mechanisms of EA might provide therapeutic targets as well as a more optimized strategy for acupoint selection and therapy dosage.

AUTHOR CONTRIBUTIONS

YX and FZ conceived the main ideas and wrote the manuscript. W-BL, MZ, and FD searched the references and designed the framework.

REFERENCES

Ahn, S. M., Kim, Y. R., Shin, Y. I., Ha, K. T., Lee, S. Y., Shin, H. K., et al. (2018). Therapeutic potential of a combination of electroacupuncture and trkb-expressing mesenchymal stem cells for ischemic stroke. *Mol. Neurobiol.* doi: 10.1007/s12035-018-1067-z. [Epub ahead of print].

Chang, Q. Y., Lin, Y. W., and Hsieh, C. L. (2018). Acupuncture and neuroregeneration in ischemic stroke. *Neural Regen. Res.* 13, 573–583. doi: 10.4103/1673-5374.230272

Chen, A., Lin, Z., Lan, L., Xie, G., Huang, J., Lin, J., et al. (2012). Electroacupuncture at the Quchi and Zusanli acupoints exerts neuroprotective role in cerebral ischemia-reperfusion injured rats via activation of the PI3K/Akt pathway. *Int. J. Mol. Med.* 30, 791–796. doi: 10.3892/ijmm.2012.1074

Chen, B., Tao, J., Lin, Y., Lin, R., Liu, W., and Chen, L. (2015a). Electro-acupuncture exerts beneficial effects against cerebral ischemia and promotes the proliferation of neural progenitor cells in the cortical peri-infarct area through the Wnt/beta-catenin signaling pathway. *Int. J. Mol. Med.* 36, 1215–1222. doi: 10.3892/ijmm.2015.2334

Chen, C., Zhang, W., Lou, B. D., Pan, J., Cao, Y., Zhong, F., et al. (2015b). [Effect of electroacupuncture stimulation of acupoints of the pericardium meridian on serum NGF and Nogo-A contents and cerebral NGF and Nogo-A expression in cerebral ischemia rats]. *Zhen Ci Yan Jiu* 40, 94–98. doi: 10.13702/j.1000-0607.2015.02.002

Chen, F., Yan, Z. K., and Yang, B. (2009). [Effects of electroacupuncture on cerebral Bcl-2 and caspase-3 expression after cerebral ischemia reperfusion in rats]. *Zhen Ci Yan Jiu* 34, 363–367. doi: 10.13702/j.1000-0607.2009.06.003

Chen, S., Wang, M., Yang, H., Mao, L., He, Q., Jin, H., et al. (2017). LncRNA TUG1 sponges microRNA-9 to promote neurons apoptosis by up-regulated Bcl2l11 under ischemia. *Biochem. Biophys. Res. Commun.* 485, 167–173. doi: 10.1016/j.bbrc.2017.02.043

Cheng, S., Ma, M., Ma, Y., Wang, Z., Xu, G., and Liu, X. (2009). Combination therapy with intranasal NGF and electroacupuncture enhanced cell proliferation and survival in rats after stroke. *Neurol. Res.* 31, 753–758. doi: 10.1179/174313209X382557

Chi, L., Du, K., Liu, D., Bo, Y., and Li, W. (2018). Electroacupuncture brain protection during ischemic stroke: a role for the parasympathetic nervous system. *J. Cereb. Blood Flow Metab.* 38, 479–491. doi: 10.1177/0271678X17697988

Deng, B., Bai, F., Zhou, H., Zhou, D., Ma, Z., Xiong, L., et al. (2016). Electroacupuncture enhances rehabilitation through miR-181b targeting PirB after ischemic stroke. *Sci. Rep.* 6:38997. doi: 10.1038/srep38997

Feng, X., Yang, S., Liu, J., Huang, J., Peng, J., Lin, J., et al. (2013). Electroacupuncture ameliorates cognitive impairment through inhibition of NF-kappaB-mediated neuronal cell apoptosis in cerebral ischemia-reperfusion injured rats. *Mol. Med. Rep.* 7, 1516–1522. doi: 10.3892/mmr.2013.1392

Glick, D., Barth, S., and Macleod, K. F. (2010). Autophagy: cellular and molecular mechanisms. *J. Pathol.* 221, 3–12. doi: 10.1002/path.2697

Guo, J., Li, R., Zhao, P., and Cheng, J. (2002). Effect of taurine in combination with electroacupuncture on neuronal damage following transient focal cerebral ischemia in rats. *Acupunct. Electrother. Res.* 27, 129–136. doi: 10.3727/036012902816026086

Guo, J. C., Gao, H. M., Chen, J., Zhao, P., Cao, X. D., Li, Y., et al. (2004). Modulation of the gene expression in the protective effects of electroacupuncture against cerebral ischemia: a cDNA microarray study. *Acupunct. Electrother. Res.* 29, 173–186. doi: 10.3727/036012904815901434

Han, B., Lu, Y., Zhao, H., Wang, Y., Li, L., and Wang, T. (2015). Electroacupuncture modulated the inflammatory reaction in MCAO rats via inhibiting the TLR4/NF-kappaB signaling pathway in microglia. *Int. J. Clin. Exp. Pathol.* 8, 11199–11205. doi: 10.13935/j.cnki.sjzx.150631

Hong, J., Wu, G., Zou, Y., Tao, J., and Chen, L. (2013). Electroacupuncture promotes neurological functional recovery via the retinoic acid signaling pathway in rats following cerebral ischemia-reperfusion injury. *Int. J. Mol. Med.* 31, 225–231. doi: 10.3892/ijmm.2012.1166

Huang, J., Ye, X., You, Y., Liu, W., Gao, Y., Yang, S., et al. (2014). Electroacupuncture promotes neural cell proliferation *in vivo* through activation of the ERK1/2 signaling pathway. *Int. J. Mol. Med.* 33, 1547–1553. doi: 10.3892/ijmm.2014.1702

Huang, J., You, X., Liu, W., Song, C., Lin, X., Zhang, X., et al. (2017a). Electroacupuncture ameliorating post-stroke cognitive impairments via inhibition of peri-infarct astroglial and microglial/macrophage P2 purinoceptors-mediated neuroinflammation and hyperplasia. *BMC Complement. Altern. Med.* 17:480. doi: 10.1186/s12906-017-1974-y

Huang, S., Huang, D., Zhao, J., and Chen, L. (2017b). Electroacupuncture promotes axonal regeneration in rats with focal cerebral ischemia through the downregulation of Nogo-A/NgR/RhoA/ROCK signaling. *Exp. Ther. Med.* 14, 905–912. doi: 10.3892/etm.2017.4621

Jiang, J., Luo, Y., Qin, W., Ma, H., Li, Q., Zhan, J., et al. (2017). Electroacupuncture suppresses the NF-kappaB signaling pathway by upregulating cylindromatosis to alleviate inflammatory injury in cerebral ischemia/reperfusion rats. *Front. Mol. Neurosci.* 10:363. doi: 10.3389/fnmol.2017.00363

Kim, J. H., Choi, K. H., Jang, Y. J., Bae, S. S., Shin, B. C., Choi, B. T., et al. (2013a). Electroacupuncture acutely improves cerebral blood flow and attenuates moderate ischemic injury via an endothelial mechanism in mice. *PLoS ONE* 8:e56736. doi: 10.1371/journal.pone.0056736

Kim, J. H., Choi, K. H., Jang, Y. J., Kim, H. N., Bae, S. S., Choi, B. T., et al. (2013b). Electroacupuncture preconditioning reduces cerebral ischemic injury via BDNF and SDF-1alpha in mice. *BMC Complement. Altern. Med.* 13:22. doi: 10.1186/1472-6882-13-22

Kim, M. W., Chung, Y. C., Jung, H. C., Park, M. S., Han, Y. M., Chung, Y. A., et al. (2012). Electroacupuncture enhances motor recovery performance with brain-derived neurotrophic factor expression in rats with cerebral infarction. *Acupunct. Med.* 30, 222–226. doi: 10.1136/acupmed-2011-010126

Kim, Y. R., Ahn, S. M., Pak, M. E., Lee, H. J., Jung, D. H., Shin, Y. I., et al. (2018). Potential benefits of mesenchymal stem cells and electroacupuncture on the trophic factors associated with neurogenesis in mice with ischemic stroke. *Sci. Rep.* 8:2044. doi: 10.1038/s41598-018-20481-3

Kim, Y. R., Kim, H. N., Ahn, S. M., Choi, Y. H., Shin, H. K., and Choi, B. T. (2014). Electroacupuncture promotes post-stroke functional recovery via enhancing endogenous neurogenesis in mouse focal cerebral ischemia. *PLoS ONE* 9:e90000. doi: 10.1371/journal.pone.0090000

Lan, L., Tao, J., Chen, A., Xie, G., Huang, J., Lin, J., et al. (2013). Electroacupuncture exerts anti-inflammatory effects in cerebral ischemia-reperfusion injured rats via suppression of the TLR4/NF-kappaB pathway. *Int. J. Mol. Med.* 31, 75–80. doi: 10.3892/ijmm.2012.1184

Li, C., Zhang, T., Yu, K., Xie, H., Bai, Y., Zhang, L., et al. (2017a). Neuroprotective effect of electroacupuncture and upregulation of hypoxia-inducible factor-1alpha during acute ischaemic stroke in rats. *Acupunct. Med.* 35, 360–365. doi: 10.1136/acupmed-2016-011148

Li, J., He, J., Du, Y., Cui, J., Ma, Y., and Zhang, X. (2014). Electroacupuncture improves cerebral blood flow and attenuates moderate ischemic injury via Angiotensin II its receptors-mediated mechanism in rats. *BMC Complement. Altern. Med.* 14:441. doi: 10.1186/1472-6882-14-441

Li, X., Wang, M. H., Qin, C., Fan, W. H., Tian, D. S., and Liu, J. L. (2017b). Fingolimod suppresses neuronal autophagy through the mTOR/p70S6K pathway and alleviates ischemic brain damage in mice. *PLoS ONE* 12:e0188748. doi: 10.1371/journal.pone.0188748

Liao, S. L., Lin, Y. W., and Hsieh, C. L. (2017). Neuronal regeneration after electroacupuncture treatment in ischemia-reperfusion-injured cerebral infarction rats. *Biomed Res. Int.* 2017:3178014. doi: 10.1155/2017/3178014

Lin, R., Lin, Y., Tao, J., Chen, B., Yu, K., Chen, J., et al. (2015a). Electroacupuncture ameliorates learning and memory in rats with cerebral ischemia-reperfusion injury by inhibiting oxidative stress and promoting p-CREB expression in the hippocampus. *Mol. Med. Rep.* 12, 6807–6814. doi: 10.3892/mmr.2015.4321

Lin, R., Wu, Y., Tao, J., Chen, B., Chen, J., Zhao, C., et al. (2016). Electroacupuncture improves cognitive function through Rho GTPases and enhances dendritic spine plasticity in rats with cerebral ischemia-reperfusion. *Mol. Med. Rep.* 13, 2655–2660. doi: 10.3892/mmr.2016.4870

Lin, X. M., Chen, L. P., and Yao, X. (2015b). [The impact of different duration of EA-pretreatment on expression of MMP-9 and VEGF in blood-brain barrier in rats with cerebral ischemia-reperfusion injury]. *Zhen Ci Yan Jiu* 40, 40–44. doi: 10.13702/j.1000-0607.2015.01.008

Lin, X. M., Tan, K. P., Zhang, A. J., and He, L. H. (2009). [Effect of electroacupuncture on the permeability of blood-brain barrier for nerve growth factor and its relevance to PKC pathway in cerebral ischemia rats]. *Zhen Ci Yan Jiu* 34, 110–113. doi: 10.13702/j.1000-0607.2009.02.009

Lin, Y. W., and Hsieh, C. L. (2010). Electroacupuncture at Baihui acupoint (GV20) reverses behavior deficit and long-term potentiation through N-methyl-d-aspartate and transient receptor potential vanilloid subtype 1 receptors in middle cerebral artery occlusion rats. *J. Integr. Neurosci.* 9, 269–282. doi: 10.1142/S0219635210002433

Liu, L., and Cheung, R. T. (2013). Effects of pretreatment with a combination of melatonin and electroacupuncture in a rat model of transient focal cerebral ischemia. *Evid. Based Complement. Alternat. Med.* 2013:953162. doi: 10.1155/2013/953162

Liu, W., Mukherjee, M., Sun, C., Liu, H., and McPeak, L. K. (2008). Electroacupuncture may help motor recovery in chronic stroke survivors: a pilot study. *J. Rehabil. Res. Dev.* 45, 587–595. doi: 10.1682/JRRD.2007.11.0181

Liu, W., Shang, G., Yang, S., Huang, J., Xue, X., Lin, Y., et al. (2016a). Electroacupuncture protects against ischemic stroke by reducing autophagosome formation and inhibiting autophagy through the mTORC1-ULK1 complex-Beclin1 pathway. *Int. J. Mol. Med.* 37, 309–318. doi: 10.3892/ijmm.2015.2425

Liu, W., Wang, X., Yang, S., Huang, J., Xue, X., Zheng, Y., et al. (2016b). Electroacupunctre improves motor impairment via inhibition of microglia-mediated neuroinflammation in the sensorimotor cortex after ischemic stroke. *Life Sci.* 151, 313–322. doi: 10.1016/j.lfs.2016.01.045

Liu, W., Wang, X., Zheng, Y., Shang, G., Huang, J., Tao, J., et al. (2016c). Electroacupuncture inhibits inflammatory injury by targeting the miR-9-mediated NF-kappaB signaling pathway following ischemic stroke. *Mol. Med. Rep.* 13, 1618–1626. doi: 10.3892/mmr.2015.4745

Liu, W., Wu, J., Huang, J., Zhuo, P., Lin, Y., Wang, L., et al. (2017). Electroacupuncture regulates hippocampal synaptic plasticity via miR-134-mediated LIMK1 function in rats with ischemic stroke. *Neural Plast.* 2017:9545646. doi: 10.1155/2017/9545646

Liu, Z., Chen, X., Gao, Y., Sun, S., Yang, L., Yang, Q., et al. (2015). Involvement of GluR2 up-regulation in neuroprotection by electroacupuncture pretreatment via cannabinoid CB1 receptor in mice. *Sci. Rep.* 5:9490. doi: 10.1038/srep09490

Long, F., Li, X. Z., Gong, B., Wang, Y., Dai, E. Z., and Guo, Q. H. (2016). [Effect of electro-acupuncture on the expression of Slit2 and HSPGs in Rats with focal cerebral infarction]. *Sichuan Da Xue Xue Bao Yi Xue Ban* 47, 203–207. doi: 10.13464/j.scuxbyxb.2016.02.013

Lu, K., Li, F., Gong, B., Dai, E. Z., Wang, Y., and Zeng, Z. H. (2013). [Effect of electroacupuncture of "Neiguan" (PC 6) and "Zusanli" (ST 36) on expression of cerebral cortical slit 2/Robo 1 in the focal cerebral infarction rats]. *Zhen Ci Yan Jiu* 38, 265–270.

Lü, Y., Du, Y. H., Xu, Y. L., Cui, J. J., Yang, L. H., Gao, L., et al. (2015). [Effect of electroacupuncture at "Shuigou" (GV 26) on immunoactivity and content of protein kinase c in the middle cerebral artery in acute cerebral infarction rats]. *Zhen Ci Yan Jiu* 40, 219–223. doi: 10.13702/j.1000-0607.2015.03.009

Ma, J., and Luo, Y. (2008). Effects of electroacupuncture on expressions of angiogenesis factors and anti-angiogenesis factors in brain of experimental cerebral ischemic rats after reperfusion. *J. Tradit. Chin. Med.* 28, 217–222. doi: 10.1016/S0254-6272(08)60050-3

Ma, J. X., and Luo, Y. (2007). [Effects of electroacupuncture on expression of angiogenic growth factors and antiangiogenic growth factors in the brain tissue of the rat after focal cerebral ischemia reperfusion]. *Zhongguo Zhen Jiu* 27, 129–133. doi: 10.13703/j.0255-2930.2007.02.021

Ma, R., Yuan, B., Du, J., Wang, L., Ma, L., Liu, S., et al. (2016). Electroacupuncture alleviates nerve injury after cerebra ischemia in rats through inhibiting cell apoptosis and changing the balance of MMP-9/TIMP-1 expression. *Neurosci. Lett.* 633, 158–164. doi: 10.1016/j.neulet.2016.09.033

Michalczyk, K., and Ziman, M. (2005). Nestin structure and predicted function in cellular cytoskeletal organisation. *Histol. Histopathol.* 20, 665–671. doi: 10.14670/HH-20.665

Pan, J., Zhang, W., Yan, J., Chang, X. R., Zhang, H., Chen, W. S., et al. (2012). [Effects of electroacupuncture of acupoints of pericardium meridian on serum

VEGF content and cerebral VEGF expression in cerebral ischemia rats]. *Zhen Ci Yan Jiu* 37, 197–201. doi: 10.13702/j.1000-0607.2012.03.005

Pan, S., Zhan, X., Su, X., Guo, L., Lv, L., and Su, B. (2011). Proteomic analysis of serum proteins in acute ischemic stroke patients treated with acupuncture. *Exp. Biol. Med.* 236, 325–333. doi: 10.1258/ebm.2011.010041

Peng, Y., Wang, H., Sun, J., Chen, L., Xu, M., and Chu, J. (2012). Electroacupuncture reduces injury to the blood-brain barrier following cerebral ischemia/ reperfusion injury. *Neural Regen. Res.* 7, 2901–2906. doi: 10.3969/j.issn.1673-5374.2012.36.007

Ren, L., Fang, Y., Zhang, A., Li, X., Wang, X., Yin, Z., et al. (2010a). Effect of electroacupuncture on the expression of Nav1.1 in rat after acute cerebral ischemia. *Neurol. Res.* 32, 763–769. doi: 10.1179/016164109X12445616596481

Ren, L., Wang, Y. K., Fang, Y. N., Zhang, A. W., and Li, X. L. (2010b). Effect of electroacupuncture therapy on the expression of Na(v)1.1 and Na(v)1.6 in rat after acute cerebral ischemia. *Neurol. Res.* 32, 1110–1116. doi: 10.1179/016164110X12700393823453

Seri, B., Garcia-Verdugo, J. M., McEwen, B. S., and Alvarez-Buylla, A. (2001). Astrocytes give rise to new neurons in the adult mammalian hippocampus. *J. Neurosci.* 21, 7153–7160. doi: 10.1523/JNEUROSCI.21-18-07153.2001

Shi, J. (1999). [A study on the effect and mechanism of acupuncture suppression of neuronal apoptosis following cerebral ischemia]. *Sheng Li Ke Xue Jin Zhan* 30, 326–329.

Shi, P., Sun, L. L., Lee, Y. S., and Tu, Y. (2017). Electroacupuncture regulates the stress-injury-repair chain of events after cerebral ischemia/reperfusion injury. *Neural. Regen. Res.* 12, 925–930. doi: 10.4103/1673-5374.208574

Shin, H. K., Lee, S. W., and Choi, B. T. (2017). Modulation of neurogenesis via neurotrophic factors in acupuncture treatments for neurological diseases. *Biochem. Pharmacol.* 141, 132–142. doi: 10.1016/j.bcp.2017.04.029

Su, M. Z., Yi, W., Huang, K. B., Liu, R., and Xu, N. G. (2012). [Effect of electroacupuncture on expression of signal transducer and activator of transcription 3 in focal ischemic cerebral tissue in cerebral ischemia rats]. *Zhen Ci Yan Jiu* 37, 108–113. doi: 10.13702/j.1000-0607.2012.02.007

Sun, N., Zou, X., Shi, J., Liu, X., Li, L., and Zhao, L. (2005). Electroacupuncture regulates NMDA receptor NR1 subunit expression via PI3-K pathway in a rat model of cerebral ischemia-reperfusion. *Brain Res.* 1064, 98–107. doi: 10.1016/j.brainres.2005.09.060

Talwar, T., and Srivastava, M. V. (2014). Role of vascular endothelial growth factor and other growth factors in post-stroke recovery. *Ann. Indian Acad. Neurol.* 17, 1–6. doi: 10.4103/0972-2327.128519

Tan, F., Chen, J., Liang, Y., Gu, M., Li, Y., Wang, X., et al. (2014a). Electroacupuncture attenuates cervical spinal cord injury following cerebral ischemia/reperfusion in stroke-prone renovascular hypertensive rats. *Exp. Ther. Med.* 7, 1529–1534. doi: 10.3892/etm.2014.1619

Tan, F., Chen, J., Liang, Y. G., Li, Y. P., Wang, X. W., Meng, D., et al. (2014b). [Effect of electric acupuncture on the expression of NgR in the cerebral cortex, the medulla oblongata, and the spinal cord of hypertensive rats after cerebral infarction]. *Zhongguo Zhong Xi Yi Jie He Za Zhi* 34, 334–341. doi: 10.7661/CJIM.2014.03.0334

Tang, L., Ma, C., You, F., and Ding, L. (2015). [Impacts of the low-frequency electric stimulation at the acupoints on the content of plasma 5-HT and NE in the patients with post-stroke insomnia]. *Zhongguo Zhen Jiu* 35, 763–767. doi: 10.13703/j.0255-2930.2015.08.004

Tao, J., Zheng, Y., Liu, W., Yang, S., Huang, J., Xue, X., et al. (2016). Electro-acupuncture at LI11 and ST36 acupoints exerts neuroprotective effects via reactive astrocyte proliferation after ischemia and reperfusion injury in rats. *Brain Res. Bull.* 120, 14–24. doi: 10.1016/j.brainresbull.2015.10.011

Tian, G. H., Tao, S. S., Chen, M. T., Li, Y. S., Li, Y. P., Shang, H. C., et al. (2016). Electroacupuncture treatment alleviates central poststroke pain by inhibiting brain neuronal apoptosis and aberrant astrocyte activation. *Neural Plast.* 2016:1437148. doi: 10.1155/2016/1437148

Tian, X. S., Zhou, F., Yang, R., Xia, Y., Wu, G. C., and Guo, J. C. (2008). [Electroacupuncture protects the brain against acute ischemic injury via up-regulation of delta-opioid receptor in rats]. *Zhong Xi Yi Jie He Xue Bao* 6, 632–638. doi: 10.3736/jcim20080617

Wang, C., Yang, F., Liu, X., Liu, M., Zheng, Y., and Guo, J. (2014). Neurotrophic signaling factors in brain ischemia/reperfusion rats: differential modulation pattern between single-time and multiple electroacupuncture stimulation. *Evid. Based Complement. Alternat. Med.* 2014:625050. doi: 10.1155/2014/625050

Wang, Q., Li, X., Chen, Y., Wang, F., Yang, Q., Chen, S., et al. (2011). Activation of epsilon protein kinase C-mediated anti-apoptosis is involved in rapid tolerance induced by electroacupuncture pretreatment through cannabinoid receptor type 1. *Stroke* 42, 389–396. doi: 10.1161/STROKEAHA.110.597336

Wang, S. J., Omori, N., Li, F., Jin, G., Hamakawa, Y., Sato, K., et al. (2003). Functional improvement by electro-acupuncture after transient middle cerebral artery occlusion in rats. *Neurol. Res.* 25, 516–521. doi: 10.1179/016164103101201751

Wang, S. J., Omori, N., Li, F., Jin, G., Zhang, W. R., Hamakawa, Y., et al. (2002). Potentiation of Akt and suppression of caspase-9 activations by electroacupuncture after transient middle cerebral artery occlusion in rats. *Neurosci. Lett.* 331, 115–118. doi: 10.1016/S0304-3940(02)00866-2

Wang, Y., Shen, Y., Lin, H. P., Li, Z., Chen, Y. Y., and Wang, S. (2016). Large-conductance Ca(2+)-activated K(+) channel involvement in suppression of cerebral ischemia/reperfusion injury after electroacupuncture at Shuigou (GV26) acupoint in rats. *Neural Regen Res* 11, 957–962. doi: 10.4103/1673-5374.184495

Wicha, P., Tocharus, J., Janyou, A., Jittiwat, J., Changtam, C., Suksamrarn, A., et al. (2017). Hexahydrocurcumin protects against cerebral ischemia/reperfusion injury, attenuates inflammation, and improves antioxidant defenses in a rat stroke model. *PLoS ONE* 12:e0189211. doi: 10.1371/journal.pone.0189211

Wu, J., Lin, B., Liu, W., Huang, J., Shang, G., Lin, Y., et al. (2017). Roles of electro-acupuncture in glucose metabolism as assessed by 18F-FDG/PET imaging and AMPKalpha phosphorylation in rats with ischemic stroke. *Int. J. Mol. Med.* 40, 875–882. doi: 10.3892/ijmm.2017.3057

Xie, C., Gao, X., Luo, Y., Pang, Y., and Li, M. (2016). Electroacupuncture modulates stromal cell-derived factor-1alpha expression and mobilization of bone marrow endothelial progenitor cells in focal cerebral ischemia/reperfusion model rats. *Brain Res.* 1648(Pt A), 119–126. doi: 10.1016/j.brainres.2016.07.038

Xie, G., Yang, S., Chen, A., Lan, L., Lin, Z., Gao, Y., et al. (2013). Electroacupuncture at Quchi and Zusanli treats cerebral ischemia-reperfusion injury through activation of ERK signaling. *Exp. Ther. Med.* 5, 1593–1597. doi: 10.3892/etm.2013.1030

Xu, H., Zhang, Y., Sun, H., Chen, S., and Wang, F. (2014). Effects of acupuncture at GV20 and ST36 on the expression of matrix metalloproteinase 2, aquaporin 4, and aquaporin 9 in rats subjected to cerebral ischemia/reperfusion injury. *PLoS ONE* 9:e97488. doi: 10.1371/journal.pone.0097488

Xu, N. G., Yi, W., and Lai, X. S. (2002). [Effect of electro-acupuncture on calcium content in neurocytes of focal cerebral ischemia]. *Zhongguo Zhong Xi Yi Jie He Za Zhi* 22, 295–297. doi: 10.3321/j.issn:1003-5370.2002.04.021

Xu, Y. L., Gao, L., Shi, L., Li, J., Liu, W. H., and Du, Y. H. (2012). [Effect of electroacupuncture intervention on expression of vascular PKC in the ischemic cerebral tissue in rats with cerebral infarction]. *Zhen Ci Yan Jiu* 37, 218–223. doi: 10.13702/j.1000-0607.2012.03.009

Xue, L. W., Li, Q., and Sun, J. Q. (2007). [Clinical observation on penetration needling combined with electroacupuncture for treatment of post-stroke shoulder-hand syndrome]. *Zhongguo Zhen Jiu* 27, 491–493. doi: 10.13703/j.0255-2930.2007.07.007

Xue, X., You, Y., Tao, J., Ye, X., Huang, J., Yang, S., et al. (2014). Electro-acupuncture at points of Zusanli and Quchi exerts anti-apoptotic effect through the modulation of PI3K/Akt signaling pathway. *Neurosci. Lett.* 558, 14–19. doi: 10.1016/j.neulet.2013.10.029

Yang, L. H., Du, Y. H., and Li, J. (2017). [Effect of electroacupuncture on expression of apelin-APJ system of cerebral vascular endothelial cell in rats with cerebral infarction]. *Zhen Ci Yan Jiu* 42, 9–13. doi: 10.13702/j.1000-0607.2017.01.002

Yi, W., Xu, N. G., and Wang, G. B. (2006). [Experimental study on effects of electro-acupuncture in improving synaptic plasticity in focal cerebral ischemia rats]. *Zhongguo Zhong Xi Yi Jie He Za Zhi* 26, 710–714. doi: 10.3321/j.issn:1003-5370.2006.08.009

Yue, Z. H., Li, L., Chang, X. R., Jiang, J. M., Chen, L. L., and Zhu, X. S. (2012). [Comparative study on effects between electroacupuncture and acupuncture for spastic paralysis after stroke]. *Zhongguo Zhen Jiu* 32, 582–586. doi: 10.13703/j.0255-2930.2012.07.004

Zhan, J., Pan, R., Zhou, M., Tan, F., Huang, Z., Dong, J., et al. (2018). Electroacupuncture as an adjunctive therapy for motor dysfunction in acute stroke survivors: a systematic review and meta-analyses. *BMJ Open* 8:e017153. doi: 10.1136/bmjopen-2017-017153

Zhan, J., Qin, W., Zhang, Y., Jiang, J., Ma, H., Li, Q., et al. (2016). Upregulation of neuronal zinc finger protein A20 expression is required for electroacupuncture to attenuate the cerebral inflammatory injury mediated by the nuclear factor-kB signaling pathway in cerebral ischemia/reperfusion rats. *J. Neuroinflamm.* 13:258. doi: 10.1186/s12974-016-0731-3

Zhang, H. X., Liu, L. G., Zhou, L., Huang, H., Li, X., and Yang, M. (2007). [Effect of scalp acupuncture on inflammatory response in rats with acute cerebral ischemia-reperfusion injury]. *Zhong Xi Yi Jie He Xue Bao* 5, 686–691. doi: 10.3736/jcim20070617

Zhang, H. X., Wang, Q., Zhou, L., Liu, L. G., Yang, X., Yang, M., et al. (2009). [Effects of scalp acupuncture on acute cerebral ischemia-reperfusion injury in rats]. *Zhong Xi Yi Jie He Xue Bao* 7, 769–774. doi: 10.3736/jcim20090812

Zhang, J., Lin, X., Zhou, H., Chen, Y., Xiao, S., Jiao, J., et al. (2018). Electroacupuncture: a new approach to open the blood-brain barrier in rats recovering from middle cerebral artery occlusion. *Acupunct. Med.*. doi: 10.1136/acupmed-2017-011496

Zhang, S., Li, G., Xu, X., Chang, M., Zhang, C., and Sun, F. (2011). Acupuncture to point Baihui prevents ischemia-induced functional impairment of cortical GABAergic neurons. *J. Neurol. Sci.* 307, 139–143. doi: 10.1016/j.jns.2011.04.021

Zhang, Y., Lin, R., Tao, J., Wu, Y., Chen, B., Yu, K., et al. (2016). Electroacupuncture improves cognitive ability following cerebral ischemia reperfusion injury via CaM-CaMKIV-CREB signaling in the rat hippocampus. *Exp. Ther. Med.* 12, 777–782. doi: 10.3892/etm.2016.3428

Zhang, Y. M., Xu, H., Sun, H., Chen, S. H., and Wang, F. M. (2014). Electroacupuncture treatment improves neurological function associated with regulation of tight junction proteins in rats with cerebral ischemia reperfusion injury. *Evid. Based Compl. Alternat. Med.* 2014:989340. doi: 10.1155/2014/989340

Zhao, J., Sui, M., Lu, X., Jin, D., Zhuang, Z., and Yan, T. (2015). Electroacupuncture promotes neural stem cell proliferation and neurogenesis in the dentate gyrus of rats following stroke via upregulation of Notch1 expression. *Mol. Med. Rep.* 12, 6911–6917. doi: 10.3892/mmr.2015.4279

Zhao, L., Shi, J., Sun, N., Tian, S., Meng, X., Liu, X., et al. (2005). Effect of electroacupuncture on TRPM7 mRNA expression after cerebral ischemia/reperfusion in rats via TrkA pathway. *J. Huazhong Univ. Sci. Technol. Med. Sci.* 25, 247–250. doi: 10.1007/BF02828132

Zhao, P., and Cheng, J. (1997). Effects of electroacupuncture on extracellular contents of amino acid neurotransmitters in rat striatum following transient focal cerebral ischemia. *Acupunct. Electrother. Res.* 22, 119–126. doi: 10.3727/036012997816356743

Zhao, Y., Chen, S., Yu, W., Cai, S., Zhang, L., Wang, X., et al. (2010). [The effect of electro-acupuncture on endogenous EPCs and serum cytokines in cerebral ischemia-reperfusion rat]. *Sheng Wu Yi Xue Gong Cheng Xue Za Zhi* 27, 1322–1326. doi: 10.1016/S1876-3804(11)60004-9

Zheng, H. Z., Jiang, W., Zhao, X. F., Du, J., Liu, P. G., Chang, L. D., et al. (2016). Electroacupuncture induces acute changes in cerebral cortical miRNA profile, improves cerebral blood flow and alleviates neurological deficits in a rat model of stroke. *Neural Regen Res* 11, 1940–1950. doi: 10.4103/1673-5374.197135

Zhou, H., Yang, C., Bai, F., Ma, Z., Wang, J., Wang, F., et al. (2017). Electroacupuncture alleviates brain damage through targeting of neuronal calcium sensor 1 by miR-191a-5p after ischemic stroke. *Rejuvenation Res.* 20, 492–505. doi: 10.1089/rej.2017.1920

Zhou, Y. C., Wu, X. G., and Xiao, Y. C. (2011). [Effects of electroacupuncture at "Zusanli" (ST 36) and "Neiguan" (PC 6) on expression of GAP-43 in cerebral infarction rats]. *Zhongguo Zhen Jiu* 31, 55–59. doi: 10.13703/j.0255-2930.2011.01.016

Zou, R., Wu, Z., and Cui, S. (2015). Electroacupuncture pretreatment attenuates bloodbrain barrier disruption following cerebral ischemia/reperfusion. *Mol. Med. Rep.* 12, 2027–2034. doi: 10.3892/mmr.2015.3672

Conflict of Interest Statement: The authors declare that the research was conducted in the absence of any commercial or financial relationships that could be construed as a potential conflict of interest.

frontiers in Neuroscience

ORIGINAL RESEARCH
published: 19 February 2019
doi: 10.3389/fnins.2019.00119

Bladder Neuromodulation in Acute Spinal Cord Injury via Transcutaneous Tibial Nerve Stimulation: Cystometrogram and Autonomic Nervous System Evidence From a Randomized Control Pilot Trial

Argyrios Stampas[1], Kenneth Gustafson[2], Radha Korupolu[1], Christopher Smith[3], Liang Zhu[4] and Sheng Li[1]*

[1] Department of Physical Medicine and Rehabilitation, University of Texas Health Science Center at Houston, Houston, TX, United States, [2] Department of Bioengineering, Case Western Reserve University, Cleveland, OH, United States, [3] Department of Urology, Baylor College of Medicine, Houston, TX, United States, [4] Biostatistics and Epidemiology Research Design Core, University of Texas Health Science Center at Houston, Houston, TX, United States

OPEN ACCESS

Edited by:
Gottfried Schlaug,
Beth Israel Deaconess Medical Center, Harvard Medical School, United States

Reviewed by:
Thelma Anderson Lovick,
University of Bristol, United Kingdom
Oluwole Awosika,
University of Cincinnati, United States

***Correspondence:**
Argyrios Stampas
argyrios.stampas@uth.tmc.edu

Specialty section:
This article was submitted to Neural Technology, a section of the journal Frontiers in Neuroscience

Received: 16 July 2018
Accepted: 01 February 2019
Published: 19 February 2019

Citation:
Stampas A, Gustafson K, Korupolu R, Smith C, Zhu L and Li S (2019) Bladder Neuromodulation in Acute Spinal Cord Injury via Transcutaneous Tibial Nerve Stimulation: Cystometrogram and Autonomic Nervous System Evidence From a Randomized Control Pilot Trial. Front. Neurosci. 13:119. doi: 10.3389/fnins.2019.00119

Aim: Percutaneous tibial nerve stimulation is used to decrease incontinence in chronic neurogenic bladder. We report the findings from a subset of patients in a randomized control trial of transcutaneous tibial nerve stimulation (TTNS) for bladder neuromodulation in acute spinal cord injury (SCI) in whom heart rate variability (HRV) was recorded before and after cystometrogram (CMG). The aim was to correlate autonomic nervous system (ANS) changes associated with the CMG changes after the trial using HRV analyses.

Methods: The study was a double-blinded sham-controlled 2-week trial with consecutive acute SCI patients admitted for inpatient rehabilitation, randomized to TTNS vs. control sham stimulation. Pre- and Post- trial CMG were performed with concurrent 5-min HRV recordings with empty bladder and during filling. Primary outcomes were changes with CMG between/within groups and associations to the HRV findings.

Results: There were 10 subjects in the TTNS group and 6 in the control group. Pre-trial baseline subject characteristics, blood pressures (BPs), and CMG were similar between groups. In both groups, the pre-trial systolic BP increased during filling CMG. After the trial, the control group had significantly increased detrusor pressure and counts of detrusor-sphincter dyssynergia on CMG, not seen in the TTNS group. Also, the control group did not maintain rising BP post-trial, which was observed pre-trial and remained in the TTNS group post-trial. HRV was able to detect a difference in the ANS response to bladder filling between groups. Post-trial HRV was significant for markers of overall increased parasympathetic nervous system activity during filling in the controls, not seen in the TTNS group.

Conclusion: Preliminary evidence suggests that TTNS in acute SCI is able to achieve bladder neuromodulation via modulation of ANS functions.

Clinical Trial Registration: clinicaltrials.gov, NCT02573402.

Keywords: spinal cord injuries, heart rate variability, neuromodulation, autonomic nervous system, neurogenic urinary bladder, transcutaneous electric stimulation

INTRODUCTION

Neurogenic bladder develops over time after a period of spinal shock following acute spinal cord injury (SCI), leading to detrusor hyperreflexia (DH), detrusor sphincter dyssynergia (DSD), decreased bladder compliance and capacity, and increasing detrusor pressures. It is estimated that DH and/or DSD occurs in 95% of suprasacral SCI with up to 50% developing serious urologic complications (Weld and Dmochowski, 2000; Bacsu et al., 2012). The status quo for the management of neurogenic bladder in acute SCI is limited to maintaining safe pressures and volumes through a combination of timed voiding, catheterization, and anticholinergic bladder medications. Although significant reductions in morbidity and mortality have been achieved, little is done to mitigate the development of DH and DSD (Whiteneck et al., 1992). However, neuromodulation of the acute neurogenic bladder has the potential to alter the natural course of neurogenic bladder in SCI.

For example, when invasive sacral neuromodulation was performed in acute SCI, the group receiving the implanted device, under continuous operational condition, maintained normal bladder capacity, reported improved quality of life scores, and the detrusor did not develop hyperactivity (Sievert et al., 2010). The control group experienced the typical sequelae of SCI neurogenic bladder over time, including decreased bladder capacity and frequent UTIs complicated by sepsis and hospitalizations. Using similar proposed neural pathways, the afferent input from tibial nerve stimulation (TNS) improves bladder outcomes through neuromodulation of the spinal reflexes which may also prevent development of the pathologic reflexes suspected to cause DH/DSD (Gupta et al., 2015).

We hypothesized that neuromodulation of the bladder in acute SCI can be achieved with transcutaneous TNS as measured by cystometrogram and performed a double-blinded, randomized sham-controlled pilot trial of 19 subjects (Stampas et al., 2018). We reported the findings of safety and feasibility of 30-min sessions of TTNS in acute SCI as well as evidence of efficacy based on CMG findings of reduced bladder capacity and increased counts of DSD in controls compared to the TTNS group (Stampas et al., 2018). The CMG can provide information about the lower urinary tract physiology, which is only half of the story regarding the importance of an SCI neurogenic bladder treatment. The autonomic response to bladder stimulation and filling is an equally important component of this pathology that has remained elusive.

The most common precipitating stimulus of autonomic dysreflexia (AD), the only SCI cardiovascular condition to directly cause death characterized by sudden episodic increases in blood pressure (BP) in response to noxious simulation below the level of injury (Karlsson, 1999; Dolinak and Balraj, 2007) originates from the bladder (Lindan et al., 1980). In those with SCI levels of thoracic level 6 (T6) and above, AD is thought to occur in approximately 50–90% of people (Snow et al., 1978; Lindan et al., 1980; Curt et al., 1997; Sharif and Hou, 2017). Therefore, another goal of improving neurogenic bladder in SCI is to improve the response of the ANS to bladder stimuli and subsequently reduce or eliminate AD. A leading theory behind the development of AD is that the sympathetic preganglionic neurons below the level of injury undergo maladaptive neuroplasticity which leads to the reflexive release of massive amounts of norepinephrine resulting in AD (Sharif and Hou, 2017). Furthermore, pelvic afferent fibers are upregulated following SCI, of which the unmyelinated C-fibers play an essential role in eliciting AD (Hou et al., 2008). Therefore, it is imperative to understand whether neuromodulation of the bladder can impact the development of AD. To this end, heart rate variability (HRV) and BP measurements can be used to measure the ANS responses during bladder filling as well as the changes in the ANS as it relates to the developing neurogenic bladder.

Heart rate variability measurements, reflecting the ANS balance between the sympathetic (SNS) and parasympathetic nervous system (PNS), have the potential to be used as a clinical tool, requiring a non-invasive electrocardiogram (ECG) measurement using established guidelines for their recording and interpretation, producing frequency- and time-domain variables (Task Force of the European Society of Cardiology the North American Society of Pacing Electrophysiology, 1996). HRV has been found to be a reliable and reproducible measurement in SCI (Ditor et al., 2005). Recently, HRV measurements have been performed concurrently with CMG testing in chronic SCI and controls, with findings of significant differences between groups (Huang et al., 2016). The ability to detect differences in the ANS via HRV while filling the bladder during CMG may improve the understanding of the autonomic component of neurogenic bladder and the changes as it develops.

Many of the HRV analyses in SCI have focused on the frequency-domain findings, likely owing to the validation study in SCI (Ditor et al., 2005). According to the Task Force of the European Society of Cardiology and the North American Society of Pacing and Electrophysiology, the High-frequency (HF) spectral component represents cardiac parasympathetic control (Task Force of the European Society of Cardiology the North American Society of Pacing Electrophysiology, 1996). The Low-frequency (LF) spectral component has been generally accepted to represent baroreflex-mediated (sympathetic-driven) vagal outflow. The LF to HF ratio has been used to describe the cardiac sympathovagal balance. Total power in HRV reflects the range of overall variation of the sympathetic and parasympathetic nervous system. Largely under-reported in the SCI literature, the time-domain variables reflect the parasympathetic activity (NN50, pNN50, RMSSD). However, the standard deviation of all normal-to-normal intervals (SDNN) reflects the sympathetic and parasympathetic activity influencing HRV.

The aim of this exploratory study was to correlate CMG and ANS changes, specifically BPs and HRV, before and after TTNS during filling CMG in a subset of patients from the pilot randomized sham-control trial of TTNS in acute SCI (Stampas et al., 2018) who had concurrent ANS measurements. We hypothesized that TTNS could neuromodulate the bladder function and alter the response of the ANS during bladder filling with routine use. Specifically, we hypothesized that (1) TTNS would prevent the harmful CMG changes that would be found in the control group and (2) that ANS response to bladder filling would differ between groups based on HRV and BP recordings.

TABLE 1 | Baseline demographics.

	Control (n = 6)	TTNS (n = 10)	p-value
	Mean (SD)		
Age (years)	51.8 (9.6)	38.1 (14.2)	0.06
Duration of injury (days)	19.5 (6.7)	22.7 (9.1)	0.45
Admission FIM motor	15.5 (5.5)	17.5 (5.3)	0.45
Admission FIM bladder	1 (0)	1 (0)	
Admission FIM cognition	30.3 (4.3)	27.3 (6.1)	0.41
	Frequency (%)		
Male	1 (17%)	7 (70%)	0.12
Tetraplegia	4 (67%)	4 (40%)	0.61
Neurologic level			0.47
C1-4	3 (50%)	4 (40%)	
C5-8	1 (17%)	0	
T1-T4	1 (17%)	5 (40%)	
T5-T9	1 (17%)	1 (10%)	
AIS severity			0.46
A	3 (50%)	8 (70%)	
B	0	1 (10%)	
C	2 (33%)	1 (10%)	
D	1 (17%)	0	

TTNS, transcutaneous tibial nerve stimulation group; FIM, functional independence measure; AIS, American Spinal Injury Association (ASIA) Impairment Scale; AIS A, complete injury; AIS B, motor complete, sensory incomplete injury; AIS C, motor incomplete injury with less than half of the muscles below the level of injury with antigravity strength; AIS D, motor incomplete with at least half the muscles below the level of injury with antigravity strength.

MATERIALS AND METHODS

Patients with acute SCI were recruited for this study from July 2016 to October 2017 during admission to inpatient rehabilitation. Patients were screened using the electronic medical record (EMR) and then approached to complete verification of the inclusion/exclusion criteria and consent. Inclusion criteria were: (1) acute traumatic SCI; (2) 18–65 years old; (3) within 6 weeks of injury; (4) neurologic level of injury T9 and rostral, to avoid damage to the lower motor neurons (LMNs) of the bladder. Exclusion criteria were: (1) prior central nervous system disorder; (2) peripheral neuropathy; (3) premorbid genitourinary diagnoses; (4) known LMN injury to the bladder or its potential due to multitrauma; (5) ventilator assistance for respiration due to the challenges in performing the cystometrogram in these subjects. See **Table 1** for subject details.

Study Design

Upon consent, baseline CMG was performed and subjects were randomized into TTNS and control groups in a 2:1 ratio, stratified by areflexic bladder to ensure a balanced distribution between the two groups (**Figure 1**). After this pre-trial CMG, TTNS versus control stimulation was performed and upon completion, post-trial CMG was performed within 3 days after the final intervention. Following the CONSORT 2010 guidelines, randomization and experiments were performed by the research assistant, while the principle investigator and subjects were blinded to treatment allocation. Further details can be found in the complete pilot trial publication (Stampas et al., 2018). This study was approved by the Institutional Review Board and is registered with clinicicaltrials.gov: NCT02573402.

The Interventions

Those in the TTNS group received 30 min of TTNS per day for 10 days within a 16-day period. TTNS was applied to the right leg with the negative electrode behind the internal malleolus and the positive electrode 10 cm. superior to the negative electrode, verified by big toe flexion with rising current intensity (Amarenco et al., 2003). Stimulation frequency of 10 Hz and 200 μs duration was used with current intensity increased until toe flexion, then lowered (sub-motor) for 30 min at constant stimulation (Amarenco et al., 2003; Finazzi Agrò et al., 2005). Those in the control group received sham stimulation in which the electrodes were placed and the stimulator was activated until toe flexion, but then immediately reduced to zero intensity. The display on the device was covered in both arms to prevent subjects from reading the current intensity.

The Assessment

The urodynamic methodology complied with International Continence Society recommendations (Schafer et al., 2002). Subjects were brought to the urology procedure suite, transferred to the examination table, and catheterized to empty the bladder. Disposable adhesive electrodes were attached to each

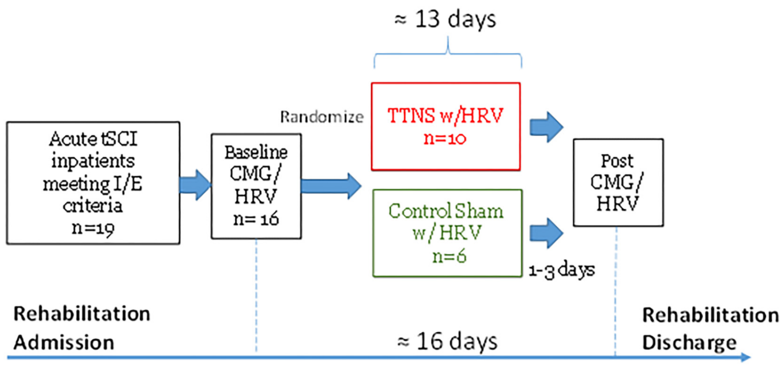

FIGURE 1 | Study Timeline. tSCI, traumatic spinal cord injury; I/E, inclusion/exclusion criteria; CMG, cystometrogram; HRV, heart rate variability; TTNS, transcutaneous tibial nerve stimulation.

electrocardiogram (ECG) lead and the white "right arm" and black "left arm" electrode leads were placed along the 1st intercostal spaces in the subclavicular area on the right and left chest wall, respectively. Subjects were asked to remain motionless without speaking as the 5-min ECG recordings were collected using the HRV heart rhythm scanner (Biocom 5000 Wireless ECG Recorder, Biocom Technologies, Poulsbo, WA, United States). After the CMG catheter was inserted and waiting 5 min with emptied bladder, ECG recordings started with Empty bladder recordings. At the initiation of bladder filling, Filling 1 recordings began for 5 min, followed by Filling 2 recordings for 5 min. ECG signals were saved for off-line HRV analyses.

Cystometry was performed with the patient supine through a double lumen 7 Fr. catheter with computerized analysis of the results using normal saline at 25 to 30°C with a filling rate of 40 ml per minute, terminating at 600 ml of bladder capacity or sooner as clinically indicated. Clinical indications for early termination of the CMG includes overflow leaking and AD. Filling 1 was 0–200 cc followed by Filling 2 with approximately 200–450 cc of infused saline, based on the volumes infused during the 5-min HRV recordings. Filling phases were used because the 5-min HRV recording could not record the entire CMG. The same procedures were followed for both pre- and post- TTNS trial measurements, with bladder empty and bladder filling, at a similar time of day. Blood pressures were measured with Welch Allyn® Vital Signs Monitor 300 before and during filling, every 5 min or sooner as clinically indicated. A rise of systolic BP greater than or equal to 20 mmHg was defined as AD (Curt et al., 1997). The Numerical Pain Scale (NPS) was recorded for each patient at the time of CMG as a possible HRV confounding variable (Karri et al., 2017).

Data Analyses

From the larger pilot trial (Stampas et al., 2018) the primary outcomes were safety and feasibility measures and the secondary outcomes were the within- and between-group CMG changes after TTNS. Measurements included: maximum detrusor pressure (cmH_2O); bladder capacity [maximum volume infused (ml)]; frequency of DSD and DH (count); volume at first involuntary detrusor contraction (ml); and subjective measures of first sensation and desire to void [based on infused volume of saline (ml)]. DH was defined as a non-volitional increase in detrusor pressure of at least 6 cm H_2O (Kaplan et al., 1991). DSD is defined as the presence of involuntary contractions of the external sphincter during detrusor contractions (Blaivas et al., 1981). Factors that may affect the bladder including medication use in the 24 h prior to the CMG and presence of an indwelling catheter were recorded and used in the analyses.

For this study cohort with ANS measures from the larger pilot trial, the primary outcome measures were the ANS differences with bladder filling within and between groups based on HRV and BP changes. Kubios HRV analysis software (University of Eastern Finland, Joensuu, Finland) was used offline to analyze the ECG recordings via time and frequency domains. Time-domain parameters included Mean R–R interval (RR is the interval between successive Rs on the QRS complex of the ECG wave), Mean HR (heart rate), STDHR (standard deviation of HR), SDNN (standard deviation of normal to normal R–R intervals), RMSSD (root mean squared of successive differences), NN50 (pairs of successive R–R beat lengths that differ by more than 50 ms), and pNN50 (the proportion of NN50 for total number of beats). Frequency domain measurements included low-frequency (LF), high-frequency (HF), the ratio LF/HF, and total power (the sum of power of all frequency bands, reflecting the range of variation of the overall autonomic regulation).

Statistical Methodology

Descriptive statistics were provided for baseline demographics for the control and TTNS groups, with comparisons using Wilcoxon Rank Sum and Fischer's exact test for continuous and categorical data, respectively (**Table 1**). We compared the CMG outcomes before and after the trial within and between the two groups (**Figure 2** and **Table 2**). For between group comparison, Wilcoxon rank sum and Fisher's exact tests were performed on continuous and categorical variables, respectively. For within group comparison before and after the trial, multilevel mixed-effects linear regression was performed controlling for subject and duration of injury variability for continuous variables, and

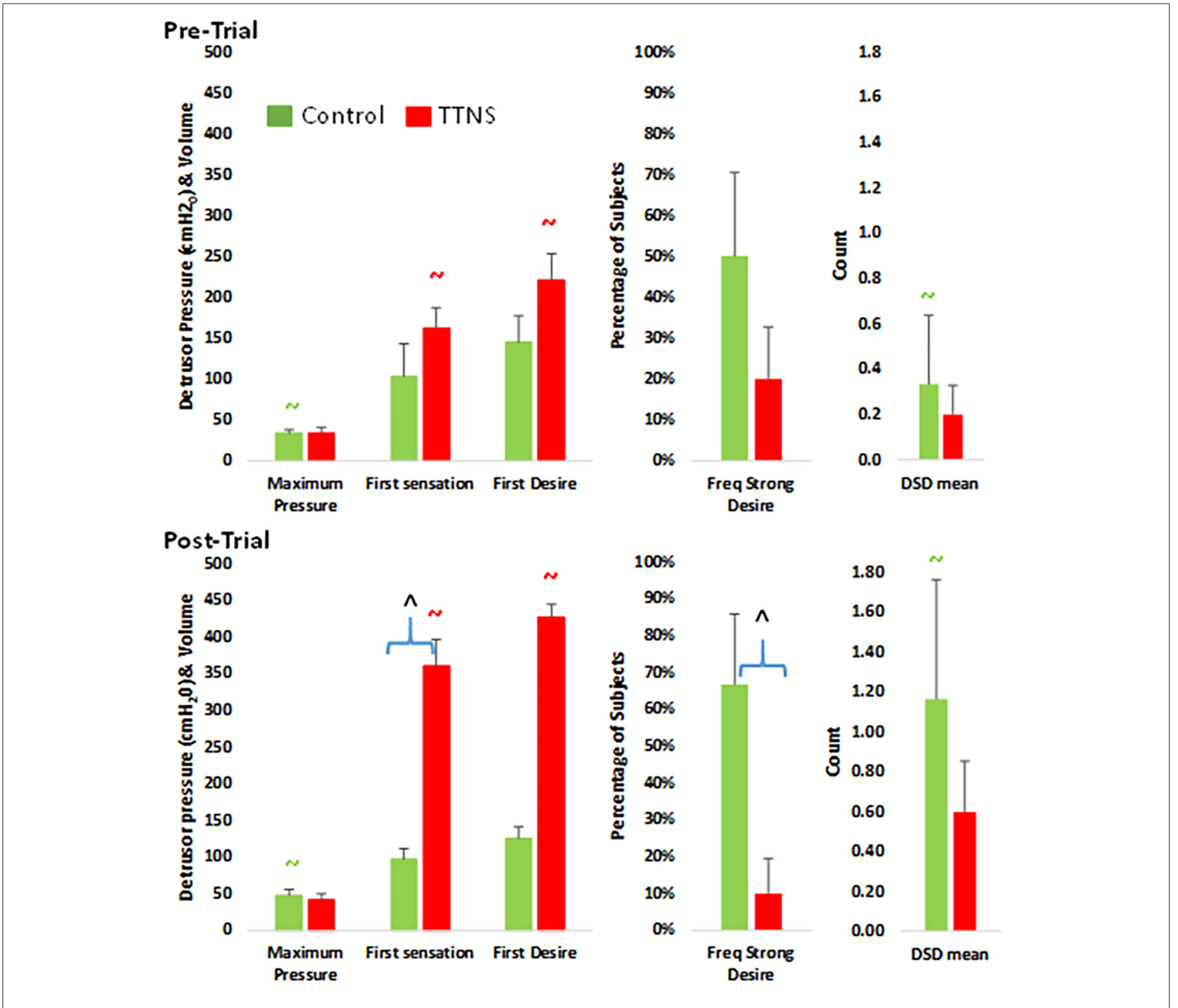

FIGURE 2 | Bar graphs of significant differences between control (green) and TTNS (red) groups, pre- **(top)** and post-trial **(bottom)**. DSD, detrusor-sphincter dyssynergia. All symbols are significant $p < 0.05$ and color-coded: ^between group difference; ~ pre- vs. post-difference.

multilevel mixed-effects logistic regression was performed for categorical variables. Using similar statistical methods used in the CMG analyses, measures of the ANS at the time of CMG after the bladder was emptied (Empty Bladder) were performed between groups and within groups pre-/post-trial (**Table 3**). Between group ANS difference during Filling 1 (first 5 min of CMG filling to approximately 200 cc) and Filling 2 (next 5 min of CMG filling to approximately 450 cc) were performed using Wilcoxon rank sum test (**Table 4**). Multilevel mixed-effects linear regression was used to compare ANS differences within the groups pre- and post-trial, as well as the ANS changes from empty to Filling 1 to Filling 2 pre- and post-trial (**Figures 3**, **4**). Finally, CMG variables that changed significantly were added as the dependent variables in multilevel mixed-effects linear modeling with the ANS variables as the independent variables. HRV variables that had significant pre-trial differences between groups were excluded. As an exploratory study, no adjustments were made for multiple comparisons, with plans to confirm all results with a larger scale study. Stata 14.0 (StataCorp., 2015) was used for the analyses, with $p < 0.05$ set for significance.

RESULTS

Pre-trial

There were six control and 10 TTNS subjects that had HRV analyses performed from within the TTNS trial. Due to technical difficulties, we were unable to perform HRV on

TABLE 2 | Cystometrogram data.

	Pre-trial			Post-trial			Pre vs. post	
	Control (*n* = 6)	TTNS (*n* = 10)		Control (*n* = 6)	TTNS (*n* = 10)		Control (*n* = 6)	TTNS (*n* = 9)
Variables	**Mean (SD)**		***p*-value**	**Mean (SD)**		***p*-value**	***p*-value**	
Maximum detrusor pressure (cmH_2O)	33 (12)	34 (21)	0.91	48 (21)	42 (27)	0.55	**0.04**	0.11
Bladder capacity (ml)	566 (88)	589 (31)	0.79	465 (171)	548 (115)	0.23	0.06	0.1
Freq. detrusor Hyperactivity	3.5 (3.8)	1 (1.5)	0.16	1.2 (1.6)	1.1 (1.4)	0.95	0.17	0.47
Freq. of detrusor-sphincter dyssynergia	0.33 (0.82)	0.2 (0.42)	1	1.2 (1.6)	0.6 (0.8)	0.55	**0.01**	0.23
	***N* (%)**			***N* (%)**				
Presence of:								
Involuntary contraction	4 (67%)	5 (50%)	0.63	4 (67%)	6 (60%)	1	0.92	0.63
First sensation	4 (67%)	4 (40%)	0.61	4 (67%)	4 (40%)	0.61	0.34	0.28
First desire	4 (67%)	3 (30%)	0.3	4 (67%)	2 (20%)	0.12	0.4	0.07
Strong desire	3 (50%)	2 (20%)	0.3	4 (67%)	1 (10%)	**0.04**	0.77	0.09
Detrusor areflexia	2 (33%)	5 (50%)	0.63	2	4	1	0.92	0.63
Spinal shock	1 (17%)	2 (30%)	1	0	1	1	0.32	0.32
Autonomic dysreflexia	0	3 (30%)	0.25	0	1 (11%)	1	NA	0.3
Indwelling catheter	2 (33%)	4 (40%)	1	3	4	1	0.42	0.15
Bladder medication	0	0		0	0		-	-
Spasm medication	4 (67%)	2 (20%)	0.12	3	3	0.61	0.96	0.97
Subgroup analysis of those with sensation/contraction Mean volumes in ml (SD)								
First involuntary contraction	226 (168)	304 (81)	0.46	258 (258)	258 (105)	0.52	0.06	0.96
First sensation	103 (116)	162 (89)	0.39	97 (41)	361 (131)	**0.02**	0.96	**0.01**
First desire	145 (91)	221 (127)	0.29	126 (43)	427 (78)	0.06	0.6	**0.03**
Strong desire	262 (262)	341 (28)	0.56	285 (179)	482	0.48	0.265	**-**

SD, standard deviation; Freq., frequency; TTNS, transcutaneous tibial nerve stimulation; cmH_2O, centimeters pressure of water; ml, milliliters; DH, detrusor hyperreflexia; DSD, detrusor-sphincter dyssynergia; AD, autonomic dysreflexia. Significant difference of bold values p < 0.05.

TABLE 3 | Autonomic nervous system data, empty bladder significant differences.

	Pre-trial			Post-trial			Pre vs. post	
	Control (*n* = 6)	TTNS (*n* = 10)		Control (*n* = 6)	TTNS (*n* = 9)		Control (*n* = 6)	TTNS (*n* = 9)
Variables	**Mean (SD)**		***p*-value**	**Mean (SD)**		***p*-value**	***p*-value**	
Systolic BP	111 (8)	110 (17)	0.95	123 (14)	116 (15)	0.44	**0.04**	0.28
SDNN (ms)	23 (16)	45 (20)	**0.02**	38 (32)	38 (22)	0.81	**0.02**	**0.04**
Total power (ms^2)	456 (509)	2300 (2366)	**0.02**	1838 (2495)	1524 (1579)	0.81	**0.03**	**0.03**

ms, milliseconds, bpm, beats per minute; BP, blood pressure; SDNN, standard deviation of normal to normal R–R intervals. Significant difference of bold values p < 0.05.

one subject in the TTNS group post-trial. There were no baseline demographic differences between groups in terms of age, duration of injury, sex, functional independence measure (FIM) scores on admission, levels of injury, and SCI severity (**Table 1**).

There were also no Pre-Trial differences on CMG between groups regarding maximum detrusor pressure, bladder capacity, frequency of DH and DSD, the occurrence of AD and filling sensations, and the volume of saline infused at the time of these sensations (**Figure 2** and **Table 2**).

Although there were no group differences in BPs during Pre-Trial measurements with Empty Bladder (**Figure 3** and **Table 3**), there was increased overall ANS activity in the TTNS group compared to the control group as reflected by SDNN and total power ($p = 0.02$ for both) (**Table 3**). This was also observed during filling CMG at Filling 1, with increased SDNN ($p = 0.02$) and total power ($p = 0.02$) in the TTNS group compared to controls (**Table 4**). The TTNS group also had increased RMSSD ($p = 0.04$) reflecting parasympathetic activity during Filling 1 compared to the controls (**Table 4**).

Both groups increased SBP during bladder filling on Pre-Trial CMG (**Figure 3A**). In the control group during Pre-trial CMG from Filling 1 to Filling 2, there was increased parasympathetic activity (increased mean RR, decreased mean HR, $p = 0.006$ for both; increased STDHR, $p = 0.008$) and increased overall ANS activity (SDNN, $p = 0.005$) (**Table 4**). STDHR also significantly

TABLE 4 | Autonomic nervous system, filling cystometrogram data comparisons, significant differences.

	Pre-trial						Post-trial						Pre vs. post			
	Control (n = 6)		TTNS (n = 10)		Between group difference		Control (n = 6)		TTNS (n = 9)		Between group difference		Control (n = 6)		TTNS (n = 9)	
	Mean/SD				*p*-value		Mean/SD				*p*-value		*p*-value			
	F1	F2	F1	F2	F1	F2	F1	F2	F1	F2	F1	F2	F1	F2	F1	F2
DBP (mmHg)	68/8	68/7	7/9	74/12	0.7	0.6	76/10	77/11	72/13	80/16	0.3	0.8	0.2*	**0.03**	0.5	0.2
SDNN (ms)	20/11	30/16	43/21	49/31	**0.02**	0.2	32/16	29/20	37/17	40/21	0.8	0.3	**<0.001**	0.8	0.5	0.4
STDHR (bpm)	2/2	3/2	3/1	3/2	0.07	0.3	3/1	3/2	3/2	3/2	0.4	0.5	**<0.001**	0.3	0.8	0.3
RMSSD (ms)	11/5	15/7	31/29	36/35	**0.04**	0.1	31/28	30/31	29/19	27/16	0.8	0.8	**0.02**	0.1	0.8	0.4
NN50 (count)	1/2	4/6	28/57	31/55	0.1	0.1	20/25	25/42	20/26	21/33	1	1	**0.02**	0.1	0.5	0.4
pNN50 (%)	0.3/0.5	1/2	13/21	15/21	0.1	0.1	8/10	10/14	13/16	10/12	0.8	1	**0.01**	0.05	1	0.4
LF (ms^2)	0.05/0.006	0.1/0.004	0.05/0.01	0.06/0.02	0.2	0.4	0.04/0.003	0.07/0.04	0.05/0.01	0.06/0.03	0.7	0.9	**0.01**	0.2	0.3	0.8
Total power (ms^2)	476/580	712/512	1582/1268	2222/3308	**0.02**	0.2	853/672	599/644	1508/1298	1824/1888	0.5	0.2	**0.04**	0.6	1	0.7

*F1, filling period 1; F2, filling period 2; ms, milliseconds; bpm, beats per minute; SDNN, standard deviation of normal to normal R–R intervals; STDHR, standard deviation of heart rate; RMSSD, root mean squared of successive differences; NN50, pairs of successive R–R beat lengths that differ by more than 50 ms; pNN50, the proportion of NN50 for total number of beats; LF, low frequency; *Wilcoxon rank-sum test used. Significant difference of bold values p < 0.05.*

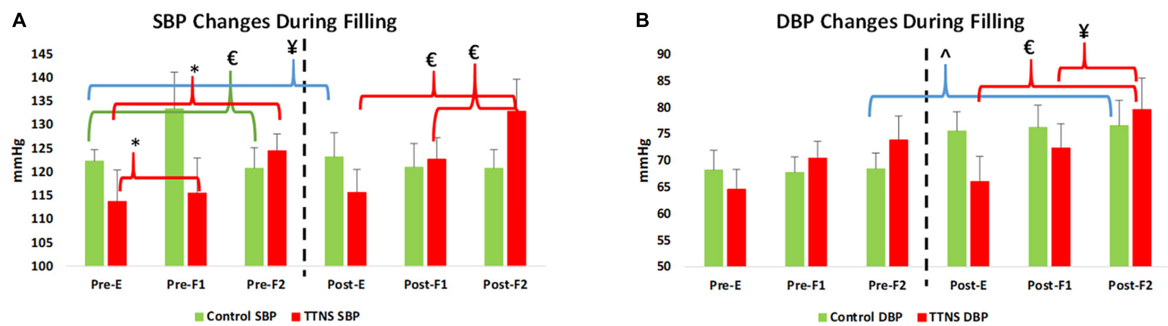

FIGURE 3 | Significant blood pressure (BP) changes during bladder filling, pre- and post-trial. Dashed line represents transition to post-trial testing, red brackets and green brackets are within group differences in the TTNS and controls, respectively. Blue brackets are pre- post-trial differences. **(A)** In both groups, SBP increases with filling pre-test. Post-test, this is only seen in the TTNS group. **(B)** Diastolic BP is significantly different in the controls post-trail compared to pre-trial. Pre, pre-trial; Post, post-trial; E, empty bladder; F1, filling phase 1; F2, filling phase 2; TTNS, transcutaneous tibial nerve stimulation; SBP, systolic blood pressure; DBP, diastolic blood pressure; ¥p = 0.04; *p = 0.01; £p < 0.01; ˆp = 0.03.

increased from Empty Bladder to Filling 2, $p = 0.035$ (**Figure 4A**). In the TTNS group, mean RR decreased from Filling 1 to Filling 2 and from Empty Bladder to Filling 2, p = 0.024, 0.006, respectively. Sympathetic tone decreased in the TTNS group as reflected by LF from Empty Bladder to Filling 1 (p = 0.004) and increased from Filling 1 to Filling 2 (p = 0.04, **Figure 4C**), and parasympathetic tone decreased (HF, p = 0.045) from Empty Bladder to Filling 2.

Post-trial

After the trial, the control group significantly increased maximum detrusor pressure (mean, SD), from 33 ± 12 to 48 ± 21 cmH_2O (p = 0.04), and increased DSD events from 0.33 ± 0.82 to 1.2 ± 1.6 (p = 0.01) (**Figure 2** and **Table 2**). There were also more in the control group (n = 4) with strong desire to void compared to the TTNS group (n = 1, p = 0.04). Comparing pre- and post-trial, there were no significant changes in the presence of involuntary bladder contractions and filling sensations in both groups. However, in those with filling sensation, the first sensation of filling was higher in the TTNS group (361 ± 131 ml) compared to the control group (97 ± 41 ml, p = 0.02). Furthermore, the TTNS group significantly increased the volumes needed for first sensation, from 162 ± 89 to 361 ± 131 ml (p = 0.01), as well as first desire to void, from 221 ± 127 ml to 427 ± 78 ml (p = 0.03).

After the trial, there were several ANS differences. In the control group, there was a significant rise in the resting SBP with empty bladder, from 111 ± 8 to 123 ± 14 mmHg (p = 0.04, **Figure 3A** and **Table 3**). The control group also significantly increased DBP during Filling 2, from 68 ± 7 to 77 ± 11 mmHg (p = 0.03, **Figure 3A** and **Table 4**). Overall ANS variability increased in the control group before and after the trial as reflected by the changes in SDNN and total power, p = 0.02 and 0.03, respectively. The control group was observed to have an overall increase in ANS activity (SDNN, total power) and PNS activity (STDHR, RMSSD, NN50, pNN50, **Figure 4B**) and a decrease in sympathetic tone (LF, **Figure 4C**) during Filling 1 (**Table 4**).

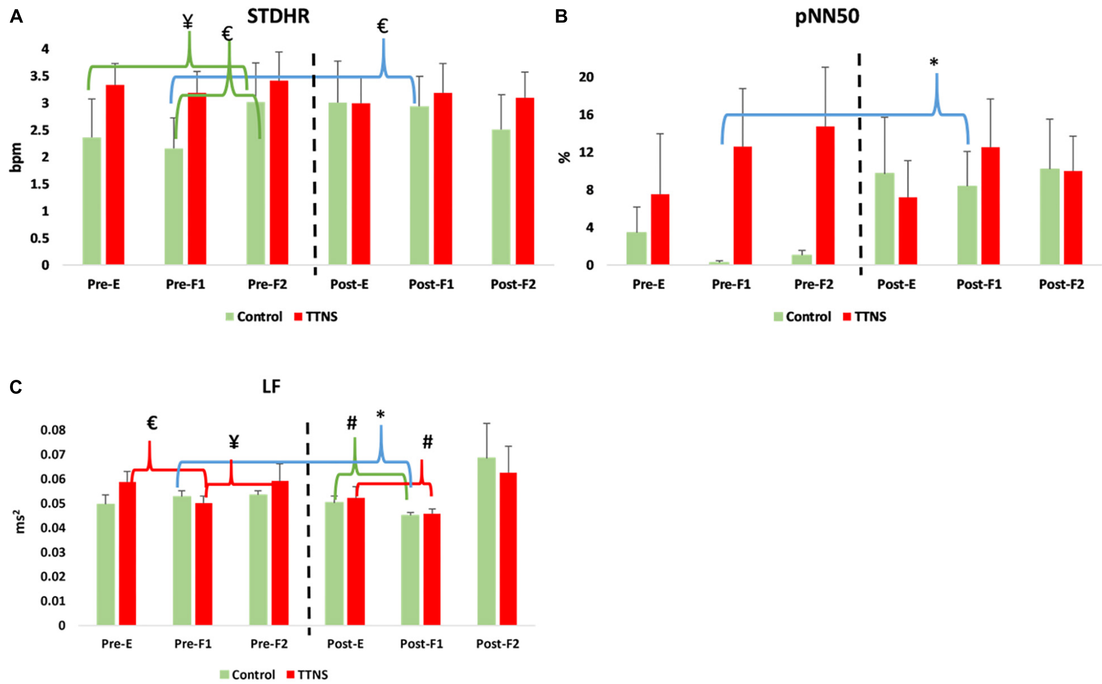

FIGURE 4 | Significant HRV changes during bladder filling, pre- and post-trial. Dashed line represents transition to post-trial testing, red brackets and green brackets are within group differences in the TTNS and controls, respectively. Blue brackets are pre- post-trial differences. **(A)** STDHR increases pre-stimulation in the controls, not seen post-test. **(B)** pNN50 increases in the controls post-test during the first filling phase. **(C)** Decrease in LF during initial filling is maintained in the TTNS group post-trial. Pre, pre-trial; Post, post-trial; E, E = empty bladder; F1, filling phase 1; F2, filling phase 2; TTNS, transcutaneous tibial nerve stimulation; STDHR, standard deviation of heart rate; bpm, beats per minute; pNN50, the proportion of pairs of successive R–R beat lengths that differ by more than 50 ms (NN50) for total number of beats. LF, low frequency; ms^2, milliseconds squared; ¥$p = 0.04$; #$p = 0.03$; *$p = 0.01$; £$p < 0.01$.

In the TTNS group, post-trial CMG was significant for increasing SBP during filling, from Filling 1 to Filling 2 ($p = 0.003$), as well as from Empty Bladder to Filling 2 ($p < 0.001$, **Figure 3A**). DBP also increased from Filling 1 to Filling 2 ($p = 0.042$) and from Empty Bladder to Filling 2 ($p < 0.001$, **Figure 3B**). This was not seen in the control group after the trial. The control groups demonstrated increased parasympathetic activity from Filling 1 to Filling 2 (Mean RR, $p = 0.02$; Mean HR, $p = 0.012$; HF, $p = 0.017$). In the TTNS group, there was decreased sympathetic activity from Empty Bladder to Filling 1 (LF, $p = 0.032$, **Figure 4C**).

Significant CMG Variables Associated to ANS Variables

In the controls, increasing parasympathetic activity was associated to: (1) increasing maximum detrusor pressure (as NN50 increased, maximum detrusor pressure increased by 0.23 cmH_2O, $p = 0.02$, 95%CI 0.04–0.43; as pNN50 increased, maximum detrusor pressure increased by 0.78 cmH_2O, $p = 0.026$, 95% CI 0.09–1.46); (2) volume to first sensation and first desire increased with increasing HF (as HF increased, volume to first sensation increased ($p = 0.021$, 95%CI 32 387) and volume to first desire increased ($p = 0.03$, 95%CI 23 397).

In the TTNS group, as LF/HF increased, DSD decreased by 0.17 ($p = 0.009$, 95%CI −0.3 −0.04). As HF increased by 0.1, volume of first sensation decreased by 158 ml ($p = 0.021$, 95%CI −292 −24). Increasing volume to first desire was significantly associated to several ANS variables: (1) as DBP increased, volume increased by 6.97 ml ($p < 0.001$, 95%CI 6.95–6.99); as SDNN increased, volume increased by 7.2 ml ($p = 0.001$, 95%CI 2.9–11.6); as NN50 increased, volume increased by 5.25 ml ($p < 0.001$, 95%CI 5.25–5.25); as total power increased, volume increased by 0.035 ($p < 0.001$, 95%CI 0.035–0.035). Volume to first desire decreased with increasing HF ($p < 0.001$, 95%CI −249 −127) and increasing LF ($p < 0.001$, 95%CI −203 −201).

DISCUSSION

In this cohort of subjects from the larger pilot trial, we observed that the previous findings of improved CMG parameters in the TTNS group were associated with paralleled ANS changes. Our concomitant findings from BP and 5-min ECG recordings with HRV analysis add to the paucity of knowledge in the developing SCI neurogenic bladder and provide insight to the effects of bladder neuromodulation with TTNS on the autonomic nervous (ANS) system response to bladder filling.

The postulated mechanism of action of percutaneous TNS and sacroneuromodulation is that stimulation of the peripheral sensory afferent fibers block competing abnormal visceral afferent signals from the bladder and prevent the reflexive, efferent motor response resulting in detrusor hyperactivity and dysynergia (Sanford and Suskind, 2016). We postulated that this mechanism can be achieved with TTNS, impacting overall sensation from the bladder, leading to prolonged times to sensation and decreased overall reflexive efferent responses causing DSD and potentially DH. The findings from our pilot data support this mechanism, with TTNS group findings of delayed bladder filling sensations and subsequent decreased reflexive motor efferent activity represented by fewer events of DSD during bladder filling. With the addition of the ANS measurements, we sought to describe the ANS response to bladder filling with TTNS compared to controls.

Similar to the reported increase in systolic BP in non-SCI subjects and chronic tetraplegia approaching maximal bladder capacities, we found an increase in SBP as the bladder fills in both the controls and TTNS group Pre-trial (**Figure 3A**) (Huang et al., 2016). Over time, this physiologic response is lost in the control group, but is maintained in the TTNS group (**Figure 3A**). Importantly, there were no pre- post-trial differences in ANS measures in the TTNS group (**Figure 4**). This may suggest that the neuromodulation from TTNS not only maintains bladder mechanical responses, but also the sensory afferent responses which are communicated to the ANS.

Unlike the TTNS group after the trial, ANS measures were able to detect several changes in the control group. The control group displayed evidence of increased parasympathetic activity during early filling (NN50, pNN50) and decreased sympathetic activity (LF) with subsequent decreased HR and increased RR during late filling. This may explain the lack of increased SBP during filling which was seen pre-trial (**Figure 3A**). Furthermore, these findings suggest that the neurogenic bladder sensory afferents may trigger an increased parasympathetic response before the normal capacity to void is achieved.

In the control group, mixed-effects linear modeling was significant for increasing volume to first sensation and first desire to void associated to increasing parasympathetic activity measured by HF. The opposite association was observed in the TTNS group, with increasing HF associated to reduced volumes to first sensation and first desire to void. Although the meaning of this relationship remains to be determined, that opposite findings were observed in the control and intervention group are noteworthy suggesting that HRV differences are associated with CMG differences and that TTNS affects the ANS response to bladder filling. Further research with larger sample sizes is warranted to clarify these relationships.

This study also highlights the need to perform urodynamic evaluations in all people with SCI. We found that completeness of injury (AIS A) did not preclude sensation during bladder filling or the desire to void during CMG. This study, as well as the findings from others, demonstrate that physical exam, including the International Standards for Neurological Classification of SCI (ISNCSCI) exam, poorly correlate with CMG findings of lower urinary tract dysfunction, even during the acute phase of injury (Weld and Dmochowski, 2000; Patki et al., 2006; Bellucci et al., 2013). Furthermore, there are very few ways to measure changes in the ANS function and response in the human neurogenic bladder, and those that exist are limited to specialized laboratory tests, including measurements of neurotransmitters and other messaging proteins (Ochodnicky et al., 2013). We propose that the addition of feasible, clinic-setting measurements of BP and HRV to measure ANS activity during serial CMG can increase the knowledge of the developing neurogenic bladder and the impact of neuromodulation. While CMG provides us with reflexive and mechanical responses, BP and HRV data provides ANS-mediated neurophysiologic responses to bladder filling.

There are several limitations to this study. The study was powered primarily based on sample size of convenience to measure safety and feasibility of TTNS in acute SCI rehabilitation, not CMG and HRV parameter changes. Findings from these pilot trials will help develop larger trials. Although baseline BP recordings were similar between groups, randomization did not balance the overall ANS activity as measured by SDNN and total power, significantly higher in the TTNS group at baseline. Also, HRV measurements may be influenced by time of day and diet, perhaps requiring a more controlled environment to precisely measure differences. Furthermore, neurologic and physiologic changes are expected to be seen in acute SCI. Serial CMGs and HRV measurements have not been performed in acute SCI and given the low numbers in the pilot trial, it is unclear how representative the changing values before and after the trial are due to TTNS versus natural history of acute SCI. That a significant difference exists between the two groups supports the hypothesis that TTNS can modulate the ANS and warrants further research. Long-term sustainability of efficacy can only be speculated based on this 2-week protocol with outcomes measured within 3 days of trial completion. Finally, the use of HRV in neurogenic bladder is novel and the analyses conducted are likely an over-simplification of the PNS and SNS response to bladder filling. The HRV variables measure different aspects of the ANS variability and therefore have differing responses. Much like the research in orthostatic hypotension in the non-SCI population, a composite of HRV variables utilizing mathematical modeling may be necessary to define correlates to CMG findings (Sannino et al., 2015). Importantly, HRV was able to detect a difference between groups. Further research is necessary to better understand the utility and knowledge gained from HRV during CMG.

CONCLUSION

Preliminary evidence suggests that TTNS in acute SCI is able to achieve bladder neuromodulation based on stable CMG findings and lack of morbid changes in the TTNS group compared to controls. The morbid CMG changes in the control group were associated with HRV markers of increased parasympathetic tone and corresponding BP findings. Further research is needed to understand the neuromodulation effects of TTNS in acute SCI neurogenic bladder and the response of the ANS during bladder filling as measured by BP and 5-min ECG recordings with HRV analyses.

ETHICS STATEMENT

This study was carried out in accordance with the recommendations of University of Texas Health Science Center at Houston and TIRR Memorial Hermann with written informed consent from all subjects. All subjects gave written informed consent in accordance with the Declaration of Helsinki. The protocol was approved by the UTHealth IRB committee.

AUTHOR CONTRIBUTIONS

AS contributed to the conception, the study design, the acquisition, the analysis, the interpretation of data, and the preparation of the manuscript. KG contributed to the study design and the editing of the manuscript. RK contributed to the acquisition of data and the editing of the manuscript. CS contributed to the study design, the interpretation of data, and editing of the manuscript. LZ contributed to the study design, the analysis, the interpretation of data, and the statistical writing. SL contributed to the interpretation of data and the editing of the manuscript.

FUNDING

This research was funded by the TIRR Rehabilitation Innovations Grant (2015) and Mission Connect [016-102], a project of the TIRR Foundation.

REFERENCES

Amarenco, G., Ismael, S. S., Even-Schneider, A., Raibaut, P., Demaille-Wlodyka, S., Parratte, B., et al. (2003). Urodynamic effect of acute transcutaneous posterior tibial nerve stimulation in overactive bladder. *J. Urol.* 169, 2210–2215. doi: 10.1097/01.ju.0000067446.17576.bd

Bacsu, C. D., Chan, L., and Tse, V. (2012). Diagnosing detrusor sphincter dyssynergia in the neurological patient. *BJU Int.* 109(Suppl. 3), 31–34. doi: 10.1111/j.1464-410X.2012.11042.x

Bellucci, C. H., Wollner, J., Gregorini, F., Birnböck, D., Kozomara, M., Mehnert, U., et al. (2013). Acute spinal cord injury–do ambulatory patients need urodynamic investigations? *J. Urol.* 189, 1369–1373. doi: 10.1016/j.juro.2012.10.013

Blaivas, J. G., Sinha, H. P., Zayed, A. A., and Labib, K. B. (1981). Detrusor-external sphincter dyssynergia: a detailed electromyographic study. *J. Urol.* 125, 545–548. doi: 10.1016/S0022-5347(17)55100-9

Curt, A., Nitsche, B., Rodic, B., Schurch, B., and Dietz, C. (1997). Assessment of autonomic dysreflexia in patients with spinal cord injury. *J. Neurol. Neurosurg. Psychiatry* 62, 473–477. doi: 10.1136/jnnp.62.5.473

Ditor, D. S., Kamath, M. V., Macdonald, M. J., Bugaresti, J., McCartney, N., and Hicks, A. L. (2005). Reproducibility of heart rate variability and blood pressure variability in individuals with spinal cord injury. *Clin. Auton. Res.* 15, 387–393. doi: 10.1007/s10286-005-0293-4

Dolinak, D., and Balraj, E. (2007). Autonomic dysreflexia and sudden death in people with traumatic spinal cord injury. *Am. J. Forensic Med. Pathol.* 28, 95–98. doi: 10.1097/PAF.0b013e3180600f99

Finazzi Agrò, E., Campagna, A., Sciobica, F., Petta, F., Germani, S., Zuccalà, A., et al. (2005). Posterior tibial nerve stimulation: is the once-a-week protocol the best option? *Minerva Urol. Nefrol.* 57, 119–123.

Gupta, P., Ehlert, M. J., Sirls, L. T., and Peters, K. M. (2015). Percutaneous tibial nerve stimulation and sacral neuromodulation: an update. *Curr. Urol. Rep.* 16:4. doi: 10.1007/s11934-014-0479-1

Hou, S., Duale, H., Cameron, A. A., Abshire, S. M., Lyttle, T. S., and Rabchevsky, A. G. (2008). Plasticity of lumbosacral propriospinal neurons is associated with the development of autonomic dysreflexia after thoracic spinal cord transection. *J. Comp. Neurol.* 509, 382–399. doi: 10.1002/cne.21771

Huang, Y. H., Chang, H. Y., Tsai, S. W., Chou, L. W., Chen, S. L., and Lin, Y. H. (2016). Comparison of autonomic reactions during urodynamic examination in patients with spinal cord injuries and able-bodied subjects. *PLoS One* 11:e0161976. doi: 10.1371/journal.pone.0161976

Kaplan, S. A., Chancellor, M. B., and Blaivas, J. G. (1991). Bladder and sphincter behavior in patients with spinal cord lesions. *J. Urol.* 146, 113–117. doi: 10.1016/S0022-5347(17)37727-3

Karlsson, A. K. (1999). Autonomic dysreflexia. *Spinal Cord* 37, 383–391. doi: 10.1038/sj.sc.3100867

Karri, J., Zhang, L., Li, S., Chen, Y. T., Stampas, A., and Li, S. (2017). Heart rate variability: a novel modality for diagnosing neuropathic pain after spinal cord injury. *Front. Physiol.* 8:495. doi: 10.3389/fphys.2017.00495

Lindan, R., Joiner, E., Freehafer, A. A., and Hazel, C. (1980). Incidence and clinical features of autonomic dysreflexia in patients with spinal cord injury. *Paraplegia* 18, 285–292.

Ochodnicky, P., Uvelius, B., Andersson, K. E., and Michel, M. C. (2013). Autonomic nervous control of the urinary bladder. *Acta Physiol.* 207, 16–33. doi: 10.1111/apha.12010

Patki, P., Woodhouse, J., Hamid, R., Shah, J., and Craggs, M. (2006). Lower urinary tract dysfunction in ambulatory patients with incomplete spinal cord injury. *J. Urol.* 175, 1784–7;discussion87. doi: 10.1016/S0022-5347(05)00979-1

Sanford, M. T., and Suskind, A. M. (2016). Neuromodulation in neurogenic bladder. *Transl. Androl. Urol.* 5, 117–126. doi: 10.3978/j.issn.2223-4683.2015.12.01

Sannino, G., Melillo, P., Stranges, S., De Pietro, G., and Pecchia, L. (2015). Blood pressure drop prediction by using hrv measurements in orthostatic hypotension. *J. Med. Syst.* 39:143. doi: 10.1007/s10916-015-0292-5

Schafer, W., Abrams, P., Liao, L., Mattiasson, A., Pesce, F., Spangberg, A., et al. (2002). Good urodynamic practices: uroflowmetry, filling cystometry, and pressure-flow studies. *Neurourol. Urodyn.* 21, 261–274. doi: 10.1002/nau.10066

Sharif, H., and Hou, S. (2017). Autonomic dysreflexia: a cardiovascular disorder following spinal cord injury. *Neural Regen. Res.* 12, 1390–1400. doi: 10.4103/1673-5374.215241

Sievert, K.-D., Amend, B., Gakis, G., Toomey, P., Badke, A., Kaps, H. P., et al. (2010). Early sacral neuromodulation prevents urinary incontinence after complete spinal cord injury. *Ann. Neurol.* 67, 74–84. doi: 10.1002/ana.21814

Snow, J. C., Sideropoulos, H. P., Kripke, B. J., Freed, M. M., Shah, N. K., and Schlesinger, R. M. (1978). Autonomic hyperreflexia during cystoscopy in patients with high spinal cord injuries. *Paraplegia* 15, 327–332. doi: 10.1038/sc.1977.49

Stampas, A., Korupolu, R., Zhu, L., Smith, C. P., and Gustafson, K. (2018). Safety, feasibility, and efficacy of transcutaneous tibial nerve stimulation in acute spinal cord injury neurogenic bladder: a randomized control pilot trial. *Neuromodulation* doi: 10.1111/ner.12855 [Epub ahead of print].

Task Force of the European Society of Cardiology the North American Society of Pacing Electrophysiology (1996). Heart rate variability: standards of measurement, physiological interpretation, and clinical use. *Circulation* 93, 1043–1065. doi: 10.1161/01.CIR.93.5.1043

Weld, K. J., and Dmochowski, R. R. (2000). Association of level of injury and bladder behavior in patients with post-traumatic spinal cord injury. *Urology* 55, 490–494. doi: 10.1016/S0090-4295(99)00553-1

Whiteneck, G. G., Charlifue, S. W., Frankel, H. L., Fraser, M. H., Gardner, B. P., Gerhart, K. A., et al. (1992). Mortality, morbidity, and psychosocial outcomes of persons spinal cord injured more than 20 years ago. *Paraplegia* 30, 617–630. doi: 10.1038/sc.1992.124

Conflict of Interest Statement: The authors declare that the research was conducted in the absence of any commercial or financial relationships that could be construed as a potential conflict of interest.

frontiers in Neuroscience

ORIGINAL RESEARCH
published: 08 March 2019
doi: 10.3389/fnins.2019.00170

Check for updates

CT-Guided Stellate Ganglion Pulsed Radiofrequency Stimulation for Facial and Upper Limb Postherpetic Neuralgia

*Yuanyuan Ding[1], Peng Yao[1], Hongxi Li[1], Zhenkai Han[1], Shimeng Wang[1], Tao Hong[1] and Guangyi Zhao[2]**

[1] Department of Pain Management, Shengjing Hospital of China Medical University, Shenyang, China, [2] Department of Anesthesiology, Shengjing Hospital of China Medical University, Shenyang, China

OPEN ACCESS

Edited by:
Gottfried Schlaug,
Beth Israel Deaconess Medical Center and Harvard Medical School, United States

Reviewed by:
Ali Yadollahpour,
Ahvaz Jundishapur University of Medical Sciences, Iran
Victor Manuel Pulgar,
Wake Forest School of Medicine, United States

***Correspondence:**
Guangyi Zhao
zhaoguangyi110004@163.com

Specialty section:
This article was submitted to Neural Technology, a section of the journal Frontiers in Neuroscience

Received: 25 October 2018
Accepted: 13 February 2019
Published: 08 March 2019

Citation:
Ding Y, Yao P, Li H, Han Z, Wang S, Hong T and Zhao G (2019) CT-Guided Stellate Ganglion Pulsed Radiofrequency Stimulation for Facial and Upper Limb Postherpetic Neuralgia. Front. Neurosci. 13:170. doi: 10.3389/fnins.2019.00170

Objective: Postherpetic neuralgia (PHN) is the most common complication of herpes zoster, manifesting as a persistent, spontaneous, knife-like pain or paroxysmal burning that seriously affects a patient's quality of life. An effective treatment of PHN is lacking. This retrospective study examined the efficacy and safety of stellate ganglion (SG) pulsed radiofrequency (PRF) on facial and upper limb PHN.

Methods: Eighty-four patients with PHN on the face or upper limbs were enrolled for the study. Patients were randomly divided into two surgical groups according to the order of enrollment; one group underwent SG block (SG-B group, $n = 42$) and the other underwent SG pulsed radiofrequency (SG-P group, $n = 42$). After surgery, patients were followed at 1 week, 2 weeks, 1 month, 3 months, and 6 months. Observation at each follow-up included basic patient characteristics, visual analog scale (VAS), quality of life (QOL) using Physical Component Summary (PCS), and Mental Component Summary (MCS) to assess, total effective rate, complications and side effects.

Results: Compared with preoperative values, VAS decreased in both groups after surgery ($P < 0.05$). In the SG-B group, VAS increased after 1 month, while in the SG-P group, VAS gradually decreased at later follow-up time points. VAS decreased more significantly in the SG-P group after 1 month ($P < 0.05$). PCS and MCS increased in both groups after the operation, and the difference was significant compared with preoperative values ($P < 0.05$). The total effective rates of the SG-B and SG-P groups were 64.3 and 83.3%, respectively. The total effective rate of the SG-P group was higher than that of the SG-B group ($P < 0.05$). The incidence of complications and side effects in the SG-B group was higher than that in the SG-P group ($P < 0.05$).

Conclusion: SG pulsed radiofrequency treatment of facial and upper limb PHN is safe and effective. It is a treatment method worth promoting.

Keywords: pulsed radiofrequency, stellate ganglion, facial and upper limb, postherpetic neuralgia, visual analog scale

INTRODUCTION

Postherpetic neuralgia (PHN) refers to the pain and discomfort that persists for more than 1 month after the disappearance of a herpes zoster (HZ) rash (Fashner and Bell, 2011). PHN is the most common complication of herpes zoster, manifesting as a persistent spontaneous, knife-like pain or paroxysmal burning that seriously affects a patient's quality of life (Johnson et al., 2010). Herpes zoster in the area of the face and limbs is a high risk factor for PHN due to the sensitivity of the affected area (Forbes et al., 2016). The mechanism of PHN is complex and lacks an effective method of treatment.

The stellate ganglion (SG) is formed by the union of the inferior cervical ganglion with the first thoracic ganglion. The dominant area of the stellate ganglion is the face and upper limbs. Stellate ganglion block (SGB) is an effective, minimally invasive treatment for neurovascular diseases in the dominant area (Jeon, 2016). Blocking the stellate ganglion can effectively improve the blood circulation of the facial and upper limb areas (Kim et al., 2018) and regulate the disordered endocrine system. At the same time, SGB may have preventive effects on PHN by reversing or preventing profound sympathetic stimulation and vasoconstriction, thereby restoring intraneural blood flow, preventing nerve ischemia and damage, alleviating neuralgia and reducing the occurrence of PHN (Boas, 1998; Makharita et al., 2012). However, due to the short duration of local anesthesia, the number of SGB treatments generally need to be increased, which increases the chance of secondary injury. Repeated treatment can lead to patient suffering, poor compliance, and poor quality of life.

Sluijter first proposed pulsed radiofrequency (PRF) for pain treatment (Sluijter, 1997). Since then, it has become a novel means of pain management. PRF delivers short bursts of radiofrequency currents (conducted through a needle) to nervous tissue without damaging the tissue. PRF has a 480 ms pulse intermission period that diffuses the generated temperature so that the temperature of the electrode does not exceed 42°C. This temperature does not cause nerve damage, and thus avoids complications such as hypoesthesia, paresthesia, and dyskinesia. PRF exerts analgesia mainly through neuromodulation. PHN is commonly treated with a combination of therapies.

Postherpetic neuralgia is one of the causes of complex regional pain syndrome (CRPS). While there are a few reports of SG pulsed radiofrequency being used for CRPS (Singh Rana et al., 2015; Kim et al., 2017), there are no reports of SG pulsed radiofrequency being used for PHN in facial and upper limb areas.

In this study, SG pulsed radiofrequency was used to treat facial and upper limb PHN; its clinical efficacy, safety, and long-term quality of life compared with SGB were evaluated.

MATERIALS AND METHODS

Patients

From January 2015 to December 2016, 84 patients with PHN on the face or upper limbs were enrolled at the Department of Pain Management, Shengjing Hospital of China Medical University (**Figure 1**). Postherpetic pigmentation or lesions were distributed unilaterally; included were 24 cases of lesions in the area of trigeminal innervation, 18 cases of lesions in the area of facial nerve innervation, and 42 cases of lesions in the upper limbs. Patients were randomly divided into two surgical groups according to the order of enrollment: one group underwent SG block (SG-B group, n = 42) and the other group underwent SG pulse radiofrequency (SG-P group, n = 42). The study was approved by the Ethics Committee of Shengjing Hospital affiliated with China Medical University. Before surgery, all patients were informed of surgical risks and complications. Written informed consent according to the Declaration of Helsinki was obtained from all patients.

The inclusion criteria were as follows: (1) visual analog scale (VAS) was >5 points within 24 h of enrollment; (2) lesions of the face and upper limbs had healed, but severe intractable pain, local skin hyperalgesia, numbness, and abnormal sensation persisted; (3) the natural course of the disease exceeded 1 month; (4) age >30 years; (5) no nausea, vomiting, dizziness, constipation, or urinary retention before randomization.

The exclusion criteria were as follows: epilepsy, trigeminal neuralgia, intracranial space-occupying lesions, hematological disorders, or abnormal blood coagulation, history of severe liver and kidney dysfunction or history of severe cardiopulmonary disease, pregnancy, and history of drug abuse.

Surgical Procedure

The patients were placed in a supine position, and the appropriate needle, under CT guidance, was positioned at the base of the C7-T1 parapophysis. A safe route was chosen to avoid injury to the vessel, and the puncture point and puncture angle were clearly defined. After disinfecting the area, a 22G needle or radiofrequency needle was selected. The needle was inserted at the CT positioning angle and gradually advanced under CT guidance until the tip touched the base of C7 and T1 parapophysis, then withdrawn 1–2 mm. No blood or cerebrospinal fluid was drawn back. The SG-B group was injected with 5 mL of 5% lidocaine. The SG-P group was subjected to a radiofrequency test (Baylis Medical Inc., Montreal, Canada): 50 Hz, 0.1–0.3 V sensory test, no neural numbness to the upper limbs or other areas; 2 Hz, 0.4~1.0 V exercise test, no corresponding segmental muscle tremors and jumping sensation. The PRF was 42°C for 300 s (pulse width 20 ms and frequency 2 Hz). The PRF was performed for two cycles. The needle was withdrawn and pressure applied to the puncture point. No abnormalities were observed. When vital signs were stable, the patient was returned to the ward.

Since antiepileptic drugs are commonly used to treat neuropathic pain, both groups were treated with the antiepileptic drugs carbamazepine (Beijing Novartis Pharmaceutical Co., Ltd., China), gabapentin (Jiangsu Enhua Pharmaceutical Co., Ltd., China), and pregabalin (Pfizer Manufacturing Deutschland GmbH, Germany). The opioid analgesia drug oxycontin (Mundipharma Pharmaceutical Co., Ltd., China), and the neurotrophic drug neurotropin (Nippon Zoki Pharmaceutical

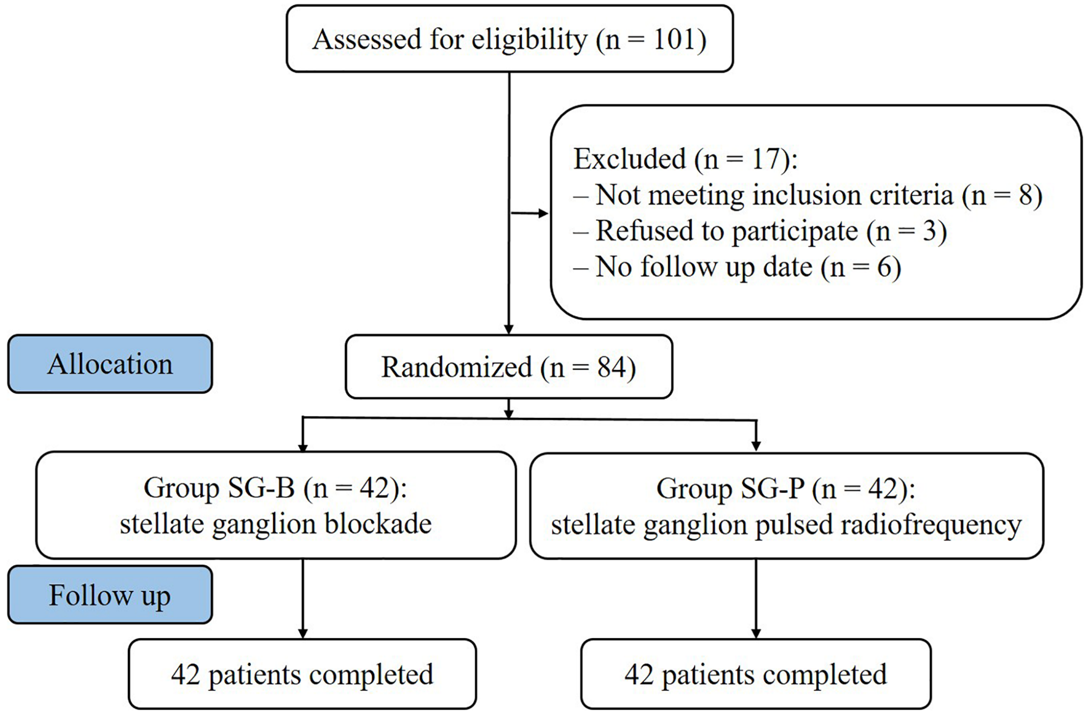

FIGURE 1 | Study flowchart. All 84 patients were included in the treatment.

Co., Ltd., Japan), were also used. The analgesic effect of all of these drugs were unsatisfactory.

Observations and Follow Up

Preoperative information included gender, age, pain duration, pain location, affected side of the body, VAS, the dosage of antiepileptic and opioid analgesia drugs.

Patients were followed at 1 week, 2 weeks, 1 month, 3 months, and 6 months with a "blind" method by the non-surgical staff. The following parameters were assessed:

(1) visual analog scale (VAS) to assess the pain level. (0 points – painless, 10 points – unbearable pain).
(2) Thirty six item short-form health survey (SF-36) (Lam et al., 2005) to assess the quality of life (QOL). The questionnaire includes 36 questions; they were used to generate eight scales, including physical, and mental states. The QOL of patients before and after surgery at each time point was assessed. Physical state includes: physical function, physical role, bodily pain, and general health. Mental state includes: vitality, social function, emotional role, and mental health. All the data were summarized to calculate Physical Component Summary (PCS), and Mental Component Summary (MCS).
(3) Total effective rate. The assessment criteria for pain relief is divided into four levels. Subjective symptoms and clinical signs were assessed at 6 months: complete remission of pain (CR, pain relief ≥75%), partial remission of pain (PR, 50%≤ pain relief <75%), mild remission of pain (MR, 25%≤ pain relief <50%), and no remission of pain (NR, pain relief <25%). Significant effective rate (%) = $[(CR + PR)/n] \times 100\%$, Total effective rate (%) = $[(CR + PR + MR)/n] \times 100\%$.
(4) Incidence of complications and side effects: including local hematoma, brachial plexus block, pneumothorax, vascular injury (common carotid artery, vertebral artery, vein, etc.), high epidural and subarachnoid block; local anesthetic related adverse reactions (vertigo, dizziness, tinnitus, chills, local anesthetic poisoning, etc.); pain induration and others such as hoarseness/aphonia, pharyngeal foreign body sensation, infection, arrhythmia, etc.

Statistical Analysis

Data were analyzed using SPSS18.0 statistical software (IBM Corporation, NY, United States). The measurement data were first tested for normality using the single-sample Kolmogorov–Smirnov test. The normal distribution variables were compared using one-way analysis of variance (ANOVA) followed by LSD pairwise comparison; values were expressed as mean ± standard deviation ($\bar{x} \pm SD$); the changes of VAS, PCS, and MCS for all time points among the groups were compared using repeated analysis of variance test. The abnormal distribution variables were compared using the Kruskal–Wallis rank sum test; values were expressed as the median±interquartile range. The enumeration data were analyzed by chi square test or Fisher's exact test. $P < 0.05$ was statistically significant.

RESULTS

Patient Characteristics

All patients completed the surgeries, and the procedures were successful. The basic condition of patients in the SG-B and SG-P groups were compared before surgery. There was no significant difference in the gender, age, pain duration, pain location and affected side, VAS, the dosage of antiepileptic and opioid analgesia drugs between the two groups ($P > 0.05$) (**Table 1**).

VAS Pain Scores

After surgery, VAS decreased in both groups, and the difference was significant compared with preoperative values ($P < 0.05$). At the early follow-up time points (1 and 2 weeks), VAS decreased in both groups, but there was no significant difference between groups. In the SG-B group, VAS increased after 1 month, while in the SG-P group VAS gradually decreased at the later follow-up time points. VAS decreased significantly in the SG-P group after 1 month, and there was a significant difference between the two groups. This difference persisted to the 6 month time point ($P < 0.05$) (**Figure 2**).

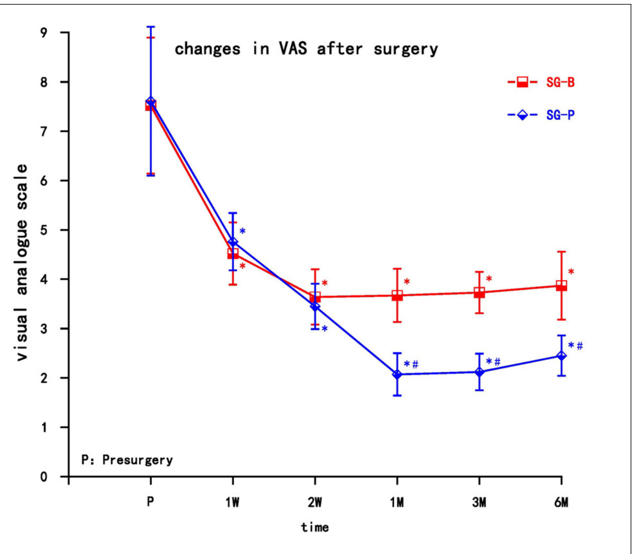

FIGURE 2 | Comparison of VAS pain scores pre-surgery and post-surgery in the two groups. At 1 and 2 weeks, VAS decreased in both groups ($P > 0.05$); VAS decreased significantly in the SG-P group after 1 month ($P < 0.05$). Results are presented as means ± SEMs. *Compared to pre-surgery, $P < 0.05$; #Compared with SG-B group, $P < 0.05$.

Quality of Life Evaluation

Both groups of patients achieved varying degrees of improvement in quality of life after pain relief, including physical function, physical role, bodily pain, general health, vitality, social function, emotional role, and mental health. The PCS and MCS increased in the two groups after the operation at each observation time point, and the difference was significant compared with preoperative levels ($P < 0.05$). At the early time points post treatment (1 and 2 weeks), both PCS and MCS gradually increased, but there was no significant difference between the two groups. In the SG-B group, PCS and MCS decreased after 1 month, while in the SG-P group, PCS and MCS continued to gradually increase, indicating a prolonged improvement in the quality of life. PCS and MCS increased significantly after 1 month in SG-P group, and there was a significant difference between the

TABLE 1 | Pre-surgery patient characteristics in SG-B and SG-P groups.

Parameters	Group		*P*-value
	SG-B	SG-P	
Patients (n)	42	42	–
Gender (F/M, %)	20 (47.6%)/22 (52.4%)	19 (45.2%)/23 (54.8%)	0.827
Age (years, range)	55.28 ± 8.35 (34–72)	56.13 ± 8.56 (35–70)	0.569
Pre-surgery pain duration (M, range)	8.32 ± 5.27 (3–17)	8.54 ± 5.42 (3–20)	0.675
Pain location (n, %)			
Trigeminal nerve	20 (47.6%)	21 (50.0%)	–
Facial nerve	6 (14.3%)	7 (16.7%)	–
Brachial plexus	16 (38.1%)	14 (33.3%)	–
Affected side (n, %)			
Right	28 (66.7%)	30 (71.4%)	–
Left	14 (33.3%)	12 (28.6%)	–
Pre-surgery VAS	7.52 ± 1.38	7.61 ± 1.51	0.416
Pre-surgery drug dosage			
Carbamazepine (mg/d, n)	558.65 ± 79.53 (23)	562.02 ± 80.19 (24)	0.493
Gabapentin (g/d, n)	2.78 ± 0.45 (10)	2.81 ± 0.52 (9)	0.715
Pregabalin (mg/d, n)	426.86 ± 73.71 (9)	428.28 ± 74.64 (9)	0.532
Oxycontin (mg/day, n)	43.62 ± 12.78 (42)	44.06 ± 11.95 (42)	0.584

SG-B, stellate ganglion blockade; SG-P, stellate ganglion pulsed radiofrequency; VAS, visual analog scale. Data are presented as numbers (%) of patients or mean ± SD.

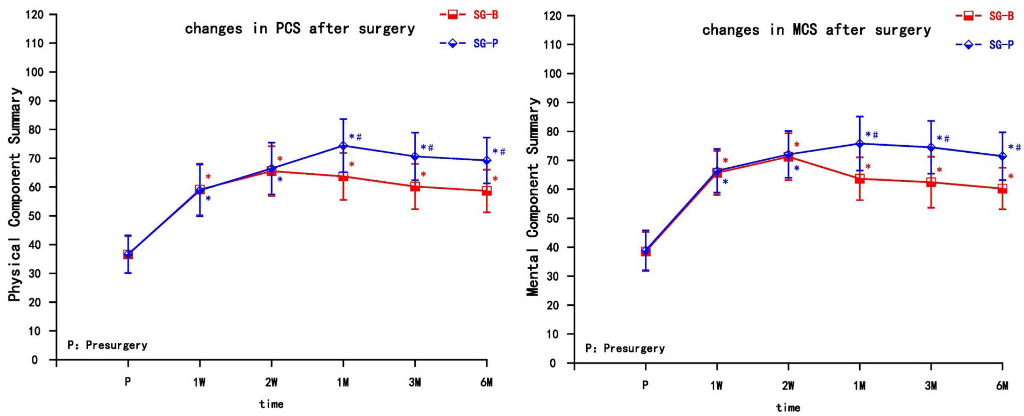

FIGURE 3 | Comparison of quality of life scores (SF-36) pre-surgery and post-surgery in the two groups. At 1 and 2 weeks, PCS and MCS increased in both groups ($P > 0.05$); PCS and MCS increased significantly in the SG-P group after 1 month ($P < 0.05$). PCS, Physical Component Summary; MCS, Mental Component Summary; Results are presented as means ± SEMs. *Compared to pre-surgery, $P < 0.05$; #Compared with SG-B group, $P < 0.05$.

two groups. This difference persisted to the 6 month follow-up time point ($P < 0.05$) (**Figure 3**).

Total Effective Rate

At 6 months post-surgery, the total effective rate of the SG-B and SG-P groups was 64.3 and 83.3%, respectively. The total effective rate of SG-P group was higher than that of SG-B group, and the difference was statistically significant ($P = 0.047$) (**Table 2**).

Incidence of Complications and Side Effects

The procedures were completed within 30 min for both groups. Postoperatively, there were no pneumothoraces, no epidural and subarachnoid blockades, no infection, no arrhythmia and no serious complications in either group.

Both groups had local hematoma, nausea and vomiting, hoarseness/aphonia, and pharyngeal foreign body sensation. After local cold compresses, the symptoms gradually resolved within 6 months without subsequent serious adverse reactions. The SG-B group experienced headache, vertigo, and dizziness; complications of brachial plexus block and pain induration also occurred; the total incidence of complications and side effect was 52.4% (22/42). There was no headache, vertigo, or dizziness, and no complication of brachial plexus block or pain induration in the SG-P group; the total incidence of complications and side effect was 16.7% (7/42). The incidence of complications and side effects in the SG-B group was higher than that in the SG-P group ($P = 0.001$) (**Table 3**).

TABLE 2 | Total effective rate in SG-B and SG-P groups (%).

Group	n	Excellent	Effective	Ineffective	The total effective rate(%)
SG-B	42	16	11	15	64.3
SG-P	42	23	12	7	83.3*

*SG-B, stellate ganglion blockade; SG-P, stellate ganglion pulsed radiofrequency; *Compared with SG-B group, P < 0.05.*

DISCUSSION

Postherpetic neuralgia is a chronic neuropathic pain. It mainly manifests as spontaneous, allodynia, and hyperalgesia. PHN is associated with the location of herpes and severity of the pain. Patients with herpes zoster in the facial and upper limb areas experience severe pain (Nagasako et al., 2002), and the damaged nerves are more prone to develop PHN. The etiology and mechanism of PHN are unclear, and there are no effective treatments. Because of the special anatomical positions of the facial and upper limb areas, the choice of treatment options is limited. Thus, it is urgent that an effective method of treatment be found.

Postherpetic neuralgia is commonly treated with a variety of drugs, including analgesics, anticonvulsants, antidepressants,

TABLE 3 | Complications and side effects in SG-B and SG-P groups (%).

Complications	Group	
	SG-B	SG-P
Hematoma, n (%)	3 (7.1)	2 (4.8)
Headache/vertigo/dizziness, n (%)	2 (4.8)	0 (0.0)
Nausea/vomiting, n (%)	4 (9.5)	2 (4.8)
Brachial plexus block, n (%)	5 (11.9)	0 (0.0)
Pain induration, n (%)	3 (7.1)	0 (0.0)
Hoarseness/aphonia, n (%)	3 (7.1)	1 (2.4)
Throat foreign body sensation, n (%)	2 (4.8)	2 (4.8)
Incidence of complications and side effect (%)	22 (52.4)	7 (16.7)*

*SG-B, stellate ganglion blockade; SG-P, stellate ganglion pulsed radiofrequency; *Compared with SG-B group, P < 0.05.*

and neurotrophic drugs. However, such treatment is generally inadequate for cases involving moderate to severe pain (Sacks, 2013). When herpes invades the area of the face and upper limbs, conventional drug therapy generally needs a longer course of treatment, which can result in a greater chance of adverse reactions. SGB can effectively relieve the acute pain of herpes and reduce the incidence of PHN (Boas, 1998; Wu et al., 2000; Makharita et al., 2012). It is an effective method to treat neurovascular diseases of the face and upper limbs and can effectively relieve the complex regional pain syndromes (CRPS) of the upper body (Datta et al., 2017).

The analgesic mechanism of SGB is still not clear, but most likely involves central and peripheral mechanisms. The central site is mainly located in the hypothalamus (Ranson et al., 1998; Westerhaus and Loewy, 2001), regulating the autonomic nervous system, endocrine system and immune system to maintain the stability of the body's internal environment (Yokoyama et al., 2000). The peripheral effect of SGB is to block the voltage-gated sodium channels on the nerve cell membrane through local anesthetics, making it difficult for the neural membrane potential to reach the action potential threshold, completely and reversibly blocking the generation and conduction of nerve impulses, blocking the spinal reflex pathway (Lynch and Elgeneidy, 1996; Lipov et al., 2009), and reducing the sympathetic nerve excitability. The functions of the vasculature, glandular secretion, muscle movement, bronchial smooth muscle contraction, and pain transmission controlled by sympathetic nerves are inhibited, thereby dilating blood vessels, increasing the blood flow in the facial and upper limbs, and reducing vascular resistance (Kang et al., 2010; Kim et al., 2018). SGB can improve the neurotrophic status, blocking the vicious cycle of pain (Reinauer et al., 1994). At the same time, it can enhance the defense function and prevent nerve damage (Boas, 1998). SGB can reduce norepinephrine (Mulvaney et al., 2010) and prostaglandins in the brain and plasma, improve ischemic, anoxic and metabolic abnormalities in local tissues, and remove inflammatory mediators by increasing local blood circulation (Park et al., 2010; Gopal et al., 2013; Kim et al., 2013). SGB can also significantly reduce the cortisol, aldosterone, angiotensin-2, 5-hydroxytryptamine and substance P in the blood of patients with pain (Wang et al., 2005; Jeon, 2016), change the lymphocyte subsets and NK cell activity (Yokoyama et al., 2000), inhibit the proinflammatory cytokines IL-1β, IL-6 and TNF-α, regulate the early inflammation responses (Liu et al., 2013), and promote nerve repair. SGB can effectively alleviate facial and upper limb PHN. However, the SG has a special anatomic location and the adjacent structures are complex. Severe complications such as hoarseness, pneumothorax, epidural block, subarachnoid space block, esophageal injury, vascular injury and hematoma formation (Hirota et al., 2017) may occur as a result of the surgery. Anesthetic drugs have a short duration of action. In order to reduce pain and improve efficacy, it is often necessary to increase the number of treatments, which may increase the occurrence of side effects and patient suffering. Therefore, it is desirable to find a therapeutic method that is effective and that can maintain analgesia for an extended period of time.

Radiofrequency is an effective treatment for chronic pain, including conventional radiofrequency (CRF) and PRF. Kastler et al. (2013) reported that CT-guided stellate ganglion CRF treatment of upper limb chronic refractory CRPS-I was more effective than SGB, with an effective rate of 67.6%. CRF produces a high-temperature effect through high-frequency currents, which causes coagulation and degeneration of pain-reducing nerve fibers (Aδ and C-type fibers) and blocks action potentials to achieve analgesia. The mechanism of PRF is different from CRF. The analgesic mechanism of pulsed radiofrequency is unclear (Lin et al., 2014), and it is currently believed that the analgesia is produced by neuromodulation (Cahana et al., 2006; Rehman et al., 2012). The radiofrequency current of PRF is intermittent. This energy transfer does not cause protein coagulation, does not destroy the anatomical basis of pain impulse transmission, and does not cause nerve damage. PRF analgesia is not achieved through temperature effects (Podhajsky et al., 2005; Hamann et al., 2006).

In this study, the decrease in reported pain resulted from a combination of treatments, including analgesic drugs, and neurotrophic drugs. VAS decreased after the operation in both groups, and the difference was significant compared with preoperative values. VAS decreased early in both groups, but VAS in the SG-B group increased after 1 month, while SG-P group still maintained VAS reduction at the later time points. This may be due to the gradual metabolism of local anesthetic drugs over time. As a result, the long-term analgesic substances metabolize and the effect gradually reduces, making it difficult to maintain long-term analgesia. The effect of PRF may be at the microscopic or even subcellular level (Cosman and Cosman, 2005). The effect of neuromodulation is slow, but it can be maintained for an extended period of time.

Inflammation and neurotrophic factors are involved in PHN (Zhao et al., 2017). PRF can regulate the expression of multiple genes in the conduction pathway, enhancing the expression of anti-inflammatory factor genes (GABAB-R1, Na/KATPase, and 5-HT3r) in the dorsal root ganglion, while decreasing the expression of proinflammatory factor genes (TNF-α and IL-6) (Vallejo et al., 2013). PRF has an immunoregulation effect, which has been shown to significantly reduce the level of $CD56^{+}$, $CD3^{-}$, IFN-γ, and NK cell frequency, and increase $CD8^{+}$ T cell frequency and IL-6 in cerebrospinal fluid (Das et al., 2018). PRF has been shown to upregulate the transcription and translation of glial cell line-derived neurotrophic factor (GDNF) in the sciatic nerve and spinal cord (Jia et al., 2016; Hailong et al., 2018) and reduce calcitonin gene-related peptide (CGRP) expression in dorsal root ganglion (Ren et al., 2018). PRF inhibited the excitatory neurotransmitter (glutamate) induced by nociception and then induced an analgesic effect on neuropathic pain (Huang et al., 2016). PRF increased histone acetylation and potassium-chloride cotransporter 2 (KCC2) expression, partially restored GABA synaptic function, alleviated inflammatory pain sensitization (Liu et al., 2017), and attenuated JNK activation in the spinal dorsal horn (Chen et al., 2014). Therefore, PRF effectively relieves pain, and can be maintained over an extended period of time. This long-term analgesic effect avoids repeated treatment of the stellate ganglion.

In addition, sensory and exercise nerve tests can be performed before PRF treatment, which will more accurately locate nerves and avoid complications. Therefore, SGB could be used to test the effect first. If the treatment was effective, then SG PRF was used to obtain the positive result. The stellate ganglion is composed of C3–C7 cervical inferior sympathetic ganglia and T1 sympathetic ganglia. The gray traffic branch is connected with the spinal nerves and contains the sympathetic nerve fibers of the brachial plexus. In this study, the SG-B patient group experienced headache, vertigo and dizziness, and there were complications of brachial plexus block and pain induration. No such complications occurred in the SG-P group. The SG-B group had more complications and side effects than SG-P group. The main complications were brachial plexus block and pain induration, which may be related to the diffusion and local injury of local anesthetic drugs. These complications and side effects could affect patient compliance and affected further treatment.

In summary, SG pulsed radiofrequency treatment of facial and upper limb PHN proved superior to SG blockage. The SG pulsed radiofrequency method is safe and effective as it alleviates PHN, improves the quality of life of the patients, and avoids the adverse reaction of local anesthetics. It is a method of treatment worth promoting.

AUTHOR CONTRIBUTIONS

TH and PY designed and conducted the study, including patient recruitment, data collection, and data analysis. HL, ZH, and SW collected the data. YD prepared the manuscript draft. GZ analyzed the data. All authors approved the final manuscript.

FUNDING

This study was supported by the Natural Science Foundation of Liaoning Province (No. 20170541032) and Shenyang Young and Middle-aged Science and Technology Innovation Talent Support Plan (No. RC170045).

REFERENCES

Boas, R. A. (1998). Sympathetic nerve blocks: in search of a role. *Reg. Anesth. Pain Med.* 23, 292–305. doi: 10.1097/00115550-199823030-00012

Cahana, A., Zundert, J., Macrea, L., van Kleef, M., and Sluijter, M. (2006). Pulsed radiofrequency: current clinical and biological literature available. *Pain Med.* 7, 411–423. doi: 10.1111/j.1526-4637.2006.00148.x

Chen, K. H., Yang, C. H., Juang, S. E., Huang, H. W., Cheng, J. K., Sheen-Chen, S. M., et al. (2014). Pulsed radiofrequency reduced complete Freund's adjuvant-induced mechanical hyperalgesia via the spinal c-Jun N-terminal kinase pathway. *Cell Mol. Neurobiol.* 34, 195–203. doi: 10.1007/s10571-013-0003-z

Das, B., Conroy, M., Moore, D., Lysaght, J., and McCrory, C. (2018). Human dorsal root ganglion pulsed radiofrequency treatment modulates cerebrospinal fluid lymphocytes and neuroinflammatory markers in chronic radicular pain. *Brain Behav. Immun.* 70, 157–165. doi: 10.1016/j.bbi.2018.02.010

Datta, R., Agrawal, J., Sharma, A., Rathore, V. S., and Datta, S. (2017). A study of the efficacy of stellate ganglion blocks in complex regional pain syndromes of the upper body. *J. Anaesthesiol. Clin. Pharmacol.* 33, 534–540. doi: 10.4103/joacp.JOACP_326_16

Fashner, J., and Bell, A. L. (2011). Herpes zoster and postherpetic neuralgia: prevention and management. *Am. Fam. Phys.* 83, 1432–1437.

Forbes, H. J., Thomas, S. L., Smeeth, L., Clayton, T., Farmer, R., Bhaskaran, K., et al. (2016). A systematic review and meta-analysis of risk factors for postherpetic neuralgia. *Pain* 157, 30–54. doi: 10.1097/j.pain.0000000000000307

Gopal, D., Singh, N. G., Jagadeesh, A. M., Ture, A., and Thimmarayappa, A. (2013). Comparison of left internal mammary artery diameter before and after left stellate ganglion block. *Ann. Card Anaesth.* 16, 238–242. doi: 10.4103/0971-9784.119161

Hailong, J., Hao, R., Zipu, J., Nan, J., and Fang, L. (2018). Pulsed radiofrequency improves neuropathic pain in chronic constriction injury rats through the upregulation of the transcription and translation levels of glial cell line-derived neurotrophic factor. *Pain Phys.* 21, 33–40.

Hamann, W., Abou-Sherif, S., Thompson, S., and Hall, S. (2006). Pulsed radiofrequency applied to dorsal root ganglia causes a selective increase in ATF3 in smallneurons. *Eur. J. Pain* 10, 171–176. doi: 10.1016/j.ejpain.2005.03.001

Hirota, K., Hirata, K., Shibata, S., Shigematsu, K., Higa, K., and Yamaura, K. (2017). Risk vessels of retropharyngeal hematoma during stellate ganglion block. *Reg. Anesth. Pain Med.* 42, 778–781. doi: 10.1097/AAP.0000000000000644

Huang, Y. H., Hou, S. Y., Cheng, J. K., Wu, C. H., and Lin, C. R. (2016). Pulsed radiofrequency attenuates diabetic neuropathic pain and suppresses formalin-evoked spinal glutamate release in rats. *Int. J. Med. Sci.* 13, 984–991. doi: 10.7150/ijms.16072

Jeon, Y. (2016). Therapeutic potential of stellate ganglion block in orofacial pain: a mini review. *J. Dent. Anesth. Pain Med.* 16, 159–163. doi: 10.17245/jdapm.2016.16.3.159

Jia, Z., Ren, H., Li, Q., Ji, N., and Luo, F. (2016). Pulsed radiofrequency reduced neuropathic pain behavior in rats associated with upregulation of GDNF expression. *Pain Phys.* 19, 49–58.

Johnson, R. W., Bouhassira, D., Kassianos, G., Leplège, A., Schmader, K. E., and Weinke, T. (2010). The impact of herpes zoster and post-herpetic neuralgia on quality-of-life. *BMC Med.* 8:37. doi: 10.1186/1741-7015-8-37

Cosman, E. R. Jr., and Cosman, E. R. Sr. (2005). Electricand thermal field effects in tissue around radiofrequency electrodes. *Pain Med.* 6, 405–424. doi: 10.1111/j.1526-4637.2005.00076.x

Kang, C. K., Oh, S. T., Chung, R. K., Lee, H., Park, C. A., Kim, Y. B., et al. (2010). Effect of stellate ganglion block on the cerebrovascular system: magnetic resonance angiography study. *Anesthesiology* 113, 936–944. doi: 10.1097/ALN.0b013e3181ec63f5

Kastler, A., Aubry, S., Sailley, N., Michalakis, D., Siliman, G., Gory, G., et al. (2013). CT-guided stellate ganglion blockade vs. radiofrequency neurolysis in the management of refractory type I complex regional pain syndrome of the upper limb. *Eur. Radiol.* 23, 1316–1322. doi: 10.1007/s00330-012-2704-y

Kim, E. D., Yoo, W. J., Kim, Y. N., and Park, H. J. (2017). Ultrasound-guided pulsed radiofrequency treatment of the cervical sympathetic chain for complex regional pain syndrome: a retrospective observational study. *Medicine* 96:e5856. doi: 10.1097/MD.0000000000005856

Kim, E. M., Yoon, K. B., Lee, J. H., Yoon, D. M., and Kim, D. H. (2013). The effect of oxygen administration on regional cerebral oxygen saturation after stellate ganglion block on the non-blocked side. *Pain Phys.* 16, 117–124.

Kim, M. K., Yi, M. S., Park, P. G., Kang, H., Lee, J. S., and Shin, H. Y. (2018). Effect of stellate ganglion block on the regional hemodynamics of the upper extremity: a randomized controlled trial. *Anesth. Analg.* 126, 1705–1711. doi: 10.1213/ANE.0000000000002528

Lam, C. L., Tse, E. Y., Gandek, B., and Fong, D. Y. (2005). The SF?36 summary scaleswere valid, reliable, and equivalent in a Chinese population. *J. Clin. Epidemiol.* 58, 815–822. doi: 10.1016/j.jclinepi.2004.12.008

Lin, M. L., Lin, W. T., Huang, R. Y., Chen, T. C., Huang, S. H., Chang, C. H., et al. (2014). Pulsed radiofrequency inhibited activation of spinal mitogen-activated protein kinases and ameliorated early neuropathic pain in rats. *Eur. J. Pain* 18, 659–670. doi: 10.1002/j.1532-2149.2013.00419.x

Lipov, E. G., Joshi, J. R., Sanders, S., and Slavin, K. V. (2009). A unifying theory linking the prolonged efficacy of the stellate ganglion block for the treatment of chronic regional pain syndrome (CRPS), hot flashes, and posttraumatic stress disorder (PTSD). *Med. Hypotheses* 72, 657–661. doi: 10.1016/j.mehy.2009.01.009

Liu, C. K., Liao, W. T., Chu, Y. C., Yang, C. H., Chen, K. H., Wu, C. H., et al. (2017). Pulsed radiofrequency attenuates complete freund's adjuvant-induced epigenetic suppression of potassium chloride cotransporter 2 expression. *Pain Med.* 18, 807–813. doi: 10.1093/pm/pnw243

Liu, M. H., Tian, J., Su, Y. P., Wang, T., Xiang, Q., and Wen, L. (2013). Cervical sympathetic block regulates early systemic inflammatory response in severe trauma patients. *Med. Sci. Monit.* 19, 194–201. doi: 10.12659/MSM.883833

Lynch, M. E., and Elgeneidy, A. K. (1996). The role of sympathetic activity in neuropathic orofacial pain. *J. Orofac. Pain* 10, 297–305.

Makharita, M. Y., Amr, Y. M., and El-Bayoumy, Y. (2012). Effect of early stellate ganglion blockade for facial pain from acute herpes zoster and incidence of postherpetic neuralgia. *Pain Phys.* 15, 467–474.

Mulvaney, S. W., McLean, B., and de Leeuw, J. (2010). The use of stellate ganglion block in the treatment of panic/anxiety symptoms with combat-related post-traumatic stress disorder; preliminary results of long-term follow-up: a case series. *Pain Pract.* 10, 359–365. doi: 10.1111/j.1533-2500.2010.00373.x

Nagasako, E. M., Johnson, R. W., Griffin, D. R., and Dworkin, R. H. (2002). Rash severity in herpes zoster: correlates and relationship to postherpetic neuralgia. *J. Am. Acad. Dermatol.* 46, 834–839. doi: 10.1067/mjd.2002.120924

Park, H. M., Kim, T. W., Choi, H. G., Yoon, K. B., and Yoon, D. M. (2010). The change in regional cerebral oxygen saturation after stellate ganglion block. *Korean J. Pain* 23, 142–146. doi: 10.3344/kjp.2010.23.2.142

Podhajsky, R. J., Sekiguchi, Y., Kikuchi, S., and Myers, R. R. (2005). The histologic effects of pulsed and continuous radiofrequency lesions at 42 degrees C to rat dorsal root ganglion and sciatic nerve. *Spine* 30, 1008–1013. doi: 10.1097/01.brs.0000161005.31398.58

Ranson, R. N., Motawei, K., Pyner, S., and Coote, J. H. (1998). The paraventricular nucleus of the hypothalamus sends efferents to the spinal cord of the rat that closely appose sympathetic preganglionic neurones projecting to the stellate ganglion. *Exp. Brain Res.* 120, 164–172. doi: 10.1007/s002210050390

Rehman, S. U., Khan, M. Z., Hussain, R., and Jamshed, A. (2012). Pulsed radiofrequency modulation for lingual neuralgia. *Br. J. Oral. Maxillofac. Surg.* 50, e4–e5. doi: 10.1016/j.bjoms.2011.06.001

Reinauer, S., Goerz, G., Hölzle, E., Heusgen, F., Dinter, W., Tarnow, J., et al. (1994). Distal edema and hyperhidrosis of the arm. Symptoms of reflex sympathetic dystrophy (Sudeck's disease). *Hautarzt* 45, 696–701. doi: 10.1007/s001050050152

Ren, H., Jin, H., Jia, Z., Ji, N., and Luo, F. (2018). Pulsed radiofrequency applied to the sciatic nerve improves neuropathic pain by down-regulating the expression of calcitonin gene-related peptide in the dorsal root ganglion. *Int. J. Med. Sci.* 15, 153–160. doi: 10.7150/ijms.20501

Sacks, G. M. (2013). Unmet need in the treatment of postherpetic neuralgia. *Am. J. Manag. Care* 19, S207–S213.

Singh Rana, S. P., Abraham, M., Gupta, V., Biswas, S., and Marda, M. (2015). Stellate ganglion pulsed radiofrequency ablation for stretch induced complex regional pain syndrome type, II. *Saudi J. Anaesth.* 9, 470–473. doi: 10.4103/1658-354X.159480

Sluijter, M. E. (1997). "Non-thermal radiofrequency proce-dures in the treatment spinal pain," in *Proceedings of the Pain in Europe; Barcelona: 2nd Annual Congress of the European Federation of IASP Chapters*, Barcelona.

Vallejo, R., Tilley, D. M., Williams, J., Labak, S., Aliaga, L., and Benyamin, R. M. (2013). Pulsed radiofrequency modulates pain regulatory gene expression along the nociceptive pathway. *Pain Phys.* 16, E601–E613.

Wang, Q. X., Wang, X. Y., Fu, N. A., Liu, J. Y., and Yao, S. L. (2005). Stellate ganglion block inhibits formalin-induced nociceptive responses: mechanism of action. *Eur. J. Anaesthesiol.* 22, 913–918. doi: 10.1017/S0265021505001559

Westerhaus, M. J., and Loewy, A. D. (2001). Central representation of the sympathetic nervous system in the central cortex. *Brain Res.* 903, 117–127. doi: 10.1016/S0006-8993(01)02453-2

Wu, C. L., Marsh, A., and Dworkin, R. H. (2000). The role of sympathetic nerve blocks in herpes zoster and postherpetic neuralgia. *Pain* 87, 121–129. doi: 10.1016/S0304-3959(00)00230-X

Yokoyama, M., Nakatsuka, H., Itano, Y., and Hirakawa, M. (2000). Stellate ganglion block modifies the distribution of lymphocyte subsets and natural-killer cell activity. *Anesthesiology* 92, 109–115. doi: 10.1097/00000542-200001000-00021

Zhao, W., Wang, Y., Fang, Q., Wu, J., Gao, X., Liu, H., et al. (2017). Changes in neurotrophic and inflammatory factors in the cerebrospinal fluid of patients with postherpetic neuralgia. *Neurosci. Lett.* 637, 108–113. doi: 10.1016/j.neulet.2016.11.041

Conflict of Interest Statement: The authors declare that the research was conducted in the absence of any commercial or financial relationships that could be construed as a potential conflict of interest.

frontiers in Neuroscience

REVIEW
published: 29 March 2019
doi: 10.3389/fnins.2019.00280

Targeted Vagus Nerve Stimulation for Rehabilitation After Stroke

Navzer D. Engineer[1]*, Teresa J. Kimberley[2], Cecília N. Prudente[1], Jesse Dawson[3], W. Brent Tarver[1] and Seth A. Hays[4,5]

[1] MicroTransponder, Inc., Austin, TX, United States, [2] Department of Physical Therapy, School of Health and Rehabilitation Sciences, MGH Institute of Health Professions, Boston, MA, United States, [3] Institute of Cardiovascular and Medical Sciences, College of Medical, Veterinary and Life Sciences, Queen Elizabeth University Hospital, University of Glasgow, Glasgow, United Kingdom, [4] Texas Biomedical Device Center, The University of Texas at Dallas, Richardson, TX, United States, [5] Department of Bioengineering, The University of Texas at Dallas, Richardson, TX, United States

Stroke is a leading cause of disability worldwide, and in approximately 60% of individuals, upper limb deficits persist 6 months after stroke. These deficits adversely affect the functional use of the upper limb and restrict participation in day to day activities. An important goal of stroke rehabilitation is to improve the quality of life by enhancing functional independence and participation in activities. Since upper limb deficits are one of the best predictors of quality of life after stroke, effective interventions targeting these deficits may represent a means to improve quality of life. An increased understanding of the neurobiological processes underlying stroke recovery has led to the development of targeted approaches to improve motor deficits. One such targeted strategy uses brief bursts of Vagus Nerve Stimulation (VNS) paired with rehabilitation to enhance plasticity and support recovery of upper limb function after chronic stroke. Stimulation of the vagus nerve triggers release of plasticity promoting neuromodulators, such as acetylcholine and norepinephrine, throughout the cortex. Timed engagement of neuromodulators concurrent with motor training drives task-specific plasticity in the motor cortex to improve function and provides the basis for paired VNS therapy. A number of studies in preclinical models of ischemic stroke demonstrated that VNS paired with rehabilitative training significantly improved the recovery of forelimb motor function compared to rehabilitative training without VNS. The improvements were associated with synaptic reorganization of cortical motor networks and recruitment of residual motor neurons controlling the impaired forelimb, demonstrating the putative neurobiological mechanisms underlying recovery of motor function. These preclinical studies provided the basis for conducting two multi-site, randomized controlled pilot trials in individuals with moderate to severe upper limb weakness after chronic ischemic stroke. In both studies, VNS paired with rehabilitation improved motor deficits compared to rehabilitation alone. The trials provided support for a 120-patient pivotal study designed to evaluate the efficacy of paired VNS therapy in individuals with chronic ischemic stroke. This manuscript will discuss the neurobiological rationale for VNS therapy, provide an in-depth discussion of both animal and human studies of VNS therapy for stroke, and outline the challenges and opportunities for the future use of VNS therapy.

Keywords: stroke, vagus nerve stimulation, plasticity, rehabilitation, neuromodulation

OPEN ACCESS

Edited by:
Gottfried Schlaug, Beth Israel Deaconess Medical Center, Harvard Medical School, United States

Reviewed by:
Kevin J. Otto, University of Florida, United States
Karim Oweiss, University of Florida, United States

***Correspondence:**
Navzer D. Engineer
navzer@microtransponder.com

Specialty section:
This article was submitted to Neural Technology, a section of the journal Frontiers in Neuroscience

Received: 31 October 2018
Accepted: 08 March 2019
Published: 29 March 2019

Citation:
Engineer ND, Kimberley TJ, Prudente CN, Dawson J, Tarver WB and Hays SA (2019) Targeted Vagus Nerve Stimulation for Rehabilitation After Stroke. Front. Neurosci. 13:280. doi: 10.3389/fnins.2019.00280

INTRODUCTION

Stroke is a leading cause of disability and a significant health burden in the United States and worldwide (Murray et al., 2013; Feigin et al., 2016). Upper limb deficits persist in approximately 60% of individuals after stroke (Wade et al., 1983), limiting their use in day to day activities and impacting quality of life of the individual (Franceschini et al., 2010; Morris et al., 2013). An important goal of stroke rehabilitation research is to develop effective, evidence-based therapies to reduce impairment, facilitate functional upper limb use and improve participation in activities without resorting to compensatory strategies after chronic stroke.

Neurophysiological and neuroimaging studies have provided an improved understanding of the neurobiological processes underlying the brain's ability to restore function by capitalizing on residual networks after stroke (Krakauer, 2004; Ward, 2004; Nudo, 2006; Murphy and Corbett, 2009; Dimyan and Cohen, 2011; Boyd et al., 2017; Sampaio-Baptista et al., 2018). One approach for improving chronic upper limb deficits is to augment this capacity to reorganize, referred to as plasticity. Rehabilitation by itself drives some reorganization of motor networks, but these changes occur within a framework of architectural and anatomical constraints which are believed to limit substantial improvements (Kleim and Jones, 2008). As a result, strategies that can enhance reorganization in conjunction with rehabilitation may support greater recovery. Here, we will describe the neurophysiological basis and implementation of VNS during rehabilitation as a means to enhance plasticity and improve post-stroke recovery.

CHOLINERGIC AND NORADRENERGIC MODULATION OF CORTICAL PLASTICITY

Activation of neuromodulatory networks is strongly linked to plasticity (Gu, 2002), thus engaging these mechanisms provides a potential strategy to enhance plasticity for stroke recovery. Cholinergic neurons within the nucleus basalis (NB) and noradrenergic neurons in the locus coeruleus (LC) are part of the ascending neuromodulatory system that projects diffusely to wide areas of the cortex. Release of acetylcholine (ACh) from NB neurons and norepinephrine (NE) from LC neurons plays an important role in many behavioral and cognitive processes including arousal, memory consolidation and attentional modulation of goal-directed behavior (Gu, 2002; Aston-Jones and Cohen, 2005; Sarter et al., 2005; Hasselmo and Sarter, 2011). The vagus nerve sends projections to the nucleus tractus solitarius (NTS), which in turn projects to the neuromodulatory nuclei. Therefore, understanding the role of these neuromodulatory networks in cortical plasticity is instructive for defining the basis for delivering VNS paired with sensory or motor events to facilitate plasticity.

In a constantly changing world, the brain must extract behaviorally relevant information to drive useful goal-directed behaviors. Neuromodulatory networks, including the cholinergic and noradrenergic systems which provide diffuse neuromodulatory innervation throughout the cortex, are uniquely poised to serve that role. Cholinergic and noradrenergic neurons show phasic discharge during specific epochs of behavior that may signal cue detection, novelty or reinforcement feedback (Hasselmo, 1995; Arnold et al., 2002; Bouret and Sara, 2004; Sarter et al., 2005, 2006, 2009; Parikh et al., 2007; Hasselmo and Sarter, 2011). For example, transient cholinergic activity in cortical neurons signals behaviorally relevant cues while decreased activity is observed with missed cues (Parikh et al., 2007). Rapid cholinergic activation provides reinforcement feedback in response to both positive and negative events (Hangya et al., 2015). Similarly, phasic discharge from LC neurons predicts correct responses in a visual discrimination task with increased cross-correlation among LC neurons (Usher et al., 1999). These studies demonstrate that brief bursts of ACh or NE are likely involved in the attentional modulation of cortical neurons to encode the behavioral relevance of stimulus-specific features during task performance.

The neuromodulator-driven attentional modulation of cortical neurons must eventually be encoded into long-lasting changes in synaptic efficacy with successful task learning (Hess and Donoghue, 1994; Hess and Krawczyk, 1996; Kirkwood et al., 1999; Rioult-Pedotti et al., 2000; Ziemann et al., 2006; Seol et al., 2007; Cohen and Maunsell, 2009; Korchounov and Ziemann, 2011; Carcea and Froemke, 2013; Hasan et al., 2013). At a systems level, the changes in synaptic efficacy may underlie reorganization of cortical maps specific to the learned features of the task (Merzenich et al., 1988; Recanzone et al., 1992, 1993; Pascual-Leone and Torres, 1993; Elbert et al., 1995; Buonomano and Merzenich, 1998; Sterr et al., 1998; Feldman and Brecht, 2005; Feldman, 2009; Froemke, 2015). Furthermore, depletion of cortical ACh or NE resulting from lesions of their respective nuclei or pharmacologic modulation with cholinergic and noradrenergic antagonists blocks cortical plasticity and impairs learning (Sato et al., 1987; Juliano et al., 1991; Heron et al., 1996; Kilgard and Merzenich, 1998; Zhu and Waite, 1998; Conner et al., 2003, 2005; Ramanathan et al., 2009; Vitrac and Benoit-Marand, 2017). Together, these studies established a causal role for the neuromodulatory networks in task-specific learning and plasticity.

The vagus nerve projects to the NTS (Foley and DuBois, 1937; Prechtl and Powley, 1990) and consequently provides rapid activation of the cholinergic and noradrenergic systems (Roosevelt et al., 2006; Nichols et al., 2011; Porter et al., 2012; Hulsey et al., 2017). Therefore, the engagement of these neuromodulatory systems by VNS led to the prediction that brief bursts of VNS paired with sensory or motor experience could enhance cortical plasticity that was specific to the paired experience. Repeatedly pairing a tone with VNS reorganized the rat auditory cortex map, resulting in an expansion for the paired tone (Engineer et al., 2011). A tone paired with trigeminal nerve stimulation did not result in specific auditory cortex plasticity, demonstrating that the enhancement of plasticity was unique to stimulation of the vagus nerve.

Neuromodulatory networks share some features in mediating plasticity in motor and auditory cortices (Gu, 2002; Ramanathan et al., 2009). Since VNS paired with sensory experience drives robust, specific plasticity in the primary sensory cortex, this raised the possibility that pairing VNS with motor training could also facilitate plasticity in naïve rat motor cortex. Indeed, repeatedly pairing VNS with a forelimb movement during motor training increased the corresponding map representation of that movement in motor cortex compared to equivalent training in rats that did not receive VNS (Porter et al., 2012). These studies laid the groundwork for using VNS paired with motor training for improving upper limb deficits after stroke.

VNS IMPROVES MOTOR FUNCTION IN ANIMAL MODELS OF STROKE

Post-stroke recovery is associated with plasticity in motor networks (Murphy and Corbett, 2009). The development of strategies to enhance this plasticity and subsequently generate greater recovery has been the focus of intense research. Based on its ability to drive training-dependent neuroplasticity in uninjured motor networks, a number of animal studies have evaluated VNS paired with rehabilitative training to support the recovery of motor function after stroke.

A study performed in an animal model of ischemic stroke tested the hypothesis that VNS paired with rehabilitative training could enhance post-stroke recovery (Khodaparast et al., 2013). This study sought to evaluate the ability of VNS delivered during motor training to improve recovery of forelimb strength, a main contributor to disability after stroke (Canning et al., 2004; Harris and Eng, 2007). Rats were trained to proficiency on a strength-based forelimb task, and then underwent ischemic lesion of the motor cortex. Rats that received brief bursts of VNS paired with forelimb movement during motor training demonstrated significantly greater recovery of volitional forelimb strength compared to rats that received equivalent training without VNS. Recovery persisted when assessed 1 week after the cessation of stimulation, consistent with the notion that VNS drives stable plasticity and providing an initial indication that the benefits of VNS therapy may be lasting.

A second study built upon these initial findings and assessed the ability of VNS to improve forelimb movement speed after stroke. Rats were pre-trained on a skilled task that measured rapid movement of the forelimb and underwent an ischemic lesion of the motor cortex (Khodaparast et al., 2014). Corroborating findings from the initial study, VNS paired with forelimb movement during rehabilitative training resulted in significant enhancement of functional recovery compared to equivalent rehabilitation training without VNS (**Figure 1A**).

Rehabilitation can become less effective with increasing time after stroke. To evaluate whether a long delay in therapy delivery would impact the efficacy of VNS, a study evaluated whether VNS paired with rehabilitative training could improve recovery in a rat model of chronic ischemic stroke (Khodaparast et al., 2016). VNS and rehabilitative training were initiated on the 7th week post-stroke in rats with chronic, stable forelimb impairment. Despite the delay in starting therapy, VNS delivered with rehabilitative training produced significantly greater forelimb recovery compared to equivalent training without stimulation (**Figure 1B**). The degree of forelimb recovery after chronic stroke was comparable to that observed in previous studies of subacute stroke (Khodaparast et al., 2013, 2014). These findings provide an initial demonstration that the efficacy of VNS paired with rehabilitative training is not dependent on time to begin the intervention after stroke. Additionally, the observation that VNS therapy improves recovery when initiated long after stroke suggests that VNS does not act by augmenting the action of pro-plasticity factors upregulated in response to stroke (Khodaparast et al., 2016). Alternatively, VNS likely acts to enhance recovery by generating repeated, temporally precise, consistent engagement of pro-plasticity neuromodulatory circuits to reinforce rehabilitation-related neural activity (Hays et al., 2013; Hays, 2016). The independence from stroke-related plasticity is consistent with the ability of VNS paired with training to drive cortical plasticity in uninjured animals (Porter et al., 2012; Hulsey et al., 2016).

Advanced age is a major risk factor for stroke and is associated with reduced plasticity, which could in turn influence the effectiveness of VNS therapy. Thus, a study sought to determine whether VNS delivered during rehabilitative training could improve post-stroke recovery in aged rats (Hays et al., 2016). Rats aged at least 18 months were pretrained on a skilled forelimb task and subsequently underwent ischemic lesions of the motor cortex. Pairing VNS with rehabilitative training generated robust improvements in recovery of forelimb strength compared to equivalent training without VNS in aged rats. The magnitude of recovery observed in aged rats that received VNS therapy was comparable to that reported in previous studies using young rats receiving the same intervention (Khodaparast et al., 2013). The similar effectiveness in aged and young rats receiving VNS is consistent with studies suggesting that age alone is not a determinant in the benefits of rehabilitation and provides initial evidence that advanced age does not preclude VNS-dependent enhancement of post-stroke recovery (Bagg et al., 2002).

Generalization of improved functional recovery to tasks that are not explicitly trained during rehabilitation is an important consideration in the translation of therapies for clinical use, as it has practical implications for administration of the therapy. Given a fixed duration for a session of rehabilitation, a therapist would need to determine whether a patient should receive a greater number of stimulation pairings during a more constrained set of rehabilitative exercises or whether to deliver fewer stimulation pairings distributed across a greater breadth of rehabilitative exercises. To provide data to guide this determination, a recent study tested whether the VNS-dependent recovery after stroke would generalize to a similar, untrained task (Meyers E.C. et al., 2018). Rats were pre-trained on a task that measured skilled forelimb rotation, then underwent an ischemic lesion to motor cortex followed by training on the same rotational task with or without VNS. Delivery of VNS paired with rehabilitative training significantly enhanced recovery of forelimb rotation compared to equivalent training without VNS. After the completion of 6 weeks of motor training on the rotation task, all rats were tested on a similar, but distinct task that

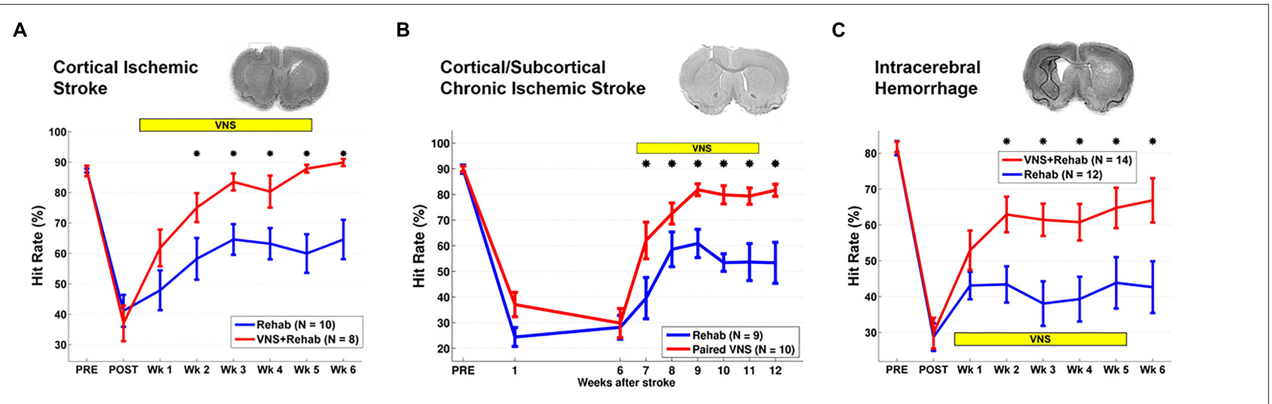

FIGURE 1 | Vagus Nerve Stimulation-dependent recovery of motor function in rat models of stroke. **(A)** VNS paired with rehabilitative training significantly improves recovery of forelimb motor function compared to equivalent training without VNS in a model of cortical ischemic stroke. The top panel shows a coronal brain section with a representative ischemic lesion. Similarly, VNS paired with rehabilitative training enhances recovery of forelimb function after **(B)** chronic combined cortical and subcortical ischemic and **(C)** intracerebral hemorrhage. The symbol "*" indicates $p < 0.05$ across groups at each time point (Adapted from Hays et al., 2014a,b; Khodaparast et al., 2016).

measured volitional forelimb strength. Rats that had previously received VNS paired with rehabilitative training on the rotation task exhibited significantly improved recovery on the volitional strength task compared to rats that had previously received rotation training without VNS, suggesting that VNS-dependent recovery may generalize to similar untrained movements. The magnitude of recovery observed on the untrained task was similar to that observed when VNS was paired with training on the primary task, providing evidence of generalization. Moreover, in this study, VNS-dependent recovery persisted at least 7 weeks following cessation of stimulation, providing additional corroborating evidence that the benefits of VNS are long-lasting.

Other studies provide insight into the implementations of VNS therapy that may be most beneficial. To determine the stimulation paradigm that yields the greatest enhancement in recovery, a study evaluated a range of distinct VNS parameters on recovery of forelimb strength after stroke (Hays et al., 2014b). Delivery of an equivalent amount of VNS that is temporally dissociated from rehabilitative training is less effective at promoting recovery than VNS that is paired with forelimb movement during rehabilitative training, suggesting that non-specific effects of stimulation that do not require precise timing, such as reduction of inflammation or neurogenesis, do not contribute to VNS-dependent enhancement of recovery. Additionally, a paradigm that delivered sixfold more stimulation in rapid succession generated significantly less recovery than VNS explicitly paired with forelimb movement rehabilitation. Together, the results from this study emphasize the need to optimize both the dose and timing of stimulation paradigms for VNS therapy.

Additional studies support the use of VNS therapy for mechanistically distinct forms of cerebrovascular injury. Intracerebral hemorrhage (ICH) is a common and devastating subtype of stroke with few post-injury treatment options. Evidence from preclinical studies indicates that reorganization of spared circuits supports recovery after ICH, similar to ischemic stroke (Auriat et al., 2010; Liang et al., 2013; Santos et al., 2013). Based on the premise that VNS enhances plasticity, a study evaluated whether VNS paired with rehabilitative training may lead to improved recovery in a model of ICH (Hays et al., 2014a). Rats were trained to proficiency on a skilled forelimb task and then received an injection of collagenase into the dorsolateral striatum to induce hemorrhage. Delivery of VNS paired with rehabilitative training significantly enhanced recovery compared to equivalent training without VNS, providing a preliminary demonstration that VNS therapy can improve motor function after ICH (**Figure 1C**). Emerging evidence extends these findings to other distinct forms of neurological damage, indicating VNS can improve recovery in models of traumatic brain injury (Pruitt et al., 2016), spinal cord injury (SCI; Ganzer et al., 2018), and peripheral nerve damage (Meyers E. et al., 2018; **Figure 2**).

Cognitive deficits are not uncommon in patients following ischemic stroke (Tatemichi et al., 1994). Preclinical studies document improvements in memory retention with VNS (Clark et al., 1995, 1998). While a small number of clinical studies provide corroborating evidence for the role of VNS in improving memory function, placebo-controlled studies in larger clinical populations are needed to determine whether VNS facilitates long-term improvement in cognitive function in humans after stroke (Hoppe et al., 2001; Boon et al., 2006; Ghacibeh et al., 2006; Sun et al., 2017). It is possible that short bursts of VNS combined with a cognitive rehabilitative training paradigm may promote plasticity and improve cognitive impairments after stroke. While considerably more development is needed, these findings raise the prospect that pairing VNS with cognitive rehabilitation may represent a potential intervention for post-stroke cognitive impairment.

Despite the evidence demonstrating VNS-dependent enhancement of recovery across a range of preclinical models of neurological injury, the mechanisms that underlie recovery are not thoroughly characterized. In the following section, we will discuss the putative mechanisms by which VNS modulates neural plasticity to support recovery of function.

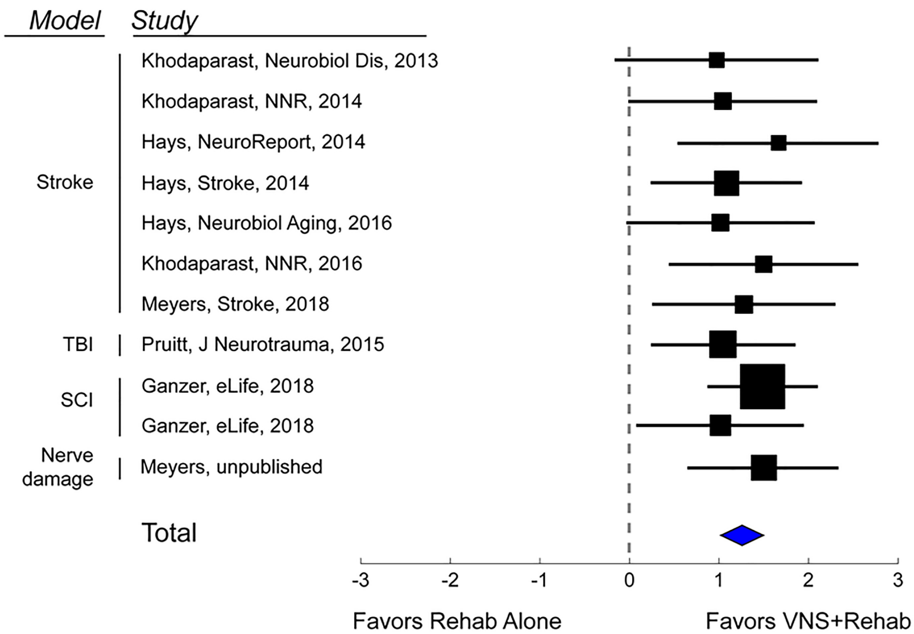

FIGURE 2 | Vagus Nerve Stimulation therapy improves recovery in a variety of models of neurological injury. A meta-analysis of recovery across a range of rat models of neurological damage demonstrates that VNS paired with rehabilitative training (VNS+Rehab) consistently improves recovery of forelimb motor function compared to equivalent rehabilitative training without VNS (Rehab Alone). The data are presented as a forest plot. Markers denote standardized mean difference for VNS+Rehab compared to Rehab Alone for each study, and horizontal lines indicate 95% confidence interval. The size of the indicator represents the number of subjects. The blue diamond represents the summary effect.

NEUROBIOLOGICAL MECHANISMS OF MOTOR RECOVERY AFTER PAIRED VNS

Structural plasticity in descending cortical spinal circuits has been associated with recovery after stroke. A recent study evaluated whether VNS paired with rehabilitative training influenced reorganization of corticospinal tract (CST) connectivity (Meyers E.C. et al., 2018). A retrograde transsynaptic tracing study in rats revealed that VNS paired with rehabilitation tripled synaptic connectivity in CST networks controlling the impaired forelimb compared to equivalent rehabilitation without VNS, providing a direct quantification of VNS-dependent plasticity in motor networks after stroke. This reorganization of CST connectivity was observed 2 months after the cessation of VNS, suggesting that this plasticity is robust and enduring, and consistent with the notion that this plasticity subserves long-term restoration of motor function (**Figure 3**).

Vagus Nerve Stimulation engages a variety of molecular and neuronal mechanisms via the ascending neuromodulatory systems that may underlie the observed reorganization of motor networks. After a stroke, treatment with brain-derived neurotrophic factor (BDNF) increases functional recovery, whereas reduction of BDNF levels prevented the benefits of rehabilitative training (Schabitz et al., 2004; Ploughman et al., 2009). In rodents, both acute and chronic VNS increased levels of BDNF in the hippocampus but the elevated BDNF levels were not associated with improvements in the forced swim or elevated plus-maze tests (Follesa et al., 2007). It remains to be determined whether elevated BDNF levels contribute to motor reorganization and stroke recovery.

Engagement of neuromodulatory networks that regulate synaptic plasticity also represents a means by which VNS likely supports recovery. VNS drives activation of multiple neuromodulatory networks, including the noradrenergic, cholinergic, and serotonergic systems (Nichols et al., 2011; Hulsey et al., 2017). These neuromodulators, in turn, act synergistically to alter spike-timing dependent plasticity (STDP) properties in active networks (Dan and Poo, 2004; Seol et al., 2007). These neuromodulators are known to act within a short window of approximately 5–10 s after neural activity, referred to as the synaptic eligibility trace, to allow STDP (He et al., 2015). Two studies provide initial evidence that VNS generates temporally precise neuromodulatory feedback within the synaptic eligibility trace to drive synaptic plasticity. First, in a study examining plasticity in auditory cortex, only tones presented concurrently with VNS were reinforced (Engineer et al., 2011). Tones delayed 15 s after VNS, which falls outside the time window for synaptic eligibility, failed to generate plasticity. Second, a study examined the requirement for a temporal association between VNS and optimal trials during rehabilitative exercises after SCI (Ganzer et al., 2018). VNS delivery immediately after or within 2 s of the optimal trials significantly enhanced recovery of motor function, while a delay of approximately 25 s from the optimal trials failed to yield any benefits compared to equivalent rehabilitation without VNS.

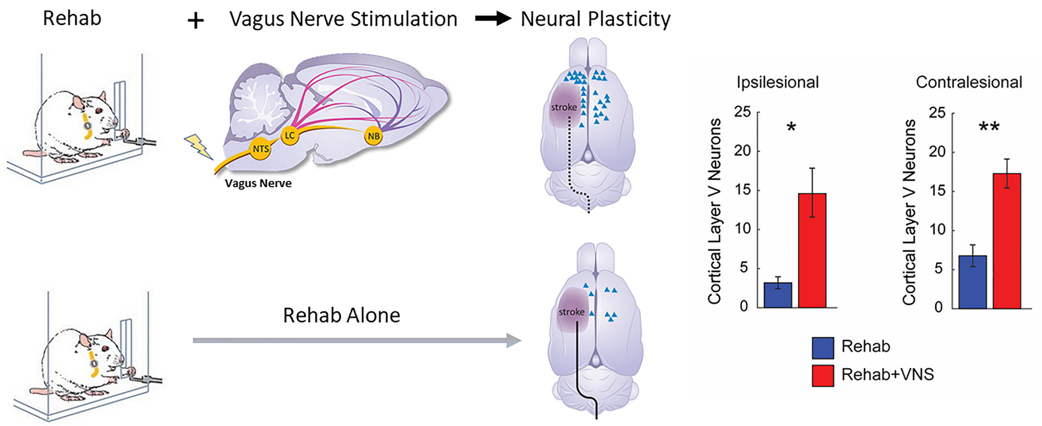

FIGURE 3 | Vagus Nerve Stimulation paired with motor training enhances synaptic reorganization after stroke. Rats that receive VNS paired with motor training (red bar) after stroke demonstrated a significantly greater increase in corticospinal tract (CST) connectivity to rehabilitated muscles compared to equivalent training without VNS (blue bar). CST connectivity originating in both the ipsilesional and contralesional hemispheres was increased. These findings indicate that VNS drives large-scale reorganization in motor networks after stroke which may underlie recovery of function (Adapted from Meyers E.C. et al., 2018). * indicates $p < 0.05$; ** indicates $p < 0.01$.

These studies align well with the time scale of the synaptic eligibility trace and provide a means by which VNS may drive temporally precise neuromodulatory release to reinforce ongoing neural activity related to the paired event.

RANDOMIZED CLINICAL TRIALS TO ASSESS SAFETY AND EFFICACY OF PAIRED VNS AFTER CHRONIC ISCHEMIC STROKE

Transitioning from basic science investigation to clinical studies moves the field closer to determining if these promising findings can translate into improvements in clinical care. Studies are now attempting to translate these preclinical VNS experiments into clinical practice through feasibility, safety, and more recently, pivotal clinical trials in individuals with chronic stroke (Dawson et al., 2016; Kimberley et al., 2018).

A single-blinded, randomized feasibility study evaluating VNS paired with motor rehabilitation was performed by Dawson et al. (2016) in 20 participants with chronic ischemic stroke who had moderate to severe upper limb weakness. Subjects were randomized to VNS paired with rehabilitation ($n = 9$; implanted) or rehabilitation alone ($n = 11$; not implanted). VNS was triggered by a therapist pushing a button during task-specific movements,

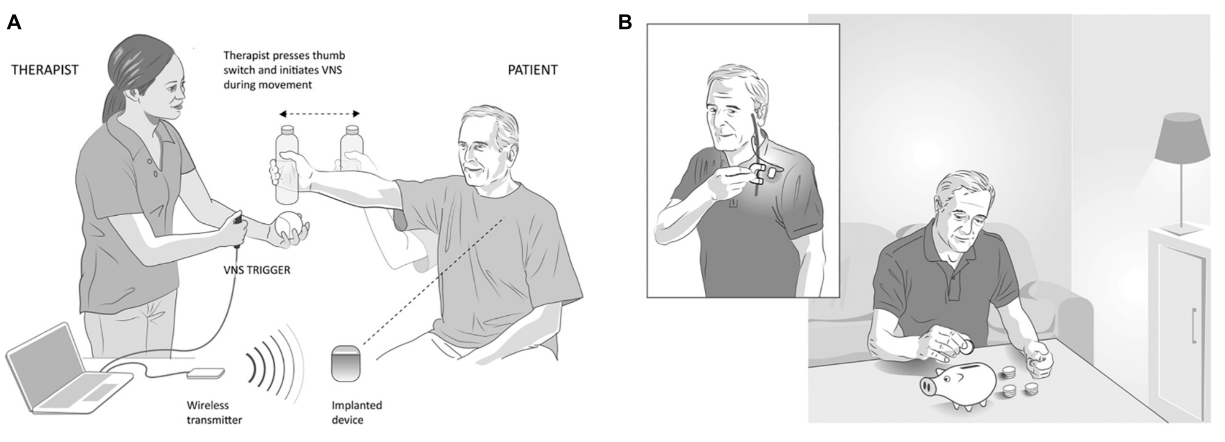

FIGURE 4 | Vagus Nerve Stimulation paired with rehabilitation in the clinic and at home, **(A)** In-clinic rehabilitation with VNS: VNS is delivered by a therapist using a push button timed with a task-specific movement. Pressing the button delivers a brief burst of VNS (0.5 s) during an active goal-directed movement. The VNS system includes an implantable pulse generator (implanted device) that is implanted under the individual's chest wall, an implantable lead, wireless transmitter (for communication between the device and computer) and custom programming software. **(B)** Home-based VNS therapy: Participants are provided a magnet (inset) to swipe over the device once before the start of each rehabilitation session to self-initiate 30 min of VNS (0.5 s burst of VNS every 10 s for 30 min). During the 30 min, participants performed at-home exercises prescribed by the therapist and adapted to their functional level and goals.

based on the notion that VNS provides timed engagement of neuromodulatory networks to support rehabilitation-dependent plasticity (**Figure 4A**). Stimulation parameters were selected based on earlier preclinical studies (Engineer et al., 2011; Porter et al., 2012; Khodaparast et al., 2013, 2014, 2016; Hays et al., 2016; Hulsey et al., 2016). The main outcome measures were a change in upper extremity Fugl-Meyer Assessment (FMA-UE) score and response rate (FMA-UE change ≥6 points was considered clinically meaningful, discussed below). After 6 weeks of in-clinic rehabilitation, participants in the paired VNS group showed a 9.6-point improvement from baseline while the control group improved by 3 points in the per-protocol analysis (between group difference = 6.5 points, CI: 0.4 to 12.6, $p = 0.038$). The response rates were 66 and 36.4% in VNS and control groups, respectively. No serious adverse device effects were reported. These results demonstrated the feasibility of using paired VNS and did not raise safety concerns. Two limitations of this study were the absence of an implanted control VNS group and the lack of assessment of long-lasting effects of paired VNS. These limitations were addressed in a second pilot study (Kimberley et al., 2018).

This second study was a multicenter, fully blinded and randomized study (Kimberley et al., 2018). All participants were implanted with the VNS device, which allowed the control group to crossover to receive paired VNS therapy after completion of blinded follow-up and permitted within-subject comparison of gains. To evaluate the lasting effects of paired VNS, home-based therapy was included as part of the study (**Figure 4B**). Differences between the two studies are highlighted in **Table 1**.

Seventeen participants with chronic ischemic stroke who had moderate to severe upper extremity impairment were enrolled at four sites, with similar surgical procedure and randomization (**Figure 5A**) to the first study. The study design is shown in **Figure 5B**. Participants performed 6 weeks of in-clinic therapy followed by home-based therapy. After 6-weeks of in-clinic therapy, participants in both groups had 1 month of at-home exercises with no VNS followed by 2 months of home-based therapy. During home therapy, participants in both groups activated the VNS device at the start of each 30-min session via a magnet swipe over the implanted pulse generator to deliver either Active or Paired VNS (0.8 mA) or Control VNS (0 mA), respectively (**Figure 4B**).

After 2 months of home-based therapy, the Paired VNS group continued the VNS therapy while the Control Group switched over to receive paired VNS (**Figure 5B**). After 6 weeks of in-clinic therapy, the FMA-UE score increased by 7.6 points for the VNS group and 5.3 points for controls. Three months after the end of in-clinic therapy (post-90), the FMA-UE increased by 9.5 in the paired VNS group and 3.8 points in controls. At post-90, response rate (FMA-UE change ≥6 points) was 88% in the VNS group and 33% in controls ($p = 0.03$) (**Figures 6A,B**).

After controls crossed-over to receive in-clinic Active VNS, FMA-UE improved by 9.8 points from baseline ($p < 0.001$) after 6 weeks. After an additional 2 months of home-based VNS, FMA-UE improvement was maintained at 9.7 points ($p = 0.01$). Therefore, the improvements in upper limb impairment more than doubled after rehabilitation paired VNS compared to rehabilitation alone, an effect of approximately the same magnitude observed in the preclinical studies of VNS for ischemic stroke (Khodaparast et al., 2013).

It is of note that controls received similar intensity of in-clinic and home rehabilitation (without VNS) and showed

TABLE 1 | Comparison of the two pilot VNS studies (Dawson et al., 2016; Kimberley et al., 2018).

	Dawson et al., 2016	Kimberley et al., 2018
Number of sites	2 United Kingdom	4 United States and United Kingdom
Study design	Randomized, single-blind (Assessor)	Randomized, blinded (Assessor, Therapist, Participant), sham-controlled, cross-over
Number of participants	20 (VNS: $n = 9$; Control: $n = 11$)	17 (VNS: $n = 8$; Control: $n = 9$)
VNS implantation	Only VNS group implanted	Both VNS and Control group implanted
Long-term home therapy	No	Yes
Inclusion criteria	ARAT (Action Research Arm Test)	FMA-UE (Fugl-Meyer Assessment – Upper Extremity)
Outcome measure end-points	End of in-clinic (6 weeks) assessment followed by a 30-day assessment	End of in-clinic (6 weeks) assessment followed by 30-day and 3-month assessment
Imaging (Structural MRI)	Yes	Yes
Safety	(One) Transient vocal cord palsy and dysphagia after implant, (Five) minor events including nausea, metallic taste in the mouth. No serious adverse device effects.	(Three) Serious adverse events related to implantation surgery including wound infection, shortness of breath with dysphagia and hoarseness. No serious adverse device effects.
Efficacy (FMA change from baseline at 6 weeks)	9.6 vs. 3 (between group difference = 6.5 points, CI: 0.4 to 12.6, $p = 0.038$). *Response rate: 66% vs. 36.4%	7.6 vs. 5.3 (between group difference = 2.3 points, CI: −1.8 to 6.4, $p = 0.2$). *Response rate: 75% vs. 33%. At 3 months, post-therapy, 9.5 vs. 3.8 (between group difference = 5.7 points, CI: −1.4 to 11.5, $p = 0.055$). *Response rate: 88% vs. 33% ($p = 0.03$).

**FMA change ≥6 points.*

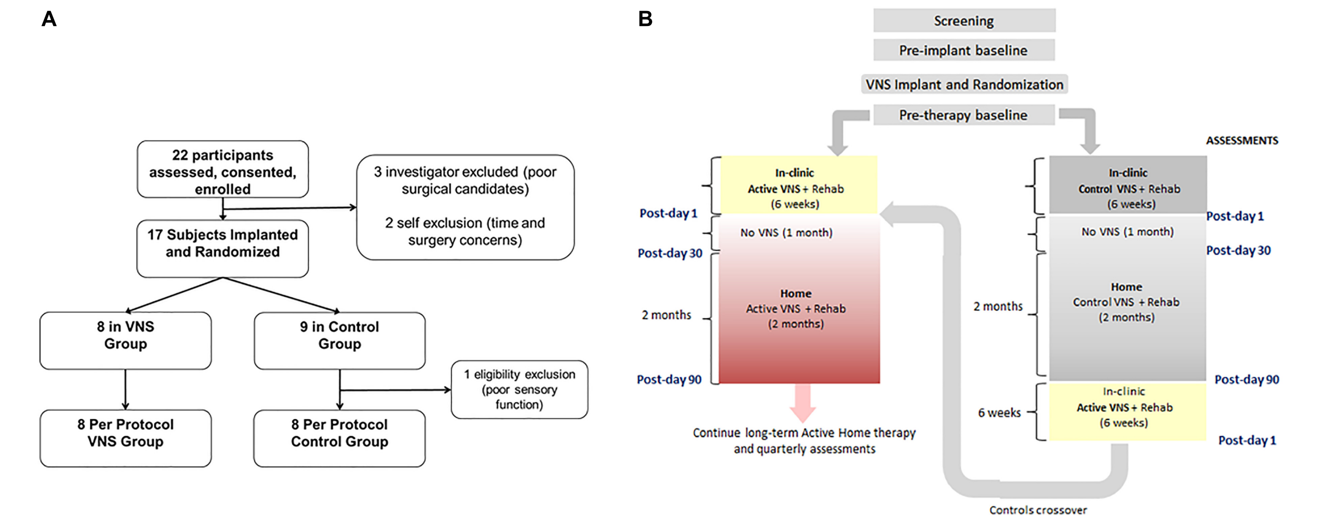

FIGURE 5 | (A) Consort Diagram for the pilot study (from Kimberley et al., 2018). Twenty-two participants were enrolled in the study of which 17 were implanted. Eight participants were randomized to the VNS group and 9 to rehabilitation only **(B)**. Clinical study flowchart. After screening and baseline evaluations, all participants were implanted with a VNS device and randomized to receive either Active (0.8 mA) or Control VNS (0.0 mA) paired with upper limb rehabilitation. Participants received 18 sessions of in-clinic therapy for 6 weeks, followed by a home-based therapy for 3 months (no VNS was delivered to either group during the 1st month of home therapy). The 3-month time point is referred to as Post-day 90. After Post-day 90, the Active VNS group continued with home-based Active VNS, and the Control group crossed over to receive 6-weeks of in-clinic therapy with Active VNS followed by home-based Active VNS, similar to the Active VNS+Rehab group. Outcome measures were evaluated at baseline, Post-day 1, Post-day 30, and Post-day 90.

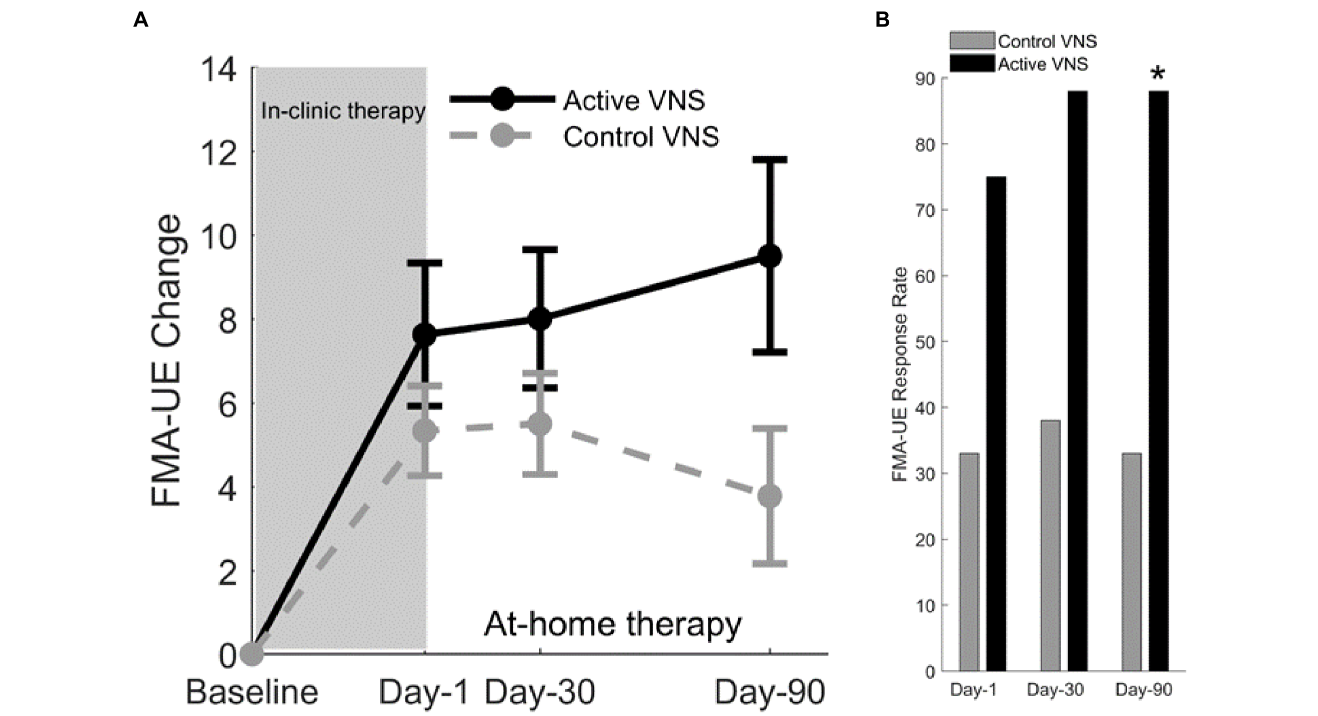

FIGURE 6 | (A) Fugl-Meyer assessment–upper extremity (Kimberley et al., 2018). Change in FMA-UE score at three posttreatment assessments from baseline for Active VNS (solid line) and Control VNS + Rehab (dashed line). Shaded area indicates 6 weeks of in-clinic therapy. Error bars indicated standard error of the mean (s.e.m). **(B)** FMA-UE responder rate (defined as FMA-UE change ≥6 points from baseline) for Active VNS (black) and Control VNS + Rehab (gray). *$p < 0.05$, Fisher exact test.

minimal improvement in the randomized portion of the study, especially as more time elapsed following the in-clinic rehabilitation. After crossover to Active VNS, the control participants showed a clinically meaningful outcome that was similar to the initial Active VNS group. This is consistent with studies suggesting that intense rehabilitation or standard of care rehabilitation for individuals with chronic stroke may be insufficient to significantly improve motor outcomes (van der Lee et al., 1999; Langhorne et al., 2009; Teasell et al., 2014).

In addition to improving motor impairment, Active VNS therapy also improved upper limb functional performance. At post-90 (3 months after the end of in-clinic therapy), the Wolf Motor Function Test (WMFT-Functional) difference between the Paired VNS and Control groups was 0.33 points (CI, 0.04 to 0.61; $p = 0.029$). Thus, participants showed significant improvements on both impairment (FMA-UE) as well as functional scales (WMFT-Functional) after Paired VNS therapy. These results suggest that improvement reflects true motor recovery rather than improved movement compensation. The study showed that rehabilitation paired with VNS was an acceptably safe and feasible intervention for patients with chronic stroke and demonstrated sufficient safety and feasibility to support a larger pivotal trial.

The benefits of Paired VNS require time to emerge and may suggest that progressive neural reorganization is facilitated by paired VNS (Porter et al., 2012; Meyers E.C. et al., 2018). VNS responders had greater cortico-spinal tract (CST) injury compared to control responders, which suggests that VNS-induced neuroplastic mechanisms could facilitate improvements in the VNS responders who would otherwise not have responded to rehabilitation alone (Dawson et al., 2016). These findings also mirror the reorganization of the CST observed with VNS therapy in preclinical models in which VNS paired with rehabilitation significantly increased synaptic connectivity in both ipsilesional and contralesional CST networks controlling the impaired forelimb (Meyers E.C. et al., 2018; **Figure 3**). Assessment of plasticity in multiple brain regions that accompanies improvements in recovery would strengthen future clinical studies by providing a more detailed description of the mechanisms that support VNS-dependent benefits.

A change in FMA-UE score of ≥ 6 points was used to indicate a clinically meaningful improvement. Previous studies have assessed FMA-UE scores using anchor-based methods to determine the clinically important change in FMA-UE from baseline. The FMA-UE change ranged from 4.24 to 7.25 points (Page et al., 2012). A $>50\%$ improvement in the overall arm and hand function, which was considered an excellent improvement, corresponded to FMA-UE change of 5.25 points. If the 9.5-point increase in FMA-UE score observed at day-90 following Paired VNS and the 9.8-point change from baseline after crossover to Paired VNS in Controls is a true effect of VNS, the therapy enhances the modest improvements seen with rehabilitation alone, up to more clinically meaningful levels.

CLINICAL AND NEUROPHYSIOLOGICAL CONSIDERATIONS FOR FUTURE CLINICAL STUDIES

Although the studies described above present initial evidence that VNS paired with rehabilitation may support recovery after stroke, there are several important considerations for continued translation of the VNS therapy.

Clinical and Neurophysiological Biomarkers

Clinical and neurophysiological biomarkers are important for predicting response to interventions, especially in a heterogeneous chronic stroke population (Milot and Cramer, 2008; Burke and Cramer, 2013; Wu et al., 2015; Boyd et al., 2017). It would be valuable to identify biomarkers in patient subpopulations that are non-responsive to the VNS therapy. Biomarker evaluation across a range of stimulation parameters, including intensity, frequency, and pulse width, would be useful to guide the selection of paradigms to maximize plasticity and recovery after stroke. Future studies with larger sample sizes may determine whether clinical and neurophysiological markers will help identify participants more or less responsive to VNS therapy.

A number of characteristics, including age, type of stroke (e.g., ischemic or hemorrhagic), stroke location (e.g., supratentorial or infratentorial), stroke severity, amount of spasticity, associated contractures that may limit movement, time since stroke onset, associated sensory loss, comorbidities (e.g., diabetes), are known to affect outcomes. Moreover, factors that directly impact neuromodulatory function, including Parkinson's disease, Alzheimer's disease and concomitant use of pharmacotherapeutic agents, may specifically impact the efficacy of VNS. These factors will be discussed below.

Supratentorial and Infratentorial Strokes

The clinical VNS studies described above included participants with supratentorial, ischemic stroke and excluded infratentorial strokes. Infratentorial or posterior strokes such as those involving the cerebellum, pons or medulla, were excluded because the behavioral benefits of paired VNS have not yet been demonstrated in preclinical models. Furthermore, individuals with posterior strokes presenting with upper limb weakness likely have other symptoms including dizziness, double vision, visual field deficits, dysphagia, clumsiness of the hand and ataxia that may impact upper limb motor training and therefore would likely require a different rehabilitation protocol. Previous studies have demonstrated that brainstem infarcts can result in the activation or reorganization of motor cortex (Kwon and Jang, 2010). It is possible that Paired VNS therapy could recruit upstream spared CSTs to regain lost function. Furthermore, studies in rat models of SCI showed that VNS paired with motor training drives plasticity in upstream motor neurons, suggesting that VNS-dependent plasticity in residual cortical or subcortical motor circuits could mediate recovery (Ganzer et al., 2018).

Hemorrhagic Stroke

In rat models of hemorrhagic stroke, rehabilitation improves motor outcomes along with changes in dendrite morphology suggesting that plasticity within residual neurons supported recovery (Auriat et al., 2010). Furthermore, studies in a rat model of ICH provide direct evidence that VNS paired with motor training significantly improves forelimb function compared to equivalent training alone (Hays et al., 2014a). However, the clinical VNS studies excluded individuals with hemorrhagic stroke to maximize the ability to detect effects in ischemic stroke patients. Considering the flexibility of VNS to enhance recovery in a wide range of neurological injury animal models including hemorrhagic stroke, future studies evaluating VNS in patients with these types of stroke is warranted.

Age

Age is an important non-modifiable risk factor for ischemic stroke (Bagg et al., 2002; Kelly-Hayes et al., 2003; Saposnik et al., 2008; Hays et al., 2016; Lui and Nguyen, 2018). Advanced age is associated with a reduction in neuroplasticity, which raises the prospect that advanced age may reduce the efficacy of VNS therapy (Kelly-Hayes et al., 2003; Burke and Barnes, 2006; Freitas et al., 2011). However, preclinical studies provide an initial demonstration that age does not limit VNS-dependent enhancement of recovery after stroke, as aged rats benefited from the therapy as much as young rats (Hays et al., 2016). The pilot clinical study (Kimberley et al., 2018) included a wide age-range of participants (37–73 years), and after 3 months of paired VNS therapy, 50% of participants over 65 years of age showed significant improvement in FMA-UE scores ($\geq$6-point change). Therefore, age by itself did not preclude VNS-dependent benefit in responders; and less improvement in non-responders suggests that other factors are involved in determining response to therapy.

Chronic Stroke

The clinical studies included individuals with chronic stroke for the following reasons: First, highlighting the need for interventions that are effective long after the acute stroke episode, an estimated 7.2 million Americans live with chronic post-stroke disability (Benjamin et al., 2018). Second, evidence from preclinical studies supports the efficacy of VNS paired with rehabilitative training when initiated several weeks after stroke (Khodaparast et al., 2016). Thus, VNS likely acted by engaging plasticity-enhancing neuromodulatory circuits during training rather than pro-plasticity factors upregulated by stroke (Meyers E.C. et al., 2018). Third, since spontaneous recovery of upper limb motor deficits is often observed during the first 6 months after stroke, any improvements in upper limb deficits obtained from interventions carried out during this acute phase would be difficult to dissociate from this spontaneous recovery. Indeed, participants with sub-chronic stroke often show greater improvements on the FMA-UE compared to participants with chronic stroke (Shelton et al., 2001; Masiero et al., 2007; Narayan Arya et al., 2011). Finally, acute stroke is a life-changing event for the majority of individuals, and it is likely that most individuals, physicians, and other healthcare professionals would be somewhat reluctant to undergo a non-emergency surgical procedure. The chronic population was therefore selected as a starting point for investigation.

Severity of Upper Limb Deficits

The VNS clinical studies excluded individuals with very severe upper limb deficits who had minimal to no movement in their upper extremity (typically FMA-UE < 15). VNS could be combined with other interventions to initiate movements in this severe population. Since paired VNS in rats facilitated recruitment of residual neurons and increased synaptic connectivity in cortico-spinal networks controlling the impaired forelimb (Meyers E.C. et al., 2018), it is possible that the severity of CST injury may not preclude recovery of the impaired limb function in humans. This would be an interesting area for study once proven effective in a moderately severe population.

Centrally Acting Drugs May Interfere With the Effects of VNS

Since VNS acts via the activation of neuromodulatory pathways, it is possible that certain medications could interfere with the effects of VNS therapy. For example, lipophilic muscarinic antagonists (e.g., scopolamine) or adrenergic antagonists (e.g., metoprolol) easily cross the blood-brain barrier and are known to have central adverse effects which could interfere with the effects of VNS. Animal studies provide supporting evidence that interfering with neuromodulatory networks prevents the plasticity enhancing effects of VNS (Hulsey et al., 2016; Hulsey, 2018). Unlike pharmacological blockade, animal studies utilized methods that resulted in a permanent, virtually complete reduction of neuromodulators. Therefore, pharmacological antagonism may differentially influence the effects of VNS. Nevertheless, given the well-documented literature regarding the central effects of some cholinergic and noradrenergic antagonists on mood, cognitive processing, behavioral performance and neurophysiological indicators of plasticity, some drug exclusions need to be considered in clinical studies.

Sensory Loss

Impaired tactile sensation, stereognosis, and proprioception are common after stroke. Sensory disruption can affect motor function and recovery, since sensorimotor integration is important for successful goal-directed movements (Xerri et al., 1998; Bolognini et al., 2016). With severe sensory loss, the motor deficits can appear to be worse, even in the absence of significant muscle weakness. The motor cortex receives significant input from somatosensory areas, and peripheral nerve lesions or lesions in the somatosensory cortex can significantly alter movement representations in motor cortex and impact motor skill learning (Donoghue and Sanes, 1987; Xerri et al., 1998). Furthermore, lesions of motor cortex can also disrupt sensory function (Nudo et al., 2000).

It is possible that repeatedly pairing VNS with tactile rehabilitation may improve sensory deficits in individuals with significant sensory loss. In a case report study involving a

72-year-old male with sensory deficits, VNS paired with tactile rehabilitation showed clinically meaningful improvements in sensory threshold, proprioception and stereognosis that were long-lasting (Kilgard et al., 2018). It is possible that the pairing narrowed receptive fields from the hand to individual fingers, which may have contributed to the improved tactile perception. Thus, individuals with motor deficits and significant sensory deficits may benefit from VNS combined with tactile training and could show improvements in both sensory as well as motor function.

Comorbid Conditions

Neurodegenerative diseases (e.g., Alzheimer's disease and Parkinson's disease) can deplete neuromodulator reserves in basal forebrain cholinergic neurons and LC neurons (Whitehouse et al., 1981; Coyle et al., 1983; Gesi et al., 2000; Zarow et al., 2003). Since cholinergic and noradrenergic modulation is essential for the effects of VNS, it is possible that decreased neuromodulator reserves may impact VNS-induced plasticity. In such individuals, it is possible that different stimulation parameters may be needed to generate appropriate activation of remaining neuromodulatory networks. Future studies evaluating VNS in both animal models and patients with neurodegenerative diseases is warranted.

Future preclinical and clinical studies in larger populations along with neurophysiological biomarkers as predictors of improvement will help adapt the VNS therapy to different patient subgroups.

OPTIMIZATION OF VNS PARAMETERS

Identification of stimulation parameters and paradigms that yield maximal recovery is an important step in the translation of VNS-based targeted plasticity therapy for stroke. Both the preclinical and clinical studies evaluating motor recovery described above utilized identical stimulation settings of 0.8 mA, 100 μs pulse width, 30 Hz frequency and a pulse train of 0.5 s (Engineer et al., 2011; Porter et al., 2012; Dawson et al., 2016; Kimberley et al., 2018).

Given that VNS-directed plasticity is believed to underlie recovery, a number of studies have characterized stimulation paradigms aimed at increasing the magnitude of VNS-dependent plasticity. The parameter that has been most thoroughly investigated is stimulation intensity. Higher intensity stimulation recruits a larger proportion of vagal fibers and triggers stronger activation of neuromodulatory nuclei, which may improve stroke recovery (Roosevelt et al., 2006; Castoro et al., 2011; Mollet et al., 2013; Hulsey et al., 2017). Paradoxically, a number of studies examining the effects of VNS on neural plasticity and memory indicate that moderate intensity stimulation generates the greatest effects compared to lower and higher intensity stimulation (Clark et al., 1995, 1998, 1999), suggesting that non-linear interactions in upstream targets may be responsible for these effects and VNS operates across a specific range of stimulation parameters.

Increasing the pulse width can compensate for a reduction in stimulation amplitude, indicating that total charge delivered to the nerve is the main predictor of VNS-dependent engagement of neuromodulatory networks and VNS-dependent plasticity (Hulsey et al., 2017; Loerwald et al., 2017). Several studies have examined the influence of varying other stimulation parameters on VNS-dependent plasticity. Increasing the interval between stimulation trains increases the magnitude of VNS-dependent plasticity, an effect ascribed to desensitization of neuromodulatory receptors (Borland et al., 2018). Additionally, similar to the effect of stimulation intensity, the pulse frequency during a VNS train also demonstrates an inverted-U relationship with plasticity. Trains consisting of pulses delivered at moderate frequency rates enhanced cortical plasticity, while slower and faster pulse rates both fail to significantly enhance plasticity (Buell et al., 2018). Taken together, the studies illustrate the influence of both the timing and intensity of stimulation parameters on the magnitude of VNS-dependent plasticity, suggesting manipulation of either or both parameters may be required to optimize efficacy for clinical implementation.

The precise mechanisms that underlie the observed inverted-U relationship between plasticity and several VNS parameters are not fully understood. However, several possibilities could explain this response, the most apparent of which is the effect of stimulation intensity. First, lower stimulation intensities could recruit pro-plasticity neuromodulatory circuits, while higher intensities recruit overriding anti-plasticity networks. As a result, moderate stimulation intensities would produce the greatest enhancement of plasticity by maximally recruiting the low threshold system while suppressing activation of the high threshold system. Other possible explanations relate to receptor activation. Noradrenergic receptors are required for VNS effects and are known to display considerable adaptation (Gainetdinov et al., 2004). Low intensity stimulation may avoid desensitization and allow repeated effective signaling and thus drive plasticity, while high intensity stimulation may produce desensitization that prohibits repeated activation and limits plasticity. Alternatively, activation of different receptor types at differing stimulation intensities could produce an inverted-U effect. Low and moderate intensities of VNS may result in appropriate norepinephrine release to engage higher-affinity α2-adrenergic receptors and promote potentiation, whereas high intensity stimulation may increase norepinephrine levels further to activate lower-affinity β-adrenergic receptors to oppose potentiation. Indeed, this concentration-dependent dichotomy in control of the polarity of plasticity by adrenergic receptors has been described previously (Salgado et al., 2012). A recent study demonstrated that stimulation frequency also imposes an inverted-U effect on the degree of plasticity, consistent with postsynaptic receptor activation as the primary mediator of the response (Buell et al., 2018). It is important to note that both the desensitizing and opposing activation models, as well as many others, may contribute to the inverted-U, as they are not mutually exclusive.

It is not known whether the inverted-U response results from a common underlying principle of cellular and network activity across all brain regions or whether differences in network architecture across different systems would produce different outcomes. It is possible that non-responders to the standard VNS therapy may benefit from a different set of stimulation parameters that operate within this range or circumvent the conditions that perturb neuromodulatory pathways, such as alterations in vagal tone or neuromodulatory function. Furthermore, given the heterogeneity of patient characteristics as well as stroke manifestations described above, it is possible that some subgroups may be more responsive to one set of stimulation settings than others. Clinical studies described above utilized a standard, non-individualized set of stimulation parameters and observed significant improvement in motor deficits in most patients, supporting the notion that a relatively wide effective therapeutic range exists and individual variability is unlikely to preclude benefits (Dawson et al., 2016; Kimberley et al., 2018). Regardless of the underlying mechanism, the differential responses to stimulation parameters highlight the utility of optimizing stimulation parameters to yield the greatest response.

NON-INVASIVE VAGUS NERVE STIMULATION

In recent years, non-invasive transcutaneous methods of stimulating the vagus nerve have emerged as a potential alternative strategy to generate VNS without necessitating a surgical implant. There are two primary ways of delivering non-invasive VNS. The first method, commonly termed tVNS or aVNS, targets the auricular branch of the vagus nerve (ABVN) and consists of the application of stimulation to the skin of the external ear on the tragus and cymba. The second is transcutaneous stimulation of the skin in the neck region over the cervical vagus nerve, commonly referred to as nVNS and targets the underlying cervical vagus.

The two main sites for auricular VNS include the tragus and cymba concha. Recent reports suggest that the extent to which vagal branches innervate the tragus is unclear (Badran et al., 2018a; Burger and Verkuil, 2018) due to inconsistencies in a human cadaver study that described the innervation of the human auricle (Peuker and Filler, 2002). Furthermore, inconsistencies in electrode placement and skin contact coupled with the effects of varying tissue impedance on nerve activation from individual to individual may be impediments to reliable stimulation with tVNS. For example, the electrode is placed over the auricular skin in a relatively small area with dense innervation and it is possible that the spread of current could activate nearby nerves such as the auriculotemporal branch of the mandibular nerve. This combined recruitment complicates the assessment and interpretation of the effects of stimulation of the vagus nerve.

Stimulation parameters using implanted cervical VNS have been well characterized and strongly influence the plasticity effects of VNS. The challenge of identifying and consistently delivering stimulation within a particular range of parameters is magnified by non-invasive stimulation strategies. While tVNS may be able to stimulate the auricular branches of the vagus, the inability to provide consistent, reliable activation may hamper the ability to observe robust effects. Furthermore, the ABVN has five times less A-β fibers compared to the cervical vagus nerve (Safi et al., 2016), which may contribute to its weaker activation of central targets (Ay et al., 2015).

Therefore, while avoiding surgical implantation has advantages, the preponderance of evidence in well-controlled studies points to the failure of these devices to sufficiently and reliably activate key brain structures. For example, in rat models of acute ischemic stroke, cervical VNS resulted in a greater reduction of infarct volume compared to non-invasive VNS (Ay et al., 2009, 2015). Non-invasive VNS also generated less intense c-fos staining in NTS neurons compared to cervical VNS, suggesting less robust activation (Ay et al., 2015). Available data from human studies describing regional brain activation in response to non-invasive VNS varies substantially from study to study (Kraus et al., 2007; Frangos et al., 2015; Yakunina et al., 2017; Badran et al., 2018a). Moreover, human studies using tVNS at the tragus failed to demonstrate significant activation of the locus coeruleus, a key brainstem nucleus in the actions of VNS, compared to sham stimulation (Yakunina et al., 2017; Badran et al., 2018b). These studies may explain the reduced efficacy of human studies with non-invasive VNS compared to cervical VNS (Bauer et al., 2016; Barbella et al., 2018).

A second non-invasive approach is stimulation delivered to the neck region above the cervical vagus nerve (nVNS). This method of non-invasive stimulation has shown efficacy for the treatment of acute episodes of cluster headaches and migraine (Silberstein et al., 2016; Goadsby et al., 2018; Grazzi et al., 2018; Tassorelli et al., 2018). The mechanism of action is thought to arise from VNS-driven activation of NTS, which in turn modulates the activity of the trigeminal cervical complex (TCC) (Moeller et al., 2018) and suppresses the transmission of nociceptive signals to higher pain processing centers (Bohotin et al., 2003). However, NTS also receives direct inputs from the trigeminal and cervical nerves. Since these nerves lie near the vagus nerve, it is possible that these nerves can also activate NTS via the spread of current. Indeed, trigeminal nerve stimulation or peripheral nerve stimulation can modulate nociceptive signals in the TCC via activation of NTS (Contreras et al., 1982; Lewis et al., 1987; Du and Zhou, 1990; Zerari-Mailly et al., 2005; Liu et al., 2014; Mercante et al., 2017) and have therefore been used for the treatment of headaches (Magis et al., 2007, 2013; Saper et al., 2011). Activation of these nerves during nVNS could contribute to headache relief (Henssen et al., 2019). Therefore, both VNS and TNS can modulate nociceptive input via NTS activation and may represent a generalized anti-nociceptive response to stimulation. In contrast, the induction of cortical plasticity is unique to VNS inputs. Repeatedly pairing a tone with cervical VNS, but not TNS, resulted in tone-specific plasticity in the auditory cortex (Engineer et al., 2011).

In addition to NTS, which receives 95% of the vagal input (Magdaleno-Madrigal et al., 2010), key brain regions activated by cervical VNS are also activated by non-invasive VNS including locus coeruleus, amygdala, hippocampus, cingulate and insula (Chae et al., 2003). This implied that the actions of non-invasive VNS were similar to cervical VNS since both methods activate similar upstream targets, and could, therefore, be used as an alternative to cervical VNS. However, many studies have demonstrated these key brain regions are also activated by peripheral nerve stimulation, trigeminal nerve stimulation, and cutaneous stimulation (Kwon et al., 2000; Rouzade-Dominguez et al., 2001; Scherder et al., 2003; Frangos and Komisaruk, 2017; De Cicco et al., 2018). Furthermore, LC neurons can be activated by both aversive stimulation (e.g., tail pinch) as well as cervical VNS (Hulsey et al., 2017). In other words, brain regions activated by VNS are also activated by tactile, arousing or aversive sensory stimuli, suggesting that the activation of these regions is not specific to the vagus nerve. Therefore, nVNS activation of common brain regions does not entail equivalence to cervical VNS.

Furthermore, cervical VNS stimulation parameters have been well characterized and have been shown to modulate plasticity effects across a twofold range of intensities and suggest the existence of a potentially useful therapeutic range of activity (Borland et al., 2016). With non-invasive VNS, the ability to deliver consistent and reliable stimulation within a particular range of parameters to induce plasticity for therapeutic use has not yet been demonstrated. Taken together, these results demonstrate that brain activation of common targets by cervical VNS and non-invasive VNS does not entail similar plasticity or behavioral outcomes. More studies are needed to determine the extent to which the vagus nerve is activated using non-invasive approaches along with a parametric characterization of stimulation parameters.

Recently, two clinical studies were conducted using non-invasive VNS combined with upper limb rehabilitation in individuals with chronic upper extremity weakness after stroke. In a study by Capone et al., (Capone et al., 2017) individuals with chronic ischemic or hemorrhagic stroke were randomized to either tVNS combined with robotic rehabilitation (n = 7) or auricular-sham VNS (ear lobe) combined with robotic rehabilitation (n = 5). The therapy was delivered for 10 days over 2 weeks. After 2 weeks, no significant differences between the tVNS and sham group were observed on the FMA-UE score (5.4 vs. 2.8 points, p = 0.16). While the results are interesting, the sample size precludes drawing distinct conclusions about tVNS efficacy.

In the second single-arm feasibility study (Redgrave et al., 2018), 13 participants more than 3 months post-stroke underwent rehabilitation combined with tVNS for 6 weeks. After tVNS rehabilitation training, the FMA-UE score increased by 17.1 $\pm$ 7.8 points with a $>$10-point change in 83% of patients. It should be noted that the FMA-UE scores used in this study combined motor, sensory, and joint components (0–126 points score) instead of the 0–66 points score that is typically used in many upper-limb stroke studies. Therefore the results are not directly comparable with the cervical VNS studies (Dawson et al., 2016; Kimberley et al., 2018). Several limitations of this study are worth considering. First, the study did not include a sham stimulation control group. Since stimulation was delivered at the maximally tolerable intensity and was thus perceptible, a placebo effect of stimulation cannot be ruled out. Second, some participants were less than 6 months post-stroke, and it is possible that spontaneous recovery could contribute to some of the improvement (Narayan Arya et al., 2011). A future randomized, blinded, placebo-controlled study in chronic stroke patients would be required to determine the efficacy of non-invasive VNS as applied to upper limb rehabilitation.

Further studies are needed to explore the effectiveness of non-invasive VNS, with a specific focus on parametric characterization. Ideally, any non-invasive VNS effects would be benchmarked against implanted VNS to determine the magnitude. As non-invasive stimulation would have demonstrable advantages for patients over implanted VNS, a thorough evaluation in robust, well-designed studies is needed to guide future clinical implementation.

CONCLUSION AND FUTURE DIRECTIONS

The studies reviewed provide a compelling demonstration that VNS-based rehabilitation is a potentially useful strategy to target plasticity and improve motor function for chronic stroke. VNS-dependent rapid engagement of neuromodulatory networks provides a signal to facilitate plasticity in pathways activated by rehabilitative exercises. While the effects of cholinergic and noradrenergic modulation on cortical plasticity have been well documented, other neuromodulators could also play a role in VNS-induced cortical plasticity. Emerging evidence highlights a similar role of serotoninergic systems in the VNS-dependent enhancement of plasticity, paralleling studies demonstrating that VNS activates these neuromodulatory systems (Manta et al., 2009, 2012; Hulsey, 2018). The neurophysiological mechanisms underlying VNS-driven cortical plasticity are complex and likely involve top-down control of neuromodulatory inputs involved in the planning of movements, reward, and decision making (Zmarowski et al., 2005; Convento et al., 2014).

The effects of VNS paired with rehabilitation have been tested across several different animal models of stroke and other neurological injuries and consistently demonstrate significantly greater recovery and enhancement of plasticity when rehabilitation is paired with VNS compared to equivalent rehabilitation without VNS. The flexibility to improve recovery across several injury models demonstrates that VNS engages a generalized mechanism to potentiate benefits specific to rehabilitation. The improved behavioral outcomes across different models along with objective evidence of plasticity after paired VNS informed clinical studies for the inclusion of appropriate patient populations who are likely to benefit from the therapy.

The encouraging findings from the two pilot clinical studies supported the design of a phase III pivotal, multi-site, double-blind, randomized trial (VNS-REHAB) of this intervention with 120 implanted participants and approximately 20 study sites. This study is powered to detect the difference seen in the FMA-UE score at the end of 6-weeks of in-clinic therapy with 80% power. The VNS-REHAB study is approximately 75% enrolled, with enrollment expected to complete in Spring 2019.

Despite the observed improvements across a range of conditions, it is possible that additional factors, including comorbid conditions, stroke etiology, individual variations in anatomy, and drugs or diseases that influence neuromodulatory function, could influence the efficacy of VNS therapy. Evaluation of the clinical effectiveness of paired VNS therapy in heterogeneous stroke populations along with continued development of stimulation parameters and rehabilitative paradigms to individualize and optimize the therapy for specific patient subgroups will improve the potential of this therapy to improve human function and well-being.

AUTHOR CONTRIBUTIONS

NE and SH wrote the manuscript. All authors participated in the discussion of the manuscript and provided significant revisions. All authors approved the final version of the manuscript for submission.

FUNDING

The work was supported by MicroTransponder, Inc. This work was supported by MicroTransponder, Inc. and by the National Institutes of Health R01 NS094384 (SAH).

REFERENCES

Arnold, H. M., Burk, J. A., Hodgson, E. M., Sarter, M., and Bruno, J. P. (2002). Differential cortical acetylcholine release in rats performing a sustained attention task versus behavioral control tasks that do not explicitly tax attention. *Neuroscience* 114, 451–460. doi: 10.1016/S0306-4522(02)00292-0

Aston-Jones, G., and Cohen, J. D. (2005). An integrative theory of locus coeruleus-norepinephrine function: adaptive gain and optimal performance. *Annu. Rev. Neurosci.* 28, 403–450. doi: 10.1146/annurev.neuro.28.061604.135709

Auriat, A. M., Wowk, S., and Colbourne, F. (2010). Rehabilitation after intracerebral hemorrhage in rats improves recovery with enhanced dendritic complexity but no effect on cell proliferation. *Behav. Brain Res.* 214, 42–47. doi: 10.1016/j.bbr.2010.04.025

Ay, I., Lu, J., Ay, H., and Gregory Sorensen, A. (2009). Vagus nerve stimulation reduces infarct size in rat focal cerebral ischemia. *Neurosci. Lett.* 459, 147–151. doi: 10.1016/j.neulet.2009.05.018

Ay, I., Napadow, V., and Ay, H. (2015). Electrical stimulation of the vagus nerve dermatome in the external ear is protective in rat cerebral ischemia. *Brain Stimul.* 8, 7–12. doi: 10.1016/j.brs.2014.09.009

Badran, B. W., Brown, J. C., Dowdle, L. T., Mithoefer, O. J., LaBate, N. T., Coatsworth, J., et al. (2018a). Tragus or cymba conchae? Investigating the anatomical foundation of transcutaneous auricular vagus nerve stimulation (taVNS). *Brain Stimul.* 11, 947–948. doi: 10.1016/j.brs.2018.06.003

Badran, B. W., Jenkins, D. D., DeVries, W. H., Dancy, M., Summers, P. M., Mappin, G. M., et al. (2018b). Transcutaneous auricular vagus nerve stimulation (taVNS) for improving oromotor function in newborns. *Brain Stimul.* 11, 1198–1200. doi: 10.1016/j.brs.2018.06.009

Bagg, S., Pombo, A. P., and Hopman, W. (2002). Effect of age on functional outcomes after stroke rehabilitation. *Stroke* 33, 179–185. doi: 10.1161/hs0102.101224

Barbella, G., Cocco, I., Freri, E., Marotta, G., Visani, E., Franceschetti, S., et al. (2018). Transcutaneous vagal nerve stimulation (t-VNS): an adjunctive treatment option for refractory epilepsy. *Seizure* 60, 115–119. doi: 10.1016/j.seizure.2018.06.016

Bauer, S., Baier, H., Baumgartner, C., Bohlmann, K., Fauser, S., Graf, W., et al. (2016). Transcutaneous Vagus Nerve Stimulation (tVNS) for treatment of drug-resistant epilepsy: a randomized, double-blind clinical trial (cMPsE02). *Brain Stimul.* 9, 356–363. doi: 10.1016/j.brs.2015.11.003

Benjamin, E. J., Virani, S. S., Callaway, C. W., Chamberlain, A. M., Chang, A. R., Cheng, S., et al. (2018). *Heart Disease and Stroke Statistics - 2018 Update: A Report from the*. Dallas, TX: American Heart Association. doi: 10.1161/CIR.0000000000000558

Bohotin, C., Scholsem, M., Multon, S., Martin, D., Bohotin, V., and Schoenen, J. (2003). Vagus nerve stimulation in awake rats reduces formalin-induced nociceptive behaviour and fos-immunoreactivity in trigeminal nucleus caudalis. *Pain* 101, 3–12. doi: 10.1016/S0304-3959(02)00301-9

Bolognini, N., Russo, C., and Edwards, D. J. (2016). The sensory side of post-stroke motor rehabilitation. *Restor. Neurol. Neurosci.* 34, 571–586. doi: 10.3233/RNN-150606

Boon, P., Moors, I., De Herdt, V., and Vonck, K. (2006). Vagus nerve stimulation and cognition. *Seizure* 15, 259–263. doi: 10.1016/j.seizure.2006.02.014

Borland, M., Vrana, W., Moreno, N., and Fogarty, E. (2016). Cortical map plasticity as a function of vagus nerve stimulation intensity. *Brain Stimul.* 9, 117–123. doi: 10.1016/j.brs.2015.08.018

Borland, M. S., Engineer, C. T., Vrana, W. A., Moreno, N. A., Engineer, N. D., Vanneste, S., et al. (2018). The interval between VNS-tone pairings determines the extent of cortical map plasticity. *Neuroscience* 369, 76–86. doi: 10.1016/j.neuroscience.2017.11.004

Bouret, S., and Sara, S. J. (2004). Reward expectation, orientation of attention and locus coeruleus-medial frontal cortex interplay during learning. *Eur. J. Neurosci.* 20, 791–802. doi: 10.1111/j.1460-9568.2004.03526.x

Boyd, L. A., Hayward, K. S., Ward, N. S., Stinear, C. M., Rosso, C., Fisher, R. J., et al. (2017). Biomarkers of stroke recovery: consensus-based core recommendations from the stroke recovery and rehabilitation roundtable. *Neurorehabil. Neural Repair* 31, 864–876. doi: 10.1177/1545968317732680

Buell, E. P., Loerwald, K. W., Engineer, C. T., Borland, M. S., Buell, J. M., Kelly, C. A., et al. (2018). Cortical map plasticity as a function of vagus nerve stimulation rate. *Brain Stimul.* 11, 1218–1224. doi: 10.1016/j.brs.2018.07.045

Buonomano, D. V., and Merzenich, M. M. (1998). Cortical plasticity: from synapses to maps. *Annu. Rev. Neurosci.* 21, 149–186. doi: 10.1146/annurev.neuro.21.1.149

Burger, A. M., and Verkuil, B. (2018). Transcutaneous nerve stimulation via the tragus: are we really stimulating the vagus nerve? *Brain Stimul.* 11, 945–946. doi: 10.1016/j.brs.2018.03.018

Burke, E., and Cramer, S. C. (2013). Biomarkers and predictors of restorative therapy effects after stroke. *Curr. Neurol. Neurosci. Rep.* 13:329. doi: 10.1007/s11910-012-0329-9

Burke, S. N., and Barnes, C. A. (2006). Neural plasticity in the ageing brain. *Nat. Rev. Neurosci.* 7, 30–40. doi: 10.1038/nrn1809

Canning, C. G., Ada, L., Adams, R., and O'Dwyer, N. J. (2004). Loss of strength contributes more to physical disability after stroke than loss of dexterity. *Clin. Rehabil.* 18, 300–308. doi: 10.1191/0269215504cr715oa

Capone, F., Miccinilli, S., Pellegrino, G., Zollo, L., Simonetti, D., Bressi, F., et al. (2017). Transcutaneous vagus nerve stimulation combined with robotic rehabilitation improves upper limb function after stroke. *Neural Plast* 2017:7876507. doi: 10.1155/2017/7876507

Carcea, I., and Froemke, R. C. (2013). Cortical plasticity, excitatory–inhibitory balance, and sensory perception. *Prog. Brain Res.* 2013, 65–90. doi: 10.1016/B978-0-444-63327-9.00003-5

Castoro, M. A., Yoo, P. B., Hincapie, J. G., Hamann, J. J., Ruble, S. B., Wolf, P. D., et al. (2011). Excitation properties of the right cervical vagus nerve in adult dogs. *Exp. Neurol.* 227, 62–68. doi: 10.1016/j.expneurol.2010.09.011

Chae, J.-H., Nahas, Z., Lomarev, M., Denslow, S., Lorberbaum, J. P., Bohning, D. E., et al. (2003). A review of functional neuroimaging studies of vagus nerve stimulation (VNS). *J. Psychiatr. Res.* 37, 443–455. doi: 10.1016/S0022-3956(03)00074-8

Clark, K. B., Krahl, S. E., Smith, D. C., and Jensen, R. A. (1995). Post-training unilateral vagal stimulation enhances retention performance in the rat. *Neurobiol. Learn. Mem.* 63, 213–216. doi: 10.1006/nlme.1995.1024

Clark, K. B., Naritoku, D. K., Smith, D. C., Browning, R. A., and Jensen, R. A. (1999). Enhanced recognition memory following vagus nerve stimulation in human subjects. *Nat. Neurosci.* 2, 94–98. doi: 10.1038/4600

Clark, K. B., Smith, D. C., Hassert, D. L., Browning, R. A., Naritoku, D. K., and Jensen, R. A. (1998). Posttraining electrical stimulation of vagal afferents with concomitant vagal efferent inactivation enhances memory storage processes in the rat. *Neurobiol. Learn. Mem.* 70, 364–373. doi: 10.1006/nlme.1998.3863

Cohen, M. R., and Maunsell, J. H. R. (2009). Attention improves performance primarily by reducing interneuronal correlations. *Nat. Neurosci.* 12, 1594–1600. doi: 10.1038/nn.2439

Conner, J. M., Chiba, A. A., and Tuszynski, M. H. (2005). The basal forebrain cholinergic system is essential for cortical plasticity and functional recovery following brain injury. *Neuron* 46, 173–179. doi: 10.1016/j.neuron.2005.03.003

Conner, J. M., Culberson, A., Packowski, C., Chiba, A. A., and Tuszynski, M. H. (2003). Lesions of the Basal forebrain cholinergic system impair task acquisition and abolish cortical plasticity associated with motor skill learning. *Neuron* 38, 819–829. doi: 10.1016/S0896-6273(03)00288-5

Contreras, R. J., Beckstead, R. M., and Norgren, R. (1982). The central projections of the trigeminal, facial, glossopharyngeal and vagus nerves: an autoradiographic study in the rat. *J. Auton. Nerv. Syst.* 6, 303–322. doi: 10.1016/0165-1838(82)90003-0

Convento, S., Bolognini, N., Fusaro, M., Lollo, F., and Vallar, G. (2014). Neuromodulation of parietal and motor activity affects motor planning and execution. *Cortex* 57, 51–59. doi: 10.1016/j.cortex.2014.03.006

Coyle, J. T., Price, D. L., and DeLong, M. R. (1983). Alzheimer's disease: a disorder of cortical cholinergic innervation. *Science* 219, 1184–1190. doi: 10.1126/science.6338589

Dan, Y., and Poo, M. (2004). Spike timing-dependent plasticity of neural circuits. *Neuron* 44, 23–30. doi: 10.1016/j.neuron.2004.09.007

Dawson, J., Pierce, D., Dixit, A., Kimberley, T. J., Robertson, M., Tarver, B., et al. (2016). Safety, feasibility, and efficacy of vagus nerve stimulation paired with upper-limb rehabilitation after ischemic stroke. *Stroke* 47, 143–150. doi: 10.1161/STROKEAHA.115.010477

De Cicco, V., Tramonti Fantozzi, M. P., Cataldo, E., Barresi, M., Bruschini, L., Faraguna, U., et al. (2018). Trigeminal, visceral and vestibular inputs may improve cognitive functions by acting through the locus coeruleus and the ascending reticular activating system: a new hypothesis. *Front. Neuroanat.* 11:130. doi: 10.3389/fnana.2017.00130

Dimyan, M. A., and Cohen, L. G. (2011). Neuroplasticity in the context of motor rehabilitation after stroke. *Nat. Rev. Neurol.* 7, 76–85. doi: 10.1038/nrneurol.2010.200

Donoghue, J. P., and Sanes, J. N. (1987). Peripheral nerve injury in developing rats reorganizes representation pattern in motor cortex. *Proc. Natl. Acad. Sci. U.S.A.* 84, 1123–1126. doi: 10.1073/pnas.84.4.1123

Du, H. J., and Zhou, S. Y. (1990). Involvement of solitary tract nucleus in control of nociceptive transmission in cat spinal cord neurons. *Pain* 40, 323–331. doi: 10.1016/0304-3959(90)91129-7

Elbert, T., Pantev, C., Wienbruch, C., Rockstroh, B., and Taub, E. (1995). Increased cortical representation of the fingers of the left hand in string players. *Science* 270, 305–307. doi: 10.1126/science.270.5234.305

Engineer, N. D., Riley, J. R., Seale, J. D., Vrana, W. A., Shetake, J. A., Sudanagunta, S. P., et al. (2011). Reversing pathological neural activity using targeted plasticity. *Nature* 470, 101–106. doi: 10.1038/nature09656

Feigin, V. L., Roth, G. A., Naghavi, M., Parmar, P., Krishnamurthi, R., Chugh, S., et al. (2016). Global burden of stroke and risk factors in 188 countries, during 1990-2013: a systematic analysis for the Global Burden of Disease Study 2013. *Lancet Neurol.* 15, 913–924. doi: 10.1016/S1474-4422(16)30073-4

Feldman, D. E. (2009). Synaptic mechanisms for plasticity in neocortex. *Annu. Rev. Neurosci.* 32, 33–55. doi: 10.1146/annurev.neuro.051508.135516

Feldman, D. E., and Brecht, M. (2005). Map plasticity in somatosensory cortex. *Science* 310, 810–815. doi: 10.1126/science.1115807

Foley, J. O., and DuBois, F. S. (1937). Quantitative studies of the vagus nerve in the cat. I. The ratio of sensory to motor fibers. *J. Comp. Neurol.* 67, 49–67. doi: 10.1002/cne.900670104

Follesa, P., Biggio, F., Gorini, G., Caria, S., Talani, G., Dazzi, L., et al.. (2007). Vagus nerve stimulation increases norepinephrine concentration and the gene expression of BDNF and bFGF in the rat brain. *Brain Res.* 1179, 28–34. doi: 10.1016/j.brainres.2007.08.045

Franceschini, M., La Porta, F., Agosti, M., and Massucci, M. (2010). Is health-related-quality of life of stroke patients influenced by neurological impairments at one year after stroke? *Eur. J. Phys. Rehabil. Med.* 46, 389–399.

Frangos, E., Ellrich, J., and Komisaruk, B. R. (2015). Non-invasive access to the vagus nerve central projections via electrical stimulation of the external ear: fMRI evidence in humans. *Brain Stimul.* 8, 624–636. doi: 10.1016/j.brs.2014.11.018

Frangos, E., and Komisaruk, B. R. (2017). Access to vagal projections via cutaneous electrical stimulation of the neck: fMRI evidence in healthy humans. *Brain Stimul.* 10, 19–27. doi: 10.1016/j.brs.2016.10.008

Freitas, C., Perez, J., Knobel, M., Tormos, J. M., Oberman, L., Eldaief, M., et al. (2011). Changes in cortical plasticity across the lifespan. *Front. Aging Neurosci.* 3:5. doi: 10.3389/fnagi.2011.00005

Froemke, R. C. (2015). Plasticity of cortical excitatory-inhibitory balance. *Annu. Rev. Neurosci.* 38, 195–219. doi: 10.1146/annurev-neuro-071714-034002

Gainetdinov, R. R., Premont, R. T., Bohn, L. M., Lefkowitz, R. J., and Caron, M. G. (2004). Desensitization of G protein-coupled receptors and neuronal functions. *Annu. Rev. Neurosci.* 27, 107–144. doi: 10.1146/annurev.neuro.27.070203.144206

Ganzer, P. D., Darrow, M. J., Meyers, E. C., Solorzano, B. R., Ruiz, A. D., Robertson, N. M., et al. (2018). Closed-loop neuromodulation restores network connectivity and motor control after spinal cord injury. *eLife* 7:e32058. doi: 10.7554/eLife.32058

Gesi, M., Soldani, P., Giorgi, F. S., Santinami, A., Bonaccorsi, I., and Fornai, F. (2000). The role of the locus coeruleus in the development of Parkinson's disease. *Neurosci. Biobehav. Rev.* 24, 655–668. doi: 10.1016/S0149-7634(00)00028-2

Ghacibeh, G. A., Shenker, J. I., Shenal, B., Uthman, B. M., and Heilman, K. M. (2006). The influence of vagus nerve stimulation on memory. *Cogn. Behav. Neurol.* 19, 119–122. doi: 10.1097/01.wnn.0000213908.34278.7d

Goadsby, P. J., de Coo, I. F., Silver, N., Tyagi, A., Ahmed, F., Gaul, C., et al. (2018). Non-invasive vagus nerve stimulation for the acute treatment of episodic and chronic cluster headache: a randomized, double-blind, sham-controlled ACT2 study. *Cephalalgia* 38, 959–969. doi: 10.1177/0333102417744362

Grazzi, L., Tassorelli, C., de Tommaso, M., Pierangeli, G., Martelletti, P., Rainero, I., et al. (2018). Practical and clinical utility of non-invasive vagus nerve stimulation (nVNS) for the acute treatment of migraine: a post hoc analysis of the randomized, sham-controlled, double-blind PRESTO trial. *J. Headache Pain* 19:98. doi: 10.1186/s10194-018-0928-1

Gu, Q. (2002). Neuromodulatory transmitter systems in the cortex and their role in cortical plasticity. *Neuroscience* 111, 815–835. doi: 10.1016/S0306-4522(02)00026-X

Hangya, B., Ranade, S. P., Lorenc, M., and Kepecs, A. (2015). Central cholinergic neurons are rapidly recruited by reinforcement feedback. *Cell* 162, 1155–1168. doi: 10.1016/j.cell.2015.07.057

Harris, J. E., and Eng, J. J. (2007). Paretic upper-limb strength best explains arm activity in people with stroke. *Phys. Ther.* 87, 88–97. doi: 10.2522/ptj.20060065

Hasan, M. T., Hernández-González, S., Dogbevia, G., Treviño, M., Bertocchi, I., Gruart, A., et al. (2013). Role of motor cortex NMDA receptors in learning-dependent synaptic plasticity of behaving mice. *Nat. Commun.* 4:2258. doi: 10.1038/ncomms3258

Hasselmo, M. E. (1995). Neuromodulation and cortical function: modeling the physiological basis of behavior. *Behav. Brain Res.* 67, 1–27. doi: 10.1016/0166-4328(94)00113-T

Hasselmo, M. E., and Sarter, M. (2011). Modes and models of forebrain cholinergic neuromodulation of cognition. *Neuropsychopharmacology* 36, 52–73. doi: 10.1038/npp.2010.104

Hays, S. A. (2016). Enhancing rehabilitative therapies with vagus nerve stimulation. *Neurotherapeutics* 13, 382–394. doi: 10.1007/s13311-015-0417-z

Hays, S. A., Khodaparast, N., Hulsey, D. R., Ruiz, A., Sloan, A. M., Rennaker, R. L., et al. (2014a). Vagus nerve stimulation during rehabilitative training improves functional recovery after intracerebral hemorrhage. *Stroke* 45, 3097–3100. doi: 10.1161/STROKEAHA.114.006654

Hays, S. A., Khodaparast, N., Ruiz, A., Sloan, A. M., Hulsey, D. R., Rennaker, R. L., et al. (2014b). The timing and amount of vagus nerve stimulation during rehabilitative training affect poststroke recovery of forelimb strength. *Neuroreport* 25, 676–682. doi: 10.1097/WNR.0000000000000154

Hays, S. A., Khodaparast, N., Sloan, A. M., Fayyaz, T., Hulsey, D. R., Ruiz, A. D., et al. (2013). The bradykinesia assessment task: an automated method to measure forelimb speed in rodents. *J. Neurosci. Methods* 214, 52–61. doi: 10.1016/j.jneumeth.2012.12.022

Hays, S. A., Ruiz, A., Bethea, T., Khodaparast, N., Carmel, J. B., Rennaker, R. L. II, et al. (2016). Vagus Nerve Stimulation during rehabilitative training enhances recovery of forelimb function after ischemic stroke in aged rats. *Neurobiol. Aging* 43, 111–118. doi: 10.1016/j.neurobiolaging.2016.03.030

He, K., Huertas, M., Hong, S. Z., Tie, X. X., Hell, J. W., Shouval, H., et al. (2015). Distinct eligibility traces for LTP and LTD in cortical synapses. *Neuron* 88, 528–538. doi: 10.1016/j.neuron.2015.09.037

Henssen, D. J. H. A., Derks, B., van Doorn, M., Verghoot, N., van Walsum, A.-M. V. C., Staats, P., et al. (2019). Vagus nerve stimulation for primary headache disorders: An anatomical review to explain a clinical phenomenon. *Cephalalgia* 1–5. doi: 10.1177/0333102419833076

Heron, C., Gould, T. J., and Bickford, P. (1996). Acquisition of a runway motor learning task is impaired by a beta adrenergic antagonist in F344 rats. *Behav. Brain Res.* 78, 235–241. doi: 10.1016/0166-4328(95)00252-9

Hess, G., and Donoghue, J. P. (1994). Long-term potentiation of horizontal connections provides a mechanism to reorganize cortical motor maps. *J. Neurophysiol.* 71, 2543–2547. doi: 10.1152/jn.1994.71.6.2543

Hess, G., and Krawczyk, R. (1996). Cholinergic modulation of synaptic transmission in horizontal connections of rat motor cortex. *Acta Neurobiol. Exp.* 56, 863–872.

Hoppe, C., Helmstaedter, C., Scherrmann, J., and Elger, C. E. (2001). No evidence for cognitive side effects after 6 months of vagus nerve stimulation in epilepsy patients. *Epilepsy Behav.* 2, 351–356. doi: 10.1006/ebeh.2001.0219

Hulsey, D. R. (2018). *Neuromodulatory Pathways Required for Targeted Plasticity Therapy*. Doctoral dissertation, The University of Texas at Dallas, Richardson, TX.

Hulsey, D. R., Hays, S. A., Khodaparast, N., Ruiz, A., Das, P., Rennaker, R. L., et al. (2016). Reorganization of motor cortex by vagus nerve stimulation requires cholinergic innervation. *Brain Stimul.* 9, 174–181. doi: 10.1016/j.brs.2015.12.007

Hulsey, D. R., Riley, J. R., Loerwald, K. W., Rennaker, R. L., Kilgard, M. P., and Hays, S. A. (2017). Parametric characterization of neural activity in the locus coeruleus in response to vagus nerve stimulation. *Exp. Neurol.* 289, 21–30. doi: 10.1016/j.expneurol.2016.12.005

Juliano, S. L., Ma, W., and Eslin, D. (1991). Cholinergic depletion prevents expansion of topographic maps in somatosensory cortex. *Proc. Natl. Acad. Sci. U.S.A.* 88, 780–784. doi: 10.1073/pnas.88.3.780

Kelly-Hayes, M., Beiser, A., Kase, C. S., Scaramucci, A., D'Agostino, R. B., and Wolf, P. A. (2003). The influence of gender and age on disability following ischemic stroke: the Framingham study. *J. Stroke Cerebrovasc. Dis.* 12, 119–126. doi: 10.1016/S1052-3057(03)00042-9

Khodaparast, N., Hays, S. A., Sloan, A. M., Fayyaz, T., Hulsey, D. R., Rennaker, R. L., et al. (2014). Vagus nerve stimulation delivered during motor rehabilitation improves recovery in a rat model of stroke. *Neurorehabil. Neural Repair* 28, 698–706. doi: 10.1177/1545968314521006

Khodaparast, N., Hays, S. A., Sloan, A. M., Hulsey, D. R., Ruiz, A., Pantoja, M., et al. (2013). Vagus nerve stimulation during rehabilitative training improves forelimb strength following ischemic stroke. *Neurobiol. Dis.* 60, 80–88. doi: 10.1016/j.nbd.2013.08.002

Khodaparast, N., Kilgard, M. P., Casavant, R., Ruiz, A., Qureshi, I., Ganzer, P. D., et al. (2016). Vagus nerve stimulation during rehabilitative training improves forelimb recovery after chronic ischemic stroke in rats. *Neurorehabil. Neural Repair* 30, 676–684. doi: 10.1177/1545968315616494

Kilgard, M. P., and Merzenich, M. M. (1998). Cortical map reorganization enabled by nucleus basalis activity. *Science* 279, 1714–1718. doi: 10.1126/science.279.5357.1714

Kilgard, M. P., Rennaker, R. L., Alexander, J., and Dawson, J. (2018). Vagus nerve stimulation paired with tactile training improved sensory function in a chronic stroke patient. *Neurorehabilitation* 42, 159–165. doi: 10.3233/NRE-172273

Kimberley, T. J., Pierce, D., Prudente, C. N., Francisco, G. E., Yozbatiran, N., Smith, P., et al. (2018). Vagus nerve stimulation paired with upper limb rehabilitation after chronic stroke. *Stroke* 49, 2789–2792. doi: 10.1161/STROKEAHA.118.022279

Kirkwood, A., Rozas, C., Kirkwood, J., Perez, F., and Bear, M. F. (1999). Modulation of long-term synaptic depression in visual cortex by acetylcholine and norepinephrine. *J. Neurosci.* 19, 1599–1609. doi: 10.1523/JNEUROSCI.19-05-01599.1999

Kleim, J. A., and Jones, T. A. (2008). Principles of experience-dependent neural plasticity: implications for rehabilitation after brain damage. *J. Speech Lang. Hear. Res.* 51, S225–S239. doi: 10.1044/1092-4388(2008/018)

Korchounov, A., and Ziemann, U. (2011). Neuromodulatory neurotransmitters influence LTP-Like plasticity in human cortex: a pharmaco-TMS study. *Neuropsychopharmacology* 36, 1894–1902. doi: 10.1038/npp.2011.75

Krakauer, J. W. (2004). Functional imaging of motor recovery after stroke: remaining challenges. *Curr. Neurol. Neurosci. Rep.* 4, 42–46. doi: 10.1007/s11910-004-0010-z

Kraus, T., Hösl, K., Kiess, O., Schanze, A., Kornhuber, J., and Forster, C. (2007). BOLD fMRI deactivation of limbic and temporal brain structures and mood enhancing effect by transcutaneous vagus nerve stimulation. *J. Neural Transm.* 114, 1485–1493. doi: 10.1007/s00702-007-0755-z

Kwon, Y., Kang, M., Ahn, C., Han, H., Ahn, B., and Lee, J. (2000). Effect of high or low frequency electroacupuncture on the cellular activity of catecholaminergic neurons in the brain stem. *Acupunct. Electrother. Res.* 25, 27–36. doi: 10.3727/036012900816356235

Kwon, Y. H., and Jang, S. H. (2010). Cortical activation pattern in hemiparetic patients with pontine infarct. *Eur. Neurol.* 64, 9–14. doi: 10.1159/000313976

Langhorne, P., Coupar, F., and Pollock, A. (2009). Motor recovery after stroke: a systematic review. *Lancet Neurol.* 8, 741–754. doi: 10.1016/S1474-4422(09)70150-4

Lewis, J. W., Baldrighi, G., and Akil, H. (1987). A possible interface between autonomic function and pain control: opioid analgesia and the nucleus tractus solitarius. *Brain Res.* 424, 65–70. doi: 10.1016/0006-8993(87)91193-0

Liang, H., Yin, Y., Lin, T., Guan, D., Ma, B., Li, C., et al. (2013). Transplantation of bone marrow stromal cells enhances nerve regeneration of the corticospinal tract and improves recovery of neurological functions in a collagenase-induced rat model of intracerebral hemorrhage. *Mol. Cells* 36, 17–24. doi: 10.1007/s10059-013-2306-9

Liu, K., Gao, X.-Y., Li, L., Ben, H., Qin, Q.-G., Zhao, Y.-X., et al. (2014). Neurons in the nucleus tractus solitarius mediate the acupuncture analgesia in visceral pain rats. *Auton. Neurosci.* 186, 91–94. doi: 10.1016/j.autneu.2014.08.004

Loerwald, K. W., Borland, M. S., Rennaker, R. L., Hays, S. A., and Kilgard, M. P. (2017). The interaction of pulse width and current intensity on the extent of cortical plasticity evoked by vagus nerve stimulation. *Brain Stimul.* 11, 271–277. doi: 10.1016/j.brs.2017.11.007

Lui, S. K., and Nguyen, M. H. (2018). Elderly stroke rehabilitation: overcoming the complications and its associated challenges. *Curr. Gerontol. Geriatr. Res.* 2018:9853837. doi: 10.1155/2018/9853837

Magdaleno-Madrigal, V. M., Martínez-Vargas, D., Valdés-Cruz, A., Almazán-Alvarado, S., and Fernández-Mas, R. (2010). Preemptive effect of nucleus of the solitary tract stimulation on amygdaloid kindling in freely moving cats. *Epilepsia* 51, 438–444. doi: 10.1111/j.1528-1167.2009.02337.x

Magis, D., Allena, M., Bolla, M., De Pasqua, V., Remacle, J.-M., and Schoenen, J. (2007). Occipital nerve stimulation for drug-resistant chronic cluster headache: a prospective pilot study. *Lancet Neurol.* 6, 314–321. doi: 10.1016/S1474-4422(07)70058-3

Magis, D., Sava, S., d'Elia, T. S., Baschi, R., and Schoenen, J. (2013). Safety and patients' satisfaction of transcutaneous Supraorbital NeuroStimulation (tSNS) with the Cefaly®device in headache treatment: a survey of 2,313 headache sufferers in the general population. *J. Headache Pain* 14:95. doi: 10.1186/1129-2377-14-95

Manta, S., Dong, J., Debonnel, G., and Blier, P. (2009). Enhancement of the function of rat serotonin and norepinephrine neurons by sustained vagus nerve stimulation. *J. Psychiatry Neurosci.* 34, 272–280.

Manta, S., El Mansari, M., and Blier, P. (2012). Novel attempts to optimize vagus nerve stimulation parameters on serotonin neuronal firing activity in the rat brain. *Brain Stimul.* 5, 422–429. doi: 10.1016/j.brs.2011.04.005

Masiero, S., Celia, A., Rosati, G., and Armani, M. (2007). Robotic-assisted rehabilitation of the upper limb after acute stroke. *Arch. Phys. Med. Rehabil.* 88, 142–149. doi: 10.1016/j.apmr.2006.10.032

Mercante, B., Enrico, P., Floris, G., Quartu, M., Boi, M., Serra, M. P., et al. (2017). Trigeminal nerve stimulation induces Fos immunoreactivity in selected brain regions, increases hippocampal cell proliferation and reduces seizure severity in rats. *Neuroscience* 361, 69–80. doi: 10.1016/j.neuroscience.2017.08.012

Merzenich, M. M., Recanzone, G. H., Jenkind, W. M., Allard, T. T., and Nudo, R. J. (1988). "Cortical representational plasticity," in *Neurobiology Neocortex*, eds P. Rakic and W. Singer (Hoboken, NJ: John Wiley & Sons Limited), 41–67. doi: 10.1152/jn.00493.2013

Meyers, E., Kasliwal, N., Lai, E., Romero-Ortega, M., Rennaker, R., Kilgard, M., et al. (2018). *Restoring Central Networks Improves Motor and Sensory Function After Nerve Damage. in Society for Neuroscience*. Available at: https://abstractsonline.com/pp8/#!/4649/presentation/29258 [accessed October 29, 2018].

Meyers, E. C., Solorzano, B. R., James, J., Ganzer, P. D., Lai, E. S., Rennaker, R. L., et al. (2018). Vagus nerve stimulation enhances stable plasticity and generalization of stroke recovery. *Stroke* 49, 710–717. doi: 10.1161/STROKEAHA.117.019202

Milot, M.-H., and Cramer, S. C. (2008). Biomarkers of recovery after stroke. *Curr. Opin. Neurol.* 21, 654–659. doi: 10.1097/WCO.0b013e3283186f96

Moeller, M., Schroeder, C. F., and May, A. (2018). Vagus nerve stimulation modulates the cranial trigeminal autonomic reflex. *Ann. Neurol.* 84, 886–892. doi: 10.1002/ana.25366

Mollet, L., Raedt, R., Delbeke, J., El Tahry, R., Grimonprez, A., Dauwe, I., et al. (2013). Electrophysiological responses from vagus nerve stimulation in rats. *Int. J. Neural Syst.* 23:1350027. doi: 10.1142/S0129065713500275

Morris, J. H., Van Wijck, F., Joice, S., and Donaghy, M. (2013). Predicting health related quality of life 6 months after stroke: the role of anxiety and upper limb dysfunction. *Disabil. Rehabil.* 35, 291–299. doi: 10.3109/09638288.2012.691942

Murphy, T. H., and Corbett, D. (2009). Plasticity during stroke recovery: from synapse to behaviour. *Nat. Rev. Neurosci.* 10, 861–872. doi: 10.1038/nrn2735

Murray, C. J. L., Atkinson, C., Bhalla, K., Birbeck, G., Burstein, R., Chou, D., et al. (2013). The state of US health, 1990-2010. *JAMA* 310, 591–608. doi: 10.1001/jama.2013.13805

Narayan Arya, K., Verma, R., and Garg, R. K. (2011). Estimating the minimal clinically important difference of an upper extremity recovery measure in subacute stroke patients. *Top. Stroke Rehabil.* 18, 599–610. doi: 10.1310/tsr18s01-599

Nichols, J. A., Nichols, A. R., Smirnakis, S. M., Engineer, N. D., Kilgard, M. P., and Atzori, M. (2011). Vagus nerve stimulation modulates cortical synchrony and excitability through the activation of muscarinic receptors. *Neuroscience* 189, 207–214. doi: 10.1016/j.neuroscience.2011.05.024

Nudo, R. J. (2006). Mechanisms for recovery of motor function following cortical damage. *Curr. Opin. Neurobiol.* 16, 638–644. doi: 10.1016/j.conb.2006.10.004

Nudo, R. J., Friel, K. M., and Delia, S. W. (2000). Role of sensory deficits in motor impairments after injury to primary motor cortex. *Neuropharmacology* 39, 733–742. doi: 10.1016/S0028-3908(99)00254-3

Page, S. J., Fulk, G. D., and Boyne, P. (2012). Clinically important differences for the upper-extremity fugl-meyer scale in people with minimal to moderate impairment due to chronic stroke. *Phys. Ther.* 92, 791–798. doi: 10.2522/ptj.20110009

Parikh, V., Kozak, R., Martinez, V., and Sarter, M. (2007). Prefrontal acetylcholine release controls cue detection on multiple timescales. *Neuron* 56, 141–154. doi: 10.1016/j.neuron.2007.08.025

Pascual-Leone, A., and Torres, F. (1993). Plasticity of the sensorimotor cortex representation of the reading finger in Braille readers. *Brain* 116(Pt 1), 39–52. doi: 10.1093/brain/116.1.39

Peuker, E. T., and Filler, T. J. (2002). The nerve supply of the human auricle. *Clin. Anat.* 15, 35–37. doi: 10.1002/ca.1089

Ploughman, M., Windle, V., McAllen, C. L., White, N., Dore, J. J., and Corbett, D. (2009). Brain-derived neurotrophic factor contributes to recovery of skilled reaching after focal ischemia in rats. *Stroke* 40, 1490–1495. doi: 10.1161/STROKEAHA.108.531806

Porter, B. A., Khodaparast, N., Fayyaz, T., Cheung, R. J., Ahmed, S. S., Vrana, W. A., et al. (2012). Repeatedly pairing vagus nerve stimulation with a movement reorganizes primary motor cortex. *Cereb. Cortex* 22, 2365–2374. doi: 10.1093/cercor/bhr316

Prechtl, J. C., and Powley, T. L. (1990). The fiber composition of the abdominal vagus of the rat. *Anat. Embryol.* 181, 101–115. doi: 10.1007/BF00198950

Pruitt, D. T., Schmid, A. N., Kim, L. J., Abe, C. M., Trieu, J. L., Choua, C., et al. (2016). Vagus nerve stimulation delivered with motor training enhances recovery of function after traumatic brain injury. *J. Neurotrauma* 33, 871–879. doi: 10.1089/neu.2015.3972

Ramanathan, D., Tuszynski, M. H., and Conner, J. M. (2009). The basal forebrain cholinergic system is required specifically for behaviorally mediated cortical map plasticity. *J. Neurosci.* 29, 5992–6000. doi: 10.1523/JNEUROSCI.0230-09.2009

Recanzone, G. H., Merzenich, M. M., Jenkins, W. M., Grajski, K. A., and Dinse, H. R. (1992). Topographic reorganization of the hand representation in cortical area 3b owl monkeys trained in a frequency-discrimination task. *J. Neurophysiol.* 67, 1031–1056. doi: 10.1152/jn.1992.67.5.1031

Recanzone, G. H., Schreiner, C. E., and Merzenich, M. M. (1993). Plasticity in the frequency representation of primary auditory cortex following discrimination training in adult owl monkeys. *J. Neurosci.* 13, 87–103. doi: 10.1523/JNEUROSCI.13-01-00087.1993

Redgrave, J. N., Moore, L., Oyekunle, T., Ebrahim, M., Falidas, K., Snowdon, N., et al. (2018). Transcutaneous auricular vagus nerve stimulation with concurrent upper limb repetitive task practice for poststroke motor recovery: a pilot study. *J. Stroke Cerebrovasc. Dis.* 27, 1998–2005. doi: 10.1016/j.jstrokecerebrovasdis.2018.02.056

Rioult-Pedotti, M. S., Friedman, D., and Donoghue, J. P. (2000). Learning-induced LTP in neocortex. *Science* 290, 533–536. doi: 10.1126/science.290.5491.533

Roosevelt, R. W., Smith, D. C., Clough, R. W., Jensen, R. A., and Browning, R. A. (2006). Increased extracellular concentrations of norepinephrine in cortex and hippocampus following vagus nerve stimulation in the rat. *Brain Res.* 1119, 124–132. doi: 10.1016/j.brainres.2006.08.048

Rouzade-Dominguez, M. L., Curtis, A. L., and Valentino, R. J. (2001). Role of Barrington's nucleus in the activation of rat locus coeruleus neurons by colonic distension. *Brain Res.* 917, 206–218. doi: 10.1016/S0006-8993(01)02917-1

Safi, S., Ellrich, J., and Neuhuber, W. (2016). Myelinated axons in the auricular branch of the human vagus nerve. *Anat. Rec.* 299, 1184–1191. doi: 10.1002/ar.23391

Salgado, H., Köhr, G., and Treviño, M. (2012). Noradrenergic 'Tone' determines dichotomous control of cortical spike-timing-dependent plasticity. *Sci. Rep.* 2:417. doi: 10.1038/srep00417

Sampaio-Baptista, C., Sanders, Z.-B., and Johansen-Berg, H. (2018). Structural plasticity in adulthood with motor learning and stroke rehabilitation. *Annu. Rev. Neurosci.* 41, 25–40. doi: 10.1146/annurev-neuro-080317-062015

Santos, M. V., Pagnussat, A. S., Mestriner, R. G., and Netto, C. A. (2013). Motor skill training promotes sensorimotor recovery and increases microtubule-associated protein-2 (MAP-2) immunoreactivity in the motor cortex after intracerebral hemorrhage in the rat. *ISRN Neurol.* 2013:159184. doi: 10.1155/2013/159184

Saper, J. R., Dodick, D. W., Silberstein, S. D., McCarville, S., Sun, M., and Goadsby, P. J. (2011). Occipital nerve stimulation for the treatment of intractable chronic migraine headache: ONSTIM feasibility study. *Cephalalgia* 31, 271–285. doi: 10.1177/0333102410381142

Saposnik, G., Cote, R., Phillips, S., Gubitz, G., Bayer, N., Minuk, J., et al. (2008). Stroke outcome in those over 80. *Stroke* 39, 2310–2317. doi: 10.1161/STROKEAHA.107.511402

Sarter, M., Gehring, W. J., and Kozak, R. (2006). More attention must be paid: the neurobiology of attentional effort. *Brain Res. Rev.* 51, 145–160. doi: 10.1016/j.brainresrev.2005.11.002

Sarter, M., Hasselmo, M. E., Bruno, J. P., and Givens, B. (2005). Unraveling the attentional functions of cortical cholinergic inputs: interactions between signal-driven and cognitive modulation of signal detection. *Brain Res. Rev.* 48, 98–111. doi: 10.1016/j.brainresrev.2004.08.006

Sarter, M., Parikh, V., and Howe, W. M. (2009). Phasic acetylcholine release and the volume transmission hypothesis: time to move on. *Nat. Rev. Neurosci.* 10, 383–390. doi: 10.1038/nrn2635

Sato, H., Hata, Y., Masui, H., and Tsumoto, T. (1987). A functional role of cholinergic innervation to neurons in the cat visual cortex. *J. Neurophysiol.* 58, 765–780. doi: 10.1152/jn.1987.58.4.765

Schabitz, W.-R., Berger, C., Kollman, R., Seitz, M., Tanay, E., Kiessling, M., et al.. (2004). Effect of brain-derived neurotrophic factor treatment and forced arm use on functional motor recovery after small cortical ischemia. *Stroke* 35, 992–997. doi: 10.1161/01.STR.0000119754.85848.0D

Scherder, E. J. A., Luijpen, M. W., and van Dijk, K. R. A. (2003). Activation of the dorsal raphe nucleus and locus coeruleus by transcutaneous electrical nerve stimulation in Alzheimer's disease: a reconsideration of stimulation-parameters derived from animal studies. *Chin. J. Physiol.* 46, 143–150.

Seol, G. H., Ziburkus, J., Huang, S., Song, L., Kim, I. T., Takamiya, K., et al. (2007). Neuromodulators control the polarity of spike-timing-dependent synaptic plasticity. *Neuron* 55, 919–929. doi: 10.1016/j.neuron.2007.08.013

Shelton, F. D., Volpe, B. T., and Reding, M. (2001). Motor impairment as a predictor of functional recovery and guide to rehabilitation treatment after stroke. *Neurorehabil. Neural Repair* 15, 229–237. doi: 10.1177/154596830101500311

Silberstein, S. D., Mechtler, L. L., Kudrow, D. B., Calhoun, A. H., McClure, C., Saper, J. R., et al. (2016). Non-invasive vagus nerve stimulation for the ACute treatment of cluster headache: findings from the randomized, double-blind, sham-controlled ACT1 study. *Headache* 56, 1317–1332. doi: 10.1111/head.12896

Sterr, A., Müller, M. M., Elbert, T., Rockstroh, B., Pantev, C., and Taub, E. (1998). Perceptual correlates of changes in cortical representation of fingers in blind multifinger Braille readers. *J. Neurosci.* 18, 4417–4423. doi: 10.1523/JNEUROSCI.18-11-04417.1998

Sun, L., Peräkylä, J., Holm, K., Haapasalo, J., Lehtimäki, K., Ogawa, K. H., et al. (2017). Vagus nerve stimulation improves working memory performance. *J. Clin. Exp. Neuropsychol.* 39, 954–964. doi: 10.1080/13803395.2017.1285869

Tassorelli, C., Grazzi, L., de Tommaso, M., Pierangeli, G., Martelletti, P., Rainero, I., et al. (2018). Noninvasive vagus nerve stimulation as acute therapy for migraine: the randomized PRESTO study. *Neurology* 91, e364–e373. doi: 10.1212/WNL.0000000000005857

Tatemichi, T. K., Desmond, D. W., Stern, Y., Paik, M., Sano, M., and Bagiella, E. (1994). Cognitive impairment after stroke: frequency, patterns, and relationship to functional abilities. *J. Neurol. Neurosurg. Psychiatry* 57, 202–207. doi: 10.1136/jnnp.57.2.202

Teasell, R., Foley, N., Salter, K., Richardson, M., Mbbs, N. H., Bhogal, S., et al. (2014). *Evidence-Based Review of Stroke Rehabilitation*, 16th Edn. Ontario: Heart and Stroke Foundation, 1–35. doi: 10.1111/j.2044-8341.1998.tb00988.x

Usher, M., Cohen, J. D., Servan-Schreiber, D., Rajkowski, J., and Aston-Jones, G. (1999). The role of locus coeruleus in the regulation of cognitive performance. *Science* 283, 549–554. doi: 10.1126/science.283.5401.549

van der Lee, J. H., Wagenaar, R. C., Lankhorst, G. J., Vogelaar, T. W., Devillé, W. L., and Bouter, L. M. (1999). Forced use of the upper extremity in chronic stroke patients: results from a single-blind randomized clinical trial. *Stroke* 30, 2369–2375. doi: 10.1161/01.STR.30.11.2369

Vitrac, C., and Benoit-Marand, M. (2017). Monoaminergic modulation of motor cortex function. *Front. Neural Circuits* 11:72. doi: 10.3389/fncir.2017.00072

Wade, D. T., Langton-Hewer, R., Wood, V. A., Skilbeck, C. E., and Ismail, H. M. (1983). The hemiplegic arm after stroke: measurement and recovery. *J. Neurol. Neurosurg. Psychiatry* 46, 521–524. doi: 10.1136/jnnp.46.6.521

Ward, N. S. (2004). Functional reorganization of the cerebral motor system after stroke. *Curr. Opin. Neurol.* 17, 725–730. doi: 10.1097/00019052-200412000-00013

Whitehouse, P. J., Price, D. L., Clark, A. W., Coyle, J. T., and DeLong, M. R. (1981). Alzheimer disease: evidence for selective loss of cholinergic neurons in the nucleus basalis. *Ann. Neurol.* 10, 122–126. doi: 10.1002/ana.410100203

Wu, J., Quinlan, E. B., Dodakian, L., McKenzie, A., Kathuria, N., Zhou, R. J., et al. (2015). Connectivity measures are robust biomarkers of cortical function and plasticity after stroke. *Brain* 138, 2359–2369. doi: 10.1093/brain/awv156

Xerri, C., Merzenich, M. M., Peterson, B. E., and Jenkins, W. (1998). Plasticity of primary somatosensory cortex paralleling sensorimotor skill recovery from stroke in adult monkeys. *J. Neurophysiol.* 79, 2119–2148. doi: 10.1152/jn.1998.79.4.2119

Yakunina, N., Kim, S. S., and Nam, E. C. (2017). Optimization of transcutaneous vagus nerve stimulation using functional MRI. *Neuromodulation* 20, 290–300. doi: 10.1111/ner.12541

Zarow, C., Lyness, S. A., Mortimer, J. A., and Chui, H. C. (2003). Neuronal loss is greater in the locus coeruleus than nucleus basalis and *Substantia nigra* in alzheimer and Parkinson diseases. *Arch. Neurol.* 60, 337–341. doi: 10.1001/archneur.60.3.337

Zerari-Mailly, F., Buisseret, P., Buisseret-Delmas, C., and Nosjean, A. (2005). Trigemino-solitarii-facial pathway in rats. *J. Comp. Neurol.* 487, 176–189. doi: 10.1002/cne.20554

Zhu, X. O., and Waite, P. M. (1998). Cholinergic depletion reduces plasticity of barrel field cortex. *Cereb. Cortex* 8, 63–72. doi: 10.1093/cercor/8.1.63

Ziemann, U., Meintzschel, F., Korchounov, A., and Ilić, T. V. (2006). Pharmacological modulation of plasticity in the human motor cortex. *Neurorehabil. Neural Repair* 20, 243–251. doi: 10.1177/1545968306287154

Zmarowski, A., Sarter, M., and Bruno, J. P. (2005). NMDA and dopamine interactions in the nucleus accumbens modulate cortical acetylcholine release. *Eur. J. Neurosci.* 22, 1731–1740. doi: 10.1111/j.1460-9568.2005.04333.x

Conflict of Interest Statement: NE, CP, and WBT are employees of MicroTransponder. JD and TK have presented some of this work at conferences and have received reimbursement.

The remaining author declares that the research was conducted in the absence of any commercial or financial relationships that could be construed as a potential conflict of interest.

frontiers in Neuroscience

ORIGINAL RESEARCH
published: 11 April 2019
doi: 10.3389/fnins.2019.00286

Single Sessions of High-Definition Transcranial Direct Current Stimulation Do Not Alter Lower Extremity Biomechanical or Corticomotor Response Variables Post-stroke

*John Harvey Kindred[1,2], Steven A. Kautz[1,2,3], Elizabeth Carr Wonsetler[1,3,4] and Mark Goodman Bowden[1,2,3]**

[1] Ralph H. Johnson, Veteran's Administration Medical Center, Charleston, SC, United States, [2] Division of Physical Therapy, College of Health Professions, Medical University of South Carolina, Charleston, SC, United States, [3] Department of Health Sciences and Research, College of Health Professions, Medical University of South Carolina, Charleston, SC, United States, [4] Department of Physical Therapy, School of Health Sciences, High Point University, High Point, NC, United States

OPEN ACCESS

Edited by:
Ioan Opris,
University of Miami, United States

Reviewed by:
Winston D. Byblow,
The University of Auckland,
New Zealand
Antonio Oliviero,
Fundación del Hospital Nacional de Parapléjicos, Spain

***Correspondence:**
Mark Goodman Bowden
bowdenm@musc.edu

Specialty section:
This article was submitted to Neural Technology, a section of the journal Frontiers in Neuroscience

Received: 05 September 2018
Accepted: 11 March 2019
Published: 11 April 2019

Citation:
Kindred JH, Kautz SA, Wonsetler EC and Bowden MG (2019) Single Sessions of High-Definition Transcranial Direct Current Stimulation Do Not Alter Lower Extremity Biomechanical or Corticomotor Response Variables Post-stroke. Front. Neurosci. 13:286. doi: 10.3389/fnins.2019.00286

Transcranial direct current stimulation (tDCS) is a non-invasive brain stimulation technique used to modulate cortical activity. However, measured effects on clinically relevant assessments have been inconsistent, possibly due to the non-focal dispersion of current from traditional two electrode configurations. High-definition (HD)-tDCS uses a small array of electrodes ($N = 5$) to improve targeted current delivery. The purpose of this study was to determine the effects of a single session of anodal and cathodal HD-tDCS on gait kinematics and kinetics and the corticomotor response to transcranial magnetic stimulation (TMS) in individuals post-stroke. We hypothesized that ipsilesional anodal stimulation would increase the corticomotor response to TMS leading to beneficial changes in gait. Eighteen participants post-stroke (average age: 64.8 years, *SD*: 12.5; average months post-stroke: 54, *SD*: 42; average lower extremity Fugl-Meyer score: 26, *SD*: 6) underwent biomechanical and corticomotor response testing on three separate occasions prior to and after HD-tDCS stimulation. In a randomized order, anodal, cathodal, and sham HD-tDCS were applied to the ipsilesional motor cortex for 20 min while participants pedaled on a recumbent cycle ergometer. Gait kinetic and kinematic data were collected while walking on an instrumented split-belt treadmill with motion capture. The corticomotor response of the paretic and non-paretic tibialis anterior (TA) muscles were measured using neuronavigated TMS. Repeated measures ANOVAs using within-subject factors of time point (pre, post) and stimulation type (sham, anodal, cathodal) were used to compare effects of HD-tDCS stimulation on measured variables. HD-tDCS had no effect on over ground walking speed ($P > 0.41$), or kinematic variables ($P > 0.54$). The corticomotor responses of the TA muscles were also unaffected by HD-tDCS (resting motor threshold, $P = 0.15$; motor evoked potential (MEP) amplitude,

$P = 0.25$; MEP normalized latency, $P = 0.66$). A single session of anodal or cathodal HD-tDCS delivered to a standardized ipsilesional area of the motor cortex does not appear to alter gait kinematics or corticomotor response post-stroke. Repeated sessions and individualized delivery of HD-tDCS may be required to induce beneficial plastic effects. Contralesional stimulation should also be investigated due to the altered interactions between the cerebral hemispheres post-stroke.

Keywords: HD-tDCS, anodal, cathodal, gait, mobility, tDCS, brain stimulation, TMS

INTRODUCTION

Less than 50% of individuals post-stroke return to independent community ambulation (Jorgensen et al., 1995) and 73% have some type of long term disability (Gresham et al., 1995). Brain plasticity, i.e., structural and functional circuit reorganization, occurs after stroke and during motor rehabilitation (Sampaio-Baptista et al., 2018; Zhao and Willing, 2018). In some cases, plasticity can be beneficial to recovery. However, maladaptive processes can also occur leading to prolonged recovery or disability. Therefore, enhancing the positive effects of adaptive neuroplasticity and minimizing maladaptive plasticity are integral in providing adequate post-stroke rehabilitation.

Non-invasive brain stimulation techniques have been proposed to enhance the beneficial plastic effects of post-stroke rehabilitation (Fregni and Pascual-Leone, 2007). One such technique is transcranial direct current stimulation (tDCS) which involves the application of direct current, usually 1–2 mA, to the scalp over a targeted cortical area (Woods et al., 2016). Combining tDCS and traditional therapies may potentially improve stroke recovery due to Hebbian principals of motor learning (Schlaug and Renga, 2008). A recent review/meta-analysis reported beneficial increases in lower extremity muscular strength and mobility, although no effects on walking speed, walking endurance, or balance function could be detected (Li et al., 2018). While some beneficial clinical effects have been seen with traditional tDCS, imaging and finite element modeling studies demonstrate that current flow may be concentrated in areas away from targeted neuronal populations when using traditional two electrode montages (Datta et al., 2010; Antal et al., 2011). To overcome this lack of specificity, modeling studies predicted that replacing the traditional two electrode setup, typically rectangular electrodes approximately 35 cm^2, with an array of smaller circular electrodes, <1.2 cm in diameter, can more precisely deliver current (Minhas et al., 2010). Delivering current with a 4 × 1 ring montage, termed High-definition (HD)-tDCS, increases the current density (Caparelli-Daquer et al., 2012). In this montage the central electrode has opposite polarity of the four reference electrodes, i.e., one central anode and four surrounding cathodes or a central cathode with four surrounding anodes. Due to the location of the sensorimotor cortical representation of the lower extremities deep within the cortex along the longitudinal fissure utilizing more targeted current delivery with HD-tDCS may enhance outcomes related to motor rehabilitation and nervous system plasticity in chronic stroke, especially when compared with traditional tDCS.

Studies using HD-tDCS in healthy individuals has shown increases in the corticomotor response and enhanced cross-facilitation in the upper extremities of healthy individuals (Caparelli-Daquer et al., 2012; Cabibel et al., 2018). However, there is currently a lack of information about the effects of HD-tDCS in the lower extremities of people post-stroke, specifically, regarding gait and the corticomotor response to transcranial magnetic stimulation (TMS). Therefore, the purpose of this study was to determine the effects of a single session of HD-tDCS on gait kinetics, kinematics, and lower extremity corticomotor response in chronic stroke. Our *a priori* hypothesis was that anodal HD-tDCS applied to the ipsilesional motor cortex would increase motor evoked potential (MEP) amplitude and decrease resting motor threshold (rMT) and MEP latency of the paretic TA. Furthermore, we expected that with an altered corticomotor response we would see beneficial changes to gait characteristics.

MATERIALS AND METHODS

Ethics Statement

All methods and procedures were approved by the local Institutional Review Board and conformed to the Declaration of Helsinki. All participants signed informed consent prior to their participation in any aspect of the study.

Participants and Study Procedures

Twenty-one individuals post-stroke were recruited from the Ralph H. Johnson VA Medical Center (VAMC)/Medical University of South Carolina (MUSC) Stroke Recovery Research Center's (SRRC) participant database. Inclusion criteria for the study were: >6 months post-stroke, able to ambulate at least 10 m with minimal use of assistive devices, have a locomotor control impairment as indicated by scoring less than the maximum, 34, on the lower extremity Fugl-Meyer assessment (Fugl-Meyer et al., 1975), and have a measurable corticomotor response. Prospective participants were invited to the VAMC/MUSC SRRC for a total of four visits: one initial visit and three experimental visits.

Initial Visit

During the first visit, participants signed informed consent and underwent clinical testing. The clinical tests included: Berg Balance Scale (Berg et al., 1995), Functional Gait Assessment (Wrisley et al., 2004), 6-min walk test, and the lower extremity Fugl-Meyer assessment. Clinical testing was performed by a licensed physical therapist. After clinical testing, participants underwent TMS examination to identify the cortical representation, i.e., hotspot, of the tibialis anterior (TA) on the paretic and non-paretic legs. The TMS assessment was performed using a double-cone coil and a Magstim BiStim2 stimulator (Magstim, Inc., Whitland, United Kingdom). Hotspot identification was guided by neuronavigation (Brainsight, Rogue Research, Montreal, QC, Canada) (Charalambous et al., 2018). Briefly, hotspots were identified using a single suprathreshold single TMS pulse applied over a 3x5 grid transposed over an average Montreal Neurological Institute MRI brain image. Two trials were performed and the spot with the greatest average response, i.e., largest MEP amplitude, was used during the subsequent experimental visits. All MEPs were evoked while the muscle was at rest. If muscle activity was noted prior to the application of the TMS pulse the trial was discarded, and another pulse was applied.

Experimental Visits

During the experimental visits, visits 2–4, participants underwent biomechanical and neurophysiological testing prior to and post-receiving HD-tDCS. Participants received sham, anodal, or cathodal HD-tDCS stimulation in a randomized order. During HD-tDCS stimulation participants also pedaled on a recumbent cycle ergometer at a self-selected cadence with minimal resistance to activate the cortical tissue receiving the HD-tDCS stimulation.

Biomechanical Assessment

Gait kinetics and kinematics were measured using an active LED marker set applied in a modified Helen Hayes setup while participants walked on an instrumented split-belt treadmill with bilateral force plates (Bertec, Corp., Worthington, OH, United States) (Dean et al., 2017). Participants performed two 30 s trials at their preferred self-selected comfortable speed with motion capture. Motion capture data was sampled at 100 Hz using a 12-camera system (PhaseSpace, San Leandro, CA, United States). Ground reaction forces (GRFs) were sampled at 1000 Hz. After treadmill walking participants performed two trials of over ground walking on a GAITRite electronic walkway (CIR Systems, Inc., Franklin, NJ, United States) at their preferred comfortable walking speed. Participants wore a harness attached to the ceiling to mitigate their chance of falling during all walking tests.

Corticomotor Response Measurement

The assessment of the corticomotor response to TMS was initiated within 10 min of completion of the walking trials. The corticomotor response, measured as a MEP, was recorded using surface EMG (sEMG). Electrodes were placed over the TA muscle bellies and signals were amplified 1000x and recorded at 5000 Hz using Signal 6.03 (Cambridge Electronic Design, Cambridge, United Kingdom) for offline analysis. After the participant was seated comfortably in an adjustable chair with sEMG electrodes over the paretic and non-paretic TA muscles, measurement of the rMT commenced using parameter estimation by sequential testing (PEST) (Mishory et al., 2004). To determine the rMT two PEST procedures were performed using the hotspot identified during the initial visit. The anatomical location of the hotspot was maintained between visits by utilizing neuronavigation. The PEST program directed the intensity of the TMS stimuli applied to the muscle's hotspot. The measurement of the rMT was performed twice, and the average of the two trials was used as the participant's rMT for that experimental session. Once the rMT was established for each muscle, 10 single TMS pulses were applied at 120% of the rMT to the paretic and non-paretic TA hotspots using a double cone coil while the muscles were at rest.

HD-tDCS Stimulation

Once initial gait and corticomotor response measurements were completed, participants received 20 min of one of three HD-tDCS (Soterix Medical, Inc., New York, NY, United States) stimulations: central anodal, central cathodal, or sham. Participants received the stimulations in a randomized order over the three experimental visits, and both participants and investigators were blinded the stimulation protocol used during that session. Electrodes were held in place using a cap with a pre-defined grid utilizing the standard 10–10 system (Chatrian et al., 1985). The central HD-tDCS electrode was positioned on either C1 or C2, whichever corresponded with the ipsilesional motor cortex (**Figure 1A**). This location was chosen from modeling performed using HDExplore (Soterix Medical, Inc.) to deliver current to the ipsilesional M1 with minimal current delivered to the contralesional cortex (**Figure 1B**). The HDExplore program used a standard MRI image to model current flow, stroke specific modeling was not available. A current of 2 mA was applied through the central electrode during anodal conditions that was returned through the four reference electrodes. During cathodal stimulation 0.5 mA was delivered through each of the four reference electrodes and returned through the central electrode. The sham condition was similar to anodal stimulation, however the HD-tDCS stimulator automatically reduced the current to zero after 30 s. To activate the motor cortex while receiving HD-tDCS participants pedaled on a recumbent cycle ergometer (Monark Exercise AB, Vansbro, Sweden) at a self-selected pace with minimal resistance. After stimulation was concluded participants immediately underwent reassessment of the corticomotor response followed by biomechanical assessment. Post-biomechanical and corticomotor response testing was conducted using the same parameters as pre-testing, e.g., equal treadmill speeds and TMS stimulator output intensity.

Data Analyses

Gait Kinetics and Kinematics Analyses

Motion capture data were low-pass filtered at 10 Hz using a 4^{th} order, zero-lag Butterworth filter. Body segment kinematics were determined using a custom model (Visual3D, Germantown, MD, United States). Segment COM locations were calculated using anthropometric and inertial properties (de Leva, 1996). Kinetic and kinematic variables included: anterior (propulsive) GRFs, posterior (braking) GRFs, ankle power, ankle work, cadence, paretic and non-paretic step length. All post-stimulation kinematic and kinetic variables were collected at speeds matched to pre-testing speeds on the instrumented treadmill.

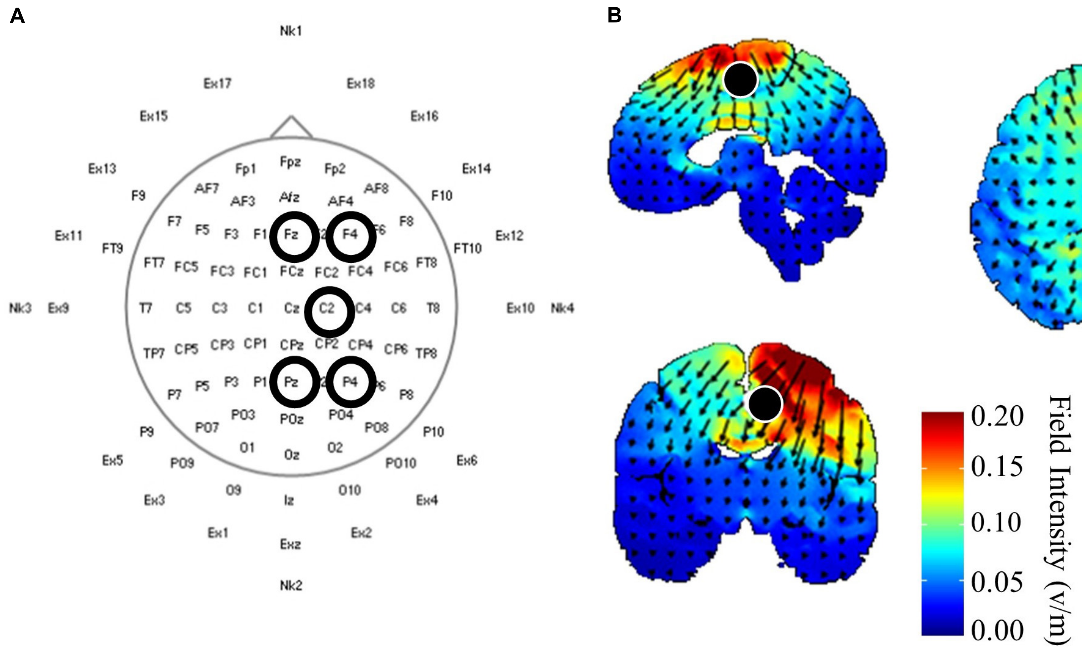

FIGURE 1 | High-definition (HD) transcranial direct current application and modeling. **(A)** HD-tDCS electrode placements according to standard 10–10 nomenclature. The central electrode was placed at C_2 with surrounding reference electrodes located at F_z, F4, P_z, P4 for participants with strokes in the right hemisphere. Left hemisphere stroke locations were C1, F_z, F3, P_z P3. **(B)** HD-tDCS current flow modeled using HDExplore (Soterix Medical, Inc.). Modeling estimated a field intensity of approximately 1 v/m at the right paracentral lobule, which is the location of the lower extremity sensorimotor representation within the cortex. Cathodal modeling showed a similar field intensity but with current moving in opposite directions.

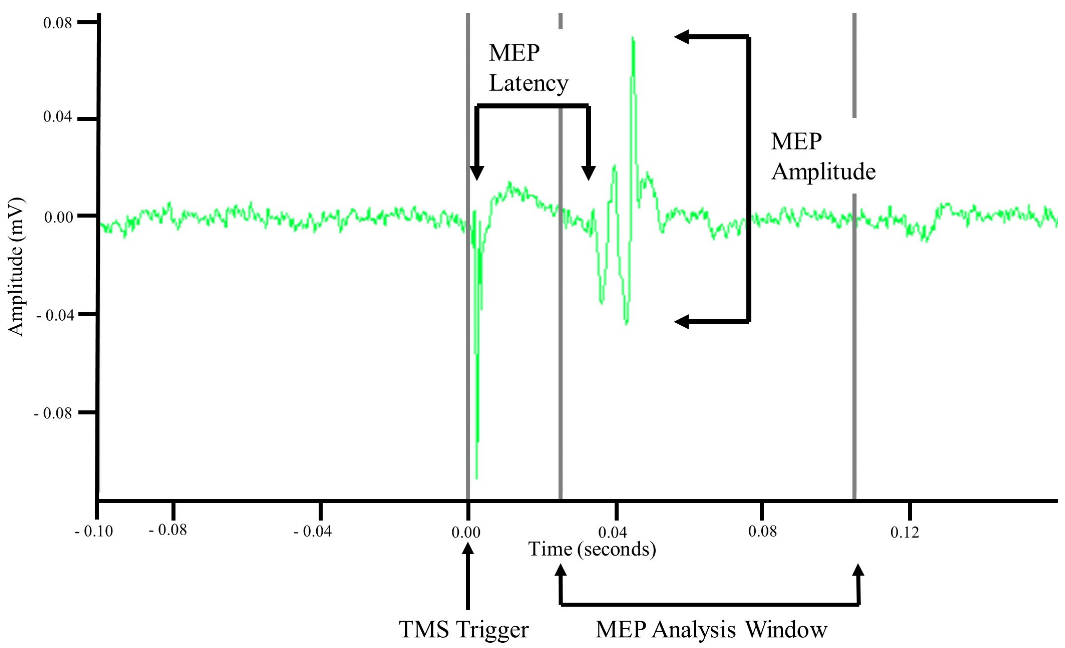

FIGURE 2 | Example motor evoked potential (MEP) recorded via surface electromyography. Unprocessed surface electromyographic signal recorded after a single TMS pulse was applied to cortical representation of the tibialis anterior (TA) muscle. MEP amplitude was measured as the difference in minimal and maximal amplitude of the signal within an 0.08 s analysis window that began 0.025 s after application of the TMS pulse. MEP latency was measured as the time between the TMS pulse and the initiation of the MEP.

MEP Analysis

Motor evoked potentials were recorded via sEMG. Using the TMS pulse trigger, a 0.5 s data window was recorded starting 0.1 s before the TMS trigger. Offline analyses of recorded EMG data were performed in MATLAB R2017b (MathWorks, Natick, MA, United States). Data were imported into MATLAB and demeaned using the average signal of the first and last 0.05 s. MEP amplitude was then calculated as the difference between the maximum and minimum values in a 0.08 s window starting at 0.025 s. Once amplitude was calculated the signal was rectified and the time from the TMS trigger pulse to the start of the MEP, i.e., latency, was measured. MEP latency was defined as the point when the rectified MEP signal amplitude was greater than the mean plus three standard deviations of the signal amplitude occurring 0.08 s before the TMS trigger pulse (Cacchio et al., 2011; Charalambous et al., 2018) for at least 0.001 s. Latency was then normalized to participant height and is reported as ms/m. Once all MEP metrics were calculated the data were exported and visually inspected to ensure the accuracy and validity of the values. For MEPs to be considered valid the following criteria had to be met: an amplitude greater than 50 μV and a non-normalized latency between 0.025 and 0.105 s. Stimulation trials that did not evoke at least 4/10 MEPs were not used for analysis. An example MEP is displayed in **Figure 2**.

Statistical Analysis

All data are reported as Mean and Standard Deviation (SD) unless otherwise noted. Variables that were comprised of values from both legs (walking speed, cadence) were analyzed using a two-factor Repeated Measures ANOVA using within-subject factors of stimulation type (sham, anodal, cathodal) and time point (pre-stimulation, post-stimulation). Additional variables that that were recorded for each leg/side (step length, GRFs, rMT, MEP amplitude, MEP normalized latency), were analyzed using a three-factor Repeated Measures ANOVA with within-subject factors of: stimulation type (sham, anodal, cathodal), leg (paretic, non-paretic), and time point (pre-stimulation, post-stimulation). Sphericity of the models was tested using Mauchly's Test of Sphericity, and in the case of significant findings Greenhouse–Geiser corrected *P-values* are reported. In all others the sphericity was assumed. When a significant *F*-test was present *post hoc* comparisons were made using Bonferroni corrections. Alpha was set to 0.05. All statistical analysis was performed using IBM SPSS Statistics for Windows, Version 24 (IBM, Corp., Somers, NY, United States).

RESULTS

Sample Demographics

Two individuals failed to screen into the study (no locomotor control impairment as assessed by achieving the maximum Fugl-Meyer score) and one participant was removed because they had no discernable corticomotor response (no MEPs elicited in the paretic or non-paretic TA) leaving a final sample of 18. The average age was 64.8 (*SD:* 12.5) years with time post-stroke of 53.7 (*SD:* 42.1) months. The average lower extremity Fugl-Meyer score was 26 (*SD*: 6) and 10 (*SD*: 3) for motor and sensory evaluations respectively. Other demographic variables are listed in **Table 1**.

TABLE 1 | Demographic variables.

Ht. (m)	Wt. (kg)	BMI	BBS	FGA	6MWT (m)
1.7	185.9	29.5	Median 50	Median 19	347.5
SD: 0.1	*SD*: 37.8	*SD*: 7.9	Range: 25–56	Range: 9–30	*SD*: 97.6

Demographic variables of the sample. Data are reported as Mean and Standard Deviation (SD) unless otherwise noted. BMI, Body Mass Index; BBS, Berg Balance Scale; FGA, Functional Gait Assessment; 6MWT, Six Minute Walk Test.

Gait Kinematic Data

Gait variables were analyzed for all participants (N = 18). Self-selected over ground walking speed, as measured via the GAITRite, did not change after HD-tDCS stimulation ($P > 0.19$). Motion capture revealed that paretic and non-paretic step length was increased after HD-tDCS stimulation ($P = 0.05$); however, the increase was not different between the different stimulation types ($P = 0.99$). Concomitant with the increase in step length, cadence was reduced after HD-tDCS stimulation ($P = 0.02$) and independent of stimulation type ($P = 0.91$). Means and SDs for all variables are displayed in **Figure 3** and all *F*-statistics and *P*-values are listed in **Table 2**.

Gait Kinetic Data

Ground Reaction Forces

Peak Propulsive (anterior direction) forces and impulse were greater in the non-paretic limb ($P < 0.02$). Peak braking (posterior direction) forces and impulses were not different between the legs ($P > 0.14$). Propulsive GRFs were not changed with the intervention ($P > 0.32$). However, there was a stimulation type × time point interaction with the peak braking GRF ($P < 0.01$). The interaction revealed an increase, more negative, in peak braking forces after cathodal stimulation. No other effects of HD-tDCS were detected for any other kinetic variables ($P > 0.07$). Means and SDs for all variables are displayed in **Figure 4** and **Table 3** contains all *F*-statistics and *P*-values.

Ankle Power and Work

Ankle power and work were greater on the non-paretic side compared to the paretic side ($P < 0.04$). However, the intervention had no effect ankle power or work ($P > 0.06$). There were no interactions for any variables ($P > 0.07$). Means and SDs for each variable are displayed in **Figure 5** and all *F*-statistics and *P*-values are listed in **Table 4**.

Corticomotor Response

We were unable to elicit a response in the paretic TA of two participants, and subsequently they were removed from the analysis (N = 16). There were no differences in rMT prior to initiation of the HD-tDCS stimulations ($P = 0.15$). However, the rMT in the paretic leg was greater compared to the non-paretic leg ($P < 0.01$). Twenty minutes of HD-tDCS and cycling did not change rMT ($P > 0.15$).

Out of 2160 single TMS pulses, 1888 (87%) valid MEPs were evoked. Due to some trials not having the required number

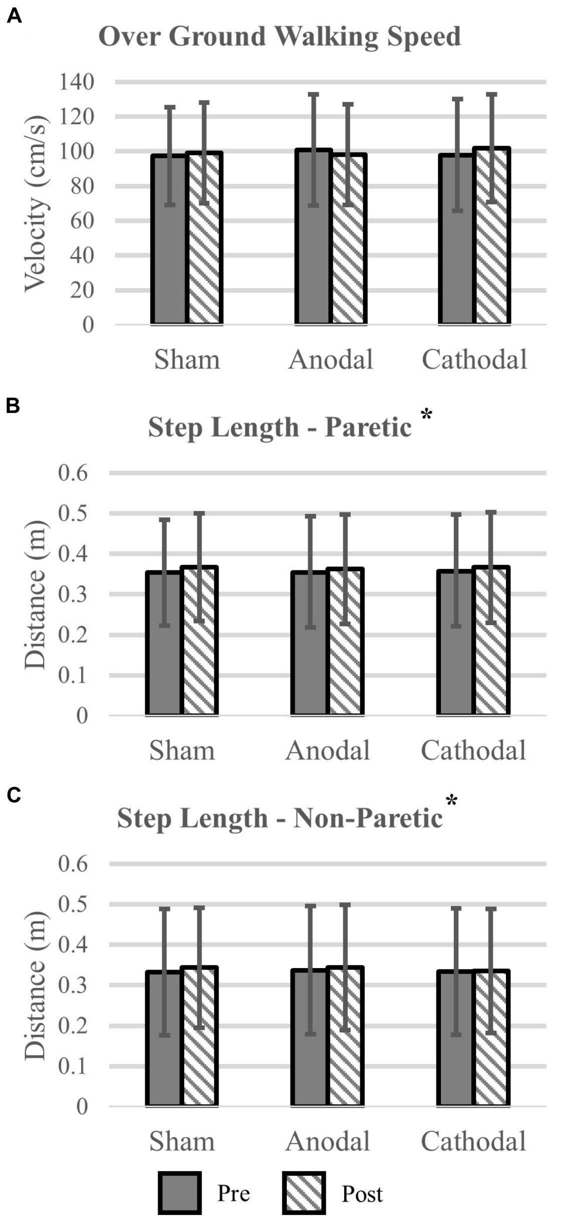

FIGURE 3 | Kinematic variables. **(A)** Over ground walking speeds were not affected by the application of HD-tDCS. **(B,C)** The step length of the paretic and non-paretic legs was increased after HD-tDCS stimulation. However, this increase was not different between the three stimulation types (Sham, Anodal, Cathodal). $^*P < 0.05$.

of valid MEPs (>4) the sample size for MEP amplitude and normalized latency comparisons were reduced to $N = 12$. MEP amplitude was not affected by HD-tDCS ($P > 0.25$) and amplitude was similar between the legs ($P = 0.60$). Normalized MEP latency of the non-paretic side was shorter compared to the paretic side ($P = 0.05$), and HD-tDCS did not affect latency values ($P > 0.18$). No interactions between the variables were identified ($P > 0.18$). Corticomotor response data are displayed in **Figure 6** and *F*-statistics and *P*-values are listed in **Table 5**.

TABLE 2 | Spatial-temporal gait variables statistics.

	Main effect of stimulation type	Main effect time point	Main effect of leg	Interaction(s)
Over ground walking speed	$F = 0.31$ $P = 0.74$	$F = 0.71$ $P = 0.41$	N/A	$F = 1.73$ $P = 0.19$
Cadence	$F = 0.09$ $P = 0.91$	$\mathbf{F = 6.32}$ $\mathbf{P = 0.02}$	N/A	$F = 0.55$ $P = 0.58$
Step length	$F = 0.01$ $P = 0.99$	$\mathbf{F = 4.58}$ $\mathbf{P = 0.05}$	$F = 1.55$ $P = 0.23$	$F < 0.63$ $P > 0.54$

Bold denotes $P < 0.05$.

DISCUSSION

The aim of this study was to identify the effects of HD-tDCS applied over ipsilesional M1 in chronic stroke. We applied three stimulation types (anodal, cathodal, and sham) to 18 participants and compared gait kinetics/kinematics and corticomotor responses pre-/post-stimulation. Contrary to our hypothesis, we were unable to detect any changes in lower extremity kinetic, kinematic, or corticomotor response variables after anodal HD-tDCS. Although, we did detect an increase in peak braking (posterior) GRFs after cathodal stimulation compared to anodal and sham. During our experiments, we did confirm previous reports of differences in kinetic, kinematic, and corticomotor response variables between the paretic and non-paretic lower extremities (Bowden et al., 2006; Allen et al., 2011; Cacchio et al., 2011). Our results seem to suggest that a single session of anodal HD-tDCS using a 4×1 montage centered on ipsilesional motor cortex (central electrode = C_2, reference electrodes = F_z, F_4, P_z, P_4) does not modulate M1 cortical activity of the lower extremities in chronic stroke.

During gait, when the heel strikes the ground a posterior GRF is applied to slow the forward progress of the body's center of mass. In this experiment we observed that the peak braking forces were increased after cathodal stimulation. However, total braking force as indicated by the posterior impulses were not different. We were also unable to detect any clinical relevant changes, in terms of gait kinematics, to accompany the increase in peak braking force. This finding leads us to believe that HD-tDCS may have effects on post-stroke gait but the clinical significance and the ability to leverage this change in a meaningful way are still unknown.

Tahtis et al. (2014) and Montenegro et al. (2016) examined the effects of a single session of bihemispheric traditional tDCS on the lower extremities in chronic stroke participants. Both reported some beneficial effects, improved timed up-and-go and force steadiness. However, they had relatively small sample sizes ($N \leq 10$) and neither identified a possible mechanism for improvement. In our study we were unable to identify any differences between the stimulation types using a within-subjects method for biomechanical and corticomotor response variables using a slightly larger sample size. Another key difference, besides traditional two-electrode versus HD-tDCS, is that in the previous studies a cathodal stimulation was applied to the contralesional side, due to the placement of the anode over

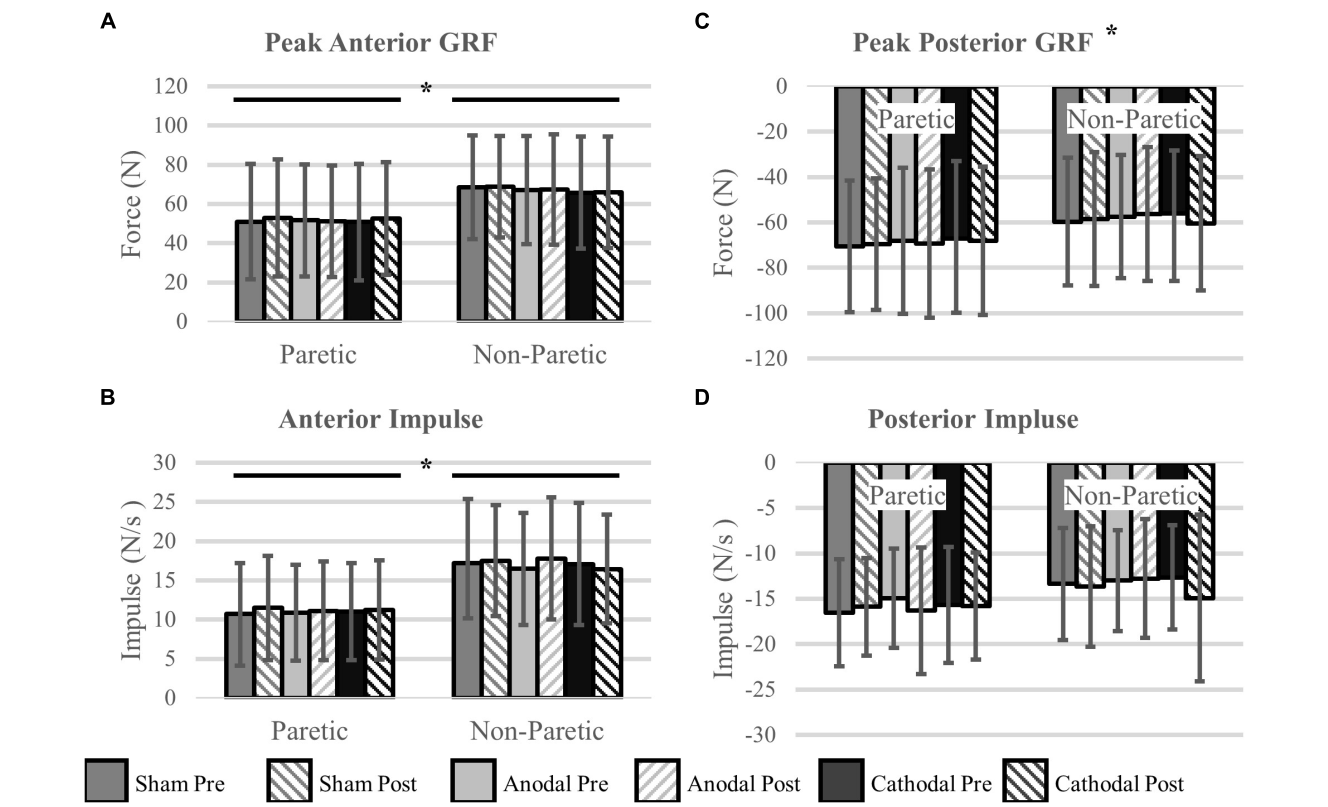

FIGURE 4 | Ground reaction forces. **(A,B)** Maximal propulsive (anterior) GRFs and impulses were not affected by HD-tDCS. The propulsive GRFs and impulses were greater in the non-paretic side compared to the paretic side, which is commonly seen in this population. **(C,D)** Maximal braking (posterior) GRFs and the posterior impulses were not different between the legs. However, there was a significant stimulation type × time point interaction revealing an increase (more negative) in peak braking forces after cathodal stimulation **(C)**. $^*P < 0.05$.

ipsilesional M1 and cathode placed over contralesional M1. It is possible that the effects seen in these earlier studies were due to a reduction in intercortical inhibition originating from the contralesional side by the cathodal stimulation. It is often seen that intercortical inhibition originating from the contralesional hemisphere is often increased post-stroke (Murase et al., 2004; Feng et al., 2013). To further demonstrate the effects of HD-tDCS on intercortical communication, Cabibel et al. (2018) showed that application of HD-tDCS to upper extremity cortical hotspots can enhance cross-facilitation, increasing excitability of unstimulated areas. Our modeling of electrode placement minimized contralesional current flow but may not have been strong enough to modulate the lesioned M1. It may be that in chronic stroke, maladaptive effects of increased intercortical inhibition originating from the contralesional hemisphere may override HD-tDCS to the ipsilesional hemisphere. Applying HD-tDCS to the contralesional M1 may provide a greater effect and requires future study. Measuring lower extremity intercortical communication in chronic stroke may allow for better targeting of current in future HD-tDCS applications.

TABLE 3 | Kinetic gait variables statistics.

	Main effect of stimulation type	Main effect time point	Main effect of leg	Interaction(s)
Peak anterior GRF	$F = 0.15$ $P = 0.87$	$F = 1.07$ $P = 0.32$	$\mathbf{F = 9.98}$ $\mathbf{P < 0.01}$	$F < 0.73$ $P > 0.49$
Anterior GRF impulse	$F = 0.20$ $P = 0.82$	$F = 1.06$ $P = 0.32$	$\mathbf{F = 7.06}$ $\mathbf{P = 0.02}$	$F < 1.54$ $P > 0.23$
Peak posterior GRF	$F = 0.31$ $P = 0.74$	$F = 0.62$ $P = 0.44$	$F = 2.46$ $P = 0.14$	$\mathbf{F = 8.11}$ $\mathbf{P < 0.01}$
Posterior GRF impulse	$F = 0.72$ $P = 0.50$	$F = 2.11$ $P = 0.17$	$F = 2.08$ $P = 0.17$	$F < 3.29$ $P > 0.07$

GRF, ground reaction force: a significant stimulation type × time point interaction was detected for cathodal stimulation only. No other interactions were significant (F < 1.65, P > 0.21). Bold denotes P < 0.05.

The brain is highly connected through a network of distinct and identifiable circuits. To compensate for damaged circuits, functional and structural remodeling occurs. The extent of damage and how circuits have reorganized can have an impact in the responsiveness to brain stimulation techniques. Diekhoff-Krebs et al. (2017) reports that individual differences in network connectivity affect the response to repetitive TMS in stroke patients. They showed that participants with greater connectivity between M1 and supplemental motor areas responded to a higher degree to intermittent theta-burst stimulation. Using tDCS in healthy individuals, Rosso et al. (2014b) showed that quicker

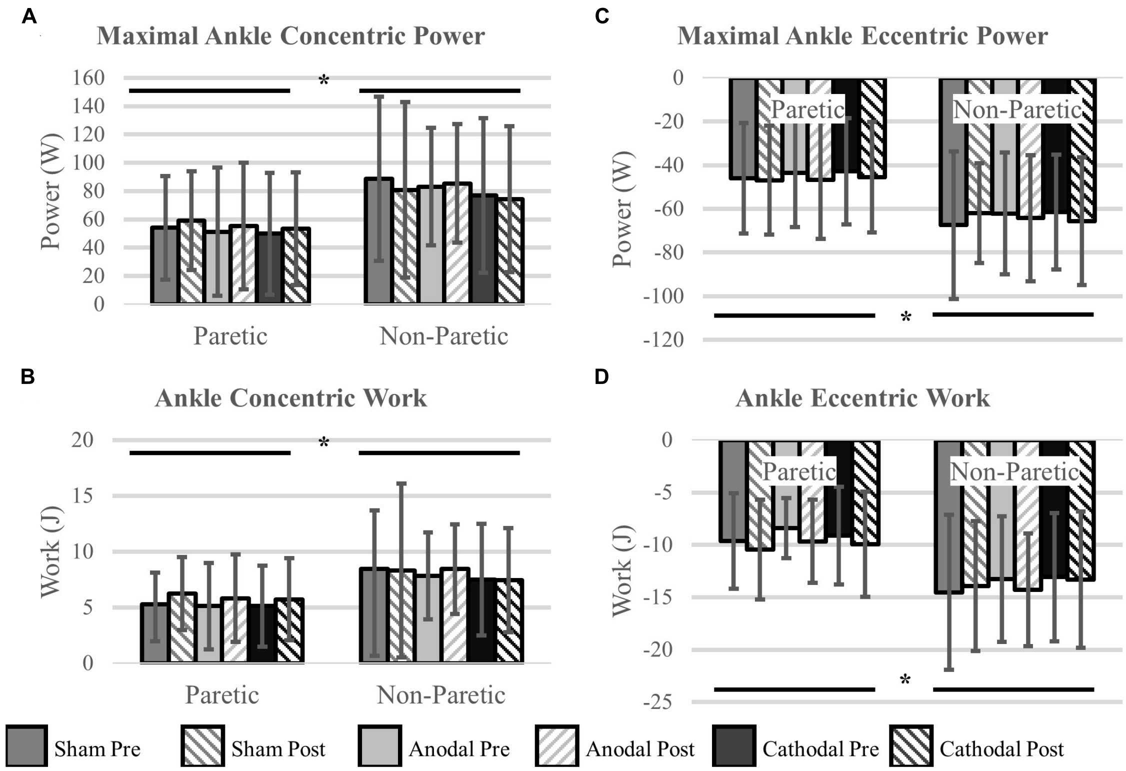

FIGURE 5 | Ankle power and work. **(A,B)** Concentric power and work were unaffected by HD-tDCS but were greater in the non-paretic ankle. **(C,D)** Eccentric power and work were unaffected by HD-tDCS but were greater in the non-paretic ankle. *Main effect of leg (paretic versus non-paretic) $P < 0.05$.

picture naming was associated with increased volume of the fiber tracts connecting the Broca's area to the supplemental motor area, as well as an increased functional connectivity between the two regions. One study of tDCS in post-stroke aphasia also indicated the anatomical location of the lesions modified the effectiveness of the stimulation (Rosso et al., 2014a). In that study, cathodal tDCS was applied to the right Broca's area in participants with lesions located within the left Broca's area, or another location within the left hemisphere. Participants with lesions located within the left Broca's area improved more than the group with locations outside that area. Depending on the innate connectivity of an individual, applying HD-tDCS to other nodes within the motor network may prove more effective. As previously mentioned, standard two-electrode tDCS montages delivers current between the anode and cathode electrodes. This may result in greater network modulation compared to HD-tDCS which likely delivers current specifically to one node. Directing HD-tDCS stimulation to different network nodes or altering the montage may lead to greater effects than those seen in this investigation. These nodes may include pre-motor areas or the cerebellum which have strong connections within the motor circuit. Modulating these areas may prove to be useful when trying to improve motor performance in chronic stroke compared to targeted M1 stimulation.

TABLE 4 | Ankle power and work statistics.

	Main effect of stimulation type	Main effect time point	Main effect of leg	Interaction(s)
Concentric ankle power	$F = 0.52$ $P = 0.60$	$F = 0.05$ $P = 0.83$	$\mathbf{F = 7.93}$ $\mathbf{P = 0.01}$	$F < 1.80$ $P > 0.20$
Eccentric ankle power	$F = 0.13$ $P = 0.88$	$F = 1.02$ $P = 0.33$	$\mathbf{F = 11.88}$ $\mathbf{P < 0.01}$	$F < 2.38$ $P > 0.11$
Concentric ankle work	$F = 0.51$ $P = 0.61$	$F = 1.90$ $P = 0.19$	$\mathbf{F = 5.01}$ $\mathbf{P = 0.04}$	$F < 0.61$ $P > 0.45$
Eccentric ankle work	$F = 0.83$ $P = 0.45$	$F = 4.01$ $P = 0.06$	$\mathbf{F = 14.17}$ $\mathbf{P < 0.01}$	$F < 1.08$ $P > 0.33$

Bold denotes $P < 0.05$.

Limitations

One of the possible reasons for the ineffectiveness of HD-tDCS to modulate the corticomotor response or biomechanical variables in this study may have been due to our stimulation location. Prior to our study, we modeled the delivery of HD-tDCS current to the TA representation of ipsilesional M1. However, when neuronavigationally determining a participant's TA hotspots, rarely was the greatest response recorded at our stimulated location (C1 or C2). It is possible that current was delivered to a less optimal location to detect changes in lower body kinetics, kinematics, and corticomotor response measures. Placing the central electrode directly over the

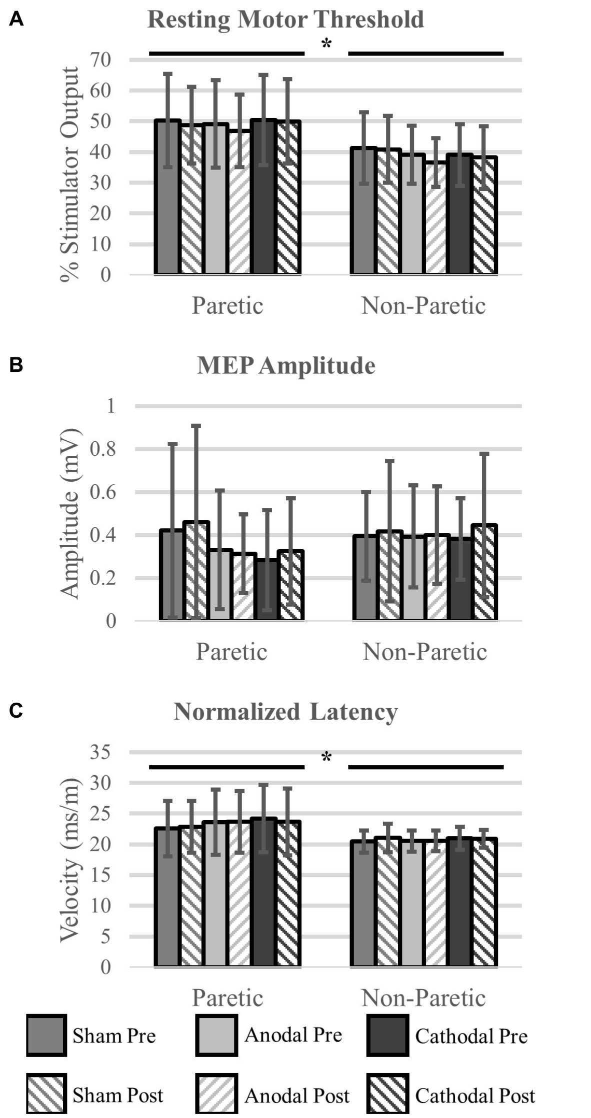

FIGURE 6 | Corticomotor response to single pulse transcranial magnetic stimulation (TMS). A single session of HD-tDCS had no effect on resting motor threshold **(A)**, MEP amplitude **(B)** or latency **(C)**. Similar to previous studies resting motor threshold and latency were greater on the paretic side compared to the non-paretic side. *Main effect of leg (paretic versus non-paretic) $P < 0.05$.

identified hotspot, as has been done previously in the upper extremities (Cabibel et al., 2018), may direct current to a more ideal location. Another important factor to consider is that current flow was modeled using a non-neurologically impaired brain. Due to technical limitations it was not possible to predict individualized current flow for each participant. It is possible that due to remodeling of the underlying neural tissue current was not delivered to an optimal location to facilitate neuromodulatory effects. Future work is certainly justified to determine the best location to deliver current in brains that have undergone motor circuit remodeling.

TABLE 5 | Corticomotor response variables statistics.

	Main effect of HD-tDCS type	Main effect of time point	Main effect of leg	Interaction(s)
Resting motor threshold	$F = 2.03$ $P = 0.15$	$F = 2.34$ $P = 0.15$	**$F = 11.90$** **$P < 0.01$**	$F < 1.84$ $P > 0.18$
MEP amplitude	$F = 0.72$ $P = 0.50$	$F = 1.46$ $P = 0.25$	$F = 0.30$ $P = 0.60$	$F < 1.16$ $P > 0.33$
Normalized latency	$F = 1.87$ $P = 0.18$	$F = 0.20$ $P = 0.66$	**$F = 4.65$** **$P = 0.05$**	$F < 1.20$ $P > 0.32$

MEP, motor evoked potential. Bold denotes $P < 0.05$.

Integrating fMRI to identify the remodeled motor networks may help investigators direct HD-tDCS stimulation to the most appropriate motor network node.

During the application of tDCS it is suggested that for effects to become evident the target area needs to be activated (Schlaug and Renga, 2008). To do this we had our participants perform recumbent cycling. However, we did not standardize or measure the forces/activity of the limbs during this exercise. Participants were instructed to cycle at a comfortable pace, but the cortically derived motor output to the paretic limb likely varied participant to participant. In previous experiments performed by members or our research group, it has been shown that activity of the non-paretic limb during cycling can induce rhythmic activity in the paretic limb (Kautz et al., 2006). It is possible that ipsilesional M1 descending drive was insufficient during rhythmic steady-state pedaling for effects of HD-tDCS to be identified. Another limitation of this modality is that there was likely a greater contribution of the quadriceps and hamstring muscles to perform the task compared to the TA. Using task that was more specific to the TA may have engaged the stimulated M1 to a greater degree and allowed for post-stimulation effects to be seen.

CONCLUSION

Twenty minutes of HD-tDCS did not alter lower extremity kinematic, kinetic, or corticomotor response variables post-stroke. Several factors likely contributed to this, and include: the number of session performed, stimulation location, and lower limb activity during stimulation. While single session experiments are often used to identify changes in physiological parameters, most researchers agree that multiple session of brain stimulation are usually required for beneficial plasticity to be identified. In the future we plan on performing similar experimental protocols over several sessions to determine if HD-tDCS can have a beneficial impact in post-stroke motor recovery.

Another area that needs further investigation is the relevance of studying MEP amplitude versus latency. MEP latency seems to be a much more stable parameter in healthy and post-stroke individuals (Charalambous et al., 2018). This was also seen in our sample, as there was less variability in latency in the paretic and non-paretic lower extremities compared to amplitude. MEP amplitude can be affected by many different physiological variables that alter electromyographic response such as hydration status, previous muscle activity, and muscle cross talk (Farina et al., 2004). These factors can change with different amounts of activity and comparing MEP amplitudes across days without some type of correction factor, e.g., reporting as a percent of maximal voluntary contraction, is likely inappropriate. Monitoring changes in latency values may prove to be a more valuable outcome measure in future investigations centered on brain stimulation in chronic stroke.

Due to differences in published protocols with tDCS, direct comparisons between traditional two electrode and HD-tDCS are difficult to make. Future studies are needed to determine which modality would most enhance current rehabilitative practices. As stated previously, during bihemispheric stimulation with traditional tDCS current passes through both the ipsilesional and contralesional sides. Alternate HD-tDCS montages may provide bihemispheric stimulation in a more targeted manner and may lead to enhanced motor recovery post-stroke compared to current clinical practices and traditional tDCS. Additionally, greater research into the standardization of HD-tDCS is needed to ensure future research can be performed in a reproducible manner and facilitate the comparison of results from different research laboratories. In conclusion we were unable to detect changes in lower extremity biomechanical or corticomotor response variables after a single session of anodal HD-tDCS to the ipsilesional M1 in chronic stroke. More work is required to determine how clinicians can best use neuromodulatory devices to improve lower extremity motor rehabilitation.

AUTHOR CONTRIBUTIONS

JK participated in data collection, analyzed and interpreted data, wrote first draft of the manuscript. SK provided conceptual framework of submitted work, critically revised manuscript for intellectual and scientific content. EW participated in data collection, critically revised manuscript for intellectual and scientific content. MB provided conceptual framework of submitted work, supervised all data collection, ensured adherence to ethical guidelines, critically revised manuscript for intellectual and scientific content, has final approval for manuscript submission.

FUNDING

Research reported in this publication was supported by the Veteran's Administration (N0787-W), by an Institutional Development Award (IDeA) from the National Institute of General Medicine Sciences of the National Institute of Health (P20GM109040) and by the NIH grant P2C-HD086844. The content is solely the responsibility fo the authors and does not necesarrily represent the official views of the VA or NIH.

ACKNOWLEDGMENTS

The authors would like to thank Mr. Brian Cence for his help with participant recruitment and data collection, as well as Dr. Christian Finetto for his help writing the MATLAB code used for the analysis.

REFERENCES

Allen, J. L., Kautz, S. A., and Neptune, R. R. (2011). Step length asymmetry is representative of compensatory mechanisms used in post-stroke hemiparetic walking. *Gait Posture* 33, 538–543. doi: 10.1016/j.gaitpost.2011.01.004

Antal, A., Polania, R., Schmidt-Samoa, C., Dechent, P., and Paulus, W. (2011). Transcranial direct current stimulation over the primary motor cortex during fMRI. *Neuroimage* 55, 590–596. doi: 10.1016/j.neuroimage.2010.11.085

Berg, K., Wood-Dauphinee, S., and Williams, J. I. (1995). The balance scale: reliability assessment with elderly residents and patients with an acute stroke. *Scand. J. Rehabil. Med.* 27, 27–36.

Bowden, M. G., Balasubramanian, C. K., Neptune, R. R., and Kautz, S. A. (2006). Anterior-posterior ground reaction forces as a measure of paretic leg contribution in hemiparetic walking. *Stroke* 37, 872–876. doi: 10.1161/01.STR.0000204063.75779.8d

Cabibel, V., Muthalib, M., Teo, W. P., and Perrey, S. (2018). High-definition transcranial direct-current stimulation of the right M1 further facilitates left M1 excitability during crossed facilitation. *J. Neurophysiol.* 119, 1266–1272. doi: 10.1152/jn.00861.2017

Cacchio, A., Paoloni, M., Cimini, N., Mangone, M., Liris, G., Aloisi, P., et al. (2011). Reliability of TMS-related measures of tibialis anterior muscle in patients with chronic stroke and healthy subjects. *J. Neurol. Sci.* 303, 90–94. doi: 10.1016/j.jns.2011.01.004

Caparelli-Daquer, E. M., Zimmermann, T. J., Mooshagian, E., Parra, L. C., Rice, J. K., Datta, A., et al. (2012). A pilot study on effects of 4x1 high-definition tDCS on motor cortex excitability. *Conf. Proc. IEEE Eng. Med. Biol. Soc.* 2012, 735–738. doi: 10.1109/embc.2012.6346036

Charalambous, C. C., Dean, J. C., Adkins, D. L., Hanlon, C. A., and Bowden, M. G. (2018). Characterizing the corticomotor connectivity of the bilateral ankle muscles during rest and isometric contraction in healthy adults. *J. Electromyogr. Kinesiol.* 41, 9–18. doi: 10.1016/j.jelekin.2018.04.009

Chatrian, G. E., Lettich, E., and Nelson, P. L. (1985). Ten percent electrode system for topographic studies of spontaneous and evoked EEG activities. *Am. J. EEG Technol.* 25, 83–92. doi: 10.1080/00029238.1985.11080163

Datta, A., Bikson, M., and Fregni, F. (2010). Transcranial direct current stimulation in patients with skull defects and skull plates: high-resolution computational FEM study of factors altering cortical current flow. *Neuroimage* 52, 1268–1278. doi: 10.1016/j.neuroimage.2010.04.252

de Leva, P. (1996). Joint center longitudinal positions computed from a selected subset of Chandler's data. *J. Biomech.* 29, 1231–1233. doi: 10.1016/0021-9290(96)00021-8

Dean, J. C., Embry, A. E., Stimpson, K. H., Perry, L. A., and Kautz, S. A. (2017). Effects of hip abduction and adduction accuracy on post-stroke gait. *Clin. Biomech.* 44, 14–20. doi: 10.1016/j.clinbiomech.2017.02.013

Diekhoff-Krebs, S., Pool, E. M., Sarfeld, A. S., Rehme, A. K., Eickhoff, S. B., Fink, G. R., et al. (2017). Interindividual differences in motor network connectivity and behavioral response to iTBS in stroke patients. *Neuroimage Clin.* 15, 559–571. doi: 10.1016/j.nicl.2017.06.006

Farina, D., Merletti, R., and Enoka, R. M. (2004). The extraction of neural strategies from the surface EMG. *J. Appl. Physiol.* 96, 1486–1495. doi: 10.1152/japplphysiol.01070.2003

Feng, W. W., Bowden, M. G., and Kautz, S. (2013). Review of transcranial direct current stimulation in poststroke recovery. *Top. Stroke Rehabil.* 20, 68–77. doi: 10.1310/tsr2001-68

Fregni, F., and Pascual-Leone, A. (2007). Technology insight: noninvasive brain stimulation in neurology-perspectives on the therapeutic potential of rTMS and tDCS. *Nat. Clin. Pract. Neurol.* 3, 383–393. doi: 10.1038/ncpneuro0530

Fugl-Meyer, A. R., Jaasko, L., Leyman, I., Olsson, S., and Steglind, S. (1975). The post-stroke hemiplegic patient. 1. a method for evaluation of physical performance. *Scand. J. Rehabil. Med.* 7, 13–31.

Gresham, G. E., Duncan, P. W., and Stason, W. B. (1995). *Post-Stroke Rehabilitation. Clinical Practice Guideline, No. 16*. Rockville, MD: U.S. Department of Health and Human Services.

Jorgensen, H. S., Nakayama, H., Raaschou, H. O., Vive-Larsen, J., Stoier, M., Olsen, T. S., et al. (1995). Outcome and time course of recovery in stroke. Part I: outcome. The Copenhagen stroke study. *Arch. Phys. Med. Rehabil.* 76, 399–405. doi: 10.1016/S0003-9993(95)80567-2

Kautz, S. A., Patten, C., and Neptune, R. R. (2006). Does unilateral pedaling activate a rhythmic locomotor pattern in the nonpedaling leg in post-stroke hemiparesis? *J. Neurophysiol.* 95, 3154–3163. doi: 10.1152/jn.00951.2005

Li, Y., Fan, J., Yang, J., He, C., and Li, S. (2018). Effects of transcranial direct current stimulation on walking ability after stroke: a systematic review and meta-analysis. *Restor. Neurol. Neurosci.* 36, 59–71. doi: 10.3233/rnn-170770

Minhas, P., Bansal, V., Patel, J., Ho, J. S., Diaz, J., Datta, A., et al. (2010). Electrodes for high-definition transcutaneous DC stimulation for applications in drug delivery and electrotherapy, including tDCS. *J. Neurosci. Methods* 190, 188–197. doi: 10.1016/j.jneumeth.2010.05.007

Mishory, A., Molnar, C., Koola, J., Li, X., Kozel, F. A., Myrick, H., et al. (2004). The maximum-likelihood strategy for determining transcranial magnetic stimulation motor threshold, using parameter estimation by sequential testing is faster than conventional methods with similar precision. *J. ECT* 20, 160–165. doi: 10.1097/00124509-200409000-00007

Montenegro, R. A., Midgley, A., Massaferri, R., Bernardes, W., Okano, A. H., Farinatti, P., et al. (2016). Bihemispheric motor cortex transcranial direct current stimulation improves force steadiness in post-stroke hemiparetic patients: a randomized crossover controlled trial. *Front. Hum. Neurosci.* 10:426. doi: 10.3389/fnhum.2016.00426

Murase, N., Duque, J., Mazzocchio, R., and Cohen, L. G. (2004). Influence of interhemispheric interactions on motor function in chronic stroke. *Ann. Neurol.* 55, 400–409. doi: 10.1002/ana.10848

Rosso, C., Perlbarg, V., Valabregue, R., Arbizu, C., Ferrieux, S., Alshawa, B., et al. (2014a). Broca's area damage is necessary but not sufficient to induce after-effects of cathodal tDCS on the unaffected hemisphere in post-stroke aphasia. *Brain Stimul.* 7, 627–635. doi: 10.1016/j.brs.2014.06.04

Rosso, C., Valabregue, R., Arbizu, C., Ferrieux, S., Vargas, P., Humbert, F., et al. (2014b). Connectivity between right inferior frontal gyrus and supplementary motor area predicts after-effects of right frontal cathodal tDCS on picture naming speed. *Brain Stimul.* 7, 122–129. doi: 10.1016/j.brs.2013.08.007

Sampaio-Baptista, C., Sanders, Z. B., and Johansen-Berg, H. (2018). Structural plasticity in adulthood with motor learning and stroke rehabilitation. *Annu. Rev. Neurosci.* 41, 25–40. doi: 10.1146/annurev-neuro-080317-062015

Schlaug, G., and Renga, V. (2008). Transcranial direct current stimulation: a noninvasive tool to facilitate stroke recovery. *Expert Rev. Med. Devices* 5, 759–768. doi: 10.1586/17434440.5.6.759

Tahtis, V., Kaski, D., and Seemungal, B. M. (2014). The effect of single session bi-cephalic transcranial direct current stimulation on gait performance in sub-acute stroke: a pilot study. *Restor. Neurol. Neurosci.* 32, 527–532. doi: 10.3233/rnn-140393

Woods, A. J., Antal, A., Bikson, M., Boggio, P. S., Brunoni, A. R., Celnik, P., et al. (2016). A technical guide to tDCS, and related non-invasive brain stimulation tools. *Clin. Neurophysiol.* 127, 1031–1048. doi: 10.1016/j.clinph.2015.11.012

Wrisley, D. M., Marchetti, G. F., Kuharsky, D. K., and Whitney, S. L. (2004). Reliability, internal consistency, and validity of data obtained with the functional gait assessment. *Phys. Ther.* 84, 906–918.

Zhao, L. R., and Willing, A. (2018). Enhancing endogenous capacity to repair a stroke-damaged brain: an evolving field for stroke research. *Prog. Neurobiol.* 163–164, 5–26. doi: 10.1016/j.pneurobio.2018.01.004

Conflict of Interest Statement: The authors declare that the research was conducted in the absence of any commercial or financial relationships that could be construed as a potential conflict of interest.

The handling Editor declared a shared affiliation, though no other collaboration, with the authors.

frontiers in Neuroscience

CLINICAL TRIAL
published: 29 May 2019
doi: 10.3389/fnins.2019.00547

Antiepileptic Effects of a Novel Non-invasive Neuromodulation Treatment in a Subject With Early-Onset Epileptic Encephalopathy: Case Report With 20 Sessions of HD-tDCS Intervention

Oded Meiron[1]*, Rena Gale[2], Julia Namestnic[2], Odeya Bennet-Back[3], Nigel Gebodh[4], Zeinab Esmaeilpour[4], Vladislav Mandzhiyev[4] and Marom Bikson[4]

[1] The Clinical Research Center for Brain Sciences, Herzog Medical Center, Jerusalem, Israel, [2] Children Respiratory Unit, Herzog Medical Center, Jerusalem, Israel, [3] Pediatric Neurology Department, Shaare Zedek Medical Center, Jerusalem, Israel, [4] Department of Biomedical Engineering, The City College of the City University of New York, New York, NY, United States

OPEN ACCESS

Edited by:
Gottfried Schlaug, Beth Israel Deaconess Medical Center, Harvard Medical School, United States

Reviewed by:
Ali Yadollahpour, Ahvaz Jundishapur University of Medical Sciences, Iran
Mouhsin Shafi, Beth Israel Deaconess Medical Center, Harvard Medical School, United States
Bernard Chang, Beth Israel Deaconess Medical Center, Harvard Medical School, United States

****Correspondence:***
Oded Meiron
oded@herzoghospital.org; neuron.o.d.m@gmail.com

Specialty section:
This article was submitted to Neural Technology, a section of the journal Frontiers in Neuroscience

Received: *09 August 2018*
Accepted: *13 May 2019*
Published: *29 May 2019*

Citation:
Meiron O, Gale R, Namestnic J, Bennet-Back O, Gebodh N, Esmaeilpour Z, Mandzhiyev V and Bikson M (2019) Antiepileptic Effects of a Novel Non-invasive Neuromodulation Treatment in a Subject With Early-Onset Epileptic Encephalopathy: Case Report With 20 Sessions of HD-tDCS Intervention. Front. Neurosci. 13:547. doi: 10.3389/fnins.2019.00547

The current clinical investigation examined high-definition transcranial direct current stimulation (HD-tDCS) as a focal, non-invasive, anti-epileptic treatment in a child with early-onset epileptic encephalopathy. We investigated the clinical impact of repetitive (20 daily sessions) cathode-centered 4 × 1 HD-tDCS (1 mA, 20 min, 4 mm ring radius) over the dominant seizure-generating cortical zone in a 40-month-old child suffering from a severe neonatal epileptic syndrome known as Ohtahara syndrome (OS). Seizures and epileptiform activity were monitored and quantified using video-EEG over multiple days of baseline, intervention, and post-intervention periods. Primary outcome measures were changes in seizure frequency and duration on the last day of intervention versus the last baseline day, preceding the intervention. In particular, we examined changes in tonic spasms, tonic-myoclonic seizures (TM-S), and myoclonic seizures from baseline to post-intervention. A trend in TM-S frequency was observed indicating a reduction of 73% in TM-S frequency, which was non-significant [$t(4) = 2.05$, $p = 0.1$], and denoted a clinically significant change. Myoclonic seizure (M-S) frequency was significantly reduced [$t(4) = 3.83$, $p = 0.019$] by 68.42%, compared to baseline, and indicated a significant clinical change as well. A 73% decrease in interictal epileptic discharges (IEDs) frequency was also observed immediately after the intervention period, compared to IED frequency at 3 days prior to intervention. Post-intervention seizure-related peak delta desynchronization was reduced by 57%. Our findings represent a case-specific significant clinical response, reduction in IED, and change in seizure-related delta activity following the application of HD-tDCS. The clinical outcomes, as noted in the current study, encourage the further investigation of this focal, non-invasive neuromodulation procedure in other severe electroclinical syndromes (e.g., West syndrome) and in larger pediatric populations diagnosed with early-onset epileptic encephalopathy.

Clinical Trial Registration: www.ClinicalTrials.gov, identifier NCT02960347, protocol ID: Meiron 2013-4.

Keywords: neonatal epileptic encephalopathy, seizure, high-definition transcranial direct current stimulation (HD-tDCS), electroencephalography (EEG), interictal epileptic discharges (IEDs)

INTRODUCTION

In the current clinical investigation, the feasibility of high-definition transcranial direct current stimulation (HD-tDCS; Datta et al., 2009) as an antiepileptic treatment in a severe pediatric epileptic syndrome case was examined. Recent findings have highlighted the potential for tDCS to significantly alleviate epileptiform activity in children ages 6 to 15 (Yook et al., 2011; Auvichayapat et al., 2013, 2016). The stimulation electrodes are typically placed on the scalp with the cathode positioned over the epileptic focus and anode is placed elsewhere or extracephallicly, with the intention to reduce excitability (Ghai et al., 2000; Brunoni et al., 2012). To the best of our knowledge, conventional tDCS has never been evaluated for its potential to serve as a focal non-invasive anti-epileptic treatment in children with significant developmental delays suffering from early-onset epileptic encephalopathy and, other than our prior investigation, had not been examined in pediatric population younger than 4 years old (Meiron et al., 2018).

Unlike traditional tDCS (in a 1 × 1 configuration) used in prior antiepileptic interventions (Datta et al., 2009; Yook et al., 2011), randomized clinical trials (Auvichayapat et al., 2016), and sham-controlled double blind studies (San-Juan et al., 2017) examining the effects of tDCS on epileptic seizures and epileptiform activity in children and adults suffering from epileptic syndromes, HD-tDCS (in a 4 × 1 configuration) is expected to produce optimized neuromodulation by focally targeting specific paroxysmal seizure-related areas and producing specific current densities at the cortical level (Dmochowski et al., 2011; Kuo et al., 2013). The focality of HD-tDCS also minimizes neuromodulatory effects outside the target area (Edwards et al., 2013; Alam et al., 2016; Karvigh et al., 2017), as compared to conventional tDCS.

Newborns with OS frequently die during infancy, and survivors manifest psychomotor impairments, as well as continuous hypsarrhythmia accompanied with epileptic infantile-spasms (Watanabe et al., 1993a; Gaily et al., 2001; Ohtahara and Yamatogi, 2006; Beal et al., 2012). Ictal and interictal electroencephalography (EEG) can help monitor disease progression and the development of region-specific epileptic foci dominance. Specific pathological and epileptic EEG patterns such as changes in paroxysmal high-voltage slow wave delta peak-activity (i.e., maximum change in spectral power) within hypsarrhythmic electroclinical conditions can be observed over particular cortical regions in age-dependent epileptic encephalopathy cases such as West syndrome (WS) and OS (Gaily et al., 2001; Ohtahara and Yamatogi, 2006; Beal et al., 2012). In support, a recent fMRI-EEG study indicated that focal hypsarrhythmic epileptiform discharges [reflected by interictal epileptic discharges (IEDs) under certain scalp electrodes in infants suffering from hypsarrhythmia, infantile spasms, and developmental delay or WS] were significantly related to corresponding-focal hemodynamic changes, and most importantly, epileptiform paroxysmal-high-voltage changes in delta power were associated with BOLD signal changes in particular cortical and subcortical regions (Siniatchkin et al., 2007). Accordingly, paroxysmal high-voltage fluctuations in delta activity in these electroclinical conditions may be considered as secondary generalized epileptiform discharges. Slow-wave delta power was positively associated with BOLD signal only in the infants suffering from hypsarrhythmia and infantile spasms, as compared to an older group suffering from temporal lobe epilepsy and WS. This is an important clinical distinction since only patients with early onset hypsarrhythmia consistently showed significant correlations between EEG delta power and BOLD signals in the brainstem, thalamus, and as a group in putamen, all of which are neural substrates associated with infantile spasms with hypsarrhythmia, and OS etiology (Watanabe et al., 1993b; Ohtahara and Yamatogi, 2006; Siniatchkin et al., 2007). Furthermore, interictal spikes were associated with significant region-specific (e.g., the caudate nucleus) changes in BOLD signal in all infants suffering from hypsarrhythmia with infantile spasms.

Ten months prior to the current investigation (when the patient was 30 months old) we evaluated the safety and feasibility of HD-tDCS in reducing epileptiform activity and seizure frequency in a dose-escalation study (Meiron et al., 2018). We applied a dynamic montage approach allowing for the adaptation to the changing daily-epileptic-foci. Stimulation dose commenced with extremely low current intensities (0.1 mA) and was gradually increased to 1 mA over a period of 2 weeks. Our preliminary findings indicated a significant reduction in IEDs (e.g., reduced sharp wave amplitudes); however, significant alleviation of seizure frequency was not observed. All vital signs and physiological parameters were unchanged throughout our preliminary clinical trial and the intervention was considered safe without any adverse effects.

In order to investigate the inhibitory effects of 4 × 1 HD-tDCS on the most salient epileptiform activity in a 40-month-old child suffering from a severe neonatal epileptic syndrome known as Ohtahara syndrome (OS), we targeted the most dominant seizure-generating networks and collected video-EEG over the course of baseline (1 week), intervention (20 days with HD-tDCS), and post-intervention (32-days following the cessation of the HD-tDCS intervention) periods. Seizure frequency and IED parameters (e.g., interictal spike frequency and amplitudes) were considered the main clinical outcome measures in assessing changes from post-intervention period (32 days after termination of 20-day intervention) versus baseline period (1 week before onset of intervention). Averaged interictal delta power, and seizure-related paroxysmal changes in mean absolute delta power served as secondary clinical outcome measures indicative of secondary epileptiform activity associated with dysfunctional circuitry that may reflect the propagation of the most dominant epileptic focus activity (Siniatchkin et al., 2007). Specifically, primary clinical outcomes included the frequency of tonic spasms, myoclonic seizures, and tonic-myoclonic seizures (TM-S), and secondary clinical outcomes included paroxysmal changes in delta power topography, and IED parameters. Daily clinical monitoring (blood testing, online vital signs, respiratory rate monitoring) and registration was ongoing throughout the entirety of the clinical trial. In contrast to our initial dose escalation HD-tDCS intervention, the current clinical investigation utilized one 4 × 1 stimulation montage and current intensity of 1 mA over the course of the intervention (4 weeks). In light of functional MRI data revealing a close link between seizure-related BOLD signals and paroxysmal EEG delta power fluctuations (Siniatchkin et al., 2007) in infants with infantile spasms and hypsarrhythmia, and most particularly since tonic-myoclonic (TM) seizure onset is related to a significant decrement in relative delta power (Rosso et al., 2006), we hypothesized a reduction in mean seizure-related delta desynchronization, associated with alleviation of interictal spike activity during the post-intervention period versus baseline, as well as a reduction in TM seizure frequency and duration.

MATERIALS AND METHODS

The study was conducted at Herzog Medical Center Jerusalem, Israel. Approval was obtained from the Israel Ministry of Health and from the institute's local institutional review board. The study was conducted in accordance with the Declaration of Helsinki, and written informed consent was obtained from the patient's parents.

Case

The patient was a 40-month-old child suffering from an early-onset epileptic syndrome called OS, which was the suspected diagnosis (based on his suppression-burst patterns and intractable seizure activity) at age 2 weeks. He was born after an uneventful, full term second pregnancy with birth weight of 3,160 g through a normal vaginal delivery, to healthy young parents with an older healthy child.

MRI scans and amino acid levels in the blood and CSF were within normal limits during the first 3 weeks after birth. Upon admission (at the Children Respiratory Unit, Herzog Medical Center, Jerusalem, Israel), at age 3 weeks, repeated seizures with bradycardic spells and oxygen desaturation episodes appeared and he was immediately ventilated through a tracheostomy, and fed through a PEG and has remained chronically ventilated and fed indefinitely. His current video-EEG displayed random asymmetrical high-voltage slow-wave spike activity referred to as hypsarrhythmia, and frequent interictal multifocal spikes with occasional irregular suppression burst (SB) patterns. Most of his ictal EEG activity was associated with intractable tonic spasms (most frequent), myoclonic seizures, and TM-S, which were the longest and most intense epileptic seizures. Seizure-related EEG activity seemed to be driven by paroxysmal changes in right hemisphere delta-frequency (1–2 Hz) spikes.

His routine antiepileptic medication included Clonazepam 1.5 mg/day, Vigabatrin 750 mg/day, and Topiramate 100 mg/day. His average seizure frequency was ranged from 50 to 100 epileptic seizures per hour. His overall EEG evolutionary changes (from age 3 months to 40 months) indicated a shift from regular SB patterns to modified hypsarrhythmia, with irregular periods of SB and slow-wave multifocal spikes. Although 75% of OS cases evolve to WS, intermittent irregular SB patterns consistently appeared in both sleeping and waking periods. This may support an OS diagnosis, which is extremely rare at this age-group, as most surviving cases after 6 months of age display hypsarrhythmia without SB patterns (Ohtahara and Yamatogi, 2006).

Study Design

The study consisted of a 5-day baseline-monitoring period prior to HD-tDCS intervention, a 20-day HD-tDCS intervention, and 32-days post-HD-tDCS intervention assessment period (**Figure 1**). The baseline-monitoring period consisted of five daily video-EEG recordings of 120 min per session (total of 600 min of baseline video-EEG), where epileptic discharge frequency and most dominant epileptic foci were monitored and quantified.

Following the baseline period, stimulation was applied according to the defined dose (see *HD-tDCS*) and was repeated over the course of 4 weeks (5-days per week). The 4 × 1 HD-tDCS montage was predetermined based on the scalp electrodes that indicated the largest paroxysmal amplitude and highest frequency of IED across frontal–temporal–parietal right-hemisphere locations, which was considered the most dominant seizure-generating neocortical area. During the intervention period, video-EEG data were acquired each day concurrently with HD-tDCS administration. For clinical monitoring purposes, intervention video-EEG data (120 min per session) were also acquired immediately after HD-tDCS sessions 12 times (120 min a day, at days 1, 3, 5, 6, 8, 10, 11, 13, 15, 16, 18, and 20; **Figure 1**) totaling 1,440 min of video-EEG indicating the child's epileptiform activity immediately post HD-tDCS sessions during the intervention period.

Post HD-tDCS antiepileptic effects were assessed using video-EEG recordings across a 32-day post-intervention period (five 120-min sessions, totaling 600 min of post-intervention video-EEG) from post-intervention days 3, 10, 18, 25, and 32. As in the baseline period, post-intervention video-EEG analyses examined seizure frequency (number of seizure over a period of 120 min), IEDs parameters (spike/sharp waves), mean delta (0.5–3.5 Hz) power, and seizure-related mean maximal delta desynchronization across 7,200 s video-EEG segments per day.

Clinical monitoring (O_2 blood saturation, pulse rate, respiratory rate, temperature, and weekly blood tests) was

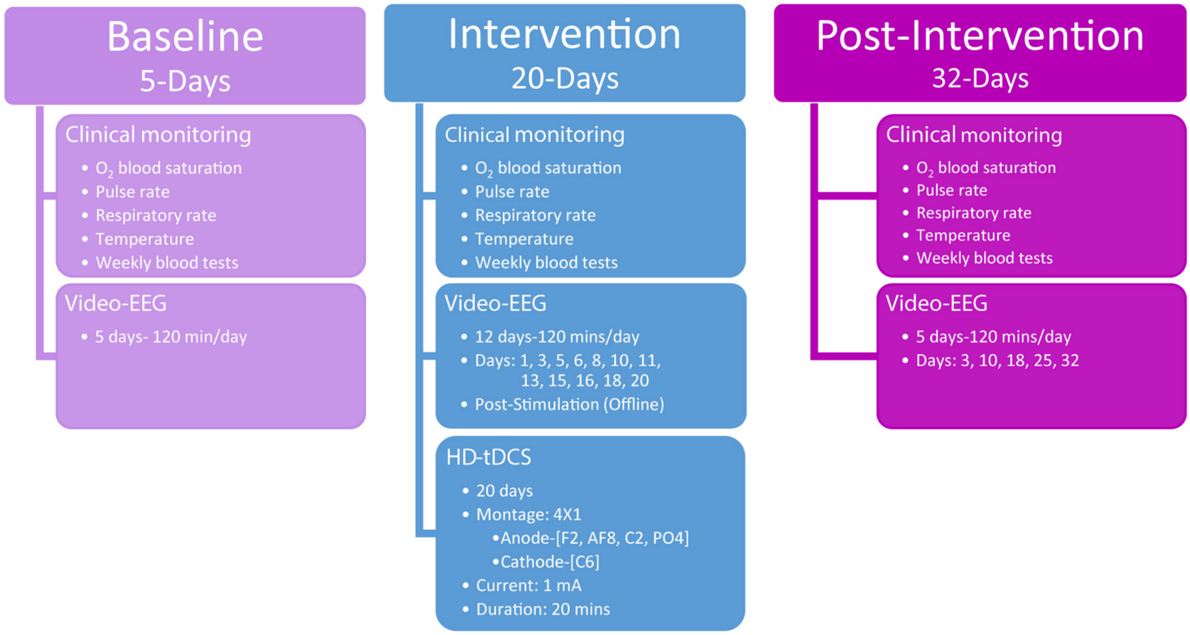

FIGURE 1 | Study overview detailing the three phases of assessments including baseline, intervention, and post-intervention. The timing and procedures administered are detailed for each of the three phases.

conducted across the entire clinical study and neurological assessments were administered at baseline (3 days prior to intervention) and immediately after the last HD-tDCS treatment session (day 20). Behavioral Pain Scale for critically ill patients (Payen et al., 2001) was administered before and after each HD-tDCS session to in order to record possible physical signs of discomfort or pain.

Video-EEG Acquisition and Analysis

During the baseline and post-intervention period scalp EEG were acquired using a 32-channel shielded cap (WaveGuard cap, ANT Neuro, Netherlands) with online 50 Hz notch filter, band-pass 0.016–256 Hz, sampling rate 512 Hz, averaged reference, grounded at AFz, and amplified using an ANT 32 channel amplifier (ANT, Netherlands). Intervention scalp EEG data were acquired using a 32-channel shielded cap (WaveGuard cap, ANT Neuro, Netherlands) with 29 integrated HD holders (Soterix Medical Inc.). Electrode positions were based on the 10/10 international system. Data were sampled at 512 Hz with a 0.016–256 Hz bandpass filter and 50 Hz notch filter, referenced to CPz, grounded at AFz, and amplified using an eego sport amplifier (ANT Neuro, Netherlands) with a bandwidth of 0–520 Hz.

Offline data analysis (including automatic spike detection analysis) of baseline and pot-intervention EEG was performed using ASALAB (4.9.3; ANT Neuro, Netherlands), and MATLAB (R2015b; MathWorks, Natick, MA, United States). Offline, baseline and post-intervention EEG was cleaned using a zero-phase 0.25–70 Hz bandpass filter (filter steepness 24 dB/oct), and using the artifact-detection function within the advance source analysis software (ASA 4.9.3, ANT, Netherlands) for noisy amplitude changes (DC correction within the ±200 μV range). Fast Fourier transformation (FFT) with epoch-length 0.5 s across the entire 7,200 s (averaging 14,400 epochs) of clean EEG (with power spectra normalized) was employed in order to review the mean spectral-power-changes in delta (0.5–3.5 Hz), theta (3.5–7.5 Hz), alpha (7.5–12.5 Hz), and beta (12.5–30 Hz) bands and their scalp topography before and after HD-tDCS intervention. Spectral power density values were subjected to a $\log_{10}$ transformation for final statistical analysis. Seizure-related spectral analysis (noting spectral density power differences between 3 s pre-seizure time-window vs. 3 s post-seizure time-window, with 0.25 s offset) generating averaged spectral power head-maps of paroxysmal delta-band (0.5–3.5 Hz) activity across all visually marked ictal events, were collected and analyzed using Advanced Source Analysis software (ASA 4.9.3, ANT-Neuro, Netherlands). Seizure-related differences in SDP from pre to post-seizure-onset window were obtained by running an averaged FFT in 500 ms steps across 6,000 ms epochs of seizure-related events. We display the results only for the delta band where topography and power changes were most consistent with seizure-onset, and associated with paroxysmal changes in IED topography (Meiron et al., 2018). **Supplementary Figure S1** provides an illustration of the raw EEG during a TM-S, and IEDs in an area representing the most dominant epileptic focus; under electrodes P4 and FC2.

The most dominant epileptic focus was predetermined during the baseline period according to the most salient topography in hypsarrhythmic slow-wave IED's (Gaily et al., 2001), and most prominent topography of averaged seizure-related power changes in delta waves (Meiron et al., 2018). Accordingly, C6 electrode location, which was the midpoint between right parietal and right frontal most dominant epileptic foci (e.g., P4 and FC2showing the highest IED frequency, and mean spike amplitude) was chosen as the target location for placing the center-cathodal HD-tDCS electrode (Meiron et al., 2018). Those scalp EEG locations consistently displayed the most paroxysmal seizure-related delta and spike activity. The rationale behind the "midpoint" method for targeting the most dominant epileptic foci is that the HD-tDCS spatial configuration inhibits all these right hemisphere locations as they fall within the 4 × 1 HD-tDCS ring montage. Thus, although P4 and FC2 are hypothesized as most dominant foci, we cannot be sure that this epileptiform activity necessarily originates from only frontal or only parietal locations, therefore, it is likely the right motor cortex location that fall between these two IED locations (such as electrode C6), possibly also contributes to the generation of clinical seizures. All right hemisphere adjacent location represent seizure related dominant areas (Meiron et al., 2018), so we made sure that the cathodal stimulation covered all these proximal seizure-related locations. Thus, utilizing a large 4 × 1 ring configuration to cover all these areas is more likely to inhibit the right-hemisphere network that generates the IED's and associated seizures.

In order to evaluate the changes in seizure frequency from baseline to post stimulation, seizures (and seizure classification) were recorded and noted by video-EEG and visually analyzed by pediatric epileptologist (i.e., child neurologist) and clinical electrophysiologist (authors OBB and OM, respectively). Epileptic tonic spasms were defined as a brief phasic contraction followed by a short tonic phase (Gaily et al., 2001) lasting around 1 s. Myoclonic seizures were defined as sudden muscle jerks, which lasted around 1–2 s. Tonic myoclonic seizures were defined as a brief tonic spasms followed immediately by myoclonic jerks last usually between 1.5–11 s. We inspected seizures of all durations (from 1 to 11 s duration), hypsarrhythmic interictal paroxysmal discharges (of random high-voltage slow waves and spikes of varying duration and location) were quantified according to Watanabe et al. (1993b) and Gaily et al. (2001) definitions of hypsarrhythmia observed in early onset electroclinical syndromes. IEDs were counted across 120 min EEG sessions using an automatic spike detection algorithm (ASA 4.9.3, ANT, Netherlands) calculating sharp waves (70–200 ms) and spike waves (0–70 ms) of negative polarity and an amplitude ratio five times larger than the averaged ongoing EEG activity. In addition to spike frequency, durations and peak amplitudes of spikes were extracted and noted by the spike-detection algorithm as well. These specific spike (sharp waves and spike wave) -parameters were previously supported as epileptiform markers associated with seizure frequency and topography in other cases of early onset epileptic encephalopathy (Watanabe et al., 1993b; Meiron et al., 2018). The spectral scalp maps for mean delta activity (2 Hz was used as it showed the maximal power peaks) were generated using MATLAB (version R2017b, with eeglab toolbox; Delorme and Makeig, 2004). The data were cleaned using automatic continuous rejection function and filter function employing a windowed sinc FIR filter algorithm with bandpass of 1–45 Hz (hamming window-type, PB dev = 0.002, SB att = −35 dB, transition bandwidth of 1 Hz). Fast Fourier Transform (FFT) was employed (Hanning window length: 512; FFT length: 512; overlap: 0) to extract the mean power of 2 Hz oscillations.

HD-tDCS

Stimulation dose consisted of 1 mA of current delivered for 20 min a day, for 20 days, with a 4 × 1 HD-tDCS montage in an open-label design. The HD-tDCS center cathode was placed at the right central C6 location (C6 electrode location was the midpoint between most dominant frontal and parietal epileptic foci), and the four surrounding anodes were placed at anterior-frontal (AF8), frontal (F2), central (C2), and parietal–occipital (PO4) locations. While principled approached for EEG inversion are proposed (Cancelli et al., 2016; Dmochowski et al., 2017), the 4 × 1 montage is robust to simple configuration rules, producing significant current flow in the brain areas circumscribed by the ring-electrodes with a polarity based on the center electrodes (Alam et al., 2016). Therefore, the frontal anodes were 3 cm anterior (F2) and 8 cm anterior (AF8) to the dominant frontal focus which was under FC2 frontal location. The electrode PO4 anode was 3 cm posterior to the parietal dominant epileptic focus (P4), and the C2 anode was 6 cm dorsal to the parietal epileptic focus (**Figure 2**). The target area was predetermined based on the most salient scalp locations indicating maximal seizure-related delta power changes and paroxysmal interictal spike topography across a 5-day baseline period (Meiron et al., 2018). Stimulation was delivered through five Ag/AgCl sintered ring electrodes (4 mm radius), held in place by specially designed plastic casings and current was supplied using a Soterix Medical 1 × 1 LTE (extra voltage limited) stimulator and a 4 × 1 HD-tDCS adaptor (Hahn et al., 2013), while using established HD-tDCS methods (Villamar et al., 2013).

HD-tDCS Computational Model

A high-resolution head model was generated based on an MRI of an age matched infant with 0.5 mm^3 resolution in order to predict current flow patterns. A computational finite element model (FEM) of the head was employed to predict the spatial distribution of electric fields in cortex and the voltage distribution over the skin for safety considerations and stimulation efficacy. Automated segmentation was first performed using Statistical Parametric Mapping (SPM8) package (Wellcome Trust Centre for Neuroimaging, London, United Kingdom) in MATLAB in order to segment images into six different tissues with conductivities assigned to each: skin (0.465 S/m), skull (0.01 S/m), air (1×10^{-15} S/m), CSF (1.65 S/m), gray matter (0.276 S/m), white matter (0.126 S/m), electrode (5.8 × 107 S/m), and gel (1.4 S/m). Residual segmentation errors were corrected in ScanIP (Simpleware, Ltd., Exeter, United Kingdom) using a combination of segmentation tools. The resulting volumetric meshes were imported into a FEM solver (COMSOL, Burlington, MA, United States) for FE computation. The center cathode received 1 mA total current whereas the four anodes received symmetric 0.25 mA of current (**Figure 2B**). Maximizing the normal component of an electric field to 0.6 V/m, the approximate electric field observed in average adult brains under 2 mA of applied current, indicated a spread of electric field across

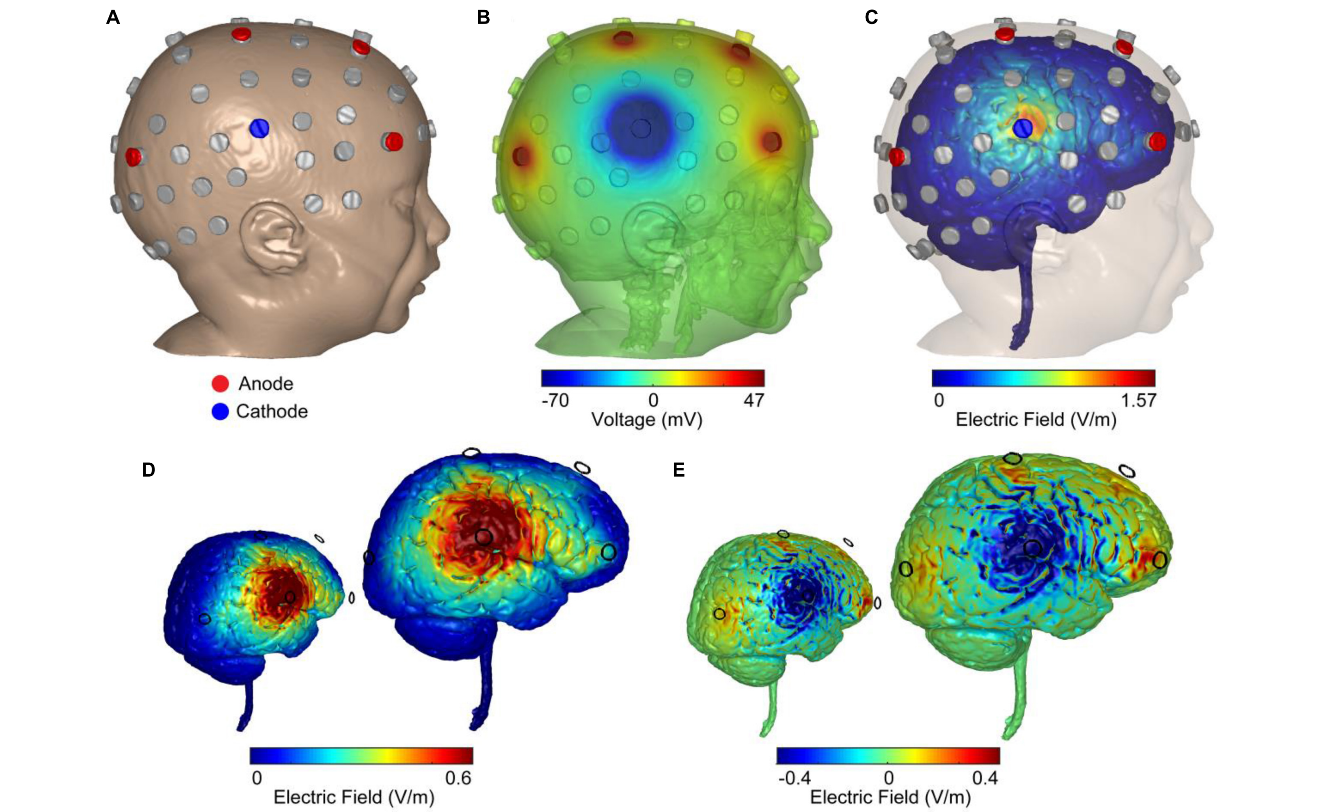

FIGURE 2 | Computer simulations of 4 × 1 HD-tDCS intervention in an age-matched MRI-derived head model. **(A)** FEM MRI-derived model of an age-matched infant with electrode positioning is based on the 10/10 International system. Locations were used for recording EEG (gray) and stimulation (blue: cathode; red: anode). **(B)** Model-based prediction from FEM indicating scalp voltages across the head and at the anodes and cathode (false color: blue minimum = –70 mV, red maximum = 47 mV, green = 0 mV). **(C)** Model-based current flow field across the brain indicating maximal electric field under the cathode (false color: blue = 0 V/m, red = 1.57 V/m). **(D)** Finite-element model predictions of the normal electric field across the brain indicating electric field under the cathode (false color: blue = 0 V/m, red = 0.6 V/m). The color scheme maximized to 0.6 V/m (seen in adult brains under 2 mA of applied current) indicated a large right temporal lobe electric field. **(E)** Model-based radial electric field distribution across the brain indicating electric field under the cathode (false color: blue = –0.4 V/m- outward-radial electric field, inhibitory; red = 0.4 V/m-inward-radial electric field, excitatory).

the right temporal lobe (**Figure 2D**). Computing the magnitude of the radial electric field represents inward and outward components of the electric field (normal to the cortical surface; **Figure 2E**). An inward-radial electric field can be interpreted as excitatory/anodal stimulation whereas the outward-radial electric field could represent inhibitory/cathodal stimulation (Nitsche and Paulus, 2000; Bikson et al., 2004; Rahman et al., 2013).

Statistical Analyses

Before examining statistically significant changes in outcome clinical variables, all seizure and epileptiform variables were subjected to normal distribution assessments using Kolmogorov–Smirnov tests. Variables that were normally distributed were subjected to parametric testing (paired sample *t*-tests), whereas non-normally distributed data were subjected to non-parametric statistical tests (Wilcoxon signed rank tests). In terms of interictal IED parameters, to avoid multiple comparisons, and because we were interested in the immediate effects following the intervention period, we compared only 1 day from post-intervention (immediately after 20 days of intervention) versus 1 day from baseline (3 days before HD-tDCS intervention). It is important to note that there were only five comparison points within baseline and within post-intervention for assessing changes in primary clinical outcome variables; thus, we acknowledge that assessing more days in future studies may further clarify the clinical benefits following a 20-day HD-tDCS intervention.

RESULTS

Tonic spasm frequency (TSF) was similar [$t(4) = -0.29$, $p = 0.78$] for both baseline ($M = 189.8$, $SD = 68.65$) and post-intervention ($M = 225$, $SD = 214.54$) periods. Post-intervention myoclonic seizure (M-S) frequency (mean: 1.2 ± 1.64) was significantly reduced [paired-samples *t*-test; $t(4) = 3.83$, $p = 0.019$] compared to baseline M-S frequency (mean: 3.8 ± 1.3; **Figure 3A**). Compared to baseline ($M = 8$, $SD = 4.47$), post-intervention ($M = 2$, $SD = 2.34$) TM-S frequency was not significantly [$t(4) = 2.05$, $p = 0.1$] lower. TM-S frequency was reduced

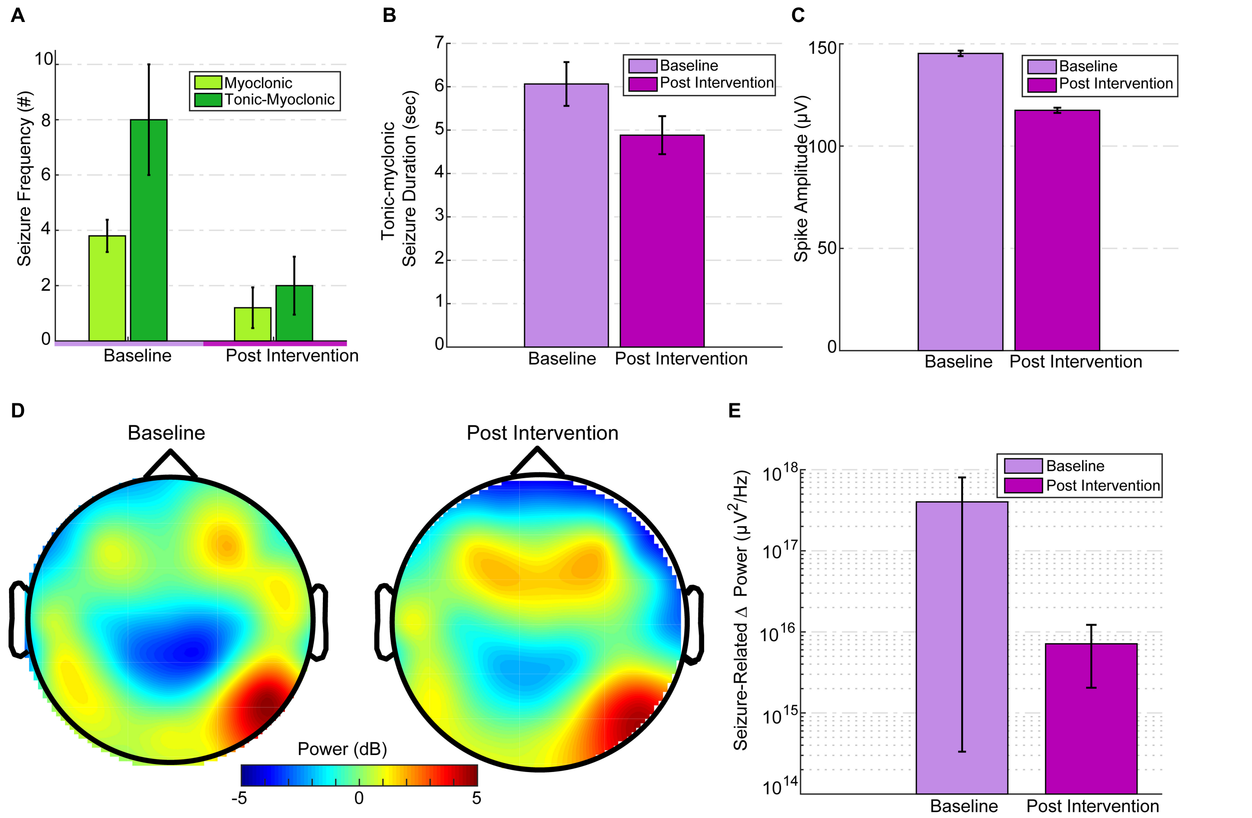

FIGURE 3 | EEG seizure baseline and post-intervention comparisons. **(A)** Seizure frequency for baseline and post intervention divided into M-S and TM-S. M-S frequency was significantly reduced ($p = 0.019$) and TM-S were reduced by more than 50% post intervention. **(B)** TM-S duration between baseline and post-intervention periods. **(C)** Mean spike amplitudes at baseline (3 days before intervention) versus intervention day 20 (immediately after the last treatment session). Spike amplitudes were significantly reduced ($p < 0.001$) compared to baseline. Spike amplitudes over the post-intervention period were significantly reduced ($p < 0.001$) compared to baseline. **(D)** Topographic scalp maps of normalized delta activity (2 Hz) comparing baseline (3 days before stimulation) and post intervention (3 days after intervention). **(E)** There was a significant difference ($p = 0.01$) between seizure-related mean peak delta desynchronization between baseline and post intervention.

by 72.88%, which constituted a clinically significant change, and represented an effective partial-response to the treatment defined as a seizure-frequency reduction >50% from baseline (**Figure 3A**). TSF, TM-S, and M-S frequencies across baseline and post-intervention periods were distributed normally. M-S ($M = 3.8$, $SD = 2.16$, range = 5) and TM-S frequency ($M = 3.2$, $SD = 3.9$, range = 7) during the intervention period (from days 5, 10, 13, 15, and 18) was similar to baseline M-S and TM-S frequency.

Since TM-S are of the longest durations (and seizure-intensity), a comparison between the TM-S durations from post-intervention (mean: 4.88 ± 1.45) versus the TM-S durations during baseline (mean: 6.06 ± 3.11) indicated that TM-S durations were non-significantly [$t(24) = 1.46$, $p = 0.1$] reduced by 19.47% at post-intervention versus baseline TM-S durations (**Figure 3B**). In order to avoid multiple comparisons, using a related samples Wilcoxon signed ranked test, we compared interictal spike frequency (summation of all spike waves; 0–70 ms, and sharp waves; 70–200 ms), spike peak amplitudes, and spike durations from intervention-day-20 (intervention day 20, immediately after the last HD-tDCS session) to the last baseline day (3 days before onset of intervention period) and found that the spike peak amplitudes were significantly reduced ($Z = -45.8$, $p < 0.001$) at post-intervention versus baseline (see **Figure 3C**). Spike durations were also significantly reduced at post-intervention versus baseline ($Z = -27.49$, $p < 0.001$). The interictal spike frequency 3 days prior to intervention was 10,876 versus 2,872 spikes at post-intervention day-20, indicating a 73.5% reduction in the frequency of IED. IED frequency during the baseline period ($M = 8330.8$, $SD = 2017.86$) was not significantly different [$t(4) = 0.43$, $p = 0.68$] from the IED frequency at post-intervention period ($M = 7344.2$, $SD = 4018.57$). The mean IED amplitudes were also not significantly changed [$t(4) = -2.1$, $p = 0.1$] at post-intervention ($M = 154.54$, $SD = 13.69$, range = 37.32) versus baseline ($M = 142.26$, $SD = 6.03$, range = 16.04).

Mean absolute spectral power of whole-brain (from 32 electrode location) delta frequency (Fast-Fourier transformed and averaged across 14,400 epochs of 0.5 s) across the 2-h baseline session (3 days before intervention) was lateralized asymmetrically and most dominant at right parietal-temporal (and slightly right-frontal) locations (see **Figure 3D**, illustrating normalized 2 Hz changes from baseline to intervention) and subdominant at contralateral temporal T7 electrode location. Post-intervention (3 days after intervention) mean whole-brain relative change in delta (0.5–3.5 Hz) power was 45.5% lower than baseline. To avoid multiple comparisons, we considered the change in mean delta power only between these two specific days before and after the intervention. This comparison reflected time-points that were closest to the onset and termination of the intervention. The mean relative change in delta power at post-intervention was reduced particularly at target electrode locations (P8-C6 and T8-F8 at right hemisphere) under the HD-tDCS 4 × 1 target-area (most dominant baseline epileptic focus), and the reduction was more pronounced over-the target-right hemisphere (**Figure 3D**).

Seizure-related delta-desynchronization (delta ERD) during post-intervention was significantly lower ($Z = 337$, $p = 0.01$) than delta-ERD at baseline (**Figure 3E**). All seizure-related (during tonic-myoclonic, tonic spasms, and myoclonic seizures only) paroxysmal delta ERD peaks (at least 500% change-in induced delta power at a 4 s interval following seizure onset relative to −0.1 to −0.3 s pre-seizure interval) were found mainly within the lower delta range (0.5 Hz–2 Hz). Across the entire baseline period (600 min of EEG) 68 delta ERD peaks were detected versus 29 delta-ERD peaks at post-intervention period (600 min of EEG), indicating a 57% reduction in ictal delta ERD activity after 20 days of HD-tDCS treatment. Therefore, not all the observed seizures were accompanied by 500% change in peak delta power and were excluded from the final peak delta ERD analysis.

The baseline neurological examination indicated severe axial hypotonia, and the child did not show any sign of communication. He responded to pain stimulation with non-specific limb movement. He was unable to make eye contact or follow an object visually and did not respond to acoustic stimuli. There were only occasional spontaneous limb movements. Contractures with limited range of motion of fingers, wrists, ankles and knees were noted bilaterally. Deep tendon reflexes were absent. There was no clonus. Plantar responses were extensor bilaterally. Face was symmetric with minimal movements and expressions. There was no titubation or dysmetria. Gag reflex was weak and corneal reflex elicited on the right but not on the left eye. At post-intervention examination there was no change in neurological status except this time the corneal reflex was elicited bilaterally.

Over the course of the HD-tDCS intervention period, IED parameters were monitored to verify a consistent decline in paroxysmal epileptiform activity. IED frequency and peak amplitudes showed the largest reduction after intervention days 1, 13, and 15, while spike durations showed the most pronounced reduction at day 10 of the intervention (**Figure 4**). No significant differences were observed between the left and right hemisphere spikes, and the IED parameters were not significantly changed within the intervention period. To observe the acute IED dynamics during the treatment intervention, treatment days 1–18 were compared. Note that mean spike frequency during the intervention period showed a pronounced decrease from baseline days ($M = 8330.8$, $SD = 2017.86$). To examine the relationship between the epileptiform activity on intervention-day 20 with post-intervention days, we examined the correlations among these measures' peak amplitudes. IED peak amplitudes on intervention-day 20 of the intervention were significantly related (all were subject to Spearman's Rho test; $-0.142 \leq R \leq -0.295$, $p < 0.001$) to IED peak amplitudes on all post-intervention days (3, 10, 18, 25, and 32 days post intervention).

DISCUSSION

The efficacy of tDCS to suppress epileptiform activity and epileptic seizures was demonstrated in animal models (Nitsche and Paulus, 2009) and patient populations with focal epilepsy due to abnormal cortical development (Fregni et al., 2006). In patient populations, 20 min of cathodal tDCS positioned at

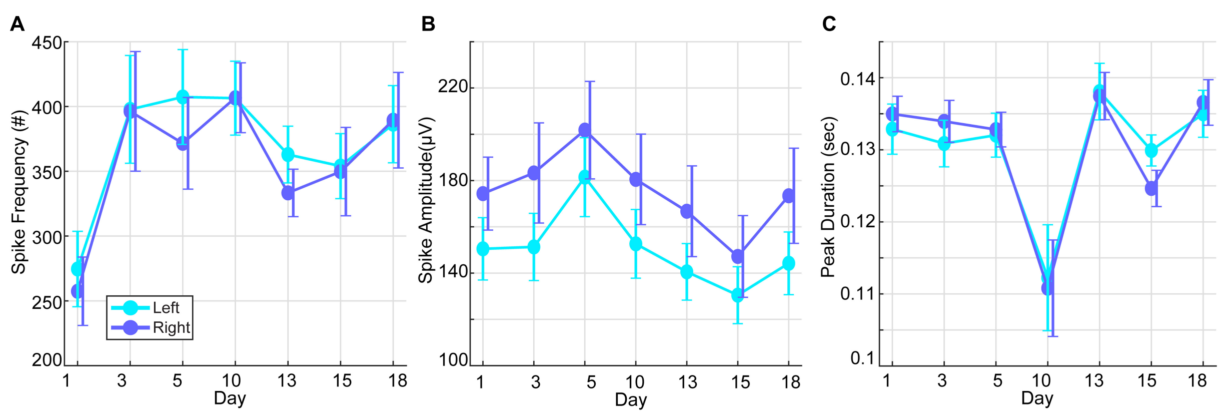

FIGURE 4 | Interictal epileptic discharges (spike waves and sharp waves) during the intervention period. **(A)** Mean spike frequency of the right and left hemisphere over days of stimulation (baseline prior to HD-tDCS: $M = 8330.8$, $SD = 2017.86$). **(B)** Mean spike amplitudes of the right and left hemisphere over days of stimulation (baseline prior to HD-tDCS: $M = 142.26$, $SD = 6.03$ μV). **(C)** Mean spike duration of the right and left hemisphere over days of stimulation (baseline prior to HD-tDCS: $M = 0.093$, $SD = 0.0044$ s).

their epileptic focus significantly reduced epileptic discharges, but had only a trend-wise effect on seizure frequency (Fregni et al., 2006). There is a broad consensus across translational animal studies and clinical trials on the putative mechanisms of direct current stimulation (Sunderam et al., 2010). tDCS will produce membrane polarization with current directed in the cathodal direction producing somatic hyperpolarization (Chan and Nicholson, 1986; Bikson et al., 2004) which reduces neuronal excitability (Gluckman et al., 1996; Bikson et al., 2004). When tDCS is sustained for minutes, it can produce lasting change in excitability (Bindman et al., 1964; Nitsche and Paulus, 2000). tDCS is among a constellation of emerging and investigational brain stimulation techniques (both invasive and non-invasive) for epilepsy (Wu and Sharan, 2013; Nune et al., 2015; Eastin and Lopez-Gonzalez, 2017; Kwon et al., 2018), but is unique in acting through direct hyperpolarizing rather than decreasing excitably secondary to neuronal activity (e.g., LTD, desynchronization).

In this case, our results suggest an effective, and significant clinical response, as well as a significant reduction in IED amplitudes immediately after the last day of intervention, via application of a focal, non-invasive neuromodulation procedure. The reduction in IED amplitudes was not sustained during the post-intervention period, while the reduction in myoclonic seizures was noted and sustained during the post-intervention period. In addition, it is important to note that although targeted dominant foci seem to receive less inhibitory field than its proximal C6 motor-network center-cathode location (see **Figure 2E**), these dominant foci locations were applied as the topographical boundaries of the seizure-generating zone, targeting the area under the HD-tDCS right-hemisphere ring configuration between the frontal and parietal foci locations. Thus, the maximal inhibitory current at the common adjacent motor-network residing between frontal–parietal dominant foci most likely generated secondary inhibitory effects at frontal–parietal dominant foci locations. Specifically, we utilized HD-tDCS to treat a 40-month-old child suffering from a severe electro-clinical syndrome (i.e., OS, organic etiology associated with brain-dysgenesis); a condition that ultimately results in severe developmental retardation, high frequency of daily seizures, and early death at infancy (Ohtahara and Yamatogi, 2006).

Importantly, there are only a few sporadic early-onset epileptic encephalopathy cases that display a sufficient response (e.g., seizure control) to conventional anti-epileptic treatments (e.g., ACTH, clonazepam, valproate, vigabatrin or ketogenic diet). Although the current investigation is limited by one case, our findings support a significant alleviation of myoclonic seizures and attenuation of epileptiform-hypsarrhythmic features that are related to electroclinical-syndrome severity and prognosis (Siniatchkin et al., 2007). Seizure-related delta reactivity during the post-intervention period and IED amplitude/durations on intervention day 20 were significantly reduced, which was clinically cross-validated by a significant reduction in myoclonic seizure frequency, and a 72% reduction in TM-S. TSF was not significantly reduced, however, it's underlying paroxysmal (high-voltage) delta activity, associated with increased brain-stem BOLD signal (Siniatchkin et al., 2007), was reduced by 57%. The observed clinical response (attenuation of M-S and TM-S frequency) was supported by significantly lower seizure-related whole-brain delta ERD at post-intervention (post-intervention days 3 to 32). More so, the IED amplitudes on intervention day 20 were significantly associated with IED amplitudes within the five different post-intervention days, possibly implying a common source of epileptiform activity. The reduction in epileptiform activity observed on intervention day 20 may have contributed to the observed clinical benefits past the active intervention period, such as the reduction in myoclonic seizures observed during the post-intervention period. The reduction in slow-wave activity was observed over the targeted seizure-generating network, indicating lower hypsarrhythmic delta activity at right parietal–temporal electrode locations, which showed the most paroxysmal IED's at baseline. This localized reduction attested to the focal effects of HD-tDCS over the targeted cortical region.

HD-tDCS can be guided to stimulate any brain regions, including deep structures, and multiple foci (Dmochowski et al., 2017; Huang et al., 2018). Ongoing studies may inform which cortical or brain-stem substructures (Siniatchkin et al., 2007) may be targeted using customized HD-tDCS montages to reduce specific epileptiform activity patterns related to tonic-spasm generation in pediatric cases suffering from early-onset epileptic encephalopathy syndromes. This case study supports ongoing HD-tDCS seizure-control trials in pediatric epilepsy including other severe electroclinical syndromes (displaying hypsarrhythmia and intractable seizures) such as early myoclonic encephalopathy, Lennox-Gastaut syndrome, and WS, and cross-validated in epileptic patients with childhood focal epilepsy.

ETHICS STATEMENT

This study was carried out in accordance with the recommendations of Herzog Medical Center Institutional review board with written informed consent from the legal guardian (parents). The subject's parents gave their informed consent in accordance with the Declaration of Helsinki. The protocol was approved by the Israel Ministry of Health and the Herzog Medical Center's Institutional Review Board.

AUTHOR CONTRIBUTIONS

All co-authors contributed significantly to the execution and supervision of the current study. OM was responsible for data collection, data analysis, interpretation of findings, overseeing the execution of the study, and the composition of the manuscript. RG was responsible for data collection, supervision, and composition of the manuscript. JN was responsible for data collection, supervision, and clinical evaluations. MB was responsible for data analysis, supervision, and manuscript composition. NG was responsible for data analysis and composition of the manuscript. OB-B was responsible for data collection including clinical evaluation and manuscript composition. ZE was responsible for data analysis. VM was responsible for data organization and data analysis.

ACKNOWLEDGMENTS

We thank the medical nursing team at the Children Respiratory Unit, for their dedication and full collaboration in facilitating the current study. We thank the Crown Foundation for partial funding support awarded to OM and the National Institutes of Health (NIH–NINDS 1R01NS101362, NIH–NIMH 1R01MH111896, NIH–NCI U54CA137788/U54CA132378, and NIH–NIMH 1R01MH109289) for partial funding support to MB.

SUPPLEMENTARY MATERIAL

The Supplementary Material for this article can be found online at: https://www.frontiersin.org/articles/10.3389/fnins.2019.00547/full#supplementary-material

FIGURE S1 | Raw EEG activity during tonic-myoclonic seizure. Red vertical lines represent the onset and offset of the seizure, orange horizontal line represents the duration of the seizure (close to 4 seconds). The left purple line represent interictal epileptic discharges on several channels (e.g., P8, C4, CP2) at approximately one second before the seizure onset. The light-blue vertical lines mark specific channels that display IED onset before (at P4 electrode) and after (at FC2 electrode) the seizure. The entire figure represents 10 seconds of EEG, each second indicated by gray vertical lines.

REFERENCES

Alam, M., Truong, D. Q., Khadka, N., and Bikson, M. (2016). Spatial and polarity precision of concentric high-definition transcranial direct current stimulation (HD-tDCS). *Phys. Med. Biol.* 61, 4506–4521. doi: 10.1088/0031-9155/61/12/4506

Auvichayapat, N., Rotenberg, A., Gersner, R., Ngodklang, S., Tiamkao, S., Tassaneeyakul, W., et al. (2013). Transcranial direct current stimulation for treatment of refractory childhood focal epilepsy. *Brain stimul.* 6, 696–700. doi: 10.1016/j.brs.2013.01.009

Auvichayapat, N., Sinsupan, K., Tunkamnerdthai, O., and Auvichayapat, P. (2016). Transcranial direct current stimulation for treatment of childhood pharmacoresistant lennox-gastaut syndrome: a pilot study. *Front. Neurol.* 7:66. doi: 10.3389/fneur.2016.00066

Beal, J. C., Cherian, K., and Moshe, S. L. (2012). Early-onset epileptic encephalopathies: ohtahara syndrome and early myoclonic encephalopathy. *Pediatr. Neurol.* 47, 317–323. doi: 10.1016/j.pediatrneurol.2012.06.002

Bikson, M., Inoue, M., Akiyama, H., Deans, J. K., Fox, J. E., Miyakawa, H., et al. (2004). Effects of uniform extracellular DC electric fields on excitability in rat hippocampal slices in vitro. *J. Physiol.* 557, 175–190. doi: 10.1113/jphysiol.2003.055772

Bindman, L. J., Lippold, O. C., and Redfearn, J. W. (1964). The action of brief polarizing currents on the cerebral cortex of the rat (1) during current flow and (2) in the production of long-lasting after-effects. *J. Physiol.* 172, 369–382. doi: 10.1113/jphysiol.1964.sp007425

Brunoni, A. R., Nitsche, M. A., Bolognini, N., Bikson, M., Wagner, T., Merabet, L., et al. (2012). Clinical research with transcranial direct current stimulation (tDCS): challenges and future directions. *Brain Stimul.* 5, 175–195. doi: 10.1016/j.brs.2011.03.002

Cancelli, A., Cottone, C., Tecchio, F., Truong, D. Q., Dmochowski, J., and Bikson, M. (2016). A simple method for EEG guided transcranial electrical stimulation without models. *J. Neural Eng.* 13:036022. doi: 10.1088/1741-2560/13/3/036022

Chan, C. Y., and Nicholson, C. (1986). Modulation by applied electric fields of Purkinje and stellate cell activity in the isolated turtle cerebellum. *J. Physiol.* 371, 89–114. doi: 10.1113/jphysiol.1986.sp015963

Datta, A., Bansal, V., Diaz, J., Patel, J., Reato, D., and Bikson, M. (2009). Gyri-precise head model of transcranial direct current stimulation: improved spatial focality using a ring electrode versus conventional rectangular pad. *Brain Stimul.* 2:207e201.

Delorme, A., and Makeig, S. (2004). EEGLAB: an open source toolbox for analysis of single-trial EEG dynamics including independent component analysis. *J. Neurosci. Methods* 134, 9–21. doi: 10.1016/j.jneumeth.2003.10.009

Dmochowski, J. P., Datta, A., Bikson, M., Su, Y., and Parra, L. C. (2011). Optimized multi-electrode stimulation increases focality and intensity at target. *J. Neural Eng.* 8:046011. doi: 10.1088/1741-2560/8/4/046011

Dmochowski, J. P., Koessler, L., Norcia, A. M., Bikson, M., and Parra, L. C. (2017). Optimal use of EEG recordings to target active brain areas with transcranial electrical stimulation. *Neuroimage* 157, 69–80. doi: 10.1016/j.neuroimage.2017.05.059

Eastin, T. M., and Lopez-Gonzalez, M. A. (2017). Stimulation and neuromodulation in the treatment of epilepsy. *Brain Sci.* 8:E2.

Edwards, D., Cortes, M., Datta, A., Minhas, P., Wassermann, E. M., and Bikson, M. (2013). Physiological and modeling evidence for focal transcranial electrical brain stimulation in humans: a basis for high-definition tDCS. *Neuroimage* 74, 266–275. doi: 10.1016/j.neuroimage.2013.01.042

Fregni, F., Thome-Souza, S., Nitsche, M. A., Freedman, S. D., Valente, K. D., and Pascual-Leone, A. (2006). A controlled clinical trial of cathodal DC polarization in patients with refractory epilepsy. *Epilepsia* 47, 335–342. doi: 10.1111/j.1528-1167.2006.00426.x

Gaily, E., Liukkonen, E., Paetau, R., Rekola, R., and Granstrom, M. L. (2001). Infantile spasms: diagnosis and assessment of treatment response by video-EEG. *Dev. Med. Child Neurol.* 43, 658–667. doi: 10.1111/j.1469-8749.2001.tb00139.x

Ghai, R. S., Bikson, M., and Durand, D. M. (2000). Effects of applied electric fields on low-calcium epileptiform activity in the CA1 region of rat hippocampal slices. *J. Neurophysiol.* 84, 274–280. doi: 10.1152/jn.2000.84.1.274

Gluckman, B. J., Neel, E. J., Netoff, T. I., Ditto, W. L., Spano, M. L., and Schiff, S. J. (1996). Electric field suppression of epileptiform activity in hippocampal slices. *J. Neurophysiol.* 76, 4202–4205. doi: 10.1152/jn.1996.76.6.4202

Hahn, C., Rice, J., Macuff, S., Minhas, P., Rahman, A., and Bikson, M. (2013). Methods for extra-low voltage transcranial direct current stimulation: current and time dependent impedance decreases. *Clin. Neurophysiol.* 124, 551–556. doi: 10.1016/j.clinph.2012.07.028

Huang, Y., Thomas, C., Datta, A., and Parra, L. C. (2018). Optimized tDCS for targeting multiple brain regions: an integrated implementation. *Conf. Proc. IEEE Eng. Med. Biol. Soc.* 2018, 3545–3548. doi: 10.1109/EMBC.2018.8513034

Karvigh, S. A., Motamedi, M., Arzani, M., and Roshan, J. H. (2017). HD-tDCS in refractory lateral frontal lobe epilepsy patients. *Seizure* 47, 74–80. doi: 10.1016/j.seizure.2017.03.005

Kuo, H. I., Bikson, M., Datta, A., Minhas, P., Paulus, W., Kuo, M. F., et al. (2013). Comparing cortical plasticity induced by conventional and high-definition 4 × 1 ring tDCS: a neurophysiological study. *Brain Stimul.* 6, 644–648. doi: 10.1016/j.brs.2012.09.010

Kwon, C. S., Ripa, V., Al-Awar, O., Panov, F., Ghatan, S., and Jette, N. (2018). Epilepsy and neuromodulation-randomized controlled trials. *Brain Sci.* 8:E69. doi: 10.3390/brainsci8040069

Meiron, O., Gale, R., Namestnic, J., Bennet-Back, O., David, J., Gebodh, N., et al. (2018). High-Definition transcranial direct current stimulation in early onset epileptic encephalopathy: a case study. *Brain Inj.* 32, 135–143. doi: 10.1080/02699052.2017.1390254

Nitsche, M. A., and Paulus, W. (2000). Excitability changes induced in the human motor cortex by weak transcranial direct current stimulation. *J. Physiol.* 527(Pt 3), 633–639. doi: 10.1111/j.1469-7793.2000.t01-1-00633.x

Nitsche, M. A., and Paulus, W. (2009). Noninvasive brain stimulation protocols in the treatment of epilepsy: current state and perspectives. *Neurotherapeutics* 6, 244–250. doi: 10.1016/j.nurt.2009.01.003

Nune, G., DeGiorgio, C., and Heck, C. (2015). Neuromodulation in the treatment of epilepsy. *Curr. Treat Options Neurol.* 17:375.

Ohtahara, S., and Yamatogi, Y. (2006). Ohtahara syndrome: with special reference to its developmental aspects for differentiating from early myoclonic encephalopathy. *Epilepsy Res.* 70(Suppl. 1), S58–S67.

Payen, J.-F., Bru, O., Bosson, J.-L., Lagrasta, A., Novel, E., Deschaux, I., et al. (2001). Assessing pain in critically ill sedated patients by using a behavioral pain scale. *Crit. Care Med.* 29, 2258–2263. doi: 10.1097/00003246-200112000-00004

Rahman, A., Reato, D., Arlotti, M., Gasca, F., Datta, A., Parra, L. C., et al. (2013). Cellular effects of acute direct current stimulation: somatic and synaptic terminal effects. *J. Physiol.* 591, 2563–2578. doi: 10.1113/jphysiol.2012.247171

Rosso, O. A., Martin, M. T., Figliola, A., Keller, K., and Plastino, A. (2006). EEG analysis using wavelet-based information tools. *J. Neurosci. Methods* 153, 163–182. doi: 10.1016/j.jneumeth.2005.10.009

San-Juan, D., Espinoza Lopez, D. A., Vazquez Gregorio, R., Trenado, C., Fernandez-Gonzalez Aragon, M., Morales-Quezada, L., et al. (2017). Transcranial direct current stimulation in mesial temporal lobe epilepsy and hippocampal sclerosis. *Brain Stimul.* 10, 28–35. doi: 10.1016/j.brs.2016.08.013

Siniatchkin, M., Van Baalen, A., Jacobs, J., Moeller, F., Moehring, J., Boor, R., et al. (2007). Different neuronal networks are associated with spikes and slow activity in hypsarrhythmia. *Epilepsia* 48, 2312–2321.

Sunderam, S., Gluckman, B., Reato, D., and Bikson, M. (2010). Toward rational design of electrical stimulation strategies for epilepsy control. *Epilepsy Behav.* 17, 6–22. doi: 10.1016/j.yebeh.2009.10.017

Villamar, M. F., Volz, M. S., Bikson, M., Datta, A., Dasilva, A. F., and Fregni, F. (2013). Technique and considerations in the use of 4x1 ring high-definition transcranial direct current stimulation (HD-tDCS). *J. Vis. Exp.* 77:e50309. doi: 10.3791/50309

Watanabe, K., Negoro, T., and Aso, K. (1993a). Benign partial epilepsy with secondarily generalized seizures in infancy. *Epilepsia* 34, 635–638. doi: 10.1111/j.1528-1157.1993.tb00440.x

Watanabe, K., Negoro, T., Aso, K., and Matsumoto, A. (1993b). Reappraisal of interictal electroencephalograms in infantile spasms. *Epilepsia* 34, 679–685. doi: 10.1111/j.1528-1157.1993.tb00446.x

Wu, C., and Sharan, A. D. (2013). Neurostimulation for the treatment of epilepsy: a review of current surgical interventions. *Neuromodulation* 16, 10–24; discussion 24. doi: 10.1111/j.1525-1403.2012.00501.x

Yook, S. W., Park, S. H., Seo, J. H., Kim, S. J., and Ko, M. H. (2011). Suppression of seizure by cathodal transcranial direct current stimulation in an epileptic patient - a case report. *Ann. Rehabil. Med.* 35, 579–582. doi: 10.5535/arm.2011.35.4.579

Conflict of Interest Statement: The City University of New York has patent on brain stimulation with MB as inventor. MB has equity in Soterix Medical Inc. which makes brain stimulation devices.

The remaining authors declare that the research was conducted in the absence of any commercial or financial relationships that could be construed as a potential conflict of interest.

frontiers in Neuroscience

ORIGINAL RESEARCH
published: 31 July 2019
doi: 10.3389/fnins.2019.00746

Electroencephalography and Functional Magnetic Resonance Imaging-Guided Simultaneous Transcranial Direct Current Stimulation and Repetitive Transcranial Magnetic Stimulation in a Patient With Minimally Conscious State

Yicong Lin[1†], Tiaotiao Liu[2†], Qian Huang[1], Yingying Su[1], Weibi Chen[1], Daiquan Gao[1], Xin Tian[2], Taicheng Huang[3], Zonglei Zhen[3], Tao Han[1], Hong Ye[1] and Yuping Wang[1,4,5]*

[1] Department of Neurology, Xuanwu Hospital, Capital Medical University, Beijing, China, [2] School of Biomedical Engineering, Tianjin Medical University, Tianjin, China, [3] State Key Laboratory of Cognitive Neuroscience and Learning and IDG/McGovern Institute for Brain Research, Beijing Normal University, Beijing, China, [4] The Beijing Key Laboratory of Neuromodulation, Beijing, China, [5] Center of Epilepsy, Beijing Institute for Brain Disorders, Capital Medical University, Beijing, China

OPEN ACCESS

Edited by:
Paolo Del Giudice,
Istituto Superiore di Sanità (ISS), Italy

Reviewed by:
Daniel Blumberger,
Centre for Addiction and Mental Health (CAMH), Canada
Jorge Leon Morales-Quezada,
Laboratory of Neuromodulation, United States

***Correspondence:**
Yuping Wang
wangyuping01@sina.cn

† These authors have contributed equally to this work

Specialty section:
This article was submitted to Neural Technology, a section of the journal Frontiers in Neuroscience

Received: *20 November 2018*
Accepted: *05 July 2019*
Published: *31 July 2019*

Citation:
Lin Y, Liu T, Huang Q, Su Y, Chen W, Gao D, Tian X, Huang T, Zhen Z, Han T, Ye H and Wang Y (2019) Electroencephalography and Functional Magnetic Resonance Imaging-Guided Simultaneous Transcranial Direct Current Stimulation and Repetitive Transcranial Magnetic Stimulation in a Patient With Minimally Conscious State. Front. Neurosci. 13:746. doi: 10.3389/fnins.2019.00746

Objective: A minimally conscious state (MCS) is characterized by discernible behavioral evidence of consciousness that cannot be reproduced consistently. This condition is highly challenging to treat. Recent studies have demonstrated the potential therapeutic effect of non-invasive brain stimulation in patients with MCS. In one patient in an MCS, we delivered simultaneous transcranial direct current stimulation (tDCS) and repetitive transcranial magnetic stimulation (rTMS) based on an individual brain network analysis and evaluated the therapeutic effect.

Methods: The directional transfer function (DTF) was calculated based on electroencephalograph (EEG) analysis. Global brain connectivity was calculated based on functional magnetic resonance imaging (fMRI) analysis. By referring to the EEG and fMRI results, we identified inferior parietal lobes (IPLs) as targets. In the 2-week treatment period, 14 sessions were applied to the identified bilateral parietal regions. Simultaneous 1.5-mA anodal tDCS and 5-Hz rTMS were delivered for 20 min per hemisphere in each session. Clinical evaluation scores were recorded weekly throughout the treatment. A second patient given the routine treatment was evaluated as a control.

Results: The clinical scores of patient 1 with MCS improved after 2 weeks of stimulation treatment, and the effect lasted for up to 1 month. EEG analysis showed a significant increase ($p < 0.001$) in the DTF value in the gamma band in a bilateral set of posterior regions, and fMRI showed a trend toward normalized activity in the IPLs. The clinical scores of patient 2 with coma did not improve much after 2 weeks of routine treatment. The EEG analysis showed a significant increase ($p = 0.021$) in the DTF value in the gamma band in a bilateral set of posterior regions.

Conclusion: The application of EEG and fMRI to characterize the functional connectivity features of the network in an MCS patient provided a reasonable and accurate stimulation target and verified the changes in functional connectivity resulting from stimulation.

Keywords: minimally conscious state, simultaneous stimulation, repetitive transcranial magnetic stimulation, transcranial direct current stimulation, functional magnetic resonance imaging

INTRODUCTION

A minimally conscious state (MCS) is characterized by discernible behavioral evidence of consciousness that cannot be reproduced consistently (Giacino et al., 2002). An MCS may result from degenerative nervous system disorders or evolve from a coma or vegetative state (VS). In MCS patients, integrated cortical functions are retained but undersustained. MCS is a highly challenging clinical condition to treat. Notably, recent studies have demonstrated the potential therapeutic effect of non-invasive brain stimulation (NIBS) in patients with MCS.

Repetitive transcranial magnetic stimulation (rTMS) and transcranial direct current stimulation (tDCS) are two NIBS techniques that have been developed in the past decades. High-frequency rTMS can decrease GABAergic activity and decrease synaptic transmission through a long-term potentiation-like mechanism (Lefaucheur et al., 2014). Anodal tDCS can change the resting membrane potential by influencing ion channels and gradients, thus increasing cortical excitability (Lefaucheur et al., 2017). These techniques have recently been employed independently in the treatment of MCS and have shown some inspiring beneficial results.

Several studies have shown that priming stimulation can alter the effect of a test stimulation on cortical excitability. Nitsche et al. (2007) found that cortical excitability was higher with simultaneous anodal tDCS and single-pulse TMS than with anodal tDCS alone. We hypothesized that a protocol of simultaneous anodal tDCS and high-frequency rTMS would produce an enhanced excitatory effect. The actual background network activity was predicted to boost the expected effect of rTMS (Muller-Dahlhaus and Ziemann, 2015).

To maximize the benefit of NIBS treatment in a patient with MCS, we designed a simultaneous stimulation protocol based on an individual brain network analysis. We identified stimulation targets and evaluated therapeutic effects by analyzing functional connections based on scalp electroencephalography (EEG) and functional magnetic resonance imaging (fMRI). As a control, we also evaluated another patient with similar structural damage who did not receive stimulation.

MATERIALS AND METHODS

Patients

Patient 1 was diagnosed with MCS according to the Coma Recovery Scale-Revised (CRS-R) (Giacino et al., 2004) due to brain stem hemorrhage 1 month prior. The patient could blink his eyes and move after stimulus, but could not consistently move to auditory command. His eyes could move from the initial target to a new target for more than 2 s. There was not any vocalization or oromotor movement. There was some discernable non-verbal communication response. On neurological examination, the pupils were equal in size and reactive to light. Corneal reflexes and gag reflexes were bilaterally present. The Babinski sign was positive bilaterally. Brain magnetic resonance imaging (MRI) showed subacute hemorrhage in the pons, left cerebral peduncle, and brachium pontis. Before stimulation, the patient's CRS-R score was 10 points based on auditory function (3), visual function (2), motor function (3), verbal function (0), communication (1), and arousal (1) criteria. The Glasgow Coma Scale (GCS) score was 10 based on eye (3), verbal (1), and motor (6) criteria. The Full Outline of UnResponsiveness (FOUR) score was 15 points. The Coma/Near Coma Scale (CNC) score was 18 points. The patient received gangliosides, ambroxol, imipenem, valsartan, captopril, and enteral nutritional suspension. The demographics, clinical data, and EEG analysis results of patient 1 are shown in detail in **Table 1**.

Patient 2 was diagnosed with coma due to brain stem hemorrhage 1 week prior. At baseline, the patient did not respond well to stimulus except for some withdraw movement to pain stimulus and avoidance to light stimulus. On neurological examination, the pupils were equal in size and slowly reactive to light. The corneal reflex was present on the left but diminished on the right. The Doll's head eye phenomenon was not present. The Babinski sign was positive on the right side. Brain computed tomography (CT) showed hemorrhage in the mid brain and pons. At the baseline, the patient's CRS-R score was 3 points based on auditory function (0), visual function (1), motor function (2), verbal function (0), communication (0), and arousal (0) criteria. The GCS score was 6 based on eye (1), verbal (1), and motor (4) criteria. The

TABLE 1 | Detailed demographics, clinical data, and EEG analysis results of the two patients studied.

No.	Age	Time to injury	Imaging characteristics	Current clinical state based on physical and standardized evaluations	Medication	Clinical EEG findings
1	31	1 month	MRI showed subacute hemorrhage in the pons, left cerebral peduncle and brachium pontis.	The pupils were equal in size and reactive to light. Corneal reflexes and gag reflexes were bilaterally present. The Babinski sign was positive bilaterally. The patient spontaneously blinked his eyes infrequently. The patient could blink his eyes after pain stimulus, but could not consistently move to acoustic command. His eyes could move from the initial target to a new target for more than 2 s. There was not any vocalization or oromotor movement.	Gangliosides, ambroxol, imipenem, valsartan, captopril, and enteral nutritional suspension	Continuous diffused slow (5–7 Hz), infrequently intermittent slow (2–4 Hz), infrequent spindle, non-reactive to stimulus.
2	83	1 week	CT showed hemorrhage in the mid brain and pons.	The pupils were equal in size and slowly reactive to light. The corneal reflex was present on the left but diminished on the right. The Doll's head eye phenomenon was not present. The Babinski sign was positive on the right side. The patient did not respond well to stimulus except for some withdraw movement to pain stimulus and avoidance to light stimulus.	Edaravone, mannitol, amlodipine, ampenem, vancomycin, reduced glutathione, ambroxol, famotidine, and enteral nutritional suspension.	Continuous diffused slow (5–7 Hz), frequently intermittent slow (2–4 Hz), non-reactive to stimulus.

MRI, magnetic resonance imaging; EEG, electroencephalogram; CT, computed tomography.

FOUR score was 5 points. The CNC score was 22 points. The patient received edaravone, mannitol, amlodipine, ampenem, vancomycin, reduced glutathione, ambroxol, famotidine, and enteral nutritional suspension. The demographics, clinical data, and EEG analysis results of patient 2 are shown in detail in **Table 1**.

EEG Analysis

EEG analysis was performed based on 1-h 32-channel scalp EEG data. The EEG signals were offline low-pass-filtered (100 Hz) and notch-filtered (49–51 Hz) and baseline correction was performed though polynomial fitting. Eye movements and significant muscle artifacts were also excluded with Automatic Artifact Removal toolbox (Gómez-Herrero, 2007). The signal-to-noise ratio (SNR) of the signal in channel i is defined as: $SNR_i = \frac{\sigma^2_{signal(i)}}{\sigma^2_{noise}}$, where $\sigma_{signal(i)}$ denotes the standard deviation of the EEG signal in channel i and σ_{noise} denotes the standard deviation of the noise signal. The noise signal is estimated using the standard deviation of the pre interval (Zhang et al., 2016). The SNRs of the signals among channels after preprocessing ranged from 7 to 10, therefore ensuring the robustness of the following causality analysis (Fasoula et al., 2013). In the framework of the multivariate autoregressive (MVAR) model, multichannel EEGs can be described as a data vector X of N source signals: $X(t) = \{x_1(t), x_2(t), ..., x_N(t)\}$.

The MVAR model can then be constructed as follows:

$$X(t) = \sum_{n=1}^{p} A_n X(t-n) + E(t) \quad (1)$$

where $E(t)$ is a vector of multivariate zero-mean uncorrelated white noise at time t, A_n is an N × N matrix of the model coefficients, and p is the model order. In the present study, the model order was calculated though the ARFIT package in eConnectome toolbox (**Supplementary Table 1**). As order selection criteria, ARFIT computes approximations to Schwarz's Bayesian Criterion (SBC) and to the logarithm of Akaike's Final Prediction Error (He et al., 2011). The MVAR model was then transformed into the frequency domain:

$$X(f) = A^{-1}(f)E(f) = H(f)E(f) \quad (2)$$

where f denotes a specific frequency and the $H(f)$ matrix is the transfer matrix defined as follows:

$$H(f) = A^{-1}(f) = \left(\sum_{i=0}^{p} A(i)e^{-j2\pi fi\Delta t}\right)^{-1}, A_0 = -I \quad (3)$$

where I is an identity matrix.

The directional transfer function (DTF) is defined by the elements of the transfer matrix H_{ij} as follows:

$$\gamma_{ij}(f)^2 = |H_{ij}|^2 / \sum_{m=1}^{N} |H_{im}(f)|^2 \quad (4)$$

where $\gamma_{ij}(f)$ expresses the ratio between inflow from node j to node i and all inflows to node i, and N is the number of nodes. Once the causal interactions from the DTF calculation for the analyzed epoch were obtained, statistical significance testing was performed to remove the links that formed spurious interactions between EEG channels. A surrogate data method was applied to each analyzed epoch in which the temporal correlation between the EEG channels was destroyed. The shuffling and connectivity estimation procedures were repeated a certain number of times (e.g., 1,000), yielding a distribution of the DTF values under the null hypothesis that no connectivity exists. Based on this empirical distribution, the critical value of significance was set at $p < 0.05$. The statistical assessment procedure was implemented for connectivity estimation to obtain real causal interactions. The DTF values among EEGs were calculated and converted into a DTF matrix (Wilke et al., 2011; Zhang et al., 2016). The DTF value is a function of frequency, which covers the major MCS rhythms. Therefore, the mean value of all the elements in the DTF matrix (DTF_{mean}) is a direct measurement of functional connectivity strength among EEGs. The results of the DTF values across different ranges have been added in the **Supplementary Materials** (**Supplementary Figure 1**).

fMRI Analysis

For fMRI analysis, we used a global brain connectivity (GBC) method (Cole et al., 2012; Wang et al., 2016) to characterize the averaged connectivity of each voxel to the rest of the voxels in the default mode network (DMN) or executive control network (ECN), which were defined from Yeo et al. (2011). The GBC method was performed by calculating the functional connectivity (i.e., correlation) of a voxel in the DMN or ECN to the rest of the voxels, one by one, and the functional connectivity was then averaged as the connectivity of each voxel to produce a GBC value. This method takes advantage of characterizing overall functional connectivity with voxelwise resolution, enabling us to examine the impairment of each network's functional connectivity in one patient.

Target Identification

Compared to eight healthy controls, patient 1 presented a significant decrease in the DTF value in gamma frequency in the bilateral posterior regions, as shown in **Figure 1**. These 15 decreased electrodes included bilateral occipital (O1, O2, Oz in 10–20 International Electrode System), parieto-occipital (PO3, PO4), parietal (P3, P4, Pz), centro-parietal (CP1, CP2), central (C3, C4), posterior temporal (T5, T6), and right centro-temporal (CP6) regions. In resting fMRI analysis, we found a profound visual decrease in brain functional connectivity in regions of the DMN, including the inferior parietal lobe (IPL), posterior cingulate cortex (PCC), and mesiofrontal region (MFR), as well as regions of the ECN, including the dorsolateral prefrontal cortex (DLPFC), as shown in **Figure 2**. Herwig et al. (2003) studied the corresponding cortical sites of the 10–20 International Electrode System using neuronavigation and found that targeting P3 mainly reached BA 40 and to a lesser extent BA 7 in the inferior part of the parietal lobe. Therefore, to better cover common regions identified by EEG and fMRI, we identified bilateral parietal regions (P3 and P4) as anodal tDCS targets and contralateral temporal regions (T4 and T3) as cathodal tDCS targets, and P3 and P4 as high-frequency TMS targets. **Figure 3** shows these targets in the individual head model.

The electric field distribution in the brain was simulated using SimNIBS 2.1.1 software (Thielscher et al., 2015). The simulation was generated based on the template head model included in the software package. We simulated the electric field distribution of the anode at P4 with the cathode at Fp1 and the anode at P4 with T3. The simulated electric field was more restricted when the anode is P4 and the cathode is T3. We also simulated the magnetic field when the target was set at P4. The simulated magnetic field and electric field were consistent.

Stimulation Protocol

For patient 1, the 14 sessions of simultaneous anodal tDCS and high-frequency rTMS were delivered over the course of 2 weeks, and a clinical evaluation was performed weekly throughout the course of treatment. Both electrical and magnetic stimulation were delivered using an Electromagnetic Stimulator (Yunshen Technology Limited Company, Beijing, China). Direct current was delivered by a pair of saline-soaked silver cloth-wrapped sponge electrodes (thickness, 0.4 cm; area of electrode, 7 cm^2, Greentek, Pty Ltd., China). rTMS was delivered through a circular coil (diameter, 74 mm; peak magnetic field, 2.0 Tesla). Forty minutes of stimulation (20 min for each hemisphere) were given per day. For the 20-min treatment on the right hemisphere, anodal tDCS was delivered over P4, and cathodal tDCS was delivered over T3. Meanwhile, 5 Hz rTMS was delivered precisely over the anodal electrode at P4. The current was ramped up to 1.5 mA (for 10 s) from the onset of stimulation, applied for 20 min, and ramped down to 0 mA (for 10 s). One rTMS train consisted of 25 pulses delivered at 5 Hz, with an intertrain interval of 55 s. In a single session, 500 pulses (20 rTMS trains) were delivered for 20 min. The strength of the stimulation was 70% of the resting motor threshold (RMT). Then, for the next 20-min treatment on the left hemisphere, anodal tDCS was delivered over P3, and cathodal tDCS was delivered over T4. Meanwhile, 5 Hz rTMS was delivered precisely over the anodal electrode at P3.

RESULTS

Clinical Assessments

During stimulation treatment, patient 1 could move to acoustic command consistently, and his eyes could open and track after verbal prompt. After stimulation, the patient improved gradually. He could recognize objects and could give consistent behavioral response to verbal prompt. The patient could spontaneously open eyes, track and fix, and could open mouth when a spoon is near. The patient had discernable non-verbal communication response. The physical examinations did not change throughout the study. The patient was evaluated on a weekly basis through these four scales. At the end of the stimulation treatment period, the CRS-R, GCS, FOUR, and CNC were 12, 10, 16, and 12 points, respectively. At 1 week after treatment, the CRS-R, GCS, FOUR, and CNC were 14, 10, 16, and 2, respectively. At 1 month after treatment, the CRS-R, GCS, FOUR, and CNC were 19, 11, 16, and 0, respectively, as shown in **Figure 4A** and **Table 2**. Further analysis of subscales of the CRS-R score in patient 1 showed that the arousal and auditory functions were the first to show improvement during stimulation (**Figure 4B**). Then, communication improved. Finally, visual function and motor function improved after stimulation treatment was completed.

Patient 2 was provided with routine treatment (without stimulation) and did not show much clinical improvement. The patient could not avoid light stimuli like before. The physical

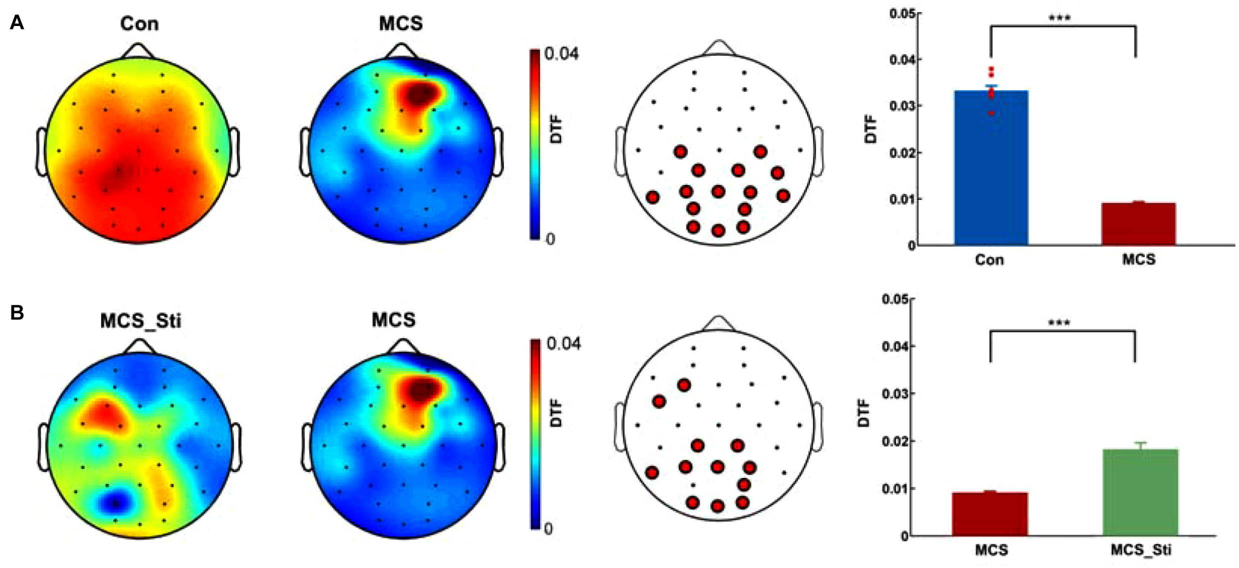

FIGURE 1 | Comparison of DTF values in the gamma frequency of EEGs between controls and patient 1 (MCS) before and after stimulation treatment. **(A)** DTF spatial distribution in healthy controls (Con) and patient 1 (MCS). The color bar denotes the DTF values. First panel: eight healthy controls. Second panel: compared to the eight healthy controls, the MCS patient showed a significantly decreased DTF value in the gamma frequency in bilateral posterior regions. Third panel: 15 electrodes with significantly reduced DTF values in patient 1 compared to those in healthy controls were identified. Fourth panel: the average DTF value of the 15 electrodes was significantly lower in the MCS patient than in Con (***$p < 0.001$, *t*-test/Wilcoxon's rank sum test). The blue bar denotes the DTF value of the 15 electrodes in eight controls. The red bar denotes the pretreatment DTF value of the 15 electrodes in the patient. The DTF value (averaged across channels) of each single healthy control is shown as a dot. **(B)** Spatial distribution of the DTF value in patient 1 before and after treatment. First panel: the MCS patient after stimulation treatment showed a significant increase in the DTF value in the gamma frequency in bilateral posterior regions. Second panel: the MCS patient before treatment. Third panel: 12 electrodes with significantly higher DTF values after treatment compared to those before treatment were identified (***$p < 0.001$). The red bar denotes the pretreatment DTF value of the 12 electrodes in the patient. The green bar denotes the post-treatment DTF value of the 12 electrodes in the patient. DTF, directional transfer function; EEG, electroencephalography; Con, controls; MCS, minimally conscious state; MCS_Sti, minimally conscious state after treatment.

examinations did not change throughout the study. The patient was also evaluated on a weekly basis through these four scales. At 1 week, the CRS-R, GCS, FOUR, and CNC were 3, 5, 5, and 22, respectively. At 2 weeks, the CRS-R, GCS, FOUR, and CNC were 4, 6, 5, and 26, respectively, as shown in **Figure 4C** and **Table 2**.

Brain Network Analysis Based on EEG

Patient 1 exhibited a significantly lower DTF value in the gamma frequency in the bilateral posterior regions than healthy controls, as shown in **Figure 1**. Fifteen electrodes, which included O1, O2, Oz, PO3, PO4, P3, P4, Pz, CP1, CP2, C3, C4, T5, T6, and CP6, showed significantly reduced DTF values (***$p < 0.001$, *t*-test/Wilcoxon's rank sum test) compared to those regions in healthy controls. After 2 weeks of stimulation, EEG analysis showed a significant increase in DTF in the gamma frequency in 12 electrodes (***$p < 0.001$) from before treatment. These 12 electrodes included F3, FC5, CP1, CP2, T5, P3, Pz, P4, PO4, O1, Oz, and O2.

In patient 2, at baseline, EEG analysis showed a significantly lower DTF value in the gamma frequency in the bilateral posterior regions than in controls, as shown in **Figure 5**. Eight electrodes, including F4, FC1, Cz, P3, Pz, P4, PO4, and CP6, showed significantly reduced DTF values (***$p < 0.001$). After 2 weeks of routine treatment, EEG analysis showed a significant increase in DTF in gamma frequency in four electrodes ($p = 0.021$) from baseline. These four electrodes included FC6, Cz, P3, and T5.

Brain Network Analysis Based on fMRI

In patient 1, the DMN identified by baseline fMRI showed decreased activity in the IPL, PCC, and MFR (shown in **Figure 2**) compared to that in healthy controls. After stimulation treatment, there was a trend toward a normalization of IPL and PCC activity due to an increase in activity. The ECN identified by baseline fMRI showed decreased activity in the DLPFC (shown in **Figure 2**) compared to that in healthy controls. After stimulation treatment, there was no trend toward a normalization of DLPFC activity or increased activity.

DISCUSSION

This is an exploratory study in which an MCS patient received simultaneous tDCS and rTMS treatment based on brain network analysis of both EEG and fMRI. rTMS with 5–20 Hz and 90–100% of RMT and tDCS with 1–2 mA have been commonly utilized in previous studies (Lefaucheur et al., 2014, 2017). We utilized rTMS with 5 Hz and 70% of the RMT, and tDCS with 1.5 mA for safety and tolerability consideration. During stimulation, the MCS patient tolerated intervention well

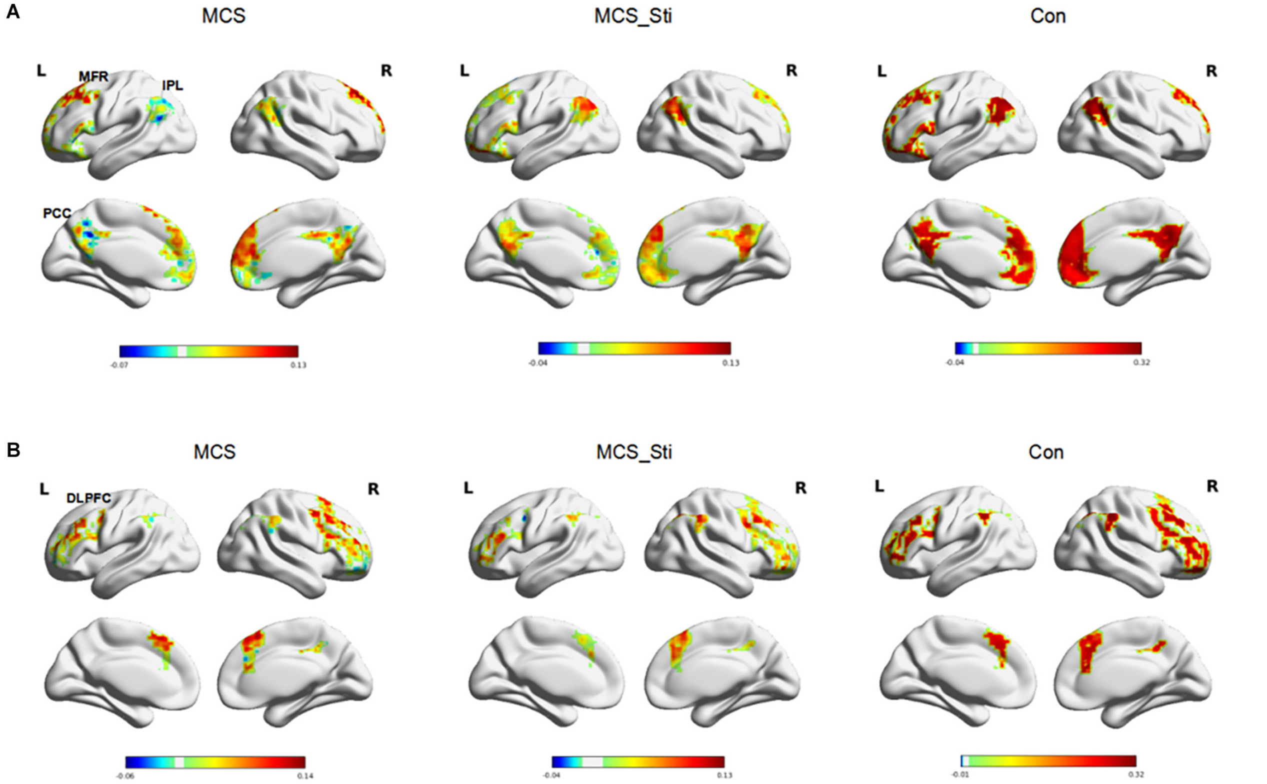

FIGURE 2 | GBC analysis of fMRI in controls (Con) and patient 1 (MCS) before and after stimulation treatment. **(A)** DMN network. First panel: before treatment, patient showed decreased activity in regions, including the IPL, MFR, and PCC. Second panel: after treatment, patient 1 showed an increase in IPL and PCC activity. Third panel: healthy controls. **(B)** ECN network. First panel: before treatment, patient 1 showed decreased activity in the DLPFC. Second panel: after treatment, patient 1 showed a decrease in DLPFC activity. Third panel: healthy controls. GBC, global brain connectivity; fMRI, functional magnetic resonance imaging; DMN, default mode network; ECN, extrinsic control network; Con, controls; MCS, minimally conscious state; MCS_Sti, minimally conscious state after treatment; MFR, mesiofrontal region; IPL, inferior parietal lobe; PCC, posterior cingulate cortex; DLPFC, dorsolateral prefrontal cortex.

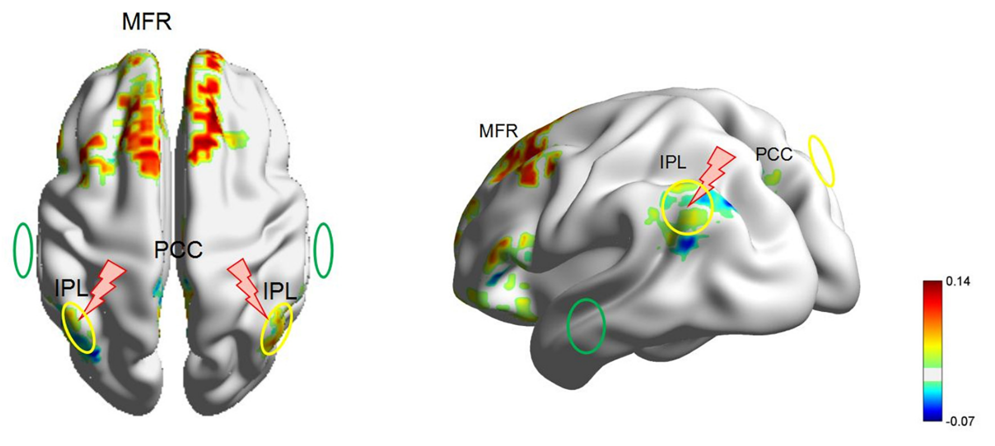

FIGURE 3 | The locations of the rTMS and tDCS targets in a head model of patient 1. The yellow circle denotes the anode electrode over P3 or P4. The green circle denotes the cathode electrode over T3 or T4. The red lightning mark denotes the rTMS site over P3 or P4. For the 20-min treatment on the right hemisphere, the anodal tDCS was delivered over P4, and the cathodal tDCS was delivered over T3. Meanwhile, 5-Hz rTMS was delivered precisely over the anodal electrode at P4. Then, for the next 20-min treatment on the left hemisphere, the anodal tDCS was delivered over P3, and the cathodal tDCS was delivered over T4. Meanwhile, 5-Hz rTMS was delivered precisely over the anodal electrode at P3. rTMS, repetitive transcranial magnetic stimulation; tDCS, transcranial direct current stimulation; fMRI, functional magnetic resonance imaging; IPL, inferior parietal lobe; PCC, posterior cingulate cortex; MFR, mesiofrontal region.

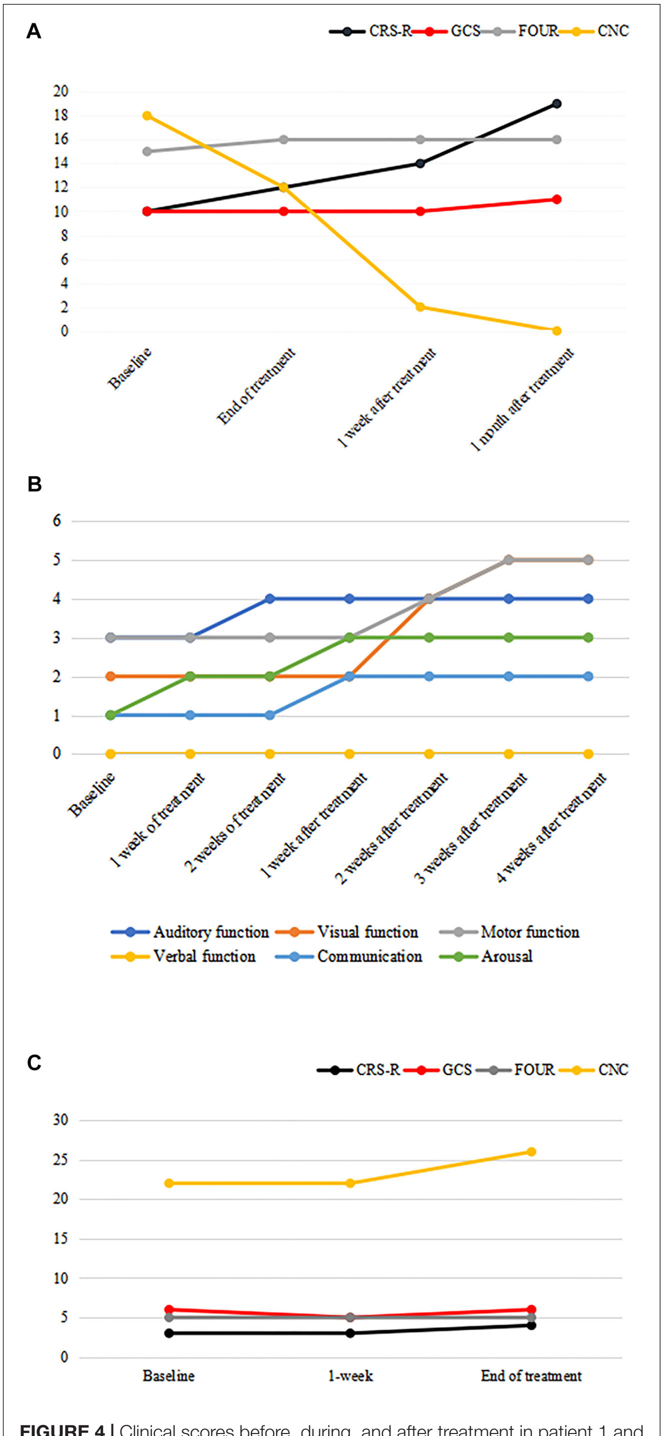

FIGURE 4 | Clinical scores before, during, and after treatment in patient 1 and patient 2. **(A)** The CRS-R, GCS, FOUR, and CNC scores in patient 1. Compared to baseline, the CRS-R and CNC scores improved considerably, and the effect lasted for up to 1 month. **(B)** The subscales of the CRS-R score in patient 1. The arousal and auditory functions were the first to show improvement during stimulation. Then, communication improved. Finally, visual function and motor function improved after stimulation treatment was completed. **(C)** The CRS-R, GCS, FOUR, and CNC scores in patient 2. Compared to baseline, the scores did not show much improvement after 2 weeks of treatment. CRS-R, Coma Recovery Scale-Revised; GCS, Glasgow Coma Scale; FOUR, Full Outline of UnResponsiveness; CNC, Coma/Near Coma Scale.

without displaying irritability and aggressiveness during head positioning or TMS/tDCS delivery. Clinical assessment showed improvement in the MCS patient. Another patient with similar structural damage was evaluated as a control and did not show much clinical improvement. Moreover, brain network analysis based on EEG and fMRI played important roles in this study. First, these tools were used to identify stimulation targets, potentially leading to more precise modulation. In addition, post-treatment analysis of the brain network was used to evaluate the treatment effect. We speculate that brain network-guided simultaneous tDCS and rTMS could be a promising treatment strategy for MCS.

IPL Modulation Helps Treat MCS

The stimulation target chosen in this study was the bilateral IPL based on combined functional and electrophysiological datasets. In patient 1, there was a significant decrease in the DTF value in the bilateral centro-parieto-occipital regions identified by EEG analysis and decreased activity in the IPLs identified by fMRI analysis. After stimulation treatment, the patient achieved obvious improvement in clinical assessment and increased activity in bilateral IPLs. The IPL is involved in the DMN, which is related to self-awareness (Greicius et al., 2003; Tian et al., 2007) and shows decreased brain activity during loss of consciousness (Di Perri et al., 2016). Positron emission computed tomography studies have shown that neuronal activity in DMN regions increases upon recovery from VS (Laureys et al., 2006). Vanhaudenhuyse et al. (2010) observed a correlation between DMN integrity and the level of consciousness. Their group found that the DMN integrity decreased when descending from normal consciousness to MCS, VS, and coma, and the authors suggested that the connective strength of the PCC within the DMN can distinguish between VS and MCS patients. The functional connections within the DMN in MCS may reflect the chance of recovery. Different connectivity patterns could influence the efficacy of tDCS in MCS patients (Cavaliere et al., 2016). The re-establishment of functional connections within DMN regions may reflect the recovery of consciousness (Laureys et al., 2005).

However, in a literature review, previously reported targets are mostly in the DLPFC, motor cortex, orbitofrontal cortex, or a parieto-occipital region (Lefaucheur et al., 2014, 2017), rather than the IPL. The DLPFC is involved in the functional ECN, which is related to external awareness (D'Esposito et al., 1998; Lieberman, 2007). In addition to the DMN, the ECN has also been demonstrated to be altered in disorders of consciousness (Vanhaudenhuyse et al., 2011; Crone et al., 2014) and restored with the recovery of consciousness (Laureys and Schiff, 2012). In our study, we further analyzed the ECN in patient 1 and found decreased activity in the bilateral DLPFC when compared with that in healthy controls. Therefore, we suspected that the patient may also benefit from stimulation over the DLPFC.

The DMN and ECN are anticorrelated to each other under normal physiological conditions. However, these two networks are hypoactivated in patients with MCS in our study, potentially reflecting a reduction in the anticorrelation. The anticorrelated

TABLE 2 | Clinical scores of the two patients throughout the study.

No.	Scale type	Baseline	1 week of treatment	2 weeks of treatment	1 week after treatment	2 weeks after treatment	3 weeks after treatment	4 weeks after treatment
1	CRS-R	10	11	12	14	17	19	19
	GCS	10	10	10	10	11	11	11
	FOUR	15	15	16	16	16	16	16
	CNC	18	14	12	2	0	0	0
2	CRS-R	3	3	4	–	–	–	–
	GCS	6	5	6	–	–	–	–
	FOUR	5	5	5	–	–	–	–
	CNC	22	22	26	–	–	–	–

CRS-R, Coma Recovery Scale-Revised; GCS, Glasgow Coma Scale; FOUR, Full Outline of UnResponsiveness; CNC, Coma/Near Coma Scale.

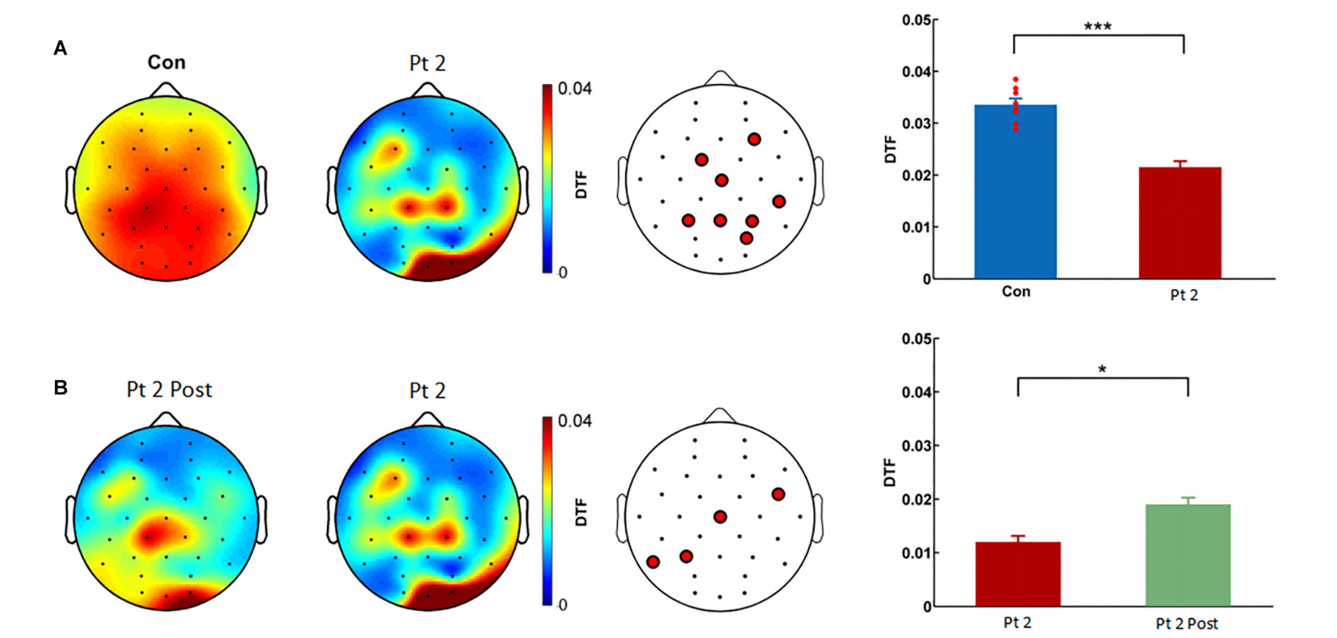

FIGURE 5 | Comparison of DTF in the gamma frequency of EEG between controls and patient 2 before and after routine treatment. **(A)** DTF spatial distribution in healthy controls (Con) and patient 2. First panel: eight healthy controls. Second panel: compared to the eight healthy controls, patient 2 showed a significantly decreased DTF value in the gamma frequency in bilateral posterior regions. Third panel: eight electrodes (F4, FC1, Cz, P3, Pz, P4, PO4, and CP6) with significantly reduced DTF values in patient 2 compared to those in Con were identified. Fourth panel: the average DTF value of the eight electrodes was significantly lower in the patient 2 than in the Con (***$p < 0.001$, *t*-test/Wilcoxon's rank sum test). The blue bar denotes the DTF value of eight electrodes in eight controls. The red bar denotes the pretreatment DTF value of eight electrodes in the patient. The DTF value (averaged across channels) of each single healthy control is shown as a dot. **(B)** Spatial distribution of the DTF in patient 2 before and after routine treatment. First panel: after routine treatment, patient 2 showed a significant increase in the DTF value in the gamma frequency in bilateral posterior regions. Second panel: patient 2 before treatment. Third panel: four electrodes (FC6, Cz, P3, and T5) with significantly higher DTF values ($p = 0.021$) after treatment compared to those before treatment were identified (*$p < 0.1$). The red bar denotes the pretreatment DTF value of the four electrodes in the patient. The green bar denotes the post-treatment DTF value of four electrodes in the patient. DTF, directional transfer function; EEG, electroencephalography; Con, controls; Pt 2 Post, patient 2 after treatment.

pattern has been shown to be of functional importance to the state of consciousness. The dynamics of the anticorrelation between the ECN and DMN during MCS have not been well-clarified. Heine et al. (2012) suspected that the anticorrelation generally diminishes or even disappears during conditions of altered consciousness. A stronger anticorrelation between the ECN and DMN has been shown to potentially reflect a better capacity to switch between internal and external modes of attention, which is necessary for maintaining conscious awareness (Leech et al., 2011; Di Perri et al., 2016). Anatomically, the superior longitudinal fascicle (SLF) connects the parietal cortex with the frontal cortex, and SLF II shows a strong connectivity to the DLPFC from the IPL (Parlatini et al., 2017). These results probably explain the accordant effect of excitatory stimulation of either the IPL or DLPFC, although further evidence is warranted.

The Synergistic Effect of tDCS and rTMS

In previous studies, the efficacy of NIBS for MCS has been mild to moderate and variable in patients. A study explored the effect of high-frequency rTMS over the motor cortex in six patients with MCS or VS and found reappearance of fast activity and an increase in slow activity upon EEG analysis and behavioral changes in one patient with MCS (Manganotti et al., 2013). A case series trial found that patients with MCS can benefit from anodal tDCS over the left DLPFC (Angelakis et al., 2014). Three randomized controlled trials of tDCS in patients with MCS showed moderately improved recovery of signs of consciousness after anodal tDCS over the left DLPFC (Thibaut et al., 2014, 2017; Martens et al., 2018).

In this study, a simultaneous combination of tDCS and rTMS was explored. The patient showed a clinical improvement and a trend toward a normalization of functional connectivity. We speculate that the simultaneous tDCS and rTMS protocol produces beneficial synergistic effects, although we can only speculate on the underlying cellular and molecular mechanisms of these synergistic effects. A candidate mechanism might be the consolidation of long-term potentiation by protein synthesis and gene transcription (Muller-Dahlhaus and Ziemann, 2015). Muller-Dahlhaus and Ziemann (2015) found that either non-homeostatic metaplasticity or homeostatic metaplasticity occurred depending on successive NIBS protocols. Non-homeostatic metaplasticity can increase NIBS-induced aftereffects on cortical excitability. We speculate that non-homeostatic metaplasticity also prevailed when tDCS and rTMS were delivered simultaneously. The non-homeostatic metaplasticity may be explained by the assumption that tDCS and TMS activate neuronal circuits without a significant physiological interaction; therefore, the resulting effect reflects an arithmetic summation of the electrical and magnetic effects (Nitsche et al., 2007).

Limitations

This is a preliminary two-case study. The patient with stimulation was in an MCS, and whether this treatment can be used in patients with other disorders of consciousness needs to be further explored. A well-designed large randomized controlled study needs to be conducted in the future. Additionally, patient 2 was not in precisely the same medical condition as patient 1. Patient 2 had coma and was enrolled in the study 1 week after stroke. All clinical scores showed a more severe condition than in patient 1. These factors likely contributed to the limited clinical improvement. More homogeneous cases need to be studied in the future, although the homogeneity of the cases may be difficult to control.

CONCLUSION

This study suggests that EEG and fMRI analysis can be used to picture the brain network, identify stimulation targets, and evaluate treatment efficacy. Large clinical trials need to be conducted to test the efficacy of repeated simultaneous tDCS and rTMS in MCS patients.

ETHICS STATEMENT

All clinical data in this case report were provided by the patient's parents or collected by our team members with the consent of the patient's parents. The study was approved by the ethics committee of the Xuanwu Hospital, Capital Medical University (ChiCTR1800014293). Written informed consent was obtained from the patient's parents for participation in the study and publication of this report.

AUTHOR CONTRIBUTIONS

YL oversaw data acquisition, reviewed the literature, and drafted the manuscript. TL analyzed and interpreted the EEG data. YW designed the study, supervised the initial drafting, and critically revised the manuscript. QH treated the patient and acquired the clinical data. YS, WC, DG, and HY managed the patient, evaluated the clinical scores, and critically revised the manuscript. XT analyzed and interpreted the EEG data. THu and ZZ analyzed and interpreted the fMRI data. THa treated the patient.

FUNDING

This work was supported by the National High Technology Research and Development Program of China (2015AA020514), the Beijing Municipal Education Commission (TJSH20161002502), and the Beijing Key Clinical Speciality Excellence Project.

SUPPLEMENTARY MATERIAL

The Supplementary Material for this article can be found online at: https://www.frontiersin.org/articles/10.3389/fnins.2019.00746/full#supplementary-material

REFERENCES

Angelakis, E., Liouta, E., Andreadis, N., Korfias, S., Ktonas, P., Stranjalis, G., et al. (2014). Transcranial direct current stimulation effects in disorders of consciousness. *Arch. Phys. Med. Rehabil.* 95, 283–289. doi: 10.1016/j.apmr.2013.09.002

Cavaliere, C., Aiello, M., Di Perri, C., Amico, E., Martial, C., Thibaut, A., et al. (2016). Functional connectivity substrates for tDCS response in minimally conscious state patients. *Front. Cell Neurosci.* 10:257. doi: 10.3389/fncel.2016.00257

Cole, M. W., Yarkoni, T., Repovs, G., Anticevic, A., and Braver, T. S. (2012). Global connectivity of prefrontal cortex predicts cognitive control and intelligence. *J Neurosci.* 32, 8988–8999. doi: 10.1523/JNEUROSCI.0536-12.2012

Crone, J. S., Soddu, A., Holler, Y., Vanhaudenhuyse, A., Schurz, M., Bergmann, J., et al. (2014). Altered network properties of the fronto-parietal network and the thalamus in impaired consciousness. *Neuroimage Clin.* 4, 240–248. doi: 10.1016/j.nicl.2013.12.005

D'Esposito, M., Ballard, D., Aguirre, G. K., and Zarahn, E. (1998). Human prefrontal cortex is not specific for working memory: a functional MRI study. *Neuroimage* 8, 274–282. doi: 10.1006/nimg.1998.0364

Di Perri, C., Bahri, M. A., Amico, E., Thibaut, A., Heine, L., Antonopoulos, G., et al. (2016). Neural correlates of consciousness in patients who have emerged from a minimally conscious state: a cross-sectional multimodal imaging study. *Lancet Neurol* 15, 830–842. doi: 10.1016/S1474-4422(16)00111-3

Fasoula, A., Attal, Y., and Schwartz, D. (2013). Comparative performance evaluation of data-driven causality measures applied to brain networks. *J. Neurosci. Methods* 215, 170–189. doi: 10.1016/j.jneumeth.2013.02.021

Giacino, J. T., Ashwal, S., Childs, N., Cranford, R., Jennett, B., Katz, D. I., et al. (2002). The minimally conscious state: definition and diagnostic criteria. *Neurology* 58, 349–353. doi: 10.1212/wnl.58.3.349

Giacino, J. T., Kalmar, K., and Whyte, J. (2004). The JFK coma recovery scale-revised: measurement characteristics and diagnostic utility. *Arch. Phys. Med. Rehabil.* 85, 2020–2029. doi: 10.1016/j.apmr.2004.02.033

Gómez-Herrero, G. (2007). *Automatic Artifact Removal (AAR) Toolbox v1.3*. Tampere: Tampere University of Technology.

Greicius, M. D., Krasnow, B., Reiss, A. L., and Menon, V. (2003). Functional connectivity in the resting brain: a network analysis of the default mode hypothesis. *Proc. Natl. Acad. Sci. U.S A.* 100, 253–258. doi: 10.1073/pnas.0135058100

He, B., Dai, Y., Astolfi, L., Babiloni, F., Yuan, H., and Yang, L. (2011). eConnectome: A MATLAB toolbox for mapping and imaging of brain functional connectivity. *J. Neurosci. Methods* 195, 261–269. doi: 10.1016/j.jneumeth.2010.11.015

Heine, L., Soddu, A., Gomez, F., Vanhaudenhuyse, A., Tshibanda, L., Thonnard, M., et al. (2012). Resting state networks and consciousness: alterations of multiple resting state network connectivity in physiological, pharmacological, and pathological consciousness states. *Front. Psychol.* 3:295. doi: 10.3389/fpsyg.2012.00295

Herwig, U., Satrapi, P., and Schönfeldt-Lecuona, C. (2003). Using the international 10-20 EEG system for positioning of transcranial magnetic stimulation. *Brain Topogr.* 16, 95–99. doi: 10.1023/b:brat.0000006333.93597.9d

Laureys, S., Boly, M., and Maquet, P. (2006). Tracking the recovery of consciousness from coma. *J. Clin. Invest.* 116, 1823–1825. doi: 10.1172/jci29172

Laureys, S., Piret, S., and Ledoux, D. (2005). Quantifying consciousness. *Lancet Neurol.* 4, 789–790. doi: 10.1016/s1474-4422(05)70230-1

Laureys, S., and Schiff, N. D. (2012). Coma and consciousness: paradigms (re)framed by neuroimaging. *Neuroimage* 61, 478–491. doi: 10.1016/j.neuroimage.2011.12.041

Leech, R., Kamourieh, S., Beckmann, C. F., and Sharp, D. J. (2011). Fractionating the default mode network: distinct contributions of the ventral and dorsal posterior cingulate cortex to cognitive control. *J. Neurosci.* 31, 3217–3224. doi: 10.1523/JNEUROSCI.5626-10.2011

Lefaucheur, J. P., Andre-Obadia, N., Antal, A., Ayache, S. S., Baeken, C., Benninger, D. H., et al. (2014). Evidence-based guidelines on the therapeutic use of repetitive transcranial magnetic stimulation (rTMS). *Clin. Neurophysiol.* 125, 2150–2206. doi: 10.1016/j.clinph.2014.05.021

Lefaucheur, J. P., Antal, A., Ayache, S. S., Benninger, D. H., Brunelin, J., Cogiamanian, F., et al. (2017). Evidence-based guidelines on the therapeutic use of transcranial direct current stimulation (tDCS). *Clin. Neurophysiol.* 128, 56–92. doi: 10.1016/j.clinph.2016.10.087

Lieberman, M. D. (2007). Social cognitive neuroscience: a review of core processes. *Annu. Rev. Psychol.* 58, 259–289. doi: 10.1146/annurev.psych.58.110405.085654

Manganotti, P., Formaggio, E., Storti, S. F., Fiaschi, A., Battistin, L., Tonin, P., et al. (2013). Effect of high-frequency repetitive transcranial magnetic stimulation on brain excitability in severely brain-injured patients in minimally conscious or vegetative state. *Brain Stimul.* 6, 913–921. doi: 10.1016/j.brs.2013.06.006

Martens, G., Lejeune, N., O'Brien, A. T., Fregni, F., Martial, C., Wannez, S., et al. (2018). Randomized controlled trial of home-based 4-week tDCS in chronic minimally conscious state. *Brain Stimul.* 11, 982–990. doi: 10.1016/j.brs.2018.04.021

Muller-Dahlhaus, F., and Ziemann, U. (2015). Metaplasticity in human cortex. *Neuroscientist* 21, 185–202. doi: 10.1177/1073858414526645

Nitsche, M. A., Roth, A., Kuo, M. F., Fischer, A. K., Liebetanz, D., Lang, N., et al. (2007). Timing-dependent modulation of associative plasticity by general network excitability in the human motor cortex. *J. Neurosci.* 27, 3807–3812. doi: 10.1523/jneurosci.5348-06.2007

Parlatini, V., Radua, J., Dell'Acqua, F., Leslie, A., Simmons, A., Murphy, D. G., et al. (2017). Functional segregation and integration within fronto-parietal networks. *Neuroimage* 146, 367–375. doi: 10.1016/j.neuroimage.2016.08.031

Thibaut, A., Bruno, M. A., Ledoux, D., Demertzi, A., and Laureys, S. (2014). tDCS in patients with disorders of consciousness: sham-controlled randomized double-blind study. *Neurology* 82, 1112–1118. doi: 10.1212/wnl.0000000000000260

Thibaut, A., Wannez, S., Donneau, A. F., Chatelle, C., Gosseries, O., Bruno, M. A., et al. (2017). Controlled clinical trial of repeated prefrontal tDCS in patients with chronic minimally conscious state. *Brain Inj.* 31, 466–474. doi: 10.1080/02699052.2016.1274776

Thielscher, A., Antunes, A., and Saturnino, G. (2015). "Field modeling for transcranial magnetic stimulation: a useful tool to understand the physiological effects of TMS? Engineering in Medicine and Biology Society (EMBC)," in *37th Annual International Conference of the IEEE*, (Milan).

Tian, L., Jiang, T., Liu, Y., Yu, C., Wang, K., Zhou, Y., et al. (2007). The relationship within and between the extrinsic and intrinsic systems indicated by resting state correlational patterns of sensory cortices. *Neuroimage* 36, 684–690. doi: 10.1016/j.neuroimage.2007.03.044

Vanhaudenhuyse, A., Demertzi, A., Schabus, M., Noirhomme, Q., Bredart, S., Boly, M., et al. (2011). Two distinct neuronal networks mediate the awareness of environment and of self. *J. Cogn. Neurosci.* 23, 570–578. doi: 10.1162/jocn.2010.21488

Vanhaudenhuyse, A., Noirhomme, Q., Tshibanda, L. J., Bruno, M. A., Boveroux, P., Schnakers, C., et al. (2010). Default network connectivity reflects the level of consciousness in non-communicative brain-damaged patients. *Brain* 133, 161–171. doi: 10.1093/brain/awp313

Wang, X., Zhen, Z., Song, Y., Huang, L., Kong, X., and Liu, J. (2016). The hierarchical structure of the face network revealed by its functional connectivity pattern. *J Neurosci.* 36, 890–900. doi: 10.1523/JNEUROSCI.2789-15.2016

Wilke, C., Worrell, G., and He, B. (2011). Graph analysis of epileptogenic networks in human partial epilepsy. *Epilepsia* 52, 84–93. doi: 10.1111/j.1528-1167.2010.02785.x

Yeo, B. T., Krienen, F. M., Sepulcre, J., Sabuncu, M. R., Lashkari, D., Hollinshead, M., et al. (2011). The organization of the human cerebral cortex estimated by intrinsic functional connectivity. *J Neurophysiol.* 106, 1125–1165. doi: 10.1152/jn.00338.2011

Zhang, D., Zhao, H., Bai, W., and Tian, X. (2016). Functional connectivity among multi-channel EEGs when working memory load reaches the capacity. *Brain Res.* 1631, 101–112. doi: 10.1016/j.brainres.2015.11.036

Conflict of Interest Statement: The authors declare that the research was conducted in the absence of any commercial or financial relationships that could be construed as a potential conflict of interest.

frontiers in Neuroscience

ORIGINAL RESEARCH
published: 02 August 2019
doi: 10.3389/fnins.2019.00792

Paired Associative Stimulation as a Tool to Assess Plasticity Enhancers in Chronic Stroke

Joshua Silverstein[1], Mar Cortes[2], Katherine Zoe Tsagaris[1], Alejandra Climent[3], Linda M. Gerber[4], Clara Oromendia[4], Pasquale Fonzetti[5,6], Rajiv R. Ratan[5,7,8], Tomoko Kitago[1,5]*, Marco Iacoboni[9,10], Allan Wu[10,11], Bruce Dobkin[12] and Dylan J. Edwards[13,14]

[1] Human Motor Recovery Laboratory, Burke Neurological Institute, White Plains, NY, United States, [2] Department of Rehabilitation and Human Performance, Icahn School of Medicine at Mount Sinai, New York, NY, United States, [3] Sant Joan de Deu Hospital, Department of Neurology, University of Barcelona, Barcelona, Spain, [4] Department of Healthcare Policy and Research, Weill Cornell Medical College, New York, NY, United States, [5] Department of Neurology, Weill Cornell Medical College, New York, NY, United States, [6] Memory Evaluation and Treatment Service, Burke Rehabilitation Hospital, White Plains, NY, United States, [7] Burke Neurological Institute, White Plains, NY, United States, [8] Feil Family Brain and Mind Research Institute, Weill Cornell Medical College, New York, NY, United States, [9] Department of Psychiatry and Biobehavioral Sciences, UCLA Semel Institute for Neuroscience and Human Behavior, Los Angeles, CA, United States, [10] Ahmanson-Lovelace Brain Mapping Center, University of California, Los Angeles, Los Angeles, CA, United States, [11] Department of Neurology, University of California, Los Angeles, Los Angeles, CA, United States, [12] Department of Neurology, Geffen School of Medicine, Reed Neurologic Research Center, University of California, Los Angeles, Los Angeles, CA, United States, [13] Moss Rehabilitation Research Institute, Elkins Park, PA, United States, [14] School of Medical and Health Sciences, Edith Cowan University, Perth, WA, Australia

OPEN ACCESS

Edited by:
Hans-Eckhardt Schaefer, University of Stuttgart, Germany

Reviewed by:
Karen Moxon, University of California, Davis, United States
Victor Manuel Pulgar, Wake Forest School of Medicine, United States

***Correspondence:**
Tomoko Kitago
tok7002@med.cornell.edu

Specialty section:
This article was submitted to Neural Technology, a section of the journal Frontiers in Neuroscience

Received: 05 October 2018
Accepted: 15 July 2019
Published: 02 August 2019

Citation:
Silverstein J, Cortes M, Tsagaris KZ, Climent A, Gerber LM, Oromendia C, Fonzetti P, Ratan RR, Kitago T, Iacoboni M, Wu A, Dobkin B and Edwards DJ (2019) Paired Associative Stimulation as a Tool to Assess Plasticity Enhancers in Chronic Stroke. Front. Neurosci. 13:792. doi: 10.3389/fnins.2019.00792

Background and Purpose: The potential for adaptive plasticity in the post-stroke brain is difficult to estimate, as is the demonstration of central nervous system (CNS) target engagement of drugs that show promise in facilitating stroke recovery. We set out to determine if paired associative stimulation (PAS) can be used (a) as an assay of CNS plasticity in patients with chronic stroke, and (b) to demonstrate CNS engagement by memantine, a drug which has potential plasticity-modulating effects for use in motor recovery following stroke.

Methods: We examined the effect of PAS in fourteen participants with chronic hemiparetic stroke at five time-points in a within-subjects repeated measures design study: baseline off-drug, and following a week of orally administered memantine at doses of 5, 10, 15, and 20 mg, comprising a total of seventy sessions. Each week, MEP amplitude pre and post-PAS was assessed in the contralesional hemisphere as a marker of enhanced or diminished plasticity. Strength and dexterity were recorded each week to monitor motor-specific clinical status across the study period.

Results: We found that MEP amplitude was significantly larger after PAS in baseline sessions off-drug, and responsiveness to PAS in these sessions was associated with increased clinical severity. There was no observed increase in MEP amplitude after PAS with memantine at any dose. Motor threshold (MT), strength, and dexterity remained unchanged during the study.

Conclusion: Paired associative stimulation successfully induced corticospinal excitability enhancement in chronic stroke subjects at the group level. However, this response did not occur in all participants, and was associated with increased clinical severity. This could be an important way to stratify patients for future PAS-drug studies. PAS was suppressed by memantine at all doses, regardless of responsiveness to PAS off-drug, indicating CNS engagement.

Keywords: paired associative stimulation, stroke, memantine, neurorehabilitation, TMS

INTRODUCTION

The capacity of the brain to make structural, physiological, and genetic adaptations following stroke, otherwise known as plasticity, is likely to be critical for improving sensorimotor impairments and functional activities. Promotion of adaptive plasticity in the central nervous system (CNS) leading to sustained functional improvement is of paramount importance, given the personal suffering and cost associated with post-stroke disability (Ma et al., 2014). In addition to rehabilitation therapies to retrain degraded motor skills, animal and human studies have tried to augment recovery with neuropharmacologic interventions. Unfortunately, few if any have had a notable effect in patients or have come into routine use (Martinsson et al., 2007; Chollet et al., 2011; Cramer, 2015; Simpson et al., 2015). Methods to screen drugs based on their presumed mechanism of action on plasticity in human motor systems could speed translation to patients. However, there is currently no accepted method in stroke patients for evaluating the potential effectiveness or individual responsiveness to putative "plasticity enhancing" drugs in an efficient, low-cost, cross-sectional manner, in order to establish target engagement in humans and to avoid the extensive time and cost of protracted clinical trials.

Paired associative stimulation (PAS) is a safe, painless, and non-invasive technique known to result in short-term modulation of corticospinal excitability in the adult human motor system, lasting ∼90 min (Stefan et al., 2000; Wolters et al., 2003). Post-PAS excitability enhancement has been considered an LTP-like response thought to relate to transient changes in synaptic efficacy in the glutamatergic system at the *N*-methyl-D-aspartate (NMDA) receptor, since both human NMDA receptor deficiency (Volz et al., 2016) and pharmacological manipulation with dextromethorphan (Stefan et al., 2002) can block the effect. While PAS has been explored as a potential therapeutic intervention in patients with residual motor deficits after stroke (Jayaram and Stinear, 2008; Castel-Lacanal et al., 2009), it has not previously been investigated for its potential use as an assay of motor system plasticity in this context. Prior studies have suggested that motor practice and PAS share the same neuronal substrates, modulating LTP and LTD-like plasticity in the human motor system (Ziemann et al., 2004; Jung and Ziemann, 2009); therefore, as an established non-invasive human neuromodulation method (Suppa et al., 2017), we reasoned that PAS would be a suitable assay in the present study to examine the effect of a drug on motor system plasticity.

Here, we examine the effect of memantine, a drug used for treatment of Alzheimer's disease, on the PAS response in patients with chronic stroke. Memantine is described pharmacologically as a low affinity, voltage dependent, non-competitive, NMDA antagonist (Rogawski and Wenk, 2003). At high concentrations, like other NMDA-R antagonists, it can inhibit synaptic plasticity. At lower, clinically relevant concentrations, memantine can, under some circumstances, promote synaptic plasticity by selectively inhibiting extra-synaptic glutamate receptor activity while sparing normal synaptic transmission, and hence may have clinical utility for rehabilitation (Xia et al., 2010). Interest in specifically using the drug for its interaction with stroke pathophysiology stems from animal models of both prevention (Trotman et al., 2015), in which pre-conditioning reduced infarct size, as well as for functional recovery, in which chronic oral administration starting >2 h post-stroke resulted in improved function through a non-neuroprotective mechanism (López-Valdés et al., 2014). In humans, memantine taken over multiple days has been used to demonstrate that the NMDA receptor is implicated in specific transcranial magnetic paired-pulse measures (Schwenkreis et al., 1999), and short-term training-induced motor map reorganization (Schwenkreis et al., 2005). In studies of neuromodulation, memantine blocked the facilitatory effect of intermittent theta-burst stimulation (iTBS) (Huang et al., 2007). Similarly, LTP-like plasticity induced by associative pairing of painful laser stimuli and TMS over primary motor cortex (M1) can also be blocked by memantine (Suppa et al., 2013). The effects of memantine on the PAS response have not yet been demonstrated, including examination of potential dose-response effects, which would be important for the potential clinical application of memantine for stroke recovery.

In our study, we set out to determine whether PAS might be a useful tool to probe the potential for plasticity after stroke in persons with chronic hemiparesis and apply PAS as an assay to look at drug effects on motor system plasticity using memantine. We hypothesized that (a) PAS would enhance corticospinal excitability in the contralesional hemisphere of stroke patients, and that (b) since PAS-induced plasticity is thought to involve a short-term change in glutamatergic synaptic efficacy, memantine would have a dose-dependent effect on PAS response. We predicted that at low doses, memantine would enhance PAS-induced plasticity through selective blockade of extrasynaptic NMDA receptors, whereas higher doses would inhibit PAS-induced plasticity.

MATERIALS AND METHODS

Participants

Participants enrolled in the study were aged ≥18 years, with unilateral ischemic stroke at least 6 months prior, and upper limb paresis (≥7 points on the Fugl-Meyer impairment scale). Exclusion criteria were as follows: contraindications to transcranial magnetic stimulation (TMS; seizure/epilepsy history, pacemaker/other electro-sensitive implants), medications or conditions that affect the metabolism of memantine, concurrent pregnancy, hemorrhagic stroke, prior stroke, and co-existing neurological disorders. Written informed consent was obtained from all participants. The study had approval from the Institutional Review Board of the Burke Rehabilitation Center.

Study Design and Drug Administration

The purpose of this experiment was to explore the potential of PAS to serve as a screening method for drugs of interest in neurorehabilitation. We used a within-subject repeated measures design to examine the effect of PAS in the contralesional hemisphere of hemiparetic persons with chronic stroke, and to test for a dose-effect of memantine on PAS response. Given the variable nature of MEPs and inter-individual responsiveness to neuromodulatory protocols, such a design is appropriate for this study. Participants attended over 5 weeks, including a screening visit and baseline assessment of clinical function and response to PAS. After the first PAS assessment, participants were given 5 mg of memantine, administered once daily for 1 week. The dosage of memantine was increased every 7 days by 5 mg to: 10, 15, and 20 mg on the 5th week. The dose of memantine was increased incrementally every week to assess for potential side effects with increasing doses. PAS response was reassessed weekly a day prior to the next dosing schedule, for a total of 5 PAS sessions per participant. The criterion measure for within session effects of PAS was MEP amplitude.

Transcranial Magnetic Stimulation and Electromyography

Participants were seated reclined with arms relaxed and supported by a pillow, with surface EMG electrodes (Biometrics Ltd., SX230 1000× gain) over the first dorsal interosseous (FDI) muscle bilaterally, and ground electrode over the ulnar styloid. Via a head stage (Biometrics Gwen+ NPII 7 Hz 8 Channel), EMG was digitized at 5 kHz (Cambridge Electronic Design, Expansion ADC12/CED Micro1401 MKII), and band-pass filtered (20–1000 Hz; Spike 2, V7.15 CED). A Lycra cap with a 1 × 1 cm coordinate system was centered over the vertex (intersection of mid-point between nasion-inion and inter-aural lines). TMS was administered over the contralesional hemisphere, with the coil (Magstim Figure-8, double 70 mm) handle posterior and rotated laterally 45° from the midline. All TMS was performed with Magstim 200^2 $BiStim^2$ (Model 3010-00). The optimal site for FDI was explored with three to four suprathreshold pulses at each grid position commencing at C3/C4.

At each visit, motor threshold (MT) was calculated at rest, using the MT assessment tool (Awiszus, 2003). For baseline MEP assessment, stimulus intensity was set as follows: steps of 5% maximal stimulator output (MSO) commencing at 120% MT, 3 pulses per intensity, ceasing when MEP peak-to-peak amplitude increase reached a plateau (MEP max). The MTAT tool was then used to adjust the stimulator intensity to obtain an MEP amplitude representative of half of the participant's MEP max. Twelve TMS pulses were delivered for each resting collection (pre/post-PAS) at ∼5–10 s intervals between pulses over 1–2 min. Resting motor threshold (RMT) and TMS intensity are reported as percentage of maximum stimulator output (%MSO) hereafter.

Paired Associative Stimulation Intervention

Ulnar nerve electrical stimulation (DS7AH Digitimer Ltd., United Kingdom) was delivered with surface electrodes (8 mm diameter, 30 mm apart; Signa® gel) positioned 3 cm above the palmar wrist crease of the unaffected arm, with cathode proximal (single 200 μs rectangular pulses). Perceptual threshold was defined as the minimum perceivable stimulator intensity (mA).

The PAS protocol approximated that described by Player et al. (2012), targeting the contralesional hemisphere, comprising 200 pairs of stimuli (TMS and ulnar nerve) given at 0.25 Hz over 13 min (Ziemann et al., 2004). In each pair, ulnar nerve stimulation (300% of perceptual threshold) preceded the TMS pulse (130% MT) by 25 ms. Baseline MEPs were collected immediately prior to the PAS intervention, followed by an immediate repeat of baseline at time 0 post, then every 10 min with a final recording at 60 min.

Clinical, Functional, and Neurophysiological Evaluation Across Weeks

An upper limb clinical impairment measure (Fugl-Meyer scale, FM) and a functional assessment (Wolf motor function test) were performed at the start and end of the study, in order to capture clinical status post 4 weeks of incremental memantine administration and PAS, relative to baseline.

Participants performed a weekly dexterity test (9-hole peg test, single trial, total time, seconds) and a strength test (maximum grip, mean of 3 trials, lbs.), with both the unaffected and the affected hand, so as to capture any potential effects of brain stimulation and drug on clinical function. Dexterity and strength tests were performed at the scheduled clinic visit prior to the PAS intervention. No upper extremity rehabilitation was provided.

RMT and sensory perceptual threshold were assessed weekly to determine stimulator intensity for the PAS protocol.

Data Analysis

Motor Evoked Potential Processing

MEPs were visually inspected offline and analyzed for peak-to-peak amplitude using Spike 2 software (Cambridge Electronic Design, Cambridge, United Kingdom). The first two pulses from each collection were routinely excluded, as were MEPs with background EMG >25 μV within 100 ms prior to the TMS stimulus. The median MEP amplitude was averaged across participants at each time point for the group analysis, repeated for each dose of drug.

Statistical Analyses

We compared the mean MEP amplitude over the 1st hour post-PAS intervention versus MEP amplitude immediately before intervention (baseline), with a non-parametric rank-sum test for paired differences, and a one-sided p-value of 0.05 testing for an increase in amplitude with PAS, for the off-drug condition and for each memantine dose.

We also explored each 10-min interval of the 1st hour post-intervention, comparing mean absolute change in MEP amplitude, and the proportion of participants who increased, using two-sided exact binomial tests. This was again repeated for each memantine dose.

To assess potential long-term effects of PAS or memantine, we compared clinical measures at the start of the study to the same assessments 1 week after the last dose, using the non-parametric rank-sum test for paired differences and a one-sided p-value of 0.05.

Exploratory Responder Analysis

In secondary analyses, we stratified participants into PAS responders and non-responders according to their response to PAS in the baseline session (off-drug), as per Müller-Dahlhaus et al. (2015) and Strube et al. (2015), where responders were defined as subjects exhibiting a post-intervention MEP amplitude increase of $>10\%$ from baseline. We evaluated clinical and neurophysiological features that were associated with having a response to PAS. Interhemispheric difference in corticospinal excitability was calculated by subtracting the ipsilesional hemisphere RMT value from the contralesional hemisphere RMT value for each subject. A RMT value of 100 was assigned for cases in which RMT was unable to be derived from the ipsilesional hemisphere (Stinear et al., 2015). We further evaluated the interaction between baseline responder status and MEP amplitude increase post-PAS with the different doses of memantine.

RESULTS

Participant Clinical Characteristics

Fourteen participants with chronic hemiparetic stroke were enrolled and completed the study (age range 48–91 years, four female/ten male, 6–161 months post-ischemic stroke; see **Table 1** for baseline clinical and neurophysiological characteristics at study entry, and **Figure 1** for imaging of lesion location). Upper limb Fugl-Meyer impairment score at study entry ranged from 7 to 60 points (mean 32.7, out of a maximum possible 66 points). PAS and memantine appeared to be safe and well tolerated by all participants; there were no adverse events related to the study medication or PAS.

Within-Session PAS Effects

Paired associative stimulation successfully increased corticospinal excitability in the contralesional hemisphere in the baseline session without memantine. The mean MEP amplitude was significantly higher after PAS intervention as shown in **Figures 2A,B** (0.504 mV pre, 0.851 mV post, 0.346 mV mean increase; 90% CI 0.055–0.638; one-sided $p = 0.028$, median increase 0.364, one-sided $p = 0.045$; sample waveforms are shown in **Figure 3**). The numerically largest increase in MEP amplitude was seen 20 min post-intervention (**Figure 2A**), where 85.7% of participants had increased MEP amplitude (one-sided $p = 0.013$), and 78.5% had increased by at least 10% (one-sided $p < 0.001$).

With all doses of memantine (5–20 mg), there was no significant increase in MEP amplitude after PAS at the group level, suggesting that memantine blocked synaptic plasticity at the

TABLE 1 | Participant characteristics at study entry.

ID	Time since onset (months)	FM-UE	WMFT (s)	rMT (%MSO)		Medication
				U	A	
P1	18	7	1613.9	47	NR	Insulin, albuterol, tamsulosin
P2	94	19	1367.1	53	NR	ASA, simvastatin, levetiracetam, levothyroxine, alendronic acid
P3	28	14	1802.6	54	NR	ASA, escitalopram
P4	100	30	674	43	NR	ASA, lisinopril
P5	27	48	54.3	48	NR	Losartan, nebivolol, atorvastatin, sertraline
P6	46	20	1452.5	55	NR	ASA, atorvastatin, escitalopram
P7	64	7	1448.1	42	NR	ASA, amlodipine, simvastatin, tamsulosin, escitalopram
P8	161	50	35.3	53	61	Warfarin, metoprolol, lisinopril, digoxin, simvastatin, metformin
P9	80	34	56.7	49	51	ASA, lisinopril, simvastatin, tamsulosin, dutasteride
P10	35	53	30.6	43	48	ASA, carvedilol, quinapril, HCTZ, atorvastatin
P11	28	48	36.3	33	34	Apixaban, sotalol, atorvastatin, pantoprazole, citalopram, gabapentin, trazodone
P12	149	24	1565.7	49	46	Clopidogrel, atorvastatin, oxybutynin, hydrocodone
P13	6	60	27.9	44	64	ASA, atorvastatin, fluoxetine, baclofen
P14	20	44	65.6	35	53	ASA, atenolol, amlodipine-benazepril, atorvastatin, duloxetine, gabapentin

FM-UE, Fugl-Meyer Upper Extremity; WMFT, Wolf Motor Function Test; rMT, resting Motor Threshold; MSO, Maximum Stimulator Output; U, Unaffected Hemisphere; A, Affected Hemisphere; NR, No Response; ASA, Aspirin; HCTZ, Hydrochlorothiazide.

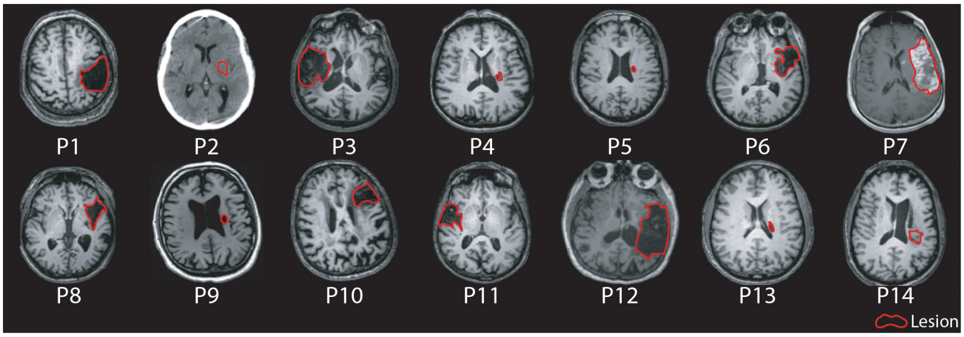

FIGURE 1 | Axial MR/CT images for individual patients illustrating the stroke lesion. Images are displayed in radiological convention. Images are labeled by participant number.

range of doses tested, contrary to our prediction that low doses would enhance PAS-induced plasticity. In the 5 mg condition[1] (**Figure 4A**), MEP amplitude was not increased from baseline following PAS intervention (0.589 mV pre, 0.597 mV post, 0.009 mV mean increase; 90% CI −0.174–0.191; p = 0.467; median increase 0.0001, p = 0.620). With 10 mg memantine (**Figure 4B**), MEP amplitude was again not found to increase from baseline (0.622 mV pre, 0.728 mV post, 0.106 mV mean increase; 90% CI −0.046–0.258; p = 0.119; median increase 0.078, p = 0.195). Similarly, MEP amplitude was not increased from baseline with 15 mg memantine (**Figure 4C**; 0.594 mV pre, 0.794 mV post, 0.200 mV mean increase; 90% CI -0.014-0.414; p = 0.061; median increase 0.164, p = 0.077) or with 20 mg memantine (**Figure 4D**; 0.642 mV pre, 0.642 mV post, 0.001 mV mean increase; 90% CI -0.181-0.181; p = 0.499; median increase 0.001, p = 0.548).

Clinical, Functional, and Neurophysiological Assessment Across Weeks

We did not observe significant changes between the first and last week of intervention in RMT in the ipsilesional hemisphere (n = 7 evaluable, average change-0.71%MSO [90%CI −2.64, 1.22], p = 0.750) nor in the contralesional hemisphere (n = 14, −0.61[3.27, 2.04], p = 0.656). We also observed no significant changes in clinical measures of grip strength (1.43lbs [−2.59, 5.44], p = 0.270; affected n = 11, 4.54 [1-0.76, 10.85], p = 0.11 unaffected, n = 14), dexterity as measured with the 9 hole peg test (−0.61s [−3.27, 2.04], p = 0.656 affected n = 6, 10.93 [−32.07, 53.94], p = 0.315 unaffected n = 14), or sensory perceptual threshold (0.350 mA [−0.375, 1.075], p = 0.204).

Exploratory Responder Analysis

Eight of fourteen participants were classified as responders to PAS, defined as subjects exhibiting a post-PAS MEP amplitude increase of >10%. Responders had a mean post-PAS increase of >200% in MEP amplitude (post/pre ratio, 2.23 [1.82; 3.33] **Figure 5**). The responders were clinically more severe as shown by increased time on the Wolf Motor Function Test (responder, mean = 1450 ± 719 SD sec;

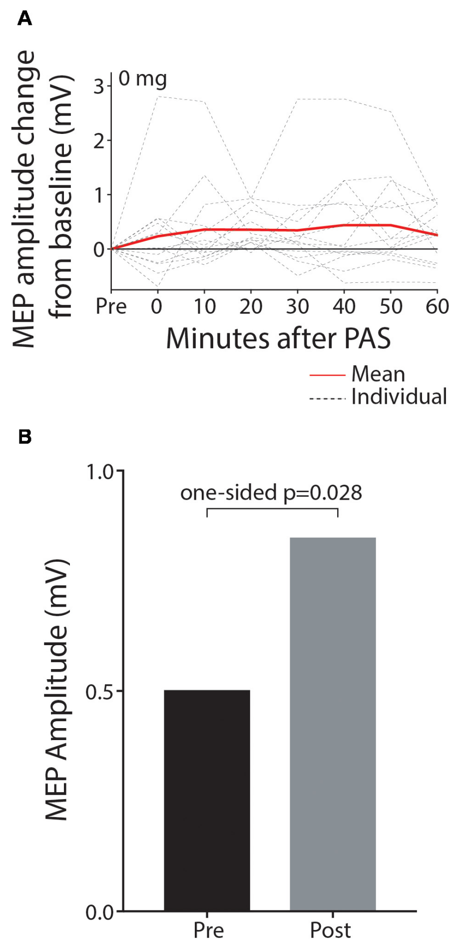

FIGURE 2 | MEP amplitude is significantly increased post-PAS intervention relative to pre-PAS amplitude in the baseline off-drug session. Data are shown depicting MEP amplitude change from baseline for individual time-points post-PAS **(A)** and mean MEP amplitude for pre and the hour post-PAS **(B)**.

[1]We conservatively removed one subject from analysis at 5 mg where the median MEP value at baseline was <50 μV, who therefore showed a disproportionately high response at over 15-fold increase.

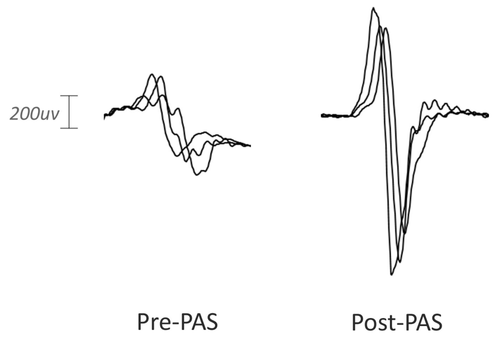

FIGURE 3 | Representative MEP waveforms from a single participant pre and post-PAS intervention. Peak-to-peak MEP amplitude was enhanced by PAS in the baseline session.

non-responder, 46 ± 541, p = 0.028), lower grip strength (responder, mean = 17.5 ± 13.3 SD lbs.; non-responder, 53 ± 27.5, p = 0.01), and TMS measures (six of eight responders had no detectable MEP on the affected side; versus one of six non-responders). Other clinical (FM) and neurophysiological (RMT difference) measures were in the same direction of greater severity, but were not statistically significant. Baseline corticospinal excitability (RMT) in the contralesional (intervention) hemisphere was comparable between responders and non-responders (mean responder, 46.4 ± 7.1; mean non-responder, 46.2 ± 6.9; median responder, 47.5 [42.8; 50.2]; median non-responder, 46.5 [43.2; 52.0] p = 1.00). There was no significant interaction between responder status and the mean increase in MEP amplitude post-PAS with any dose of memantine (see **Supplementary Table 1**) (5 mg condition; F = 0.450, p = 0.823, 10 mg condition; F = 1.681, p = 0.128, 15 mg condition; F = 2.296, p = 0.190, 20 mg condition; F = 1.297, p = 0.295).

DISCUSSION

In the present study, we examined whether PAS MEP-potentiation could be a surrogate biomarker of the likelihood that a particular medication at an optimal dose may augment plasticity. If proven viable, this methodology would be invaluable to the field, as there is currently no accepted method in stroke patients for evaluating the potential effectiveness or individual responsiveness to varying doses of putative 'plasticity enhancing' drugs in an efficient, low-cost, cross-sectional manner. This would be the first step toward trials testing therapeutic drugs in combination with training aimed at improving motor skills after disabling stroke. PAS has received interest for improving motor function post-stroke (Jayaram and Stinear, 2008; Castel-Lacanal et al., 2009), however, response to a single application as a window into the capacity for human brain plasticity has not been evaluated in this context. We showed that without memantine, PAS resulted in an after-effect of heightened excitability (MEP amplitude increase) consistent with the literature in healthy adults (Stefan et al., 2000;

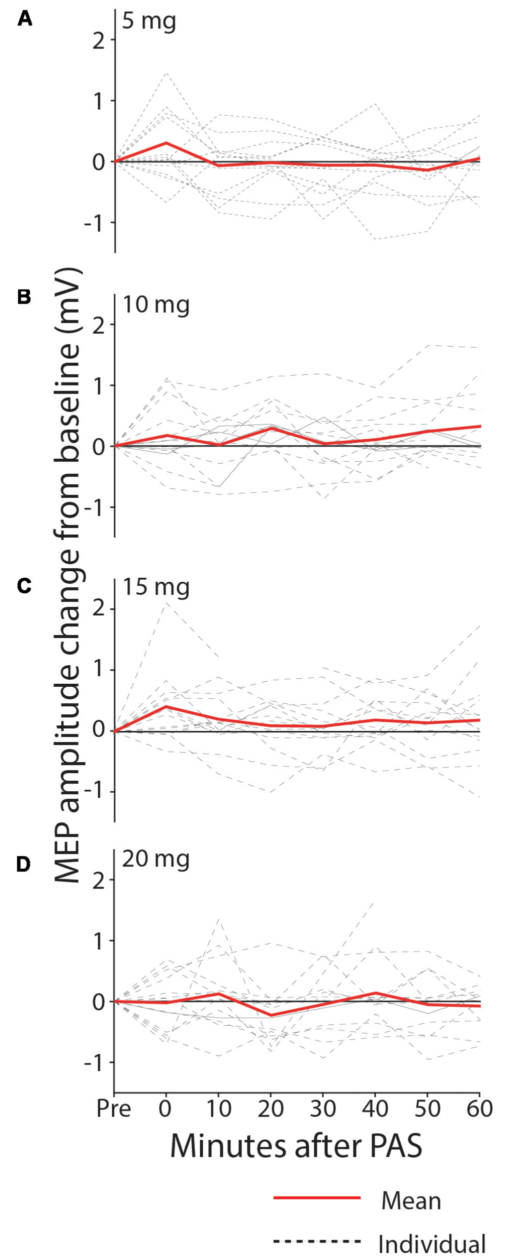

FIGURE 4 | MEP change from baseline after PAS with 5 mg **(A)**, 10 mg **(B)**, 15 mg **(C)**, and 20 mg **(D)** memantine. Group MEP amplitude over the 60 min following PAS was not significantly increased from baseline, with any dose of memantine.

Player et al., 2012). When participants were assessed following 1 week of memantine administration, at every dose evaluated (5–20 mg), excitability remained at baseline levels post-intervention, indicating that the PAS-induced excitability enhancement was blocked by memantine as assessed at steady-state. Although the predictive value of PAS for drug-induced functional recovery post-stroke has yet to be established, our data suggest that, while clinical doses of memantine can penetrate into the CNS to affect function, we found no evidence that it enhances

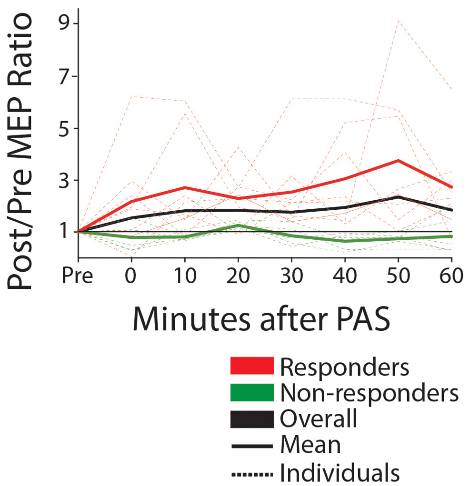

FIGURE 5 | MEP amplitude pre and post-PAS (0–60 min) for responders (mean post >10% mean pre) and non-responders, off-drug (ratio post/pre). Solid lines show group mean, dotted show individual data. Black line is the mean for the entire group. We note that approximately half of participants are responders, with a mean increase of greater than 200% post versus pre.

plasticity in the contralesional hemisphere in those with chronic hemiparetic stroke.

Effect of PAS Off-Drug

MEP amplitude was raised over the 60 min post-intervention relative to baseline, with the most consistent effect across participants occurring 20 min post-intervention. Delayed peak after-effects have been previously reported (Müller-Dahlhaus et al., 2010). Variation in both the time-course and magnitude of the PAS response could be influenced by factors including disease state, lesion location, and concurrent medications. Stroke patients typically have comorbidities (Ostwald et al., 2006), managed with medications that may affect the response to TMS (Siebner and Ziemann, 2007; Ziemann et al., 2014). In our sample, thirteen of the fourteen participants were taking drugs known to affect the response to brain stimulation, or medications that have a similar neuro-pharmacological mechanism of action to such drugs, including SSRI for the treatment of depression (Siebner and Ziemann, 2007), and anti-spasticity medication such as baclofen (Ziemann et al., 2014). PAS response may also be influenced by genotype-related differences such as BDNF and COMT polymorphism interactions (Witte et al., 2012). Experimentally, we aimed to reduce predicted variability in the quantified response by (a) using a greater sample of MEPs post-intervention, which we have previously shown can increase the sensitivity for detecting MEP amplitude change (Bastani and Jaberzadeh, 2012), and (b) by adjusting stimulus intensity to half-maximum MEP amplitude at baseline, thus accounting for individual differences and potential ceiling effects in contralesional hemisphere excitability. Although inter-subject response variation is characteristic in non-invasive neuromodulation (Wiethoff et al., 2014; Murase et al., 2015; Schambra et al., 2015), our observed variation in MEP amplitude increase post-intervention may suggest an alternative methodological approach for PAS application in post-stroke drug dosing studies (responder analysis; see below).

Drug Selection

Our selection of the drug memantine was in part based on prior studies in hippocampal microcultures by Lipton et al., (Xia et al., 2010). We hypothesized that low doses of the clinically approved, use-dependent glutamate antagonist, memantine (5–10 mg), would enhance PAS-induced excitability in the contralesional hemisphere via its ability to selectively block extrasynaptic glutamate receptors, while leaving synaptic glutamate receptors unperturbed. Extrasynaptic glutamate activity has been hypothesized to block plasticity-associated gene expression mediated via activation of synaptic glutamate (Hardingham and Bading, 2010). Contrary to our hypothesis, the current study showed that PAS-induced neuromodulation in chronic stroke was abrogated at all doses of memantine. This finding also favors a synaptic LTP-like mechanism for post-PAS excitability enhancement, and is consistent with a separate study using intermittent theta burst stimulation (iTBS) in healthy human subjects, where memantine blocked the excitability enhancing effect of iTBS (Huang et al., 2007). It remains possible that synaptic plasticity would be enhanced with memantine at lower doses (<5 mg) than those tested in this study. Additionally, Ziemann et al. (2004) demonstrated that LTP-dependent motor learning can block subsequent induction of LTP via PAS due to homeostatic metaplasticity; therefore, LTP-like plasticity induced by memantine could have blocked the effects of further LTP induction via PAS. This can be tested in future experiments using a LTD-like PAS protocol.

Stability of Electrophysiological and Clinical Measures

We did not observe significant changes in RMT, sensory perception, or motor function across the study period, indicating that both escalating drug dose, as well as weekly PAS intervention, had no cumulative effect on these measures. RMT, the individually adjusted minimum stimulator output required to elicit consistent MEPs, did not change regardless of the memantine dose, indicating high test–retest reliability and no effect of drug on this measure. RMT is thought to represent neuronal membrane excitability, since it is increased by drugs that block voltage-gated sodium channels such as carbamazepine (Ziemann et al., 1996), and is not affected by drugs influencing glutamatergic synapse activity such as riluzole (Liepert et al., 1997). Stable RMT across the study period was important experimentally, as threshold-adjusted PAS stimulus intensity remained constant, providing validity for between-dose comparisons.

Somatosensory perceptual threshold for peripheral nerve stimulation did not change across the 5 weeks of repeated PAS and daily memantine administration, indicating a neutral effect of memantine on sensory-afferent awareness and precision in detection of peripheral stimuli. There was no change in measures of impairment (Fugl-Meyer scale) or function (Wolf motor function test), thus clinical motor status remained stable over the study period. The weekly dexterity and strength measures also did not significantly vary. Taken together, these findings indicate that while PAS plasticity is not observed in the presence of memantine, there was no appreciable disruption to functional performance in either the PAS-targeted hand (unaffected) or the affected hand of chronic stroke patients, associated with weekly escalating dose of memantine, and repeated exposure to PAS.

Exploratory Responder Analysis

In the present study, approximately 57% of participants were classified as responders to PAS based on their response in the off-drug condition, which is consistent with other studies, at slightly above 50% (Müller-Dahlhaus et al., 2008; Lahr et al., 2016). We found that stroke symptom severity (measured by grip strength and WMFT) and absence of MEP in the lesioned hemisphere were predictors of response to PAS in the contralesional hemisphere, where baseline excitability was comparable across participants. This pattern of clinical and neurophysiological features associated with responsiveness to PAS is consistent with results described by Ferris et al. (2018). Plasticity induction occurred more readily in the contralesional hemisphere of more severe stroke patients, which could plausibly be due to a greater propensity for hyperexcitability in the contralesional hemisphere. We note that the degree of MEP amplitude increase post-intervention in our responder population (mean 100–300%) was higher than previous reports in the literature for healthy subjects, which ranges from 20 to 78% (Ziemann et al., 2004; Fratello et al., 2006; Müller-Dahlhaus et al., 2008; Ceccanti et al., 2018). However, the relatively scarce studies of PAS response in stroke subjects describe a wider range of response variability, with MEP facilitation ranging from 40% to over 300% (Castel-Lacanal et al., 2009; Palmer et al., 2018). We observed that five of the eight responders in our population were taking SSRI medications, which have been reported to enhance single pulse MEP amplitude (Siebner and Ziemann, 2007) as well as augment PAS effects (Batsikadze et al., 2013).

The effect of memantine was observed in both the PAS responder (more clinically affected) and non-responder (less clinically affected) groups. However, if a plasticity-enhancing drug could be beneficial for a subgroup of patients who are more severely affected but more susceptible to plasticity, this could have important implications in stroke recovery and improve precision in therapeutic prescription.

Limitations and Future Directions

As we tested the contralesional hemisphere, it is possible that a differential effect of memantine occurs in the ipsilesional hemisphere. We pursued to study the contralesional hemisphere due to concerns of reliability and validity of the PAS protocol in the ipsilesional hemisphere, as per Ferris et al. (2018). Reduced efferent and/or afferent conduction, or absent response completely, could impact the effectiveness of PAS, which is considered to be dependent on a narrow window of arrival of the peripheral stimulus afferent volley with the transcranial motor cortex stimulation. Our current findings suggest that the contralesional hemisphere is a suitable target for assessing PAS-induced plasticity, since the RMT was not reduced (hyper-excitable) in relation to our prior studies in chronic stroke (Schambra et al., 2015), and was comparable in both responder and non-responder participants.

While our sample size may not be large, one must appreciate the extent of the investigation that was conducted. This study comprised a total of seventy PAS sessions, each involving the collection of 96 MEPs. This represents one of the largest trials utilizing PAS in the stroke population, with the exception of a single study examining PAS as a potential therapeutic intervention for stroke recovery (Tarri et al., 2018). An aim of this investigation was to explore PAS as a potential screening method for drugs of interest in neurorehabilitation, prior to investing additional time and resources in a more extensive trial. Our results neither support nor preclude the use of PAS as an effective screening tool for drug effects on plasticity. Further investigation is warranted to determine whether the observations gleaned from this trial are the results of homeostatic metaplasticity.

Since PAS-induced excitability modulation is thought involve the NMDA receptor, as supported by our results with memantine, future studies in a stroke population could test the effects of other commonly used agents acting on the NMDA receptor, specifically with drugs that enhance activation of the NMDA receptor complex such as D-cycloserine (Lanthorn, 1994), or a newer generation of memantine, nitromemantine (Takahashi et al., 2015). The specific strategy advocated here was to determine the optimal dose for stimulating plasticity in the human brain by using PAS potentiation as a surrogate marker of enhanced plasticity. For example, PAS may have been useful to identify whether the dose of D-cycloserine employed was optimal before the longitudinal intervention trial in stroke rehabilitation (Butler et al., 2015) which did not show a drug benefit.

Here, we studied a chronic stroke population, though our approach could be applied in the early post-stroke period to examine impact on plasticity with emerging neuroprotective/neuroplasticity agents such as NA-1 (Tat-NR2B9c), an inhibitor of postsynaptic density-95 protein (Hill et al., 2012; Dobkin, 2017), or maraviroc, a CCR5 antagonist (Sorce et al., 2010). The use of PAS as plasticity marker should be contingent upon the reproducibility of studies of PAS in stroke. We recommend first assessing response to PAS and reproducibility prior to an individual entering the drug arm of a study.

Finally, while our finding of PAS corticospinal excitability enhancement serves as a motor domain specific effect that might be useful in post-stroke hemiparesis, PAS could plausibly be a surrogate for drug-effects on plasticity in non-motor domains.

CONCLUSION

We report the first study using non-invasive neuromodulation to assay plasticity in the post-stroke human motor system for the purpose of testing a clinically used neuroplasticity drug with potential utility in neurorehabilitation. We showed that PAS is effective for increasing corticospinal output in the contralesional hemisphere in chronic post-stroke upper limb paresis, and may serve as an assay for CNS target engagement for drugs of interest in post-stroke motor recovery. Applying this model to test a candidate drug, memantine, we found that memantine blocked PAS-induced plasticity, indicating CNS target engagement, but our findings do not support the use of memantine at the doses tested for enhancing motor system plasticity for rehabilitation.

ETHICS STATEMENT

The study had approval from the Institutional Review Board of the Burke Rehabilitation Center. All procedures performed in studies involving human participants were in accordance with the ethical standards of the institutional and/or national research committee and with the 1964 Helsinki declaration and its later amendments or comparable ethical standards. Informed consent was obtained from all individual participants included in the study.

AUTHOR CONTRIBUTIONS

JS: writing, data interpretation, data analysis, data collection, protocol revisions, figures, and literature search. MC: writing, data collection, and literature search. KT: data collection and figures. AC: writing, data analysis, data collection, protocol revisions, figures, and literature search. CO and LG: writing, statistical analysis, and figures. PF: physician, data interpretation, and literature search. RR: study design, writing, data interpretation, and literature search. TK: writing, data interpretation, and literature search. MI: study design, writing, data interpretation, protocol revisions, figures, literature search, and figures. BD and AW: study design, writing, data interpretation, protocol revisions, and literature search. DE: study design, writing, data interpretation, data analysis, protocol revisions, figures, and literature search.

FUNDING

This study was funded by the Dr. Miriam and Sheldon G. Adelson Medical Research Foundation; Grant # N/A 1/1/2013-9/30/2018.

ACKNOWLEDGMENTS

The authors would like to thank Stuart Mackenzie, Choi Deblieck, and Yeun Kim for their helpful discussion.

SUPPLEMENTARY MATERIAL

The Supplementary Material for this article can be found online at: https://www.frontiersin.org/articles/10.3389/fnins.2019.00792/full#supplementary-material

REFERENCES

Awiszus, F. (2003). TMS and threshold hunting. *Suppl. Clin. Neurophysiol.* 56, 13–23.

Bastani, A., and Jaberzadeh, S. (2012). A higher number of TMS-Elicited MEP from a combined hotspot improves intra- and inter-session reliability of the upper limb muscles in healthy individuals. *PLoS One* 7:e47582. doi: 10.1371/journal.pone.0047582

Batsikadze, G., Paulus, W., Kuo, M.-F., and Nitsche, M. A. (2013). Effect of serotonin on paired associative stimulation-induced plasticity in the human motor cortex. *Neuropsychopharmacology* 38, 2260–2267. doi: 10.1038/npp.2013.127

Butler, A. J., Kallos, J., Housley, S. N., Laplaca, M. C., Traynelis, S. F., and Wolf, S. L. (2015).). Randomized, placebo-controlled, double-blind pilot study of D-Cycloserine in chronic stroke. *Rehabil. Res. Pract.* 2015:534239. doi: 10.1155/2015/534239

Castel-Lacanal, E., Marque, P., Tardy, J., Boissezon, X. D., Guiraud, V., Chollet, F., et al. (2009). Induction of cortical plastic changes in wrist muscles by paired associative stimulation in the recovery phase of stroke patients. *Neurorehabil. Neural Repair* 23, 366–372. doi: 10.1177/1545968308322841

Ceccanti, M., Onesti, E., Rubino, A., Cambieri, C., Tartaglia, G., Miscioscia, A., et al. (2018). Modulation of human corticospinal excitability by paired associative stimulation in patients with amyotrophic lateral sclerosis and effects of Riluzole. *Brain Stimul.* 11, 775–781. doi: 10.1016/j.brs.2018.02.007

Chollet, F., Tardy, J., Albucher, J.-F., Thalamas, C., Berard, E., Lamy, C., et al. (2011). Fluoxetine for motor recovery after acute ischaemic stroke (FLAME): a randomised placebo-controlled trial. *Lancet Neurol.* 10, 123–130. doi: 10.1016/S1474-4422(10)70314-8

Cramer, S. C. (2015). Drugs to enhance motor recovery after stroke. *Stroke J. Cereb. Circul.* 46, 2998–3005.

Dobkin, B. (2017). ClinicalTrials.gov (Identifier NCT03172026). *Maraviroc to Augment Rehabilitation Outcomes After Stroke (MAROS)*. Bethesda, MD: United States National Library of Medicine. Available at: https://clinicaltrials.gov/ct2/show/NCT03172026

Ferris, J. K., Neva, J. L., Francisco, B. A., and Boyd, L. A. (2018). Bilateral motor cortex plasticity in individuals with chronic stroke, induced by paired associative stimulation. *Neurorehabil. Neural Repair* 32, 671–681. doi: 10.1177/1545968318785043

Fratello, F., Veniero, D., Curcio, G., Ferrara, M., Marzano, C., Moroni, F., et al. (2006). Modulation of corticospinal excitability by paired associative stimulation: reproducibility of effects and intraindividual reliability. *Clin. Neurophysiol.* 117, 2667–2674.

Hardingham, G. E., and Bading, H. (2010). Synaptic versus extrasynaptic NMDA receptor signalling: implications for neurodegenerative disorders. *Nat. Rev. Neurosci.* 11, 682–696. doi: 10.1038/nrn2911

Hill, M. D., Martin, R. H., Mikulis, D., Wong, J. H., Silver, F. L., Terbrugge, K. G., et al. (2012). Safety and efficacy of NA-1 in patients with iatrogenic stroke after endovascular aneurysm repair (ENACT): a phase 2, randomised, double-blind, placebo-controlled trial. *Lancet Neurol.* 11, 942–950. doi: 10.1016/S1474-4422(12)70225-9

Huang, Y.-Z., Chen, R.-S., Rothwell, J. C., and Wen, H.-Y. (2007). The after-effect of human theta burst stimulation is NMDA receptor dependent. *Clin. Neurophysiol.* 118, 1028–1032.

Jayaram, G., and Stinear, J. W. (2008). Contralesional paired associative stimulation increases paretic lower limb motor excitability post-stroke. *Exp. Brain Res.* 185, 563–570.

Jung, P., and Ziemann, U. (2009). Homeostatic and nonhomeostatic modulation of learning in human motor cortex. *J. Neurosci.* 29, 5597–5604. doi: 10.1523/JNEUROSCI.0222-09.2009

Lahr, J., Paßmann, S., List, J., Vach, W., Flöel, A., and Klöppel, S. (2016). Effects of different analysis strategies on paired associative stimulation. a pooled data analysis from three research labs. *PLoS One* 11:e0154880. doi: 10.1371/journal.pone.0154880

Lanthorn, T. H. (1994). D-Cycloserine: agonist turned antagonist. *Amino Acids* 6, 247–260. doi: 10.1007/BF00813745

Liepert, J., Schwenkreis, P., Tegenthoff, M., and Malin, J.-P. (1997). The glutamate antagonist riluzole suppresses intracortical facilitation. *J. Neural. Transm.* 104, 1207–1214.

López-Valdés, H. E., Clarkson, A. N., Ao, Y., Charles, A. C., Carmichael, S. T., Sofroniew, M. V., et al. (2014). Memantine enhances recovery from stroke. *Stroke J. Cereb. Circulat.* 45, 2093–2100.

Ma, V., Chan, L., and Carruthers, K. (2014). The incidence, prevalence, costs and impact on disability of common conditions requiring rehabilitation in the US: stroke, spinal cord injury, traumatic brain injury, multiple sclerosis, osteoarthritis, rheumatoid arthritis, limb loss, and back pain. *Arch. Phys. Med. Rehabil.* 95:986-995.e1.

Martinsson, L., Hårdemark, H.-G., and Eksborg, S. (2007). Amphetamines for improving recovery after stroke. *Cochrane Database Syst. Rev.* CD002090. doi: 10.1002/14651858.CD002090.pub2

Müller-Dahlhaus, F., Lücke, C., Lu, M.-K., Arai, N., Fuhl, A., Herrmann, E., et al. (2015). Augmenting LTP-Like Plasticity in Human Motor Cortex by Spaced Paired Associative Stimulation. *PLoS One* 10:e0131020. doi: 10.1371/journal.pone.0131020

Müller-Dahlhaus, F., Ziemann, U., and Classen, J. (2010). Plasticity resembling spike-timing dependent synaptic plasticity: the evidence in human cortex. *Front. Synaptic Neurosci.* 2:34. doi: 10.3389/fnsyn.2010.00034

Müller-Dahlhaus, J. F. M., Orekhov, Y., Liu, Y., and Ziemann, U. (2008). Interindividual variability and age-dependency of motor cortical plasticity induced by paired associative stimulation. *Exp. Brain Res.* 187, 467–475. doi: 10.1007/s00221-008-1319-7

Murase, N., Cengiz, B., and Rothwell, J. C. (2015). Inter-individual variation in the after-effect of paired associative stimulation can be predicted from short-interval intracortical inhibition with the threshold tracking method. *Brain Stimul.* 8, 105–113. doi: 10.1016/j.brs.2014.09.010

Ostwald, S. K., Wasserman, J., and Davis, S. (2006). Medications, comorbidities, and medical complications in stroke survivors: the CAReS study. *Rehabil. Nurs.* 31, 10–14.

Palmer, J. A., Wolf, S. L., and Borich, M. R. (2018). Paired associative stimulation modulates corticomotor excitability in chronic stroke: a preliminary investigation. *Restor. Neurol. Neurosci.* 36, 183–194. doi: 10.3233/RNN-170785

Player, M. J., Taylor, J. L., Alonzo, A., and Loo, C. K. (2012). Paired associative stimulation increases motor cortex excitability more effectively than theta-burst stimulation. *Clin. Neurophysiol.* 123, 2220–2226. doi: 10.1016/j.clinph.2012.03.081

Rogawski, M. A., and Wenk, G. L. (2003). The neuropharmacological basis for the use of memantine in the treatment of alzheimer's disease. *CNS Drug Rev.* 9, 275–308.

Schambra, H. M., Ogden, R. T., Martínez-Hernández, I. E., Lin, X., Chang, Y. B., Rahman, A., et al. (2015). The reliability of repeated TMS measures in older adults and in patients with subacute and chronic stroke. *Front. Cell. Neurosci.* 9:335. doi: 10.3389/fncel.2015.00335

Schwenkreis, P., Witscher, K., Janssen, F., Addo, A., Dertwinkel, R., Zenz, M., et al. (1999). Influence of the N-methyl-D-aspartate antagonist memantine on human motor cortex excitability. *Neurosci. Lett.* 3, 137–140.

Schwenkreis, P., Witscher, K., Pleger, B., Malin, J.-P., and Tegenthoff, M. (2005). The NMDA antagonist memantine affects training induced motor cortex plasticity – a study using transcranial magnetic stimulation [ISRCTN65784760]. *BMC Neurosci.* 6:35. doi: 10.1186/1471-2202-6-35

Siebner, H. R., and Ziemann, U. (2007). *Das TMS-Buch: Handbuch Der Transkraniellen Magnetstimulation*. Berlin: Springer-Verlag.

Simpson, D., Goldenberg, J., and Kasner, S. (2015). Dalfampridine in chronic sensorimotor deficits after ischemic stroke: a proof of concept study. *J. Rehabil. Med.* 47, 924–931. doi: 10.2340/16501977-2033

Sorce, S., Bonnefont, J., Julien, S., Marq-Lin, N., Rodriguez, I., Dubois-Dauphin, M., et al. (2010). Increased brain damage after ischaemic stroke in mice lacking the chemokine receptor CCR5. *Br. J. Pharmacol.* 160, 311–321. doi: 10.1111/j.1476-5381.2010.00697.x

Stefan, K., Kunesch, E., Benecke, R., Cohen, L. G., and Classen, J. (2002). Mechanisms of enhancement of human motor cortex excitability induced by interventional paired associative stimulation. *J. Physiol.* 543, 699–708.

Stefan, K., Kunesch, E., Cohen, L. G., Benecke, R., and Classen, J. (2000). Induction of plasticity in the human motor cortex by paired associative stimulation. *Brain* 123, 572–584.

Stinear, C., Petoe, M., and Byblow, W. (2015). Primary motor cortex excitability during recovery after stroke: implications for neuromodulation. *Brain Stimul.* 8, 1183–1190. doi: 10.1016/j.brs.2015.06.015

Strube, W., Bunse, T., Malchow, B., and Hasan, A. (2015). Efficacy and interindividual variability in motor-cortex plasticity following anodal tDCS and paired-associative stimulation. *Neural Plast.* 2015:10.

Suppa, A., Biasiotta, A., Belvisi, D., Marsili, L., La Cesa, S., Truini, A., et al. (2013). Heat-evoked experimental pain induces long-term potentiation-like plasticity in human primary motor cortex. *Cereb. Cortex* 23, 1942–1951. doi: 10.1093/cercor/bhs182

Suppa, A., Quartarone, A., Siebner, H., Chen, R., Di Lazzaro, V., Del Giudice, P., et al. (2017). The associative brain at work: evidence from paired associative stimulation studies in humans. *Clin. Neurophysiol.* 128, 2140–2164. doi: 10.1016/j.clinph.2017.08.003

Takahashi, H., Xia, P., Cui, J., Talantova, M., Bodhinathan, K., Li, W., et al. (2015). Pharmacologically targeted NMDA receptor antagonism by nitromemantine for cerebrovascular disease. *Sci. Rep.* 5:14781. doi: 10.1038/srep14781

Tarri, M., Brihmat, N., Gasq, D., Lepage, B., Loubinoux, I., De Boissezon, X., et al. (2018). Five-day course of paired associative stimulation fails to improve motor function in stroke patients. *Ann. Phys. Rehabil. Med.* 61, 78–84. doi: 10.1016/j.rehab.2017.11.002

Trotman, M., Vermehren, P., Gibson, C. L., and Fern, R. (2015). The dichotomy of memantine treatment for ischemic stroke: dose-dependent protective and detrimental effects. *J Cereb. Blood Flow Metab.* 35, 230–239. doi: 10.1038/jcbfm.2014.188

Volz, M. S., Finke, C., Harms, L., Jurek, B., Paul, F., Flöel, A., et al. (2016). Altered paired associative stimulation-induced plasticity in NMDAR encephalitis. *Ann. Clin. Trans. Neurol.* 3, 101–113. doi: 10.1002/acn3.277

Wiethoff, S., Hamada, M., and Rothwell, J. C. (2014). Variability in response to transcranial direct current stimulation of the motor cortex. *Brain Stimul.* 7, 468–475.

Witte, A. V., Kürten, J., Jansen, S., Schirmacher, A., Brand, E., Sommer, J., et al. (2012). Interaction of BDNF and COMT polymorphisms on paired-associative stimulation-induced cortical plasticity. *J. Neurosci.* 32, 4553–4561. doi: 10.1523/JNEUROSCI.6010-11.2012

Wolters, A., Sandbrink, F., Schlottmann, A., Kunesch, E., Stefan, K., Cohen, L. G., et al. (2003). A temporally asymmetric hebbian rule governing plasticity in the human motor cortex. *J. Neurophysiol.* 89:2339.

Xia, P., Chen, H. S. V., Zhang, D., and Lipton, S. A. (2010). Memantine preferentially blocks extrasynaptic over synaptic nmda receptor currents in hippocampal autapses. *J. Neurosci.* 30, 11246–11250. doi: 10.1523/JNEUROSCI.2488-10.2010

Ziemann, U., Iliać, T. V., Pauli, C., Meintzschel, F., and Ruge, D. (2004). Learning modifies subsequent induction of long-term potentiation-like and long-term depression-like plasticity in human motor cortex. *J. Neurosci.* 24, 1666–1672.

Ziemann, U., Lonnecker, S., Steinhoff, B. J., and Paulus, W. (1996). Effects of antiepileptic drugs on motor cortex excitability in humans: a transcranial magnetic stimulation study. *Ann. Neurol.* 3, 367–368.

Ziemann, U., Reis, J., Schwenkreis, P., Rosanova, M., Strafella, A., Badawy, R., et al. (2014). TMS and drugs revisited 2014. *Clin. Neurophysiol.* 126, 1847–1868. doi: 10.1016/j.clinph.2014.08.028

Conflict of Interest Statement: The authors declare that the research was conducted in the absence of any commercial or financial relationships that could be construed as a potential conflict of interest.

frontiers in Neuroscience

ORIGINAL RESEARCH
published: 24 October 2019
doi: 10.3389/fnins.2019.01109

Check for updates

Fornix Stimulation Induces Metabolic Activity and Dopaminergic Response in the Nucleus Accumbens

Hojin Shin[1], Sang-Yoon Lee[2], Hyun-U Cho[1], Yoonbae Oh[3], In Young Kim[4], Kendall H. Lee[3,5], Dong Pyo Jang[1]* and Hoon-Ki Min[3,6]*

[1] Graduate School of Biomedical Science & Engineering, Hanyang University, Seoul, South Korea, [2] Department of Neuroscience, College of Medicine, Gachon University, Incheon, South Korea, [3] Department of Neurologic Surgery, Mayo Clinic, Rochester, MN, United States, [4] Department of Biomedical Engineering, Hanyang University, Seoul, South Korea, [5] Department of Physiology and Biomedical Engineering, Mayo Clinic, Rochester, MN, United States, [6] Department of Radiology, Mayo Clinic, Rochester, MN, United States

The Papez circuit, including the fornix white matter bundle, is a well-known neural network that is involved in multiple limbic functions such as memory and emotional expression. We previously reported a large-animal study of deep brain stimulation (DBS) in the fornix that found stimulation-induced hemodynamic responses in both the medial limbic and corticolimbic circuits on functional resonance imaging (fMRI) and evoked dopamine responses in the nucleus accumbens (NAc), as measured by fast-scan cyclic voltammetry (FSCV). The effects of DBS on the fornix are challenging to analyze, given its structural complexity and connection to multiple neuronal networks. In this study, we extend our earlier work to a rodent model wherein we characterize regional brain activity changes resulting from fornix stimulation using fludeoxyglucose (^{18}F-FDG) micro positron emission tomography (PET) and monitor neurochemical changes using FSCV with pharmacological confirmation. Both global functional changes and local changes were measured in a rodent model of fornix DBS. Functional brain activity was measured by micro-PET, and the neurochemical changes in local areas were monitored by FSCV. Micro-PET images revealed increased glucose metabolism within the medial limbic and corticolimbic circuits. Neurotransmitter efflux induced by fornix DBS was monitored at NAc by FSCV and identified by specific neurotransmitter reuptake inhibitors. We found a significant increase in the metabolic activity in several key regions of the medial limbic circuits and dopamine efflux in the NAc following fornix stimulation. These results suggest that electrical stimulation of the fornix modulates the activity of brain memory circuits, including the hippocampus and NAc within the dopaminergic pathway.

Keywords: fornix, nucleus accumbens, deep brain stimulation, dopamine, positron emission tomography, fast-scan cyclic voltammetry

OPEN ACCESS

Edited by:
Laura Ballerini, International School for Advanced Studies (SISSA), Italy

Reviewed by:
Vassiliy Tsytsarev, University of Maryland, United States
Cornelia Helbing, German Center for Neurodegenerative Diseases (DZNE), Germany

***Correspondence:**
Dong Pyo Jang
dongpjang@gmail.com
Hoon-Ki Min
Min.Paul@mayo.edu

Specialty section:
This article was submitted to Neural Technology, a section of the journal Frontiers in Neuroscience

Received: *07 November 2018*
Accepted: *01 October 2019*
Published: *24 October 2019*

Citation:
Shin H, Lee S-Y, Cho H-U, Oh Y, Kim IY, Lee KH, Jang DP and Min H-K (2019) Fornix Stimulation Induces Metabolic Activity and Dopaminergic Response in the Nucleus Accumbens. Front. Neurosci. 13:1109. doi: 10.3389/fnins.2019.01109

INTRODUCTION

The Papez circuit is a well-known neural network that is involved in multiple limbic functions such as memory and emotional expression (Rajmohan and Mohandas, 2007). The circuit consists of the hippocampus, fornix, mammillary body, anterior nucleus of the thalamus, cingulate cortex, parahippocampal gyrus, and entorhinal cortex (Mesulam, 2000). Studies show that the interactions between the Papez circuit (medial limbic) and mesocorticolimbic circuits, including the amygdala (AM), nucleus accumbens (NAc), and prefrontal cortex (PFC) are vital to consolidation and retrieval of memory (Hamann et al., 1999; Lisman and Grace, 2005; Carr et al., 2011; Badre et al., 2014; Schedlbauer et al., 2014; Horner et al., 2015). Also, in dementia patients, memory decline has been shown to correlate with the dysfunction of intrinsic connectivity between the hippocampus, PFC, and striatum (Greicius et al., 2004; Buckner et al., 2005; Zhou and Seeley, 2014). These findings highlight the importance of studying the interaction between the medial limbic and mesocorticolimbic circuits (Ito et al., 2008; Mikell et al., 2009; Kahn and Shohamy, 2013; Bagot et al., 2015).

The fornix serves as the major structure between the hippocampus and the mammillary bodies with additional projections to the hypothalamus. Animal studies have demonstrated that lesions or transection of the fornix will hinder memory function in experimental behavior tests (Charles et al., 2004; Fletcher et al., 2006; Mala et al., 2012). A clinical trial investigating deep brain stimulation (DBS) of limbic circuitry as a treatment for morbid obesity resulted in unexpected effects on specific memory functions, evoking detailed autobiographical memories, and enhancing performance on associative memory tasks (Hamani et al., 2008). Based on this finding, DBS was applied to the fornix to address the memory dysfunction associated with dementia in a small cohort of patients with Alzheimer's disease (AD) (Laxton et al., 2010; Fontaine et al., 2013; Holroyd et al., 2015; Lozano et al., 2016; Ponce et al., 2016). Although the results of the clinical trial were favorable, we do not fully understand the mechanism by which electrically stimulating the fornix bundle affects memory function, nor its broader effects on other circuits with which the fornix bundle interacts (Vann, 2013; Ross et al., 2016).

The major challenge in determining the effects of fornix DBS is the complexity of the neuroanatomic and functional connections of the fornix. It is involved in numerous cognitive processes that have diverse axonal pathways, such as the medial limbic and the mesocorticolimbic circuit components. Adding to the complexity is a wide range of axonal fiber effects involving the hippocampus, medial temporal lobe, and NAc (Saint Marie et al., 2010; Kahn and Shohamy, 2013; Bagot et al., 2015). In a large-animal functional magnetic resonance imaging (fMRI) study, we previously demonstrated that fornix DBS elicits functional interactions between the medial limbic and mesocorticolimbic circuits and partially regulates major excitatory input into and through the NAc (Ross et al., 2016).

There have been few systematic studies of the functional network effects of fornix stimulation or the neurochemical changes that it can induce. The goal of the present study was to characterize both the regional brain activity and the specific neurochemical changes associated with fornix stimulation in rodents. To do so, we used micro positron emission tomography (PET) imaging to measure the uptake and accumulation of fludeoxyglucose (^{18}F-FDG) as a tracer for brain activity. Molecular imaging systems with specific tracers have been proposed as a biomarker-based approach to investigating the neural mechanisms for neurodegenerative diseases such as Parkinson's disease (PD), AD, and epilepsy (Lenkov et al., 2013; Joutsa et al., 2017; Matarazzo et al., 2018; Valotassiou et al., 2018). This technique was developed to monitor specific regional brain activity in small animals (Mirrione et al., 2007; Jang et al., 2009a, 2012; Frankemolle et al., 2010). To monitor specific neurotransmitter changes, we used fast-scan cyclic voltammetry (FSCV), which is a real-time electrochemical monitoring system (Agnesi et al., 2009; Bledsoe et al., 2009).

MATERIALS AND METHODS

Subjects

All procedures were performed in accordance with the National Institutes of Health Guidelines for Animal Research (Guide for the Care and Use of Laboratory Animals), and the Hanyang University Institutional Animal Care and Use Committee approved all experimental procedures. The subjects consisted of adult male Sprague Dawley rats (300–350 g, Koatech, Korea) (total n = 18; n = 15 for the PET study, and n = 3 for the FSCV study). Subjects were housed in cages containing two or three animals each, with 12-h light and dark cycles, 50–60% humidity, and *ad libitum* access to food and water.

Stereotactic Surgery

All subjects were anesthetized with Zoletil (0.1 mL/100 g, 5 mg/mL, Virbac, France) 30 min before surgery and were positioned into a stereotaxic frame (David Kopf Instruments, United States). Body temperature was maintained at 37°C with a heating pad (TCAT-2, Harvard Apparatus, United States). A burr hole was drilled into the skull according to coordinates based on Paxinos and Watson's Rat Brain Atlas (Paxinos and Watson, 1997). A twisted bipolar stainless steel electrical stimulation electrode (diameter 125 μm, 500 μm exposure, Polyimide coated, Plastics One, United States) was implanted into the fornix (AP: −1.88 mm, ML: +1.3 mm, DV: −8.3 mm) (**Figure 1B**). Once the stimulating electrode was positioned at the optimal location for targeting the fornix, it was fixed firmly to the skull with three to four screws that were fixed in place with light curing dental cement (CharmmFil Flow, DenKist, Korea). Subjects were monitored for a week of recovery post-surgery.

Micro-PET Acquisition

Two micro-PET (Focus 120 MicroPET, Concorde Microsystems, Knoxville, TN, United States) scans were conducted for each of 15 subjects with either "stimulation on" or "stimulation off," as outlined in **Figure 1A**. The 15 subjects were randomly assigned to one of two groups: "stimulation on" (n = 8) or "stimulation off" (n = 7) in the first week. In week 2, the conditions were reversed so that the eight subjects who had been scanned during "stimulation on" in the first week were scanned with "stimulation off," and the seven subjects who had "stimulation off" in week 1 were scanned with "stimulation on" in week 2. Prior to micro-PET scanning, subjects were kept in cages for 30 min in a room maintained at 30°C to maximize ^{18}F-FDG uptake, as previously described (Fueger et al., 2006). ^{18}F-FDG (500 μCi/100 g) was injected into the tail vein under light anesthesia with Zoletil

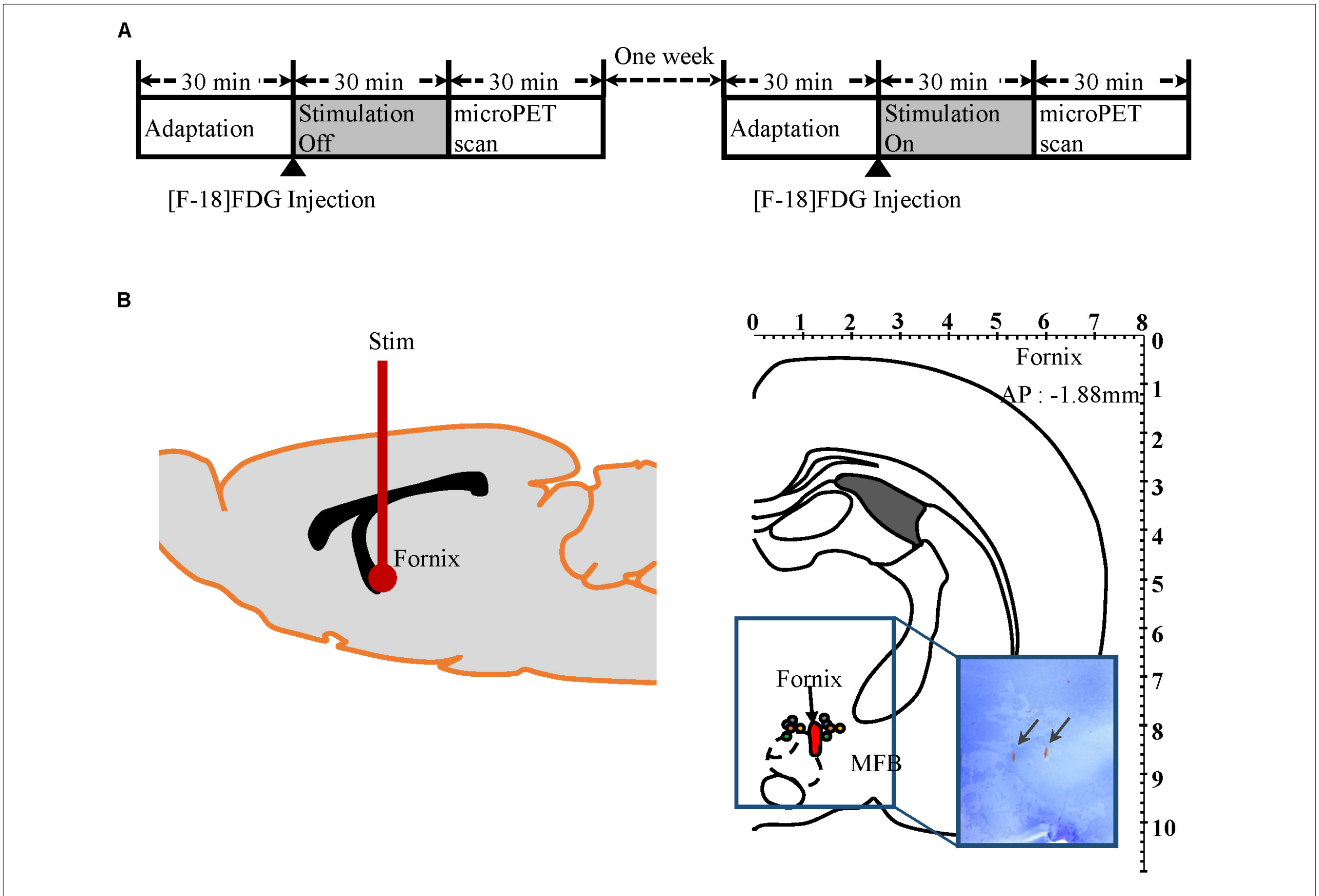

FIGURE 1 | Micro-PET experiment protocol and electrodes placement verification by histology. **(A)** Mirco-PET experiment protocol diagram. **(B)** Left: Diagram of electrode location in rat brain. Right: Location of stimulation electrodes implanted into the fornix (AP −1.88 mm, Paxinos and Watson). Each pair of colored circles marks the tip of the stimulation electrode. Arrows in rectangular image indicate where electrode tips are located in brain histology slices.

(0.03 mL/100 g, 5 mg/mL, Virbac, France). Subjects then stayed in an awake state in the cage for another 30 min for ^{18}F-FDG uptake with or without electrical stimulation (100 μA amplitude pulses at 120 Hz and a pulse width of 2 ms, biphasic). After 30 min of uptake, subjects were put into the PET scanner. The transition time took <1 min. During the PET scan, subjects were under 2% isoflurane anesthesia.

PET Post-processing and Statistical Analysis

Fludeoxyglucose micro-PET images were reconstructed using the ordered subset expectation maximization (OSEM) algorithm with 10 iterations. Using MRIcro (MRIcro Software, Georgia Institute of Technology, Atlanta, GA, United States), an individual mask was applied to extract the whole brain only. These images were normalized to an ^{18}F-FDG rat brain template (Ref, Jang) using a statistical parametric mapping (SPM) program applying six-affine rigid-body transformation smoothed with an isotropic Gaussian kernel (1 mm FWHM). Proportional signal scaling was applied for global normalization. A general linear model was applied, conducting paired t-tests comparing stimulation on–off effects across subjects (n = 15) in SPM. The statistical threshold was set at $P < 0.05$ (false discovery rate, FDR). The ^{18}F-FDG rat brain template has a matching T1-weighted magnetic resonance imaging (MRI) template that matches to Paxinos-atlas space (Schweinhardt et al., 2003; Jang et al., 2009b). The t-value map was overlaid onto the T1 MRI for display in **Figure 2**. The maximum t-value coordinate for each brain region was extracted based on the MRI template and Paxinos atlas. From these maximum t-value coordinates, individual raw FDG PET data were further extracted and normalized to the individual cerebellum value creating standard uptake values ratio (SUVR) used for **Figure 3**.

Fast-Scan Cyclic Voltammetry

Three subjects that were not part of the micro-PET study underwent FSCV recording in NAc during fornix stimulation. Electrochemical changes were recorded using conventional electrochemical sensing carbon fiber microelectrodes (CFMs) fabricated as described previously (7 μm diameter; 50–100 μm length exposed) (Chang et al., 2012). All procedures were conducted under anesthesia with Zoletil (0.1 mL/100 g, 5 mg/mL, Virbac, France). Surgical procedures similar to those for inserting

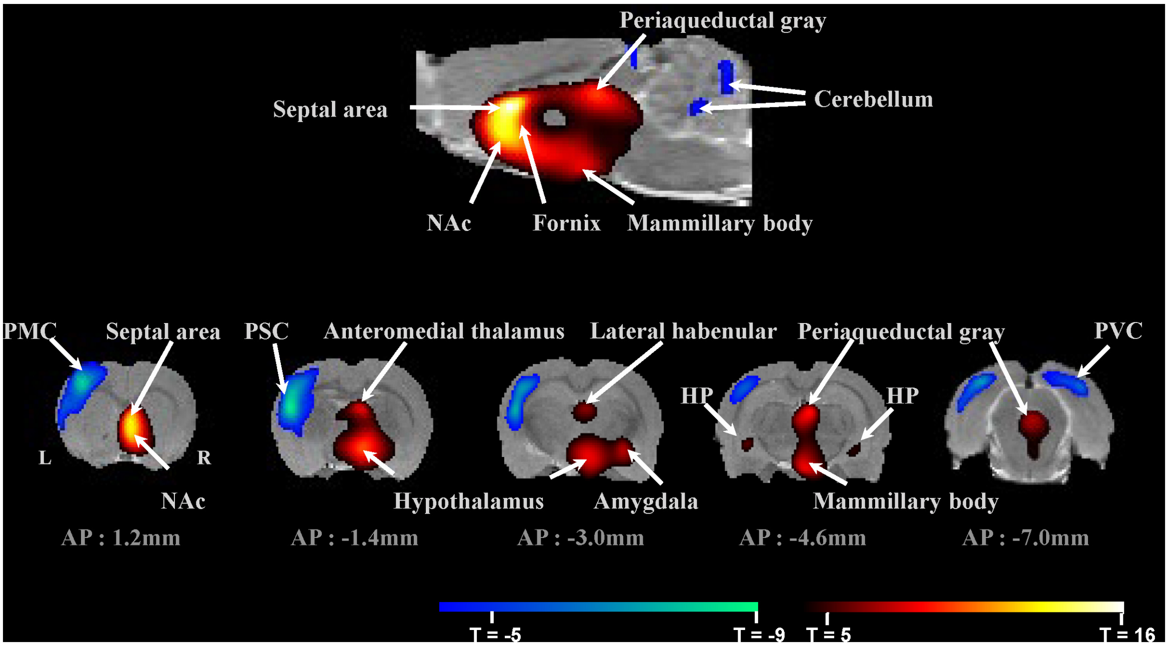

FIGURE 2 | Micro-PET imaging of fornix stimulation-induced brain regional activity averaged across 15 subjects. Brain areas with significant changes in glucose metabolism induced by fornix electrical stimulation (FDR < 0.05, n = 15). **Top:** Mirco-PET image of sagittal section. **Bottom:** Micro-PET images of coronal sections through the rat brain from AP 1.2 mm to AP –7.0 mm. PMC, primary motor cortex; PSC, primary somatosensory cortex; PVC, primary visual cortex; NAc, nucleus accumbens; and HP, hippocampus.

the stimulating electrode were followed when two additional burr holes were made for (1) CFM implantation into the NAc (AP: +1.2 mm, ML: +1.4 mm, DV: −6.5 mm to −7.8 mm) and (2) a reference electrode (Ag/AgCl) implanted into the contralateral hemisphere. Neurotransmitter changes in the NAc during fornix stimulation were measured using the Wireless Instantaneous Neurotransmitter Concentration Sensor (WINCS) system (Agnesi et al., 2009; Bledsoe et al., 2009). Conventional triangular waveforms (−0.4 to 1.5 V versus Ag/AgCl at 400 V/s) were applied at 10 Hz. Background subtraction was performed by subtracting the average of 10 voltammograms acquired prior to electrical stimulation from each voltammogram acquired after stimulation. FSCV recording began after the stabilization of the electrode. Once the stimulation electrode was fixed at the fornix, the dopamine release by electrical stimulation was measured by lowering the CFM 100 μm into the NAc each time, with 10 min interval for recovery. Electrical stimulation was applied by an isolated pulse stimulator system utilizing the parameters: 300 μA amplitude pulses at 120 Hz and a pulse width of 2 ms, biphasic, for 2 s, additional details are available in the **Supplementary Figure S1** (A–M system Model 2100, United States). A pharmacological confirmation of NAc neurochemical changes due to fornix electrical stimulation was conducted in all three FSCV subjects (Lee et al., 2006). A dopamine selective reuptake inhibitor was administered after neurotransmitter detection. Nomifensine was obtained from Sigma–Aldrich (20 mg/kg, St. Louis, MO, United States) and dissolved in 0.9% NaCl saline and injected into the intraperitoneal space.

Histology and Staining

At the end of the experiment after euthanization, target site confirmation was conducted by histology in five subjects randomly selected from the micro-PET experimental group to confirm the fornix site and in the three FSCV subjects to confirm the NAc site. Each subject was exposed to a high current (1 mA for 10 s) to mark electrolytic lesions with the electrodes. The brains were removed and stored for 24 h in 4% paraformaldehyde solution [40 g/L in phosphate-buffered saline (PBS)] at 4°C. The brains were then immersed in a 30% sucrose in PBS solution for 48 h until they sank to the bottom of the container. The brains were then sliced into 50-μm-thick sections and mounted on glass slides. Brain slices were placed directly into chloroform for 30 min and then rehydrated by applying decreasing concentrations (100, 95, and 70%) of ethyl alcohol in distilled water. Brain slices were stained with 0.1% cresyl violet solution and examined microscopically to determine the location of each electrode tip in the brain.

RESULTS

Histological Verification of Electrode Positions

After the completion of the measurements, the positions of the electrodes for the micro-PET study were histologically verified (n = 5, **Figure 1B**). The histological analysis showed that the

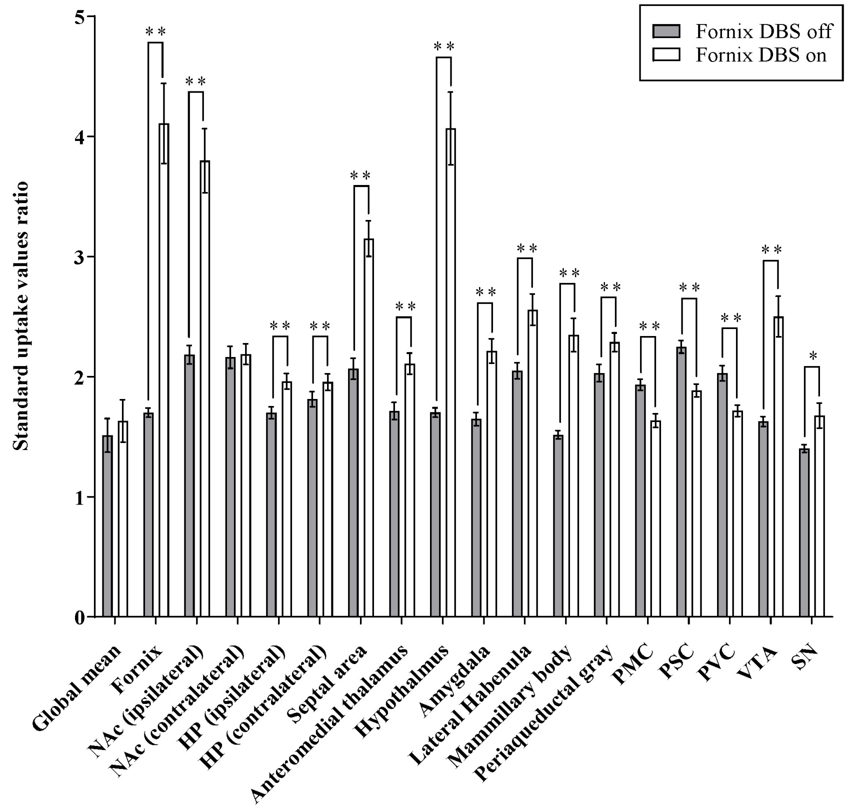

FIGURE 3 | Effects of fornix deep brain stimulation on glucose metabolism. Comparisons of ^{18}F-FDG uptake in the brain regions shown as increase/decrease relative to fornix stimulation "on" and fornix stimulation "off." Data presented are mean ± SEM values. *Values that differ significantly between fornix DBS off and on according to paired *t*-test (*$p < 0.05$, **$p < 0.001$). NAc, nucleus accumbens; HP, hippocampus; PMC, primary motor cortex; PSC, primary somatosensory cortex; PVC, primary visual cortex; VTA, ventral segmental area; and SN, substantia nigra.

twisted bipolar stainless steel electrical stimulation electrodes had been implanted in the fornix area accurately. In targeting the fornix, we avoided the medial forebrain bundle (mfb), which contains direct dopaminergic fibers from the ventral tegmental area (VTA), and histology confirmed that the stimulation electrode was not in close proximity to the mfb. Histological analysis (**Figure 4B**) for the FSCV experiment showed that the CFM had been implanted accurately close to the NAc in all three FSCV subjects.

Fornix Electrical Stimulation Results in Micro-PET Images Show Increased Glucose Metabolism Within the Medial Limbic and Corticolimbic Circuits

Figure 3 summarizes glucose metabolism changes during fornix electrical stimulation and their relative statistical significance, as determined by paired *t*-tests comparing "stimulation on" with "stimulation off." Micro-PET imaging revealed that fornix stimulation induced a significant glucose metabolism increase in the medial limbic and corticolimbic circuits, including the hippocampus, mammillary body, and anteromedial thalamus (FDR < 0.05, $n = 15$) (**Figure 2**). Fornix stimulation also generated a robust glucose metabolism increase in the ipsilateral NAc as well as increases in numerous other regions, including the lateral habenular, periaqueductal gray, AM, and septal area. We also observed significant decreases in glucose metabolism in several regions, including the primary motor cortex (PMC), primary somatosensory cortex (PSC), primary visual cortex (PVC), and cerebellum. The global mean of FDG uptake revealed no significant differences between the fornix electrical stimulation on and stimulation off conditions. However, specific brain regions, including the fornix, NAc (ipsilateral), hippocampus, septal area, anteromedial thalamus, hypothalamus, AM, lateral habenula, mammillary body, periaqueductal gray, PMC, PSC, PVC, VTA, and substantia nigra (SN) did reveal significant differences in FDG uptake between the stimulation on and stimulation off conditions (*$p < 0.05$, **$p < 0.001$). There were no significant differences in the contralateral NAc relative to the stimulation on and stimulation off conditions.

Neurotransmitter Efflux Induced by Fornix Electrical Stimulation

We used FSCV to measure neurochemical changes in the NAc during fornix stimulation ($n = 3$). During phasic fornix stimulation (2 s), dopamine release was detected *in vivo*

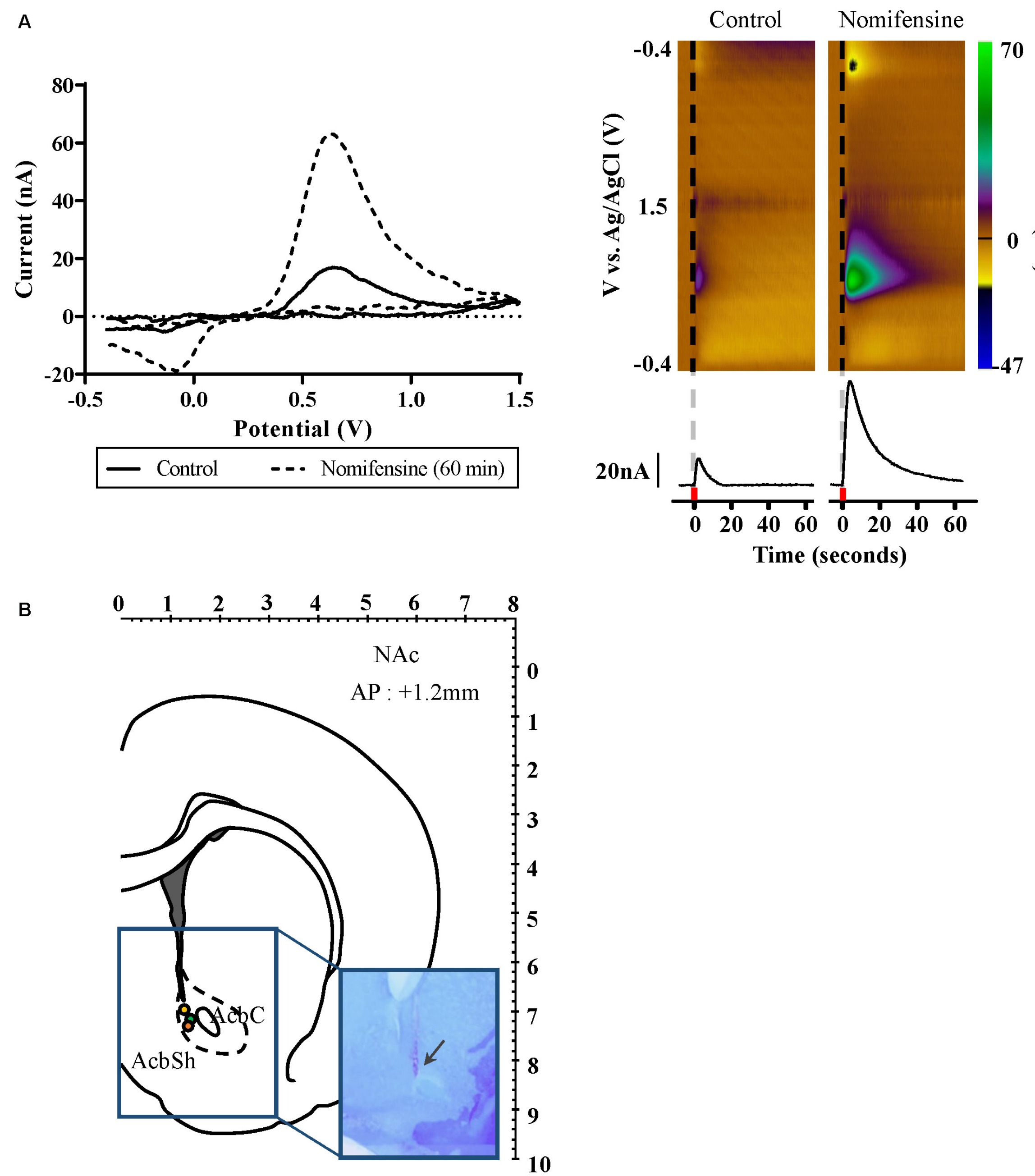

FIGURE 4 | Dopamine release as measured by FSCV in the nucleus accumbens during fornix stimulation. **(A)** Left: Confirmation of dopamine release by using dopamine selective reuptake inhibitor; control (solid), and 60 min after dopamine reuptake inhibitor administered (dash). Background subtracted voltammogram from 60 min after dopamine reuptake inhibitor administered showed significant increase compared to control. Right: Representative color plots of dopamine *in vivo*. Black vertical line (dash) denotes time of fornix stimulation. Current versus time plot at +0.6 V comparing DA release before and after dopamine reuptake inhibitor administered. Red square indicates 2 s when fornix stimulation was applied. **(B)** Location of FSCV CFM electrodes implanted into the NAc (AP 1.2 mm, Paxinos and Watson). Each colored circle marks the tip of the FSCV CFM electrodes. Arrow in rectangular image indicates where CFM tip is located in the brain histology slices. FSCV, fast-scan cyclic voltammetry; CFM, carbon fiber microelectrode; and NAc, nucleus accumbens.

in the NAc (**Figure 4**). The current–voltage curve confirms the oxidation peak at 0.6 V and the reduction peak at −0.2 V, showing characteristic FSCV dopamine markers. For further confirmation, we administered nomifensine, an inhibitor specific to dopamine reuptake. As shown in **Figure 4A**, the dopamine reuptake inhibitor showed a significant increase of neurotransmitter efflux 60 min after administration compared to the control condition by fornix stimulation alone. As shown in **Figure 4B**, histologic analysis confirmed that the CFM had been accurately implanted close to the NAc in all three FSCV subjects.

DISCUSSION

In the present study, we confirmed that fornix stimulation within the Papez circuit could induce NAc activity and further efflux of dopamine. These findings are consistent with our large-animal fMRI and FSCV study of fornix stimulation (Ross et al., 2016) and a relevant recent rat study that showed that chronic forniceal DBS significantly reduces amyloid deposition in the hippocampus and cortex, decreases astrogliosis and microglia activation, and lowers neuronal loss (Leplus et al., 2019). The micro-PET results revealed that fornix stimulation increases glucose metabolism in medial limbic circuits, including the hippocampus, mammillary bodies, and anteromedial thalamus. Other regions, such as the septal area, lateral habenula, AM, and periaqueductal gray, also showed increased glucose metabolism. In contrast, glucose metabolism was decreased in the PMC, PSC, and PVC. These increases and decreases in brain activity suggest that the fornix is part of a major limbic system pathway, the Papez circuit, which is primarily involved in certain aspects of cortical control of emotional processing and memory storage.

Additionally, fornix stimulation significantly increased activation in the NAc. In particular, encoding and consolidation of memories require the stimulation of dopamine receptors as part of a hippocampal–striatal–prefrontal loop that orchestrates the formation of new memories (Lisman and Grace, 2005; Axmacher et al., 2010). This finding may reflect the strategic position of the fornix in the brain, in that ventral hippocampal glutamatergic afferent bundles pass through the fornix to NAc medium spiny neurons (French and Totterdell, 2002, 2003; Sesack and Grace, 2010; Britt et al., 2012; MacAskill et al., 2012).

The NAc works as an interface between the limbic cortex and the midbrain structures involved in motor performance. The fornix carries limbic inputs to the ventral striatum, which then projects them to the NAc. It also carries fibers arising in the septal area that project to the hippocampal formation and to other areas of the rostral forebrain (Boeijinga et al., 1993). Another study suggests that there may be indirect connections between the fornix and the NAc from the dorsal CA3 (*Cornu Ammonis* areas) via the VTA (Luo et al., 2011). A non-human primate study found that the fornix contains 500,000 fibers projecting to and from various regions, including projections from the CA3 that target the mammillary bodies and the NAc (Talakoub et al., 2016). An fMRI study previously reported that fornix DBS could serve as a functional connection between the medial limbic and mesocorticolimbic circuits and may modulate presynaptic dopamine efflux in the NAc (Ross et al., 2016). The combination of these anatomic and functional studies suggests that fornix stimulation drives NAc input and output, which triggers the activity of the hippocampus and/or the thalamus.

Several research papers have verified the neuronal framework for dopamine efflux in the NAc induced by fornix stimulation. One rodent study suggested that stimulation of the ventral subiculum of the hippocampus evoked dopamine release in the NAc by synaptic activation of both ionotropic and metabotropic glutamate receptors (Blaha et al., 1997). The majority of cells in the NAc are GABAergic neurons with predominantly extrinsic innervation via excitatory glutamatergic projections from the hippocampus, PFC, and AM (Kelley and Domesick, 1982; Friedman et al., 2002; Sesack and Grace, 2010). NAc dopamine is known to play an important role in motor activity and in behaviors governed by drugs and natural reinforcers, as well as in non-associative forms of learning (Mele et al., 2004). Because the fornix is part of the Papez circuit, fornix stimulation-driven efflux of dopamine in the NAc may carry information related to memory and emotion (Halbig et al., 2011). Previously, it was shown that synchronized electrical stimulation of the dopamine pathway and the hippocampal pathway generates an additive fMRI response in the NAc, suggesting a modulatory role for dopamine in the hippocampal pathway (Krautwald et al., 2013). By modulating hippocampal activity, dopamine is thought to play a role in the motivational relevance of memory content (Shohamy and Adcock, 2010).

We do not have a good explanation for the decreased metabolism in the PMC, PSC, and PVC. All of the positive metabolism brain areas correspond well with the Papez circuit, but these decreased-metabolism brain areas are not in the Papez circuit. First, looking for a possible circuitry connection and not discussing the decreased signal, one possible explanation of the effect in the PMC, PSC, and PVC is the role of the AM. The amygdaloid complex contains many nuclei involved in both sensory and motor functions (Vann and Nelson, 2015). The NAc and septal area also have sensory-motor connections, so there could be a possible secondary connection. This could be further supported by the NAc having a bilateral connection to both hemispheres. The NAc also has connections from the AM, supporting our finding of metabolic changes in the AM and neurochemical changes in the NAc after fornix stimulation. Our previous study (Ross et al., 2016) showed both ipsilateral and contralateral somatosensory BOLD responses, which indicated circuit involvement between the hippocampus and PSC. In terms of the functional distribution of the forniceal fibers, part of the fornix carries fibers from the caudal hippocampus that process exteroceptive signals (Raslau et al., 2015), and lesion or damage to the fornix lead to visual discrimination deficits (Lech et al., 2016). Another possible explanation of the decreases is that electrical stimulation affected not only the fornix but also brain regions near the fornix such as the hypothalamic area. Hypothalamic DBS studies reported that functional imaging revealed stimulation-induced deactivations in the PSC (May et al., 2006; May, 2008). The final possibility is that the observed changes are artifacts of the PET analysis method, for example, the proportional scaling for global normalization. This method would work well for focal changes induced by experimental treatments but could bias the statistical analysis when relatively wide brain areas are involved. Because local changes can be smeared in wide brain areas due to the low spatial resolution of [F-18]FDG micro-PET in rat neuroimaging, the proportional scaling may cause type I or type II errors in the analysis due to over- or under-estimation of global activity.

Among the limitations of the present study is the fact that the evoked dopamine findings represent the effects of short-term stimulation (2 s) due to the inherent long-term drifting of FSCV for longer periods (Heien et al., 2005), while FDG-PET can measure 30 min of continuous stimulation effects. Further study is needed to understand if these phasic dopamine findings would impact behavioral memory test scores. Secondly, experiments, such as this one, conducted under anesthesia may not represent the activation effects found when subjects are conscious. The micro-PET FDG protocol can be used to measure conscious-state brain activity (Mizuma et al., 2010), and thus this study likely confirms a platform from which to conduct conscious-state behavioral tests during FDG uptake and PET imaging. Lastly, an inherent limitation of electrical stimulation is that it can activate unwanted and non-specific brain areas near the targeted region. For this reason, we took a cautious approach to avoided possible direct stimulation of the mfb, which contains dopaminergic fibers, given that the electrical current spread for rodent-use micro-electrodes is reported to be <1 mm (Lozano et al., 2002). Although there are inherent limitations to translating findings from healthy small animals to human pathologic conditions, the global and local patterns of molecular imaging in this study reveal potential neuronal mechanisms underlying fornix DBS (Ross et al., 2016; Fu et al., 2018).

CONCLUSION

In conclusion, the results of this rodent study provide a platform to investigate the interactions between the Papez and mesolimbic circuits related to certain aspects of memory function. Our findings support the concept that electrical stimulation of the fornix increases brain activity and controls dopamine efflux in the NAc and suggests that further exploration of the neuromodulatory effects of fornix DBS is warranted relative to its potential therapeutic impact on certain aspects of memory and emotional processing.

ETHICS STATEMENT

All procedures were performed in accordance with the National Institutes of Health Guidelines for Animal Research (Guide for the Care and Use of Laboratory Animals), and the Hanyang University Institutional Animal Care and Use Committee approved all experimental procedures.

AUTHOR CONTRIBUTIONS

H-KM and DJ supervised all aspects of this work equally. HS, IK, KL, DJ, and H-KM designed the analyses. HS and H-KM conducted the analyses. HS, S-YL, H-UC, and YO collected the data. S-YL, KL, and DJ provided the resources and consultation on the section "Materials and Methods." HS, DJ, and H-KM wrote the manuscript. All authors commented on and accepted the final version of the manuscript.

FUNDING

This study was supported by the National Research Foundation of Korea (NRF-2019M3C7A1031278) and the Korea Health Technology R&D Project through the Korea Health Industry Development Institute (KHIDI), funded by the Ministry for Health and Welfare, Korea (HI14C1135).

SUPPLEMENTARY MATERIAL

The Supplementary Material for this article can be found online at: https://www.frontiersin.org/articles/10.3389/fnins.2019.01109/full#supplementary-material

FIGURE S1 | Electrical stimulation evoked dopamine response changes by stimulation frequency and amplitude. **(A)** Dopamine oxidation current versus stimulation frequency from 10Hz to 200Hz. **(B)** Dopamine oxidation versus stimulation amplitude from 50 μA to 400 μA.

REFERENCES

Agnesi, F., Tye, S. J., Bledsoe, J. M., Griessenauer, C. J., Kimble, C. J., Sieck, G. C., et al. (2009). Wireless instantaneous neurotransmitter concentration system-based amperometric detection of dopamine, adenosine, and glutamate for intraoperative neurochemical monitoring. *J. Neurosurg.* 111, 701–711. doi: 10.3171/2009.3.JNS0990

Axmacher, N., Cohen, M. X., Fell, J., Haupt, S., Dumpelmann, M., Elger, C. E., et al. (2010). Intracranial EEG correlates of expectancy and memory formation in the human hippocampus and nucleus accumbens. *Neuron* 65, 541–549. doi: 10.1016/j.neuron.2010.02.006

Badre, D., Lebrecht, S., Pagliaccio, D., Long, N. M., and Scimeca, J. M. (2014). Ventral striatum and the evaluation of memory retrieval strategies. *J. Cogn. Neurosci.* 26, 1928–1948. doi: 10.1162/jocn_a_00596

Bagot, R. C., Parise, E. M., Pena, C. J., Zhang, H. X., Maze, I., Chaudhury, D., et al. (2015). Ventral hippocampal afferents to the nucleus accumbens regulate susceptibility to depression. *Nat. Commun.* 6:7062.

Blaha, C. D., Yang, C. R., Floresco, S. B., Barr, A. M., and Phillips, A. G. (1997). Stimulation of the ventral subiculum of the hippocampus evokes glutamate receptor-mediated changes in dopamine efflux in the rat nucleus accumbens. *Eur. J. Neurosci.* 9, 902–911. doi: 10.1111/j.1460-9568.1997.tb01441.x

Bledsoe, J. M., Kimble, C. J., Covey, D. P., Blaha, C. D., Agnesi, F., Mohseni, P., et al. (2009). Development of the wireless instantaneous neurotransmitter concentration system for intraoperative neurochemical monitoring using fast-scan cyclic voltammetry. *J. Neurosurg.* 111, 712–723. doi: 10.3171/2009.3.JNS081348

Boeijinga, P. H., Mulder, A. B., Pennartz, C. M., Manshanden, I., and Lopes Da Silva, F. H. (1993). Responses of the nucleus accumbens following fornix/fimbria stimulation in the rat. Identification and long-term potentiation of mono- and polysynaptic pathways. *Neuroscience* 53, 1049–1058. doi: 10.1016/0306-4522(93)90488-2

Britt, J. P., Benaliouad, F., Mcdevitt, R. A., Stuber, G. D., Wise, R. A., and Bonci, A. (2012). Synaptic and behavioral profile of multiple glutamatergic inputs to the nucleus accumbens. *Neuron* 76, 790–803. doi: 10.1016/j.neuron.2012.09.040

Buckner, R. L., Snyder, A. Z., Shannon, B. J., Larossa, G., Sachs, R., Fotenos, A. F., et al. (2005). Molecular, structural, and functional characterization of Alzheimer's disease: evidence for a relationship between default activity, amyloid, and memory. *J. Neurosci.* 25, 7709–7717. doi: 10.1523/jneurosci.2177-05.2005

Carr, M. F., Jadhav, S. P., and Frank, L. M. (2011). Hippocampal replay in the awake state: a potential substrate for memory consolidation and retrieval. *Nat. Neurosci.* 14, 147–153. doi: 10.1038/nn.2732

Chang, S. Y., Kim, I., Marsh, M. P., Jang, D. P., Hwang, S. C., Van Gompel, J. J., et al. (2012). Wireless fast-scan cyclic voltammetry to monitor adenosine in patients with essential tremor during deep brain stimulation. *Mayo Clin. Proc.* 87, 760–765. doi: 10.1016/j.mayocp.2012.05.006

Charles, D. P., Gaffan, D., and Buckley, M. J. (2004). Impaired recency judgments and intact novelty judgments after fornix transection in monkeys. *J. Neurosci.* 24, 2037–2044. doi: 10.1523/jneurosci.3796-03.2004

Fletcher, B. R., Calhoun, M. E., Rapp, P. R., and Shapiro, M. L. (2006). Fornix lesions decouple the induction of hippocampal arc transcription from behavior but not plasticity. *J. Neurosci.* 26, 1507–1515. doi: 10.1523/jneurosci.4441-05.2006

Fontaine, D., Deudon, A., Lemaire, J. J., Razzouk, M., Viau, P., Darcourt, J., et al. (2013). Symptomatic treatment of memory decline in Alzheimer's disease by deep brain stimulation: a feasibility study. *J. Alzheimers Dis.* 34, 315–323. doi: 10.3233/JAD-121579

Frankemolle, A. M., Wu, J., Noecker, A. M., Voelcker-Rehage, C., Ho, J. C., Vitek, J. L., et al. (2010). Reversing cognitive-motor impairments in Parkinson's disease patients using a computational modelling approach to deep brain stimulation programming. *Brain* 133, 746–761. doi: 10.1093/brain/awp315

French, S. J., and Totterdell, S. (2002). Hippocampal and prefrontal cortical inputs monosynaptically converge with individual projection neurons of the nucleus accumbens. *J. Comp. Neurol.* 446, 151–165. doi: 10.1002/cne.10191

French, S. J., and Totterdell, S. (2003). Individual nucleus accumbens-projection neurons receive both basolateral amygdala and ventral subicular afferents in rats. *Neuroscience* 119, 19–31. doi: 10.1016/s0306-4522(03)00150-7

Friedman, D. P., Aggleton, J. P., and Saunders, R. C. (2002). Comparison of hippocampal, amygdala, and perirhinal projections to the nucleus accumbens: combined anterograde and retrograde tracing study in the Macaque brain. *J. Comp. Neurol.* 450, 345–365. doi: 10.1002/cne.10336

Fu, J. F., Klyuzhin, I., Liu, S., Shahinfard, E., Vafai, N., Mckenzie, J., et al. (2018). Investigation of serotonergic Parkinson's disease-related covariance pattern using [(11)C]-DASB/PET. *Neuroimage Clin.* 19, 652–660. doi: 10.1016/j.nicl.2018.05.022

Fueger, B. J., Czernin, J., Hildebrandt, I., Tran, C., Halpern, B. S., Stout, D., et al. (2006). Impact of animal handling on the results of 18F-FDG PET studies in mice. *J. Nucl. Med.* 47, 999–1006.

Greicius, M. D., Srivastava, G., Reiss, A. L., and Menon, V. (2004). Default-mode network activity distinguishes Alzheimer's disease from healthy aging: evidence from functional MRI. *Proc. Natl. Acad. Sci. U.S.A.* 101, 4637–4642. doi: 10.1073/pnas.0308627101

Halbig, T. D., Assuras, S., Creighton, J., Borod, J. C., Tse, W., Frisina, P. G., et al. (2011). Differential role of dopamine in emotional attention and memory: evidence from Parkinson's disease. *Mov. Disord.* 26, 1677–1683. doi: 10.1002/mds.23728

Hamani, C., Mcandrews, M. P., Cohn, M., Oh, M., Zumsteg, D., Shapiro, C. M., et al. (2008). Memory enhancement induced by hypothalamic/fornix deep brain stimulation. *Ann. Neurol.* 63, 119–123. doi: 10.1002/ana.21295

Hamann, S. B., Ely, T. D., Grafton, S. T., and Kilts, C. D. (1999). Amygdala activity related to enhanced memory for pleasant and aversive stimuli. *Nat. Neurosci.* 2, 289–293. doi: 10.1038/6404

Heien, M. L., Khan, A. S., Ariansen, J. L., Cheer, J. F., Phillips, P. E., Wassum, K. M., et al. (2005). Real-time measurement of dopamine fluctuations after cocaine in the brain of behaving rats. *Proc. Natl. Acad. Sci. U.S.A.* 102, 10023–10028. doi: 10.1073/pnas.0504657102

Holroyd, K. B., Fosdick, L., Smith, G. S., Leoutsakos, J. M., Munro, C. A., Oh, E. S., et al. (2015). Deep brain stimulation targeting the fornix for mild Alzheimer dementia: design of the ADvance randomized controlled trial. *Open Access J. Clin. Trials* 7, 63–76.

Horner, A. J., Bisby, J. A., Bush, D., Lin, W. J., and Burgess, N. (2015). Evidence for holistic episodic recollection via hippocampal pattern completion. *Nat. Commun.* 6:7462. doi: 10.1038/ncomms8462

Ito, R., Robbins, T. W., Pennartz, C. M., and Everitt, B. J. (2008). Functional interaction between the hippocampus and nucleus accumbens shell is necessary for the acquisition of appetitive spatial context conditioning. *J. Neurosci.* 28, 6950–6959. doi: 10.1523/JNEUROSCI.1615-08.2008

Jang, D. P., Lee, S. H., Lee, S. Y., Park, C. W., Cho, Z. H., and Kim, Y. B. (2009a). Neural responses of rats in the forced swimming test: [F-18]FDG micro PET study. *Behav. Brain Res.* 203, 43–47. doi: 10.1016/j.bbr.2009.04.020

Jang, D. P., Lee, S. H., Park, C. W., Lee, S. Y., Kim, Y. B., and Cho, Z. H. (2009b). Effects of fluoxetine on the rat brain in the forced swimming test: a [F-18]FDG micro-PET imaging study. *Neurosci. Lett.* 451, 60–64. doi: 10.1016/j.neulet.2008.12.024

Jang, D. P., Min, H. K., Lee, S. Y., Kim, I. Y., Park, H. W., Im, Y. H., et al. (2012). Functional neuroimaging of the 6-OHDA lesion rat model of Parkinson's disease. *Neurosci. Lett.* 513, 187–192. doi: 10.1016/j.neulet.2012.02.034

Joutsa, J., Rinne, J. O., Karrasch, M., Hermann, B., Johansson, J., Anttinen, A., et al. (2017). Brain glucose metabolism and its relation to amyloid load in middle-aged adults with childhood-onset epilepsy. *Epilepsy Res.* 137, 69–72. doi: 10.1016/j.eplepsyres.2017.09.006

Kahn, I., and Shohamy, D. (2013). Intrinsic connectivity between the hippocampus, nucleus accumbens, and ventral tegmental area in humans. *Hippocampus* 23, 187–192. doi: 10.1002/hipo.22077

Kelley, A. E., and Domesick, V. B. (1982). The distribution of the projection from the hippocampal formation to the nucleus accumbens in the rat: an anterograde- and retrograde-horseradish peroxidase study. *Neuroscience* 7, 2321–2335. doi: 10.1016/0306-4522(82)90198-1

Krautwald, K., Min, H. K., Lee, K. H., and Angenstein, F. (2013). Synchronized electrical stimulation of the rat medial forebrain bundle and perforant pathway generates an additive BOLD response in the nucleus accumbens and prefrontal cortex. *Neuroimage* 77, 14–25. doi: 10.1016/j.neuroimage.2013.03.046

Laxton, A. W., Tang-Wai, D. F., Mcandrews, M. P., Zumsteg, D., Wennberg, R., Keren, R., et al. (2010). A phase I trial of deep brain stimulation of memory circuits in Alzheimer's disease. *Ann. Neurol.* 68, 521–534. doi: 10.1002/ana.22089

Lech, R. K., Koch, B., Schwarz, M., and Suchan, B. (2016). Fornix and medial temporal lobe lesions lead to comparable deficits in complex visual perception. *Neurosci. Lett.* 620, 27–32. doi: 10.1016/j.neulet.2016.03.002

Lee, K. H., Blaha, C. D., Harris, B. T., Cooper, S., Hitti, F. L., Leiter, J. C., et al. (2006). Dopamine efflux in the rat striatum evoked by electrical stimulation of the subthalamic nucleus: potential mechanism of action in Parkinson's disease. *Eur. J. Neurosci.* 23, 1005–1014. doi: 10.1111/j.1460-9568.2006.04638.x

Lenkov, D. N., Volnova, A. B., Pope, A. R., and Tsytsarev, V. (2013). Advantages and limitations of brain imaging methods in the research of absence epilepsy in humans and animal models. *J. Neurosci. Methods* 212, 195–202. doi: 10.1016/j.jneumeth.2012.10.018

Leplus, A., Lauritzen, I., Melon, C., Kerkerian-Le Goff, L., Fontaine, D., and Checler, F. (2019). Chronic fornix deep brain stimulation in a transgenic Alzheimer's rat model reduces amyloid burden, inflammation, and neuronal loss. *Brain Struct. Funct.* 224, 363–372. doi: 10.1007/s00429-018-1779-x

Lisman, J. E., and Grace, A. A. (2005). The hippocampal-VTA loop: controlling the entry of information into long-term memory. *Neuron* 46, 703–713. doi: 10.1016/j.neuron.2005.05.002

Lozano, A. M., Dostrovsky, J., Chen, R., and Ashby, P. (2002). Deep brain stimulation for Parkinson's disease: disrupting the disruption. *Lancet Neurol.* 1, 225–231. doi: 10.1016/s1474-4422(02)00101-1

Lozano, A. M., Fosdick, L., Chakravarty, M. M., Leoutsakos, J. M., Munro, C., Oh, E., et al. (2016). A phase II study of fornix deep brain stimulation in mild Alzheimer's disease. *J. Alzheimers Dis.* 54, 777–787. doi: 10.3233/JAD-160017

Luo, A. H., Tahsili-Fahadan, P., Wise, R. A., Lupica, C. R., and Aston-Jones, G. (2011). Linking context with reward: a functional circuit from hippocampal CA3 to ventral tegmental area. *Science* 333, 353–357. doi: 10.1126/science.1204622

MacAskill, A. F., Little, J. P., Cassel, J. M., and Carter, A. G. (2012). Subcellular connectivity underlies pathway-specific signaling in the nucleus accumbens. *Nat. Neurosci.* 15, 1624–1626. doi: 10.1038/nn.3254

Mala, H., Rodriguez Castro, M., Pearce, H., Kingod, S. C., Nedergaard, S. K., Scharff, Z., et al. (2012). Delayed intensive acquisition training alleviates the lesion-induced place learning deficits after fimbria-fornix transection in the rat. *Brain Res.* 1445, 40–51. doi: 10.1016/j.brainres.2012.01.035

Matarazzo, M., Wile, D., Mackenzie, M., and Stoessl, A. J. (2018). PET molecular imaging in familial Parkinson's disease. *Int. Rev. Neurobiol.* 142, 177–223. doi: 10.1016/bs.irn.2018.09.003

May, A. (2008). Hypothalamic deep-brain stimulation: target and potential mechanism for the treatment of cluster headache. *Cephalalgia* 28, 799–803. doi: 10.1111/j.1468-2982.2008.01629.x

May, A., Leone, M., Boecker, H., Sprenger, T., Juergens, T., Bussone, G., et al. (2006). Hypothalamic deep brain stimulation in positron emission tomography. *J. Neurosci.* 26, 3589–3593. doi: 10.1523/jneurosci.4609-05.2006

Mele, A., Avena, M., Roullet, P., De Leonibus, E., Mandillo, S., Sargolini, F., et al. (2004). Nucleus accumbens dopamine receptors in the consolidation of spatial memory. *Behav. Pharmacol.* 15, 423–431. doi: 10.1097/00008877-200409000-00017

Mesulam, M. M. (2000). A plasticity-based theory of the pathogenesis of Alzheimer's disease. *Ann. N. Y. Acad. Sci.* 924, 42–52.

Mikell, C. B., Mckhann, G. M., Segal, S., Mcgovern, R. A., Wallenstein, M. B., and Moore, H. (2009). The hippocampus and nucleus accumbens as potential therapeutic targets for neurosurgical intervention in schizophrenia. *Stereotact. Funct. Neurosurg.* 87, 256–265. doi: 10.1159/000225979

Mirrione, M. M., Schiffer, W. K., Fowler, J. S., Alexoff, D. L., Dewey, S. L., and Tsirka, S. E. (2007). A novel approach for imaging brain-behavior relationships in mice reveals unexpected metabolic patterns during seizures in the absence of tissue plasminogen activator. *Neuroimage* 38, 34–42. doi: 10.1016/j.neuroimage.2007.06.032

Mizuma, H., Shukuri, M., Hayashi, T., Watanabe, Y., and Onoe, H. (2010). Establishment of in vivo brain imaging method in conscious mice. *J. Nucl. Med.* 51, 1068–1075. doi: 10.2967/jnumed.110.075184

Paxinos, G., and Watson, C. (1997). *The Rat Brain in Steriotaxic Coordinates*. San Diego, CA: Academic Press.

Ponce, F. A., Asaad, W. F., Foote, K. D., Anderson, W. S., Rees Cosgrove, G., Baltuch, G. H., et al. (2016). Bilateral deep brain stimulation of the fornix for Alzheimer's disease: surgical safety in the ADvance trial. *J. Neurosurg.* 125, 75–84. doi: 10.3171/2015.6.JNS15716

Rajmohan, V., and Mohandas, E. (2007). The limbic system. *Indian J. Psychiatry* 49, 132–139.

Raslau, F. D., Augustinack, J. C., Klein, A. P., Ulmer, J. L., Mathews, V. P., and Mark, L. P. (2015). Memory Part 3: the role of the fornix and clinical cases. *AJNR Am. J. Neuroradiol.* 36, 1604–1608. doi: 10.3174/ajnr.a4371

Ross, E. K., Kim, J. P., Settell, M. L., Han, S. R., Blaha, C. D., Min, H. K., et al. (2016). Fornix deep brain stimulation circuit effect is dependent on major excitatory transmission via the nucleus accumbens. *Neuroimage* 128, 138–148. doi: 10.1016/j.neuroimage.2015.12.056

Saint Marie, R. L., Miller, E. J., Breier, M. R., Weber, M., and Swerdlow, N. R. (2010). Projections from ventral hippocampus to medial prefrontal cortex but not nucleus accumbens remain functional after fornix lesions in rats. *Neuroscience* 168, 498–504. doi: 10.1016/j.neuroscience.2010.03.037

Schedlbauer, A. M., Copara, M. S., Watrous, A. J., and Ekstrom, A. D. (2014). Multiple interacting brain areas underlie successful spatiotemporal memory retrieval in humans. *Sci. Rep.* 4:6431. doi: 10.1038/srep06431

Schweinhardt, P., Fransson, P., Olson, L., Spenger, C., and Andersson, J. L. (2003). A template for spatial normalisation of MR images of the rat brain. *J. Neurosci. Methods* 129, 105–113. doi: 10.1016/s0165-0270(03)00192-4

Sesack, S. R., and Grace, A. A. (2010). Cortico-Basal Ganglia reward network: microcircuitry. *Neuropsychopharmacology* 35, 27–47. doi: 10.1038/npp.2009.93

Shohamy, D., and Adcock, R. A. (2010). Dopamine and adaptive memory. *Trends Cogn. Sci.* 14, 464–472. doi: 10.1016/j.tics.2010.08.002

Talakoub, O., Gomez Palacio Schjetnan, A., Valiante, T. A., Popovic, M. R., and Hoffman, K. L. (2016). Closed-loop interruption of hippocampal ripples through fornix stimulation in the non-human primate. *Brain Stimul.* 9, 911–918. doi: 10.1016/j.brs.2016.07.010

Valotassiou, V., Malamitsi, J., Papatriantafyllou, J., Dardiotis, E., Tsougos, I., Psimadas, D., et al. (2018). SPECT and PET imaging in Alzheimer's disease. *Ann. Nucl. Med* 32, 583–593. doi: 10.1007/s12149-018-1292-6

Vann, S. D. (2013). Dismantling the Papez circuit for memory in rats. *eLife* 2:e00736. doi: 10.7554/eLife.00736

Vann, S. D., and Nelson, A. J. (2015). The mammillary bodies and memory: more than a hippocampal relay. *Prog. Brain Res.* 219, 163–185. doi: 10.1016/bs.pbr.2015.03.006

Zhou, J., and Seeley, W. W. (2014). Network dysfunction in Alzheimer's disease and frontotemporal dementia: implications for psychiatry. *Biol. Psychiatry* 75, 565–573. doi: 10.1016/j.biopsych.2014.01.020

Conflict of Interest: The authors declare that the research was conducted in the absence of any commercial or financial relationships that could be construed as a potential conflict of interest.

frontiers in Neuroscience

ORIGINAL RESEARCH
published: 13 December 2019
doi: 10.3389/fnins.2019.01342

High-Resolution Transcranial Electrical Simulation for Living Mice Based on Magneto-Acoustic Effect

Xiaoqing Zhou[1], Shikun Liu[1], Yuexiang Wang[2], Tao Yin[1], Zhuo Yang[2] and Zhipeng Liu[1]**

[1] *Chinese Academy of Medical Sciences & Peking Union Medical College, Institute of Biomedical Engineering, Tianjin, China,*
[2] *College of Medicine, State Key Laboratory of Medicinal Chemical Biology, Nankai University, Tianjin, China*

Transcranial electrical stimulation is an important neuromodulation tool, which has been widely applied in the cognitive sciences and in the treatment of neurological and psychiatric diseases. In this work, a novel non-invasive method of transcranial electrical stimulation with high-resolution transcranial magneto-acoustic stimulation (TMAS) method has been tested experimentally in living mice for the first time. It can achieve spatial resolution of 2 mm in the cortex and even in the deep brain regions. The induced electrical field of TMAS was simulated and measured using a test sample. Then, an animal experimental system was built, and the healthy as well as Parkinson's disease (PD) mice were simulated by TMAS *in vivo*. To investigate the effect of transcranial ultrasound stimulation (TUS) at the same time as TMAS, a TUS group was added in the experiments and its results compared with those of the TMAS group. The results not only demonstrate the high-resolution ability and safety of TMAS, but also show that both TMAS and TUS improved the synaptic plasticity of the PD mice and might improve the spatial learning and memory ability of the healthy mice and the PD mice, although the improvement performance of the TMAS group was superior to that of the TUS-group. Based on the *in vivo* TMAS studies, we propose that TMAS functions as a dual-mode stimulation combining the electric field of the magneto-acoustic effect and the mechanical force of TUS. Our results also provide an explanation of the mechanism of TMAS. This research suggests that future use of US stimulation in magnetic resonance imaging (MRI)-guided studies should involve careful consideration of the induced magneto-acoustic electrical field caused by the static magnetic field of MRI.

Keywords: transcranial focused electrical simulation, transcranial magneto-acoustic stimulation, animal experiment, transcranial ultrasound stimulation, neuromodulation

OPEN ACCESS

Edited by:
Gottfried Schlaug,
Beth Israel Deaconess Medical Center and Harvard Medical School, United States

Reviewed by:
Surjo R. Soekadar,
Charité Medical University of Berlin, Germany
Vincenzo Di Lazzaro,
Campus Bio-Medico University, Italy

****Correspondence:***
Zhuo Yang
zhuoyang@nankai.edu.cn
Zhipeng Liu
lzpeng67@163.com

Specialty section:
This article was submitted to Neural Technology, a section of the journal Frontiers in Neuroscience

Received: *17 July 2018*
Accepted: *28 November 2019*
Published: *13 December 2019*

Citation:
Zhou X, Liu S, Wang Y, Yin T, Yang Z and Liu Z (2019) High-Resolution Transcranial Electrical Simulation for Living Mice Based on Magneto-Acoustic Effect. Front. Neurosci. 13:1342. doi: 10.3389/fnins.2019.01342

INTRODUCTION

Transcranial electromagnetic stimulations have been widely applied in the cognitive sciences and in the treatment of neurological and psychiatric diseases (Fregni and Pascual-Leone, 2007; Bergmann et al., 2016; Grossman et al., 2017). They directly create electrical fields (E-fields), which influence the electrical activities of neurons in the brain by electrical current injection or magnetic induction.

At present, transcranial magnetic stimulation (TMS) (Rotenberg et al., 2014) is the most popular form of non-invasive transcranial electromagnetic stimulation. It utilizes magnetic energy that passes through the skull without attenuation to modulate neural activities and has been used to treat various brain disorders, including tremors, depression, seizures, schizophrenia, pain, and tinnitus (Theodore et al., 2002; Loo and Mitchell, 2005; Borckardt et al., 2006; Lu et al., 2015; Amiaz et al., 2016). However, given that electromagnetic fields obey Laplace's equation, it is impossible to create local maxima in the field intensity, no matter what the configuration of the source coils (Norton, 2003). TMS often does not achieve adequate spatial resolution on the millimeter scale, and it is helpless for specific activation of neuronal cells in a region less than 5 mm (Deng et al., 2013; Markovitz et al., 2015; Guo et al., 2018). In addition, because its magnetic focusing becomes poorer as the penetration depth increases, TMS is not suitable for the stimulation of deep brain tissues. Usually, deep brain stimulation (DBS) (Pereira et al., 2007; Khabarova et al., 2018) is used to stimulate deep brain areas accurately by placing electrodes in the inner area of the brain. However, this involves neurosurgical surgery, which makes it a highly invasive method.

Norton (2003) proposed the novel idea of using ultrasound (US) for focused electrical stimulation by Lorentz forces. This was expected to achieve a focused electrical field with spatial resolution of millimeter scale in the cortex and even in the deep regions. According to Norton, the stimulating electrical field would be induced not by an electric or magnetic field directly, but by the combined action of a US wave and a static magnetic field based on the magneto-acoustic effect. The ion motion created by an ultrasonic wave would form a Hall electric field generated by Lorentz forces. In theory, the induced electric field is consistent with the focused ultrasonic field in a homogeneous medium. In 2006, Zhang et al. (Hongmiao et al., 2005) tested Norton's theoretical format. They analyzed the electrical signals in a gel saline phantom resulting from a combination of ultrasonic signals and static magnetic field and found that the electrical signals were consistent with the ultrasonic signals in the frequency domain. Yuan et al. (2016) focused on the neuronal firing pattern of Norton's method, which they called transcranial magneto-acoustic stimulation (TMAS). They investigated the stimulatory mechanism of TMAS using the Hodgkin–Huxley neuron model and presented simulation results for the neuronal firing pattern. Zhang et al. (2018) improved the stimulatory mechanism of this method by considering the membrane capacitance of neuron changes under an ultrasonic radiation force, based on the Izhikevich model, and also produced simulation results for the firing activity of neurons.

In this paper, we evaluate this novel high-resolution transcranial electrical simulation method, which we also call TMAS, using simulations and measurements of the induced electrical field, as well as *in vivo* animal experiments for the first time. Here, a TMAS system was built and the intensity and distribution of the focused electrical field were measured using a short copper wire. Based on this system, we designed parameters to form a proper stimulated electrical field to stimulate both healthy mice and mouse models of Parkinson's disease (PD) by TMAS *in vivo*. Behavioral tests and electrophysiology studies were performed to explore the biological effects of this novel TMAS.

Moreover, we achieved high-resolution electrical stimulation by utilizing a highly collimated ultrasonic beam in the energy of a static magnetic field, showing that the TMAS process inevitably contains US stimulation, owing to their similar systems and physical principles. In recent years, multiple studies have demonstrated that US can successfully modulate neural activity in the brain at different frequencies (0.3–5 MHz) and different intensity levels (0.02–1000 W/cm^2) in wild-type animals and humans (Tufail et al., 2011; Baek et al., 2017; Sato et al., 2018). Here, we also investigated the effects of transcranial ultrasound stimulation (TUS) on the TMAS process. In the animal experiments, a TUS treatment group was compared with the TMAS treatment group with respect to the behavioral and electrophysiology results. The electrophysiology results show that both TMAS and TUS improved the synaptic plasticity of the PD mice. And the behavioral results suggested that both TMAS and TUS might improve the learning and memory ability of both the healthy mice and the PD mice as supplementary, due to the limitation by the sample size of the behavioral tests (3 or 4 mice per treatment group). In addition, both the healthy and the PD mice, the TMAS group showed better performance than the TUS group. Based on the *in vivo* results, we suggest that TMAS is a complex stimulation combining the electric field of the magneto-acoustic effect and the mechanical force of TUS. The results also provide an explanation of the mechanism of TMAS. Finally, we suggest that the use of TUS in magnetic resonance imaging (MRI) scanners may in future require consideration of the induced magneto-acoustic electrical field (E-field) caused by the strong static magnetic field of MRI.

MATERIALS AND METHODS

Theory of TMAS

The TMAS method is based on the magneto-acoustic effect of conductive tissue, illustrated as the central region in **Figure 1**. The longitudinal particle motion of an ultrasonic wave causes the ion to oscillate back and forth in the medium with velocity **V**. In the presence of a static magnetic field, $\mathbf{B}_0$, the ions are subjected to the Lorentz force $\mathbf{F}_{\mathrm{L}}$ and form the equivalent electrical field **E**, i.e., the simulated electrical field of TMAS:

$$\begin{cases} F_{\mathrm{L}z} = qV_yB_{0x} \\ F_{\mathrm{E}z} = qE_z \end{cases} \tag{1}$$

Considering the $\mathrm{F}_{\mathrm{E}z} = \mathrm{F}_{\mathrm{L}z}$:

$$E_z = V_yB_{0x} \tag{2}$$

Eq. 2 can also be written as the vector expression: $\mathbf{E} = \mathbf{V} \times \mathbf{B}_0$.

As $\mathbf{J} = \sigma\mathbf{E}$, where σ is the conductivity of the tissue, the current density in the tissue can be written as:

$$J_z = \sigma V_yB_{0x} \tag{3}$$

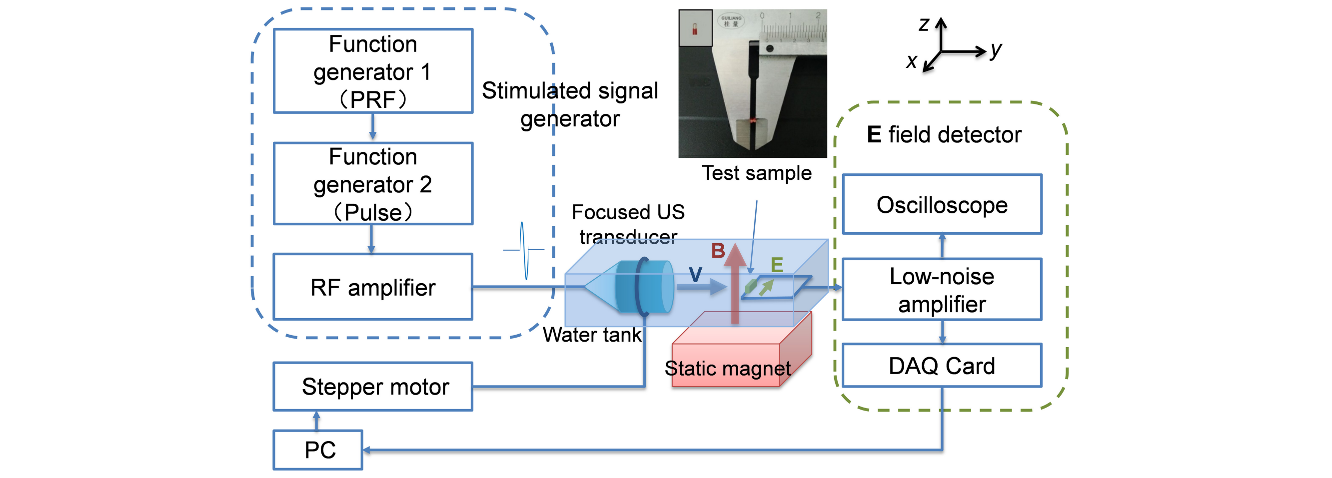

FIGURE 1 | E-field distribution detection system for TMAS.

For the plane cosine wave, the relationship between the acoustic pressure P_y and the vibration velocity V_y can be expressed as:

$$P_y = \rho c_s V_y \tag{4}$$

where ρ is the density of the tissue and c_s denotes the acoustic speed in a tissue. Then Eq. 1 can be written as:

$$\begin{cases} E_z = \frac{1}{\rho c_s} P_y B_{0x} \\ J_z = \frac{\sigma}{\rho c_s} P_y B_{0x} \end{cases} \tag{5}$$

Using Eq. 5, it can be shown that the induced (or coupled) electrical field **E** is simultaneously perpendicular to the direction of the static magnetic field $\mathbf{B}_0$, as well as the acoustic field propagation. The intensity of **E** is related to the values ρ, σ, c_s of the tissue, B_0, and the applied acoustic pressure P. The distribution of **E** is consistent with the distribution of an acoustic field in a homogeneous medium. This means that we can obtain high-resolution electrical stimulation by utilizing a highly collimated ultrasonic beam and the energy of the static magnetic field. In addition, the stimulation of cortical tissue can be highly localized in this way, as well as being achieved at greater depths in the brain.

Experimental Setup for TMAS

To measure and evaluate the distribution and intensity of the E-field in TMAS, an experimental system was set up, as shown in **Figure 1**.

Function generator 1 (TFG6920A, Shuying, China) was used to trigger US pulses and to define the pulse repetition frequency (PRF) and the pulse number of the stimulus waveform. Function generator 2 (AFG3252, Tektronix, United States) was used to define the US frequency and the number of cycles per pulse. The pulsed signals were fed to an RF amplifier (GA2500, RITEC, United States) and used to stimulate a focused US transducer (FP-1M, IOA-AC, China) with a central frequency of 1 MHz and a bandwidth of 400 kHz. The focus size and focal length of the transducer were 2 and 23 mm, respectively. The US transducer was positioned by a holder linked to a three-dimensional stepper motor. The static magnetic field was provided by a permanent magnet. The magnetic field strength B_0 of the magnet was detected by a Gauss meter (Model 475, Lakeshore, United States). The test sample was a 2 mm copper wire located in an adjusting seat. The induced electric signals of the test sample were amplified by a low-noise amplifier (5660C, Olympus, Japan) and acquired using an oscilloscope (MSO4104, Tektronix, United States) or a data acquisition card (PXI-5122, NI, Japan). The sample and the transducer were both immersed in deionized water as an acoustic coupling agent.

To evaluate the TMAS method *in vivo*, an experimental system for small animals based on that in **Figure 1** was set up, as shown in **Figure 2**.

The stimulated signal generator part was the same as **Figure 1**. In this case, the US transducer was positioned using a stereotaxic instrument (SR-6M, Narishige, Japan) and used to perform brain stimulation of targets in the mouse brain. To acquire better localization, a US collimator filled with US coupling gel was used between the US transducer (FP-1M, IOA-AC, China) and the mouse's head. The mouse was laid on a heating pad and fixed by a mouse holder. A permanent magnet was set up beside the

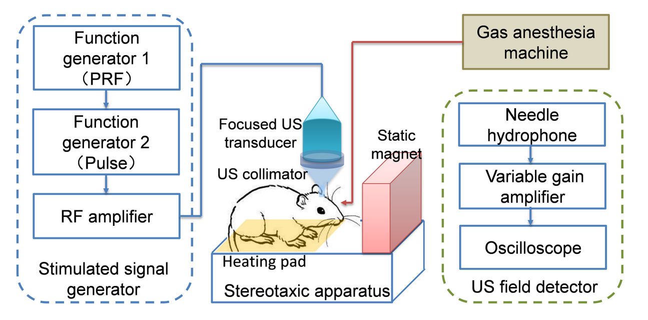

FIGURE 2 | Schematic diagram of the TMAS system for small animals.

mouse. The direction of the magnetic field was perpendicular to the US direction; this setup could produce an ionic current (i.e., a stimulated E-field) pulse along the sagittal direction in the mouse brain. A gas anesthesia machine (R580S, RWD, China) was used to provide anesthesia for the mouse during the TMAS treatments. To acquire the US intensity in real time, a US field detector containing a standard needle hydrophone (NH-1, IOA-AC, China) and a data acquisition device was established.

For TMAS, the static magnetic field is an indispensable element. Without the static magnetic field, the TMAS system in **Figure 2** would be a normal TUS system. Therefore, we could set up or remove the permanent magnet to perform TMAS and TUS, respectively.

Simulation of the Induced Electrical Field in TMAS

To prove the relationship between the E-field and the US field, we simulated the US field distribution of the transducer used in our experiments based on the wave equation written as Eq. 6 and the induced E-field distribution from Eq. 5.

$$\nabla^2 p(\mathbf{r}, t) - \frac{1}{c_s^2}\frac{\partial^2 p(r, t)}{\partial t^2} = S(\mathbf{r}, t) \tag{6}$$

where $p(\mathbf{r}, t)$ denotes the acoustic pressure at location $\mathbf{r}$ and time t, c_s is the acoustic speed in a medium and $S(\mathbf{r}, t)$ denotes the source item induced by the US transducer. The intensity of the E-field at different US pressures was also simulated. The specification of the transducer used in the simulation is shown in **Figure 3**.

In the simulation, a homogeneous medium with the same acoustic and electrical parameters as biological tissue was employed. Values of $\rho = 1000$ kg/m^3, $c_s = 1450$ m/s, and $\sigma = 1$S were used in Eq. 5.

Measurement of the Induced Electrical Field in TMAS

To validate the simulation results, the distribution and intensity of the E-field in TMAS was measured using the system shown in **Figure 2**. The US pressure field distribution of the transducer and the induced E-field distribution were measured and compared. The distribution of the US pressure field was measured using an Acertara acoustic measurement system (AMT, Acertara, United States). In this system, the ultrasonic transducer is positioned by a holder linked to a three-dimensional stepper motor and a hydrophone is used to measure the ultrasonic pressure signal in 3D space at the specified steps. The distribution of the induced E-field was measured with 2 mm steps at the x–y section and x–z section. We also measured the induced voltage of the test sample at different US pressures by changing the stimulated signal.

TMAS Treatment for Living Small Animals

Adult specific-pathogen free (SPF) male C57BL mice of 8 weeks of age were purchased from the Experimental Animal Center of Chinese Academy of Medical Sciences. All experiments were performed according to protocols approved by the Committee for Animal Care of Nankai University and in accordance with the practices outlined in the National Institutes of Health Guide for the Care and Use of Laboratory Animals.

Healthy Mice Stimulation

First, nine healthy mice were stimulated using the system shown in **Figure 2**. In order to investigate the relative contribution of TUS to the TMAS effect, the nine mice were divided into three groups in random: TMAS, TUS, and control (Con).

The mice (20–22 g) were anesthetized with 4% isoflurane, then fixed by the mouse holder of the stereotaxic apparatus. US coupling gel was applied and gently wiped on the mouse's scalp. During the stimulation, the mice were subjected to light anesthesia with 1% isoflurane. The TMAS group received TMAS treatment with US stimulation focused at the substantia nigra of the mouse brain [centered at anteroposterior (AP) −3.4 mm, mediolateral (ML) 1.5 mm, dorsoventral (DV) 4.5 mm] within a static magnetic field of 0.2 T, while the TUS group received TUS treatment at the same target region without the static magnetic field. The con groups received sham stimulation by turning off the US stimulated signal on the mouse head, with the same static magnetic field and the same conditions as the TMAS and TUS groups.

Considering the induced electric field intensity and the security of ultrasonic treatment, the US stimulated signal was chosen as in **Figure 4**.

The frequency of the US stimulated signal was 1 MHz. The pulse duration (PD) was 200 μm with 1 Hz PRF. We measured the intracranial US pressure of a mouse using the US field detector shown in **Figure 2**. The intracranial US pressure P_{in} was approximately 3 MPa, and the spatial-peak temporal-average intensity I_{spta} was approximately 60 mW/cm^2. The duration of stimulation was set to 2 min and contained 120 pulses. All the mice received TMAS, TUS, or sham stimulation once each day for consecutive 10 days. After 10 days of treatment, animal behavior tests were carried out, including the elevated plus-maze test (Okonogi et al., 2018), the open field behavior test (Aulich, 1976) and the Morris Water Maze (MWM) test (Vorhees and Williams, 2006) to assess the emotion and the learning and memory abilities of the healthy mice.

Behavioral Test Methods

The elevated plus-maze was made of black plastic boards and consisted of four arms (two open arms without walls and two enclosed by 15-cm-high walls) 30 cm long and 5 cm wide. Each test began with a mouse placed on the central platform and made to face an open arm. Mouse activities were recorded with a camera located 100 cm above the maze and analyzed on a computer.

The open field arena was made of black plastic (30 cm × 30 cm × 15 cm). Each test began by placing a mouse at a central point, and mouse activities were recorded for 5 min with a video camera located 100 cm above the arena. The arena was equally divided into 16 squares on the computer, and the four squares in the center were defined as the "center" area.

The MWM system (RB-100A type; Beijing, China) contained a 90-cm-diameter swimming arena filled with warm water

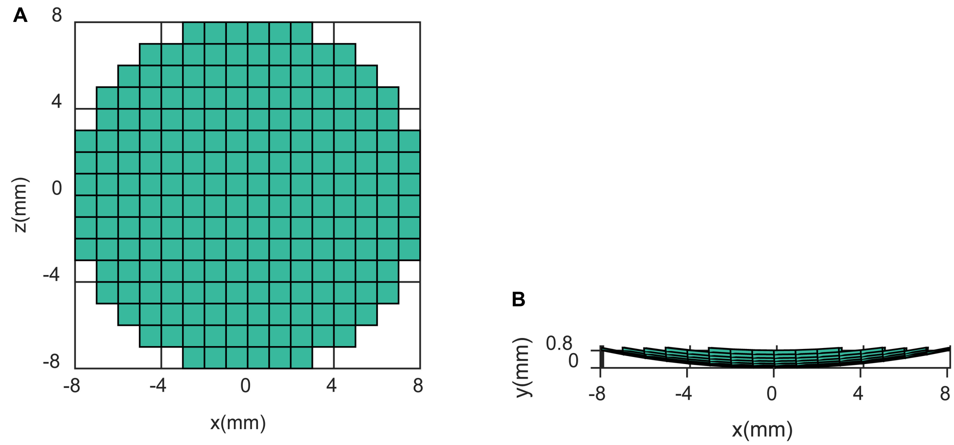

FIGURE 3 | Specification of the transducer at **(A)** the *x–z* section and **(B)** the *x–y* section.

(25°C ± 1°C) that was stained white with non-toxic TiO_2 powder. The swimming activities of mice were recorded by a video camera and analyzed by a computer. On the computer software, the swimming arena was equally divided into four quadrants (I–IV) and a 9-cm-diameter platform was placed in the center of quadrant I and submerged 0.5–1 cm below water surface during the initial training stage. During the initial training stage, all the mice were trained for 4 days with four trials each day. In each trial, the mouse was gently put onto water surface at a random point of each quadrant. The time spent to find the hidden platform (escape latency) of each mouse were monitored. If the mouse failed to find the platform within 60 s, the experimenter would guide the mouse and keep the mouse stay on the platform for 10 s, and the escape latency of this mouse would be recorded as 60 s. The time interval between trials was no less than 10 min to make sure all the mice got sufficient rest. After 4 days of training, all the mice were subjected to spatial probe test 24 h after the last training trial. During the spatial probe test, the platform was removed and the mouse was gently put into water at the opposite quadrant (IV). The mouse was allowed to swim freely for 60 s. The platform crossings and target quadrant dwell time (percentage of time spent in quadrant I) were recorded.

PD Model Mice Stimulation

The 30 PD model mice were used to further evaluate the novel stimulation method. The PD mice received a dosage of 25 mg/kg 1-methyl-4-phenyl-1,2,3,6-tetrahydropyridine (MPTP) (Patil et al., 2014) intraperitoneally (i.p.) each day for 5 days to generate PD-like behavioral phenotypes. The 30 PD mice were also divided into three groups in random: TMAS, TUS, and Con. The stimulation parameters and the experimental conditions for the PD mice were the same as those used for the healthy mice, as described in section "Healthy Mice Stimulation." After 10 days of treatment, the 18 PD (n = 6 in each group) mice were subjected to *in vivo* electrophysiological experiments. And the other 12 PD mice (n = 4 in each group) were subjected to the MWM test to assess the spatial learning and memory abilities.

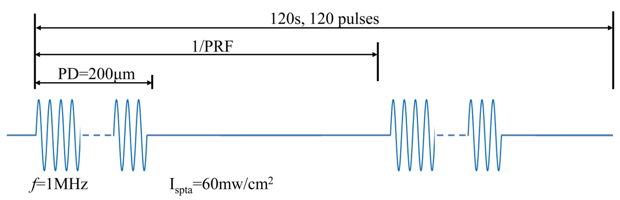

FIGURE 4 | Ultrasound stimulated signal for TMAS in live animal experiments.

In vivo Electrophysiological Study

The mice were positioned on a stereotaxic frame (SR-6 N; Narishige, Japan) after being anesthetized with 30% (w/w) urethane (0.4 mL/kg, i.p.). A bipolar stimulating electrode and recording electrode were implanted in the perforant pathway (−3.8 mm AP, 3.0 mm ML, 1.5 mm DV) and the dentate gyrus (DG) of the hippocampus (−2.0 mm AP, 1.4 mm ML, 1.5 mm DV), respectively. A stimulation current that could evoke a field excitatory postsynaptic potential (fEPSP) of 50–60% of the maximal fEPSP was used. Long-term potentiation (LTP) was induced by theta burst stimulation (30 trains of six pulses at 100 Hz with the inter-train interval of 200 ms) after 30 min of basal fEPSP recording (once every 60 s). Then, the single stimulating pulse-evoked fEPSP was recorded every 60 s for 90 min. Afterward, depotentiation (DP) was induced by low-frequency stimulation (900 pulses of 1 Hz for 15 min), and evoked fEPSP was recorded every 60 s for 90 min (Gao et al., 2015).

RESULTS

The Simulation Results Induced Electrical Field in TMAS

Figure 5 shows the (I) simulated US field distribution and (II) simulated electrical field distribution at (A) the x–y section when y = 0 mm and (B) the x–z section when y = 23 mm. The simulated focus size and focal length of the US field were nearly 2 and

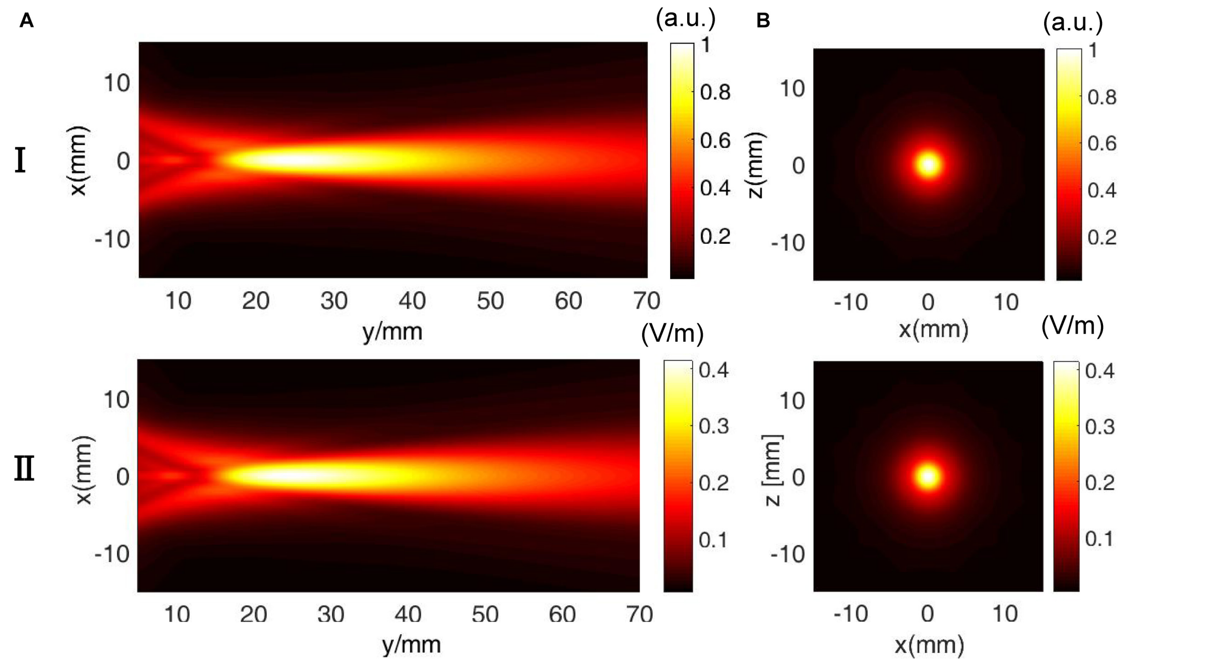

FIGURE 5 | Comparison of the (I) ultrasound pressure field distribution and (II) electrical field intensity distribution at **(A)** the *x–y* section (*y* = 0 mm) and **(B)** *x–z* section (*y* = 23 mm) in the simulation.

23 mm, respectively (**Figure 5I**), and the focus size and focal length of the induced **E** (**Figure 5II**) were also 2 and 23 mm, respectively. The distribution of **E** was highly consistent with the distribution of the US pressure field of the transducer in a homogeneous medium. As shown in **Figure 5II**, the maximal electrical field intensity was 0.4 V/m when $P = 3$ MPa and $B_0 = 0.2$ T. **Figure 6** shows the linear relationship between the intensity of the E-field and the US pressure. Clearly, a stronger E-field was obtained as the US pressure increased.

Measurement of the Induced Electrical Field in TMAS

Figure 7 shows measurements of (I) the ultrasound pressure field distribution and (II) the electrical field intensity distribution at (**Figure 7A**) the *x–y* section when $y = 0$ and (**Figure 7B**) the *x–z* section when $y = 23$ mm by normalization. The focus size and focal length of the US field (**Figure 7I**) were nearly 2 and 23 mm, respectively, as were the focus size and focal length of the induced **E** (**Figure 5II**). The distribution of **E** was consistent with the distribution of the US pressure field of the transducer using the test sample. **Figure 8** shows the relationship between the induced voltage and the US pressure. The induced voltage (E-field) was linearly correlated with the stimulated US pressure, the same as in the simulation.

Behavioral Results From Stimulation Experiments in Healthy Mice

Figure 9 illustrates the behavior results of the stimulation experiments on nine healthy mice described in section "Healthy Mice Stimulation." The behavior tests included the elevated plus-maze test and the open field behavior test. **Figures 9A,B** show the average open arm duration as a percentage of the total time, and the average open arm distance as a percentage of the total distance in the elevated plus-maze test. **Figure 9C** shows the average center duration in the open field behavior test.

As shown in **Figures 9A,B**, both the duration (%) and the distance (%) of the TMAS group and the TUS group were higher than those of the Con group. Moreover, the duration (%) and the distance (%) of the TMAS group exceeded those of the TUS group by about 23 and 22%, respectively. As shown in **Figure 9C**, the center duration times of the TMAS group and TUS group were

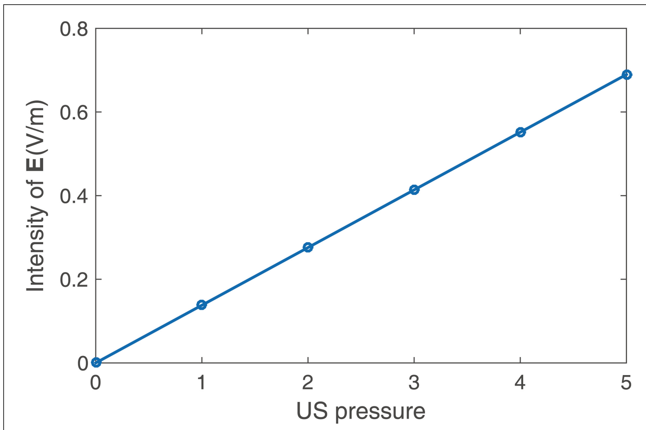

FIGURE 6 | Intensity of the E-field at different US pressures in the simulation.

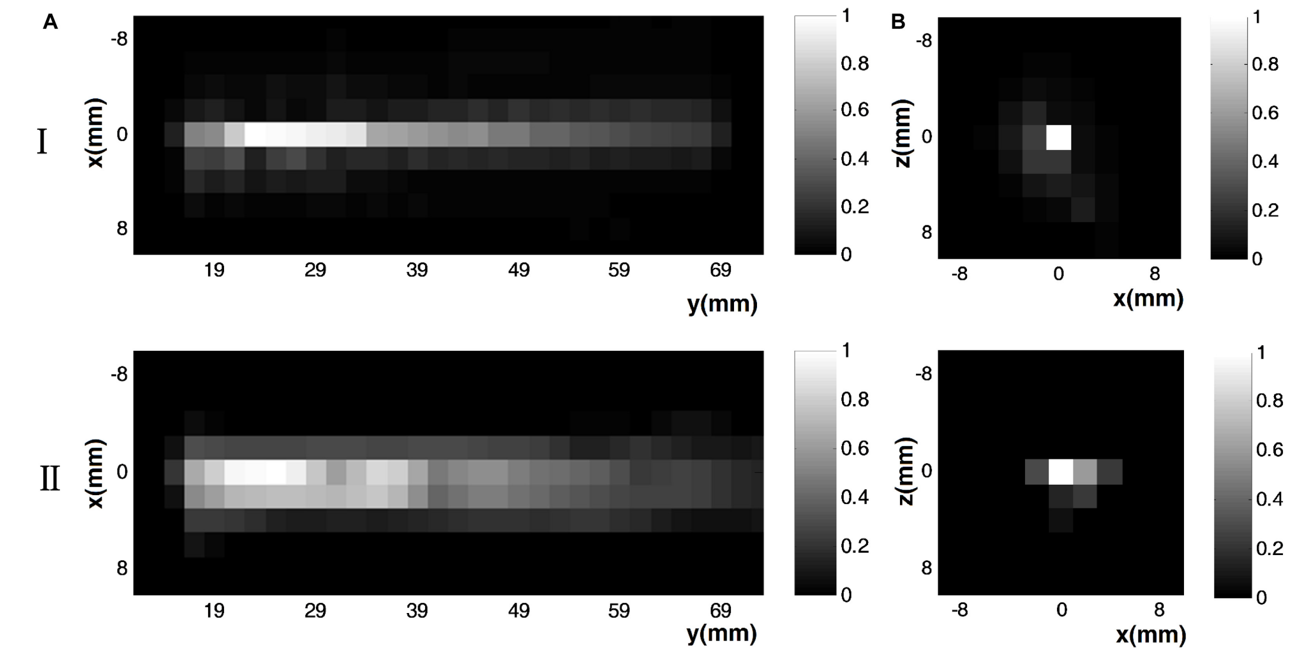

FIGURE 7 | Measurement results of (I) the ultrasound pressure field distribution and (II) the electrical field intensity distribution at **(A)** the *x–y* section (*y* = 0 mm) and **(B)** *x–z* section (*y* = 23 mm) by normalization.

higher than those of the Con group, while the center duration of the TMAS group exceeded the TUS group by about 14%.

As shown in **Figure 10A**, in the training process, the escape latencies in all groups decreased in the following days as compared to the first training day. And the rate of descent of the TMAS group is greater than the TUS group and the Con group. The rate of descent of the TUS group is greater than the Con group, too. Furthermore, the average escape latency in TMAS group is 29.64 ± 3.35 s, which is much shorter than the average escape latency in Con group (36.34 ± 5.29 s) and shorter than the average escape latency in TUS group (32.08 ± 3.60 s). In the probing test process, the platform crossings and the percentage of duration spent in the target quadrant were analyzed, as shown in **Figures 10B,C**. For the platform crossings results (**Figure 10A**), the difference between the TMAS group and Con group was significant (p = 0.0166). And the platform crossings times of the TMAS group (10.25 ± 1.72) is more than the TUS group (8.50 ± 0.42) and more than the Con group (5.00 ± 1.16). For the percentage of duration spent in the target quadrant results (**Figure 10C**), the TMAS group (62.51 ± 3.13%) is more than the TUS group (59.46 ± 4.14%) and more than the Con group (48.64 ± 5.99%). The results in **Figures 10B,C** show the same changing trend as those in **Figure 10A**.

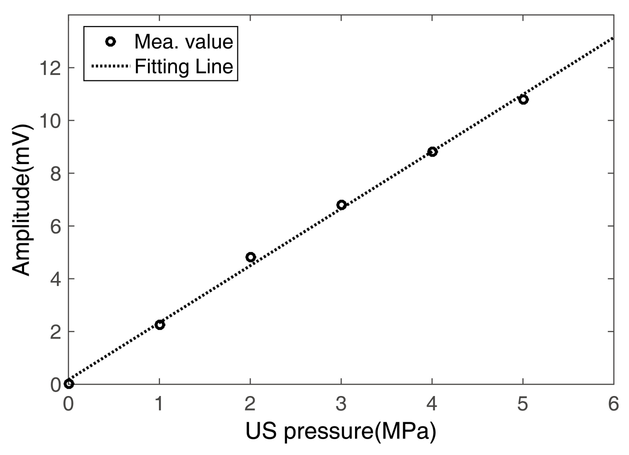

FIGURE 8 | Induced voltage of the test sample at different US pressures.

Besides, both the healthy mice involved in behavioral tests were in good physical and mental state during the 10 days treatment and didn't show any obvious discomfort after the TMAS and TUS.

Electrophysiological Results and MWM Results of the Stimulation Experiments in PD Mice

The results of the *in vivo* electrophysiological experiments on 18 PD mice described in section "PD Model Mice Stimulation" are shown in **Figures 11**, **12**.

As shown in **Figure 11**, the TMAS treatment improved LTP substantially in PD mice. At the end of the LTP recording, the slope of fEPSP in the TMAS group reached 343.9 ± 11.6% of the baseline, which much higher than the increase seen for the Con group (74.4 ± 1.4%). The TUS treatment also improved the LTP effect in PD mice. The slope of fEPSP in the TUS group reached 154.8 ± 2.3% at the end of the LTP

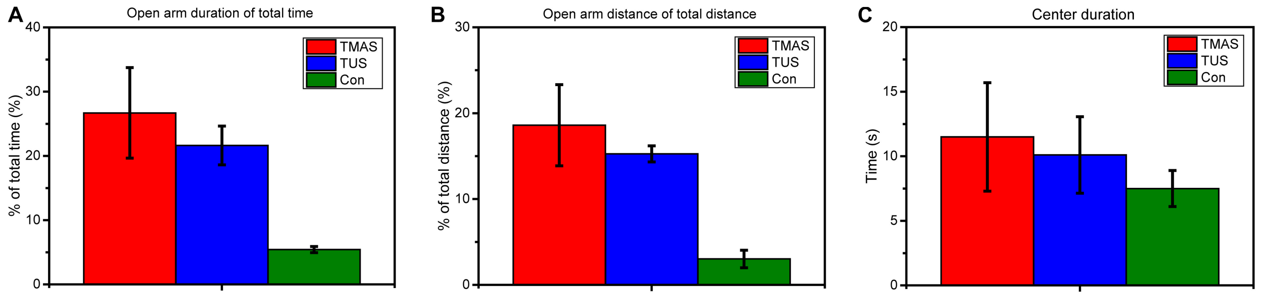

FIGURE 9 | Elevated plus-maze test and open field behavior test results from stimulation experiments in healthy mice (n = 3). **(A)** The open arm duration (the time that mouse spent in the open arms during the test) of total time (%) and **(B)** the open arm distance (the distance that mouse traveled in the open arms during test) of total distance (%) in the elevated plus-maze test. **(C)** The center duration time (the time that mouse spent in the center area) in the open field behavior test.

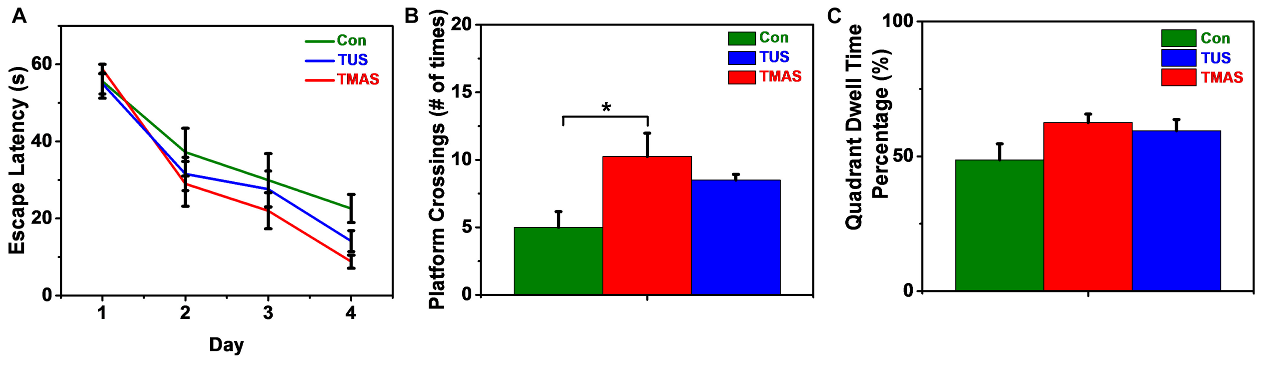

FIGURE 10 | MWM training and test results of the healthy mice (n = 3). **(A)** Escape latencies during training days. **(B)** Platform crossings on probing test day. **(C)** Percentage of duration spent in the target quadrant. $^*p < 0.05$.

recording, compared with 74.4 ± 1.4% in the Con group. We quantified the extent of LTP and DP by calculating the averages of the last 10 min of LTP recording or DP recording for each group of mice, as illustrated in **Figure 12**. For the LTP results

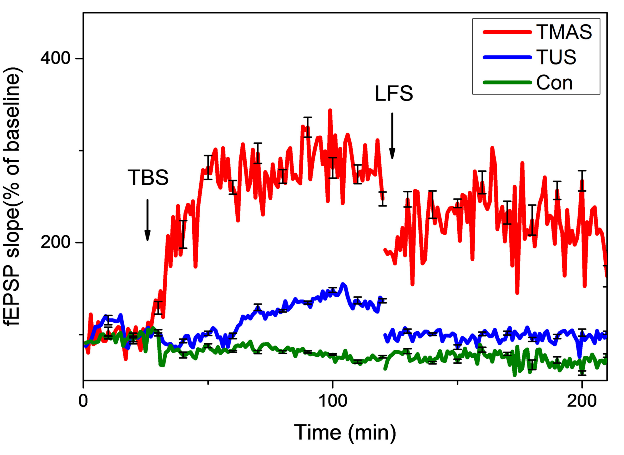

FIGURE 11 | Normalized slopes of fEPSPs in hippocampus of PD mice (n = 6). Red line, blue line, and green line denote the TMAS group, TUS group, and Con group, respectively.

(**Figure 12A**), the difference between the TMAS group and Con group was significant ($p < 0.001$), as was the difference between the TUS group and Con group ($p < 0.001$). Moreover, there was a significant difference between the TMAS group and TUS group ($p < 0.001$). Similarly, the DP results (**Figure 12B**) showed significant differences between the TMAS group and Con group ($p < 0.001$), and between the TUS group and Con group ($p < 0.01$). There was significant difference between TMAS group and TUS group ($p < 0.001$), too. The results in **Figure 12** show the same changing trend as those in **Figure 10**, and further confirm the conclusions drawn from **Figure 11**.

As shown in **Figure 13A**, in the training process, the escape latencies in all groups decreased in the following days as compared to the first training day. And the rate of descent of the TMAS group is greater than the TUS group and the Con group. The rate of descent of the TUS group is greater than the Con group, too. Furthermore, the average escape latency in TMAS group is 30.28 ± 3.14 s, which is much shorter than the average escape latency in Con group (35.81 ± 3.74 s) and slightly shorter than the average escape latency in TUS group (30.67 ± 3.59 s). In the probing test process, the platform crossings and the percentage of duration spent in the target quadrant were analyzed, as shown in **Figures 13B,C**. For the platform crossings results (**Figure 13A**), the platform crossings times of the TMAS group (7.33 ± 0.55) is more than the TUS

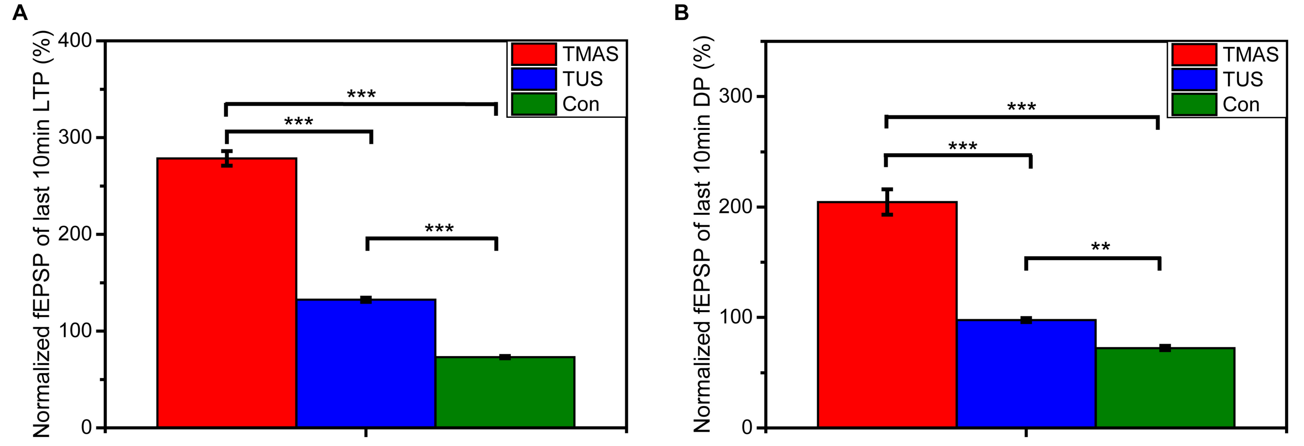

FIGURE 12 | Normalized fEPSPs of **(A)** the last 10 min of LTP and **(B)** the last 10 min of DP ($n = 6$). Data were plotted as mean ± SEM. Red, blue, and green denote the TMAS group, TUS group, and Con group, respectively. $^{**}p < 0.01$, $^{***}p < 0.001$.

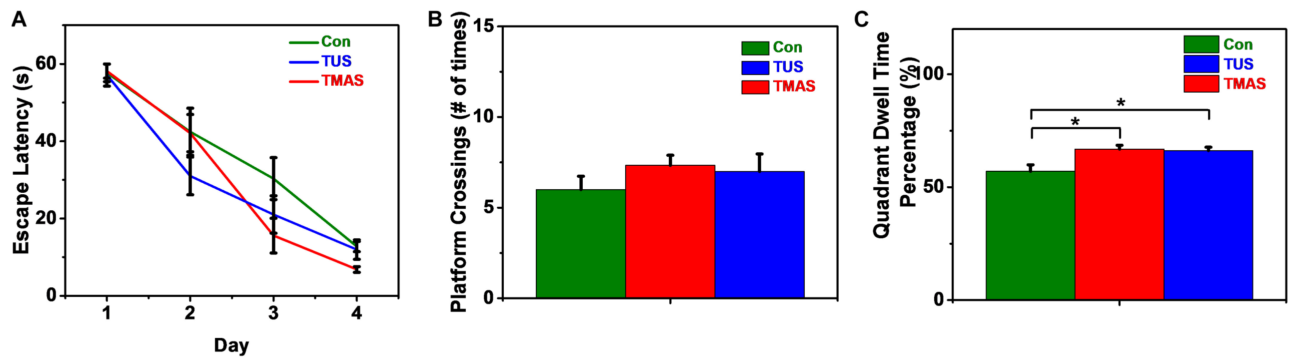

FIGURE 13 | MWM training and test results of the PD mice ($n = 4$). **(A)** Escape latencies during training days. **(B)** Platform crossings on probing test day. **(C)** Percentage of duration spent in the target quadrant. $^{*}p < 0.05$.

group (7.00 ± 0.97) and more than the Con group (6.00 ± 0.73). For the percentage of duration spent in the target quadrant results (**Figure 13C**), the difference between the TMAS group and Con group was significant ($p = 0.0143$), as was the difference between the TUS group and Con group ($p = 0.0223$). And the percentage result of TMAS group (66.86 ± 1.69%) is more than the TUS group (66.17 ± 1.54%). The results in **Figures 13B,C** show the same changing trend as those in **Figure 13A**.

Besides, both the PD mice involved in electrophysiological study and MWM tests were in good physical and mental state during the 10 days treatment and didn't show any obvious discomfort after the TMAS and TUS.

DISCUSSION

As shown in **Figures 5** and **7**, the distribution of **E** was consistent with the distribution of the US pressure field in both simulation and measurement, confirming the high-resolution ability of the TMAS method when employing a highly collimated ultrasonic beam. In our experiments, TMAS could achieve a focused electrical field with 2 mm focal size at the focal length of the transducer (23 mm). We could also acquire a series of intensities for **E** by changing the stimulated US pressure, as shown in **Figures 6** and **8**.

The open arm duration as a percentage of total time and the open arm distance as a percentage of total distance in the elevated plus-maze test reflect the emotion condition of mice. The center duration time in the open field behavior test reflects the active learning ability of mice. The results demonstrate the efficacy and the safety of the TMAS treatment. Limited by the sample size of the behavioral tests (three mice per treatment group), the results shown in **Figure 9** only suggest that both the TMAS treatment and TUS treatment might relieve the anxiety emotion and improve the learning ability of the healthy mice. Moreover, the TMAS group showed better performance than the TUS group.

The escape latency in the MWM test reflects the spatial learning ability of mice. The platform crossings and the percentage of duration spent in the target quadrant in the MWM test reflect the spatial memory ability of mice. Similarly, limited by the sample size in the MWM tests (three mice per treatment group), the results shown in **Figure 10** might suggest that both the TMAS treatment and TUS treatment might improve the learning ability and memory ability of the healthy mice. Moreover, the TMAS group showed better performance than the TUS group. The results demonstrate the efficacy and the safety of the TMAS treatment, too.

The results shown in **Figures 11** and **12** illustrate that TMAS treatment and TUS treatment could potentially alleviate the memory impairments caused by MPTP treatment by improving the LTP effect in the hippocampus. The LTP effect reflects the synaptic plasticity of mice. The synaptic plasticity in hippocampus is related to the spatial learning and memory abilities. Both the TMAS treatment and TUS treatment could improve the synaptic plasticity of the PD mice. Moreover, the TMAS group showed better performance than the TUS group. The results further demonstrate the efficacy of TMAS in PD mice, as well as the safety of the TMAS treatment.

Similarly, the MWM results shown in **Figure 13** suggest that both the TMAS treatment and TUS treatment might improve the spatial learning ability and memory ability of the PD mice. Moreover, the TMAS group showed better performance than the TUS group. Due to the small sample size (four mice per treatment group) in the MWM test, the MWM results could be a supplementary proof to further demonstrate the efficacy of TMAS in PD mice. The MWM results also demonstrate the efficacy and the safety of the TMAS treatment, too.

As illustrated in **Figures 9–13**, we could find that the synaptic plasticity of the PD mice was significantly improved by the TMAS treatments based on the electrophysiological results. And the synaptic plasticity in hippocampus is related to the spatial learning and memory abilities. According to the behavioral results, the learning and memory ability of the healthy mice might be significantly improved by the TMAS treatments. However, due to the small sample size (3 or 4 mice per treatment group) in the behavioral tests, it should admit that the behavioral results have certain limitations. So, the behavioral results could be a supplementary proof to further demonstrate the efficacy of TMAS in healthy mice and PD mice. We shall increase the sample size of the behavioral tests in the next work to improve our research. These *in vivo* results suggest that TMAS could focus on the substantia nigra of the mouse brain with a high resolution (2 mm) and have the ability to activate a small target region effectively. In addition, TUS treatments also improved the synaptic plasticity of the PD mice and might improve the learning and memory ability of the healthy mice and the PD mice compared with the Con group, although the improvement in performance of the TMAS group was superior to that of the TUS group. As described in sections "Theory of TMAS" and "Experimental Setup for TMAS," the TMAS process inevitably contains the TUS process, based on their similar systems and the theory of TMAS. In our animal experiments, the TMAS contained a focused electrical field with $E = 0.4$ V/m and a focused US field with $I_{spta} = 60$ mW/cm^2, simultaneously. Based on the results shown in **Figures 9–13**, we can speculate that the TMAS is not only a focused electrical stimulation but also a complex stimulation combining the electric field of the magneto-acoustic effect and the mechanical force of TUS, both of which play a part in TMAS treatments.

However, it is a novel finding that using an E-field with $E = 0.4$ V/m and US with $I_{spta} = 60$ mW/cm^2 can have such a marked effect in animal experiments. When designing our *in vivo* TMAS studies, we chose the stimulation parameters (the PD, PRF, etc.) to form a proper electrical field mode by considering typical electrical stimulations. Therefore, based on recent research about TUS, the PD, the duty cycle, and the intensity of our US stimulated signal were all much lower than those of the usual stimulation wave in TUS studies (Tufail et al., 2010; Li et al., 2016; Guo et al., 2018). That is, the US stimulation used in our TMAS process was not a typical one. Furthermore, the electric field intensity ($E = 0.4$ V/m) was also much lower than the electric field intensity of typical electrical stimulations by electromagnetic induction, such as TMS and DBS. The electrical stimulation used in our TMAS experiments was really a subconvulsant electrical stimulation, since $E = 0.4$ V/m is lower than the threshold of the action potentials (Nicholls et al., 2012) of neurons.

This means that the performance of TMAS can be attributed to a combination of the electric field and the US field. The mechanism of TUS has been explored in many studies. It is generally considered that the mechanical force of US can change the threshold of ion channels in the cytomembrane (Tyler et al., 2008, 2018; Li et al., 2016; Baek et al., 2017). In the TMAS process, perpendicular mechanical forces are added to the induced E-field at the target region. The mechanical force of US waves may change the ion channels, and the E-field stimulation could achieve much better activity, accordingly. On the other hand, a perpendicular E-field is added to the mechanical force at the target region. The electrical field or electrical electricity influences the local potential or the ion channel threshold, and the US stimulation could also achieve better activity in this way. In brief, based on the *in vivo* TMAS studies, we propose that TMAS is a dual-mode stimulation, simultaneously combining an electrical stimulation by the magneto-acoustic effect and an orthogonal mechanical wave stimulation. This also provides an explanation of the mechanism of TMAS. To date, there has been no other research into the mechanism of TMAS; further studies are needed to evaluate our viewpoint.

Compared with TUS, the static magnetic field in TMAS provides an additional energy source and produces an induced E-field by the magneto-acoustic effect, which involves non-negligible neurobiological effects. TUS is an important tool in neurosciences, and is often combined with MRI and used for MRI-guided brain stimulation (Rizzitelli et al., 2015; Cho et al., 2017; Meng et al., 2017). According to the *in vivo* results, we suggest that future US stimulation in MRI-guided studies should involve careful consideration of the spatio-temporal E-field caused by the strong static magnetic field of MRI.

CONCLUSION

In this paper, a novel non-invasive transcranial electrical stimulation TMAS method was, for the first time, performed experimentally and used in live mice. The induced electrical field of TMAS was simulated and measured. The results demonstrated the high-resolution ability of the TMAS method by employing a highly collimated ultrasonic beam. We built an animal experiment system, in which healthy mice and PD model mice were simulated by TMAS *in vivo*. In order to explore the relative contribution of TUS to the TMAS effect, a TUS group was added. The behavioral and electrophysiology results validate that TMAS could focus on the mouse brain with a high resolution (2 mm) and activate a small target region effectively. The results also showed that both TMAS and TUS improved the synaptic plasticity of the PD mice and might improve the learning and memory ability of the healthy mice and the PD mice, with the TMAS group being superior to the TUS group in terms of improvement in performance. Based on the *in vivo* TMAS studies, we propose that TMAS is a dual-mode stimulation combined by the electric field of the magneto-acoustic effect and the mechanical force of TUS. Our results also provide an explanation of the mechanism of TMAS. In addition, we suggest that in the future, US stimulation in MRI-guided studies should involve careful consideration of the spatio-temporal E-field caused by the strong static magnetic field.

ETHICS STATEMENT

This study was carried out in accordance with the recommendations of the practices outlined in the National Institutes of Health Guide for the Care and Use of Laboratory Animals. The protocol was approved by the Committee for Animal Care of Nankai University.

AUTHOR CONTRIBUTIONS

XZ set up the experiment system, prepared the experiments, analyzed the experimental data and drafted the manuscript. SL carry out the animal stimulations and the behavioral tests. YW prepared the PD model mice and performed the electrophysiological experiments. TY designed the initial experimental system and gave many advices to this method. ZY conceived the animal experiments. ZL proposed this study and design the whole research programme. All authors revised the final version of this manuscript.

FUNDING

This research was supported by the National Natural Science Foundation of China (81601633, 81772003, and 81772004) and the CAMS Initiative for Innovative Medicine (No. 2016-I2M-1004).

REFERENCES

Amiaz, R., Vainiger, D., Gershon, A. A., Weiser, M., Lavidor, M., and Javitt, D. C. (2016). Applying transcranial magnetic stimulation (TMS) over the dorsal visual pathway induces schizophrenia-like disruption of perceptual closure. *Brain Topogr.* 29, 552–560. doi: 10.1007/s10548-016-0487-1

Aulich, D. (1976). Escape versus exploratory activity: an interpretation of rats' behavior in the open field and a light-dark preference test. *Behav. Process.* 1, 153–164. doi: 10.1016/0376-6357(76)90035-8

Baek, H., Pahk, K. J., and Kim, H. (2017). A review of low-intensity focused ultrasound for neuromodulation. *Biomed. Eng. Lett.* 7, 135–142. doi: 10.1007/s13534-016-0007-y

Bergmann, T. O., Karabanov, A., Hartwigsen, G., Thielscher, A., and Siebner, H. R. (2016). Combining non-invasive transcranial brain stimulation with neuroimaging and electrophysiology: current approaches and future perspectives. *Neuroimage* 140, 4–19. doi: 10.1016/j.neuroimage.2016.02.012

Borckardt, J. J., Smith, A. R., Hutcheson, K., Johnson, K., Nahas, Z., Anderson, B., et al. (2006). Reducing pain and unpleasantness during repetitive transcranial magnetic stimulation. *J. ECT* 22, 259–264. doi: 10.1097/01.yct.0000244248.40662.9a

Cho, H., Pahk, K., and Kim, H. (2017). Development of low-intensity focused ultrasound (LIFU) based MRI-compatible brain stimulation system. *Brain Stimul.* 10:386. doi: 10.1016/j.brs.2017.01.139

Deng, Z. D., Lisanby, S. H., and Peterchev, A. V. (2013). Electric field depth–focality tradeoff in transcranial magnetic stimulation: simulation comparison of 50 coil designs. *Brain Stimul.* 6, 1–13. doi: 10.1016/j.brs.2012.02.005

Fregni, F., and Pascual-Leone, A. (2007). Technology insight: noninvasive brain stimulation in neurology—perspectives on the therapeutic potential of rTMS and tDCS. *Nat. Rev. Neurol.* 3, 383–393. doi: 10.1038/ncpneuro0530

Gao, J., Zhang, X., Yu, M., Ren, G., and Yang, Z. (2015). Cognitive deficits induced by multi-walled carbon nanotubes via the autophagic pathway. *Toxicology* 337, 21–29. doi: 10.1016/j.tox.2015.08.011

Grossman, N., Bono, D., Dedic, N., Kodandaramaiah, S. B., Rudenko, A., Suk, H. J., et al. (2017). Noninvasive deep brain stimulation via temporally interfering electric fields. *Cell* 169, 1029.e16–1041.e16. doi: 10.1016/j.cell.2017.05.024

Guo, H., Hamilton, I. I. M., Offutt, S. J., Gloeckner, C. D., Li, T., Kim, Y., et al. (2018). Ultrasound produces extensive brain activation via a cochlear pathway. *Neuron* 98, 1020.e4–1030.e4.

Hongmiao, Z., Jun, L., Shaohua, Y., Zhengguo, L., and Guang, L. (2005). Measurement of bioelectric currents based on the coupling of electric and magnetic field. *Conf. Proc. IEEE Eng. Med. Biol. Soc.* 3, 3001–3003.

Khabarova, E. A., Denisova, N. P., Dmitriev, A. B., Slavin, K., and Verhagen, M. L. (2018). Deep brain stimulation of the subthalamic nucleus in patients with Parkinson disease with prior pallidotomy or thalamotomy. *Brain Sci.* 8:E66.

Li, G. F., Zhao, H. X., Zhou, H., Yan, F., Wang, J. Y., Xu, C. X., et al. (2016). Improved anatomical specificity of non-invasive neuro-stimulation by high frequency (5 MHz) ultrasound. *Sci. Rep.* 6:24738. doi: 10.1038/srep24738

Loo, C. K., and Mitchell, P. B. (2005). A review of the efficacy of transcranial magnetic stimulation (TMS) treatment for depression, and current and future strategies to optimize efficacy. *J. Affect. Disord.* 88, 255–267. doi: 10.1016/j.jad.2005.08.001

Lu, M. K., Chiou, S. M., Ziemann, U., Huang, H. C., Yang, Y. W., and Tsai, C. H. (2015). Resetting tremor by single and paired transcranial magnetic stimulation in Parkinson's disease and essential tremor. *Clin. Neurophysiol.* 126, 2330–2336. doi: 10.1016/j.clinph.2015.02.010

Markovitz, C. D., Smith, B. T., Gloeckner, C. D., and Lim, H. H. (2015). Investigating a new neuromodulation treatment for brain disorders using synchronized activation of multimodal pathways. *Sci. Rep.* 5:9462. doi: 10.1038/srep09462

Meng, Y., Huang, Y., Solomon, B., Hynynen, K., Scantlebury, N., Schwartz, M. L., et al. (2017). MRI-guided focused ultrasound thalamotomy for patients with medically-refractory essential tremor. *J. Vis. Exp.* 130:e56365 doi: 10.3791/56365

Nicholls, J. G., Martin, A. R., Wallace, B. G., and Fuchs, P. A. (2012). *From Neuron to Brain*, 5th Edn. Sunderland, MA: Sinauer Associates.

Norton, S. J. (2003). Can ultrasound be used to stimulate nerve tissue? *Biomed. Eng. Online* 2:6.

Okonogi, T., Nakayama, R., Sasaki, T., and Ikegaya, Y. (2018). Characterization of peripheral activity states and cortical local field potentials of mice in an elevated plus maze test. *Front. Behav. Neurosci.* 12:62. doi: 10.3389/fnbeh.2018.00062

Patil, S. P., Jain, P. D., Ghumatkar, P. J., Tambe, R., and Sathaye, S. (2014). Neuroprotective effect of metformin in MPTP-induced Parkinson's disease in mice. *Neuroscience* 277, 747–754. doi: 10.1016/j.neuroscience.2014.07.046

Pereira, E. A., Green, A. L., Nandi, D., and Aziz, T. Z. (2007). Deep brain stimulation: indications and evidence. *Exp. Rev. Med. Dev.* 4, 591–603.

Rizzitelli, S., Giustetto, P., Cutrin, J. C., Castelli, D. D., Boffa, C., Ruzza, M., et al. (2015). Sonosensitive theranostic liposomes for preclinical in vivo MRI-guided visualization of doxorubicin release stimulated by pulsed low intensity non-focused ultrasound. *J. Control Release* 202, 21–30. doi: 10.1016/j.jconrel.2015.01.028

Rotenberg, A., Horvath, J. C., and Pascual-Leone, A. (2014). *Transcranial Magnetic Stimulation*. New York: Springer.

Sato, T., Shapiro, M. G., and Tsao, D. Y. (2018). Ultrasonic neuromodulation causes widespread cortical activation via an indirect auditory mechanism. *Neuron* 98, 1031.e5–1041.e5. doi: 10.1016/j.neuron.2018.05.009

Theodore, W. H., Hunter, K., Chen, R., Vega–Bermudez, F., Boroojerdi, B., Reeves–Tyer, P., et al. (2002). Transcranial magnetic stimulation for the treatment of seizures: a controlled study. *Neurology* 59, 560–562.

Tufail, Y., Matyushov, A., Baldwin, N., Tauchmann, M. L., Georges, J., Yoshihiro, A., et al. (2010). Transcranial pulsed ultrasound stimulates intact brain circuits. *Neuron* 66, 681–694. doi: 10.1016/j.neuron.2010.05.008

Tufail, Y., Yoshihiro, A., Pati, S., Li, M. M., and Tyler, W. J. (2011). Ultrasonic neuromodulation by brain stimulation with transcranial ultrasound. *Nat. Protoc.* 6, 1453–1470. doi: 10.1038/nprot.2011.371

Tyler, W. J., Shane, W. L., and Grace, M. H. (2018). Ultrasonic modulation of neural circuit activity. *Curr. Opin. Neurobiol.* 50, 222–231. doi: 10.1016/j.conb.2018.04.011

Tyler, W. J., Tufail, Y., Finsterwald, M., Tauchmann, M. L., Olson, E. J., and Majestic, C. (2008). Remote excitation of neuronal circuits using low-intensity, low-frequency ultrasound. *PLoS One* 3:e3511. doi: 10.1371/journal.pone.0003511

Vorhees, C. V., and Williams, M. T. (2006). Morris water maze: procedures for assessing spatial and related forms of learning and memory. *Nat. Protoc.* 1, 848–858. doi: 10.1038/nprot.2006.116

Yuan, Y., Chen, Y., and Li, X. (2016). Theoretical analysis of transcranial magneto-acoustical stimulation with Hodgkin-Huxley neuron model. *Front. Comput. Neurosci.* 10:35. doi: 10.3389/fncom.2016.00035

Zhang, S., Cui, K., Zhang, X., Shi, X., Ge, M., Zhao, M., et al. (2018). Effect of transcranial ultrasonic–magnetic stimulation on two types of neural firing behaviors in modified Izhikevich model. *IEEE Trans. Magnet.* 54, 1–4. doi: 10.1109/tmag.2017.2773086

Conflict of Interest: The authors declare that the research was conducted in the absence of any commercial or financial relationships that could be construed as a potential conflict of interest.

Advantages of publishing in Frontiers

OPEN ACCESS
Articles are free to read for greatest visibility and readership

FAST PUBLICATION
Around 90 days from submission to decision

HIGH QUALITY PEER-REVIEW
Rigorous, collaborative, and constructive peer-review

TRANSPARENT PEER-REVIEW
Editors and reviewers acknowledged by name on published articles

Frontiers
Avenue du Tribunal-Fédéral 34
1005 Lausanne | Switzerland

Visit us: www.frontiersin.org
Contact us: info@frontiersin.org | +41 21 510 17 00

REPRODUCIBILITY OF RESEARCH
Support open data and methods to enhance research reproducibility

DIGITAL PUBLISHING
Articles designed for optimal readership across devices

FOLLOW US
@frontiersin

IMPACT METRICS
Advanced article metrics track visibility across digital media

EXTENSIVE PROMOTION
Marketing and promotion of impactful research

LOOP RESEARCH NETWORK
Our network increases your article's readership